Cofilin and drebrin mediated regulation of the neuronal cytoskeleton in development and disease

Submitted by *Holly Hardy*, to the University of Exeter as a thesis for the degree of *Doctor of Philosophy in Medical Studies*, *August 2017*.

……

ACKNOWLEDGEMENTS

I would like to express my gratitude to Dr. John Chilton and Dr. Helen Dawe for their guidance, advice and encouragement. I also wish to thank the University of Exeter Medical School for funding this research.

A special thanks to my colleagues, past and present, for their knowledge and help in the lab, and for the laughs and coffee when they were needed most.

The continual love and support from my friends and family has carried me through. Thanks for always believing in me when I didn’t believe in myself.

Finally, my sincerest appreciation to Joe Rainger for being the light in the depths of the valley.

SUMMARY

The brain is a highly complex structure; neurons extend axons which follow precise paths to make connections with their targets. This extension is guided by a specialised and highly motile structure at the axon tip —the growth cone— which integrates guidance cues to steer the axon through the environment. Aberrant pathfinding is likely to result in developmental impairments causing disruption to brain functions underlying emotion learning and memory. Furthermore, pre-existing connections are constantly remodelled, the ability to do so declines with age, and can have huge impacts on quality of life and well-being. Examining how changes in growth cone behaviour triggered by external cues occurs is crucial for understanding processes in both development and disease.

Controlled reorganisation of growth cone cytoskeletal components, such as actin filaments, generate membrane protrusions forming lamellipodia and filopodia. Filopodium formation is commonly associated with sensing the mechanical and chemical environment of the cell. Despite our understanding of the guidance choices that can be made, how filopodia transmit information at a molecular level leading to profound changes in morphology, motility and directionality remains largely unknown. Various actin-binding proteins regulate the number, stability and branching of filopodia. They may therefore have a key role in priming or abrogating the ability of the growth cone to respond to a given guidance cue.

I have shown that the actin binding proteins drebrin and cofilin, whilst displaying opposing molecular activities on actin filaments, work synergistically in a temporally regulated manner. A fluorescent membrane marker combined with tagged cofilin and drebrin enabled accurate correlation of cofilin and drebrin dynamics with growth cone morphology and filopodial turnover in live neurons. In contrast to previous *in vitro* experiments, cofilin was found to enhance the effect of drebrin to promote filopodia formation in intact neurons, and that growth cone spread was significantly constrained when cofilin was knocked down. Importantly, this adds to our understanding of how the two actin binding proteins contribute to directed motility in neuronal growth cone filopodia during guidance. Furthermore, following acute treatment with low concentrations of the repulsive guidance cue semaphorin-3A, neuronal growth cones expressing cofilin displayed increased morphological complexity and filopodial stability. This suggests that traditional collapse signals may serve as pause signals allowing neurons to increase the surface area to sense the environment adequately and enable precise wiring decisions.

Remodeling of the cytoskeleton is perturbed in a number of degenerative diseases including Alzheimer's, Huntington's, and Amyotrophic Lateral Sclerosis. These conditions are associated with widespread synaptic loss, resulting in memory loss, cognitive impairment, and movement disorders which leads to severe deterioration in quality of life for those afflicted in addition to wider negative socioeconomic impacts.

How widespread synaptic loss occurs is poorly understood. One common characteristic is neuronal stress which can be initiated through different conditions such as neuroinflammation, energetic stress, glutamate excitotoxicity, and accumulation of misfolded proteins, all of which have been associated with

perturbation of the actin cytoskeleton and the initiation of the cofilin-actin rod stress response. Dysfunction of the cytoskeleton can lead to the disruption of synaptic activity by blocking the delivery of elements such as organelles and proteins required for maintenance of the synapse. Modulating this stress response offers an approach to protecting the integrity of normal synaptic function.

Actin interacting protein-1 is a conserved actin binding protein that enhances the filament disassembly activity of cofilin. I have discovered that AIP-1 has a potent ability to prevent the formation of cofilin rods which are thought to contribute to the neuronal dysfunction in several neurodegenerative disorders, even when they are treated with amyloid-β or subjected to metabolic stress. This is the first study to demonstrate a molecular mechanism for preventing rod formation in the presence of a neuronal stressor and has the potential to protect against rod formation by other stressors associated with disease such as inflammation and excitotoxicity. AIP-1 offers the exciting possibility of a means to reverse cofilin rod formation and the subsequent cytoskeletal pathology associated with dementia and has potential for therapeutic exploitation in human disease. Furthermore, it is the first study to demonstrate that AIP-1 localises to areas of rapid actin remodeling in neuronal growth cones. Exploiting the action of AIP-1 therefore represents an exciting and novel therapeutic avenue to tackle neurodegeneration.

CONTENTS

DECLARATION ..... **- 1 -**

ACKNOWLEDGEMENTS ..... **- 3 -**

SUMMARY ..... **- 5 -**

CONTENTS ..... **- 7 -**

LIST OF FIGURES ..... **- 11 -**

LIST OF TABLES ..... **- 13 -**

ABBREVIATIONS ..... **- 15 -**

CHAPTER 1

INTRODUCTION ..... **- 19 -**

1.1 The neuronal cytoskeleton ..... - 21 -
1.2 Fundamental principles of nervous system formation ..... - 23 -
1.3 Axon guidance and the growth cone ..... - 25 -
1.4 Actin cytoskeleton ..... - 35 -
1.5 Neuronal growth cone actin ..... - 36 -
1.6 Filopodia in synaptogenesis ..... - 39 -
1.7 Actin binding proteins ..... - 40 -
1.8 Cofilin ..... - 46 -
1.9 Actin interacting protein-1 ..... - 61 -
1.10 Drebrin ..... - 66 -
1.11 Identifying the gaps ..... - 74 -

CHAPTER 2

MATERIALS AND METHODS ..... **- 75 -**

2.1 Buffers, reagents and stock materials ..... - 77 -
2.2 Constructs ..... - 79 -
2.3 Generation of specific chick Cofilin-1 and AIP-1 hairpins ..... - 82 -
2.4 DNA Plasmid preparation ..... - 85 -
2.4.1 Streaking out of bacterial stab cultures ..... *- 85 -*
2.4.2 Micropreps ..... *- 85 -*
2.4.3 Minipreps ..... *- 86 -*
2.4.4 Midipreps ..... *- 87 -*
2.4.5 Maxipreps ..... *- 89 -*
2.5 Glycerol stocks ..... - 90 -
2.6 Primer design ..... - 90 -
2.7 Polymerase chain reaction ..... - 92 -
2.8 PCR product purification ..... - 92 -
2.9 Gel purification of DNA ..... - 93 -
2.10 Ligation ..... - 94 -
2.11 Bacterial transformation ..... - 94 -
2.12 Primary cell culture techniques ..... - 95 -
2.12.1 Isolation and embryonic chick dorsal root ganglia ..... *- 95 -*
2.12.2 Preparation of explant cultures ..... *- 96 -*
2.12.3 Preparation of dissociated cultures ..... *- 97 -*
2.12.4 Electroporation ..... *- 98 -*
2.13 Cell line culture ..... - 99 -
2.13.1 Transient transfection ..... *- 99 -*
2.14 Western blotting ..... - 99 -
2.14.1 Preparation of cell lysates ..... *- 99 -*
2.14.2 Preparation of embryonic chicken brain lysates ..... *- 100 -*

2.14.3 Protein quantification..... *- 101 -*
2.14.4 SDS-PAGE separation of proteins..... *- 102 -*
2.14.5 Membrane transfer..... *- 103 -*
2.14.6 Immunodetection and visualisation..... *- 104 -*
2.15 Immunocytochemistry ..... - 105 -
2.16 Preparation of J20 mouse brain slices ..... - 106 -
2.17 Immunohistochemistry ..... - 107 -
2.18 Microscopy..... - 107 -
2.19 Image analysis ..... - 108 -
2.20 Statistical analysis..... - 108 -

CHAPTER 3

Drebrin is required to stabilise and maintain actin filaments during growth cone filopodia formation and maintenance ..... - 111 -
3.1 Introduction ..... - 113 -
3.2 Results..... - 119 -
3.2.1 Drebrin localisation in fixed & DRG neuronal growth cones..... *- 119 -*
3.2.2 Effect of drebrin overexpression on the stability of filopodia ..... *- 121 -*
3.2.3 Growth cone complexity & phasic behaviour visualised……*- 126 -*
3.3 Discussion ..... - 133 -

CHAPTER 4

Drebrin and cofilin interact to modulate growth cone dynamics..... - 141 -
4.1 Introduction ..... - 143 -
4.2 Results..... - 149 -
4.2.1 Drebrin and cofilin increase morphological complexity in fibroblasts ..... *- 149 -*
4.2.2 Cofilin association with dynamic peripheral area of the growth cone. ..... *- 154 -*
4.2.3 Cofilin & drebrin synergistically drive protrusion formation in neurons ..... *- 156 -*
4.2.4 Cofilin knockdown constrains drebrin-induced growth cone spread..... *- 161 -*
4.2.5 Cofilin and drebrin display minimal overlap in live neurons..... *- 166 -*
4.2.6 Cofilin drives protrusion formation in the presence of sema 3A ..... *- 166 -*
4.3 Discussion ..... - 170 -

CHAPTER 5

Cofilin Rods ..... - 177 -
5.1 Introduction ..... - 179 -
5.2 Results..... - 186 -
5.2.1 Cofilin-actin rods form in cofilin overexpression & energetic stress..... *- 186 -*
5.2.2 Rods are formed by endogenous cofilin ..... *- 193 -*
5.2.5 AIP blocks cofilin rod formation in cofilin overexpression..... *- 202 -*
5.2.6 AIP-1 blocks rods formed by amyloid-β treatment ..... *- 205 -*
5.2.7 AIP-1 blocks rods formed by 2-DG treatment ..... *- 207 -*
5.3 Discussion ..... - 213 -

CHAPTER 6

CONCLUDING DISCUSSION..... - 219 -

APPENDICES..... - 225 -
Appendix A ..... - 227 -
Supplementary Media File 1
Appendix B ..... - 228 -
Supplementary Media File 2
Appendix C ..... - 229 -
Supplementary Media File 3 & 4
Appendix D ..... - 230 -
Supplementary Media File 5, 6, 7 & 8
Appendix E ..... - 231 -

Supplementary Media File 9
Appendix F .....- 232 -
Supplementary details of expression vector maps and cloning schemes for key genes
Appendix G.....- 239 -
Custom MATLAB scripts
REFERENCES..... - 263 -

LIST OF FIGURES

CHAPTER 1

Fig. 1-1. Classic growth cone structure with cytoskeletal components……..... -26-
Fig. 1-2. Molecular mechanisms underlying axon guidance…… -28-
Fig. 1-3. Model of Sema 3A signalling through Plexin-A……..... -33-
Fig. 1-4. The growth cone interprets cues……..….. -38-
Fig. 1-5. Actin self-assembly and the dynamic structure of filaments……..... -42-
Fig. 1-6. Actin architecture & function is governed by actin binding proteins……..... -44-
Fig. 1-7. Sequences of Human cofilin/AFD family……..……..... -48-
Fig. 1-8. Canonical cofilin regulation……..….. -54-
Fig. 1-9. Phosphatidylinositol 4,5-bisphosphate signalling downstream of receptor tyrosine kinases……..….. -56-
Fig. 1-10. AIP-1 structure, & sequences of Human AIP-1 & Chick AIP-1……. -63-
Fig. 1-11. Switching of drebrin E isoform expression……..... -67-

CHAPTER 2

Fig. 2-1 Schematics of fusion proteins……..... -81-
Fig. 2-2 Schematic of pRFPRNAiC vector used for hairpin expression…….. -84-

CHAPTER 3

Fig. 3-1. Schematic of drebrin protein domains……..…..... -115-
Fig. 3-2. Drebrin is restricted to the distal growth cone…….. -120-
Fig. 3-3. Drebrin modifies stability of filopodia……..……. -122-
Fig. 3-4. Drebrin overexpression results in shorter filopodia……..... -125-
Fig. 3-5. R-pre RFP expression in 3T3 fibroblasts…….……..... -128-
Fig. 3-6. R-Pre-mRFP as a membrane marker……..…..... -129-
Fig. 3-7. Live cell imaging of filopodia demonstrates periodicity of extension and retraction rates……..……. -132-

CHAPTER 4

Fig. 4-1. Cofilin & drebrin may have opposing effects on filopodial dynamics……..... -147-
Fig. 4-2. Circularity factor equation…….……. -150-
Fig. 4-3. Ectopic expression of drebrin and cofilin increases morphological complexity in NIH/3T3 fibroblasts……..…… -151-
Fig. 4-4. Increased cofilin activity drives protrusion formation in the presence of full-length drebrin……..…..... -153-
Fig. 4-5. Cofilin is associated with dynamic growth cone periphery……..…….. -155-
Fig. 4-6. Cofilin GFP fusion construct validation by western blot……..... -158-
Fig. 4-7. Use of tip to base ratio to assess filopodial branching……..….. -159-
Fig. 4-8. Cofilin inactivation results shorter filopodia…….. -160-
Fig. 4-9 Validation of cofilin short hairpin interfering RNA by immunofluorescence……..…… -163-
Fig. 4-10. Growth cone spread induced by drebrin is constrained when cofilin is knocked down…….……..... -165-
Fig. 4-11. Drebin and cofilin overlap minimally…….. -167-

Fig. 4-12. Cofilin drives protrusion formation in the presence of sema 3A……..... -169-
Fig. 4-13. Proposed model of cofilin and drebrin synergy in neuronal growth cones…… -173-

CHAPTER 5

Fig. 5-1. Cofilin-actin rod stress response…….…….. -181-
Fig. 5-2. Disassembly of actin structures by cofilin and AIP-1……..... -184-
Fig. 5-3. Cofilin stabilises actin filaments at high concentrations…….... -187-
Fig. 5-4. Cofilin rods form in neurons in response to acute energetic stress…….. -190-
Fig. 5-5. Automated analysis of cofilin rods……..……... -191-
Fig. 5-6. 2-DG induces rod formation in DRG…… -192-
Fig. 5-7. R21Q Cofilin mutant can be used as a genetic reporter for rods……...…….. -194-
Fig. 5-8. R21Q Cofilin mutant is only incorporated into rods formed by endogenous cofilin……... -196-
Fig. 5-9. Cofilin rod formation in growth cones of live neurons…….….... -197-
Fig. 5-10. Cofilin must be activated to form rods……..….. -199-
Fig. 5-11. Growth cone displaying large rod aggregate……...……. -200-
Fig. 5-12. Cofilin rods form in the brains of J20 mice……...……. -201-
Fig. 5-13. AIP redistributes Cofilin and blocks rod formation…..... -203-
Fig. 5-14. Quantification of rod frequency……..... -204-
Fig. 5-15. AIP-1 expression prevents cofilin rod induction by amyloid-β exposure…….….... -206-
Fig. 5-16. AIP-1 overexpression blocks 2-DG induced rod formation.... -208-
Fig. 5-17. AIP-1 localises to areas of rapid actin turnover……... -209-
Fig. 5-18. The effects of altering levels of AIP-1 expression…… -211-
Fig. 5-19. Rods display a variation in form……... -212-
Fig. 5-20. Proposed mechanism of action of AIP-1 in rescuing cytoskeletal dysfunction in neurodegeneration…….. -215-

LIST OF TABLES

CHAPTER 2

Table 2-1. Solutions……..... *-78-*
Table 2-2. Constructs……..…… *-80-*
Table 2-3. Sequences for hairpin primers…….……..... -83-
Table 2-4. Custom designed primers…….……...…….….. -91-
Table 2-5. SDS-PAGE gel percentages……...……..……..... -102-
Table 2-6. Gel recipes……...…….……..... -103-
Table 2-7. Primary antibodies……...…….. -105-
Table 2-8. Secondary antibodies…….. -105-

ABBREVIATIONS

For the convenience of the reader, listed below are the abbreviations used in this thesis.

°C	degrees Celsius
2-DG	2-deoxy-D-glucose
ABP	actin binding protein
ADF	actin depolymerising factor
ADP	adenosine diphosphate
AIP-1	actin interacting protein 1
ALS	amyotrophic lateral sclerosis
APP	amyloid precursor protein
APS	ammonium persulphate
ATP	adenosine triphosphate
BCA	bicinchoninic acid
BCS	bovine calf serum
BMP	Bone Morphogenic Protein
C-	carboxy-terminus
Ca^{2+}	calcium ion
CCD	charge-coupled device
Cdk-5	cyclin-dependent kinase-5
cDNA	complementary deoxyribonucleic acid
CMV	cytomeglavirus
CNS	central nervous system
CO_2	carbon dioxide
DAPI	4,6-diamidino-2-phenylindole, dihydrochloride
dATP	deoxyadenosine triphosphate
DCC	Deleted in Colorectal Carcinoma,
dCTP	deoxycytidine triphosphate
dd.H20	double distilled water
dGTP	deoxyguanosine triphosphate
DMEM	Dulbecco's Modified Eagle's Medium
DMSO	dimethyl sulfoxide
DNA	deoxyribonucleic acid
DNase	deoxyribonuclease
dNTP	deoxynucleotide triphosphate
Drebrin-A	drebrin-adult
Drebrin-E	drebrin-embryonic
DRG	dorsal root ganglia
DTT	dithiothreitol

dTTP	deoxythymidine triphosphate
E	embryonic day
E1	embryonic 1
E2	embryonic 2
EB	elution buffer
EB3	end-binding protein-3
EDTA	ethylenediaminetetraacetic Acid
EGF	epidermal growth factor
EtOH	ethanol
F-actin	filamentous-actin
FBS	foetal bovine serum
g	grams
G-actin	globular-actin
GFP	green fluorescent protein
GTP	guanosine-5'-triphosphate
HBSS	Hank's balanced salt solution
HE	HEPES-EDTA
HEK	human embryonic kidney
HEPES	4-(2-hydroxyethyl)-1-piperazineethanesulfonic acid
HH	Hamburger Hamilton
HI	heat-inactivated
HRP	horseradish peroxidase
ICC	immunocytochemistry
Ig	immunoglobulin
IHC	immunohistochemistry
IQR	interquartile range
kb	kilobase
kDa	kilodalton
l	litres
LB	Luria-Bertani
LIMK	LIM-Kinase
M	molar
mA	milliamps
MeOH	methanol
mg	milligrams
Mg^{2+}	magnesium ion
$MgCl_2$	magnesium chloride
min	minutes
ml	millilitres
mM	millimolar
mm	millimeter
mRFP	monomeric RFP
mRNA	messenger ribonucleic acid
MW	molecular weight

N-	amino-terminus
NaCl	sodim chloride
NaOH	sodium hydroxide
ng	nanogram
NMDA	N-methyl-D-aspartate
Npn	neuropilin
PBS	phosphate-buffered saline
PCR	polymerase chain reaction
PDGF	platelet-derived growth factor
PDL	poly-D-lysine
PFA	paraformaldehyde
PG	paraformaldehyde-glutaraldehyde
pH	potential of hydrogen
PI3K	phosphatidylinositol 3-kinase
PIP2	phosphatidylinositol 4,5-bisphosphate
PLC	phospholipase C
pMAP	phosphorylated microtubule-associated protein
PMSF	phenylmethylsulfonyl fluoride
PNS	peripheral nervous system
PSD-95	post-synaptic density-95
PTEN	phosphatase and tensin homologue
PVDF	polyvinylidene difluoride
RFP	red fluorescent protein
RGC	retinal ganglion cell
RNase	ribonuclease
RNAi	ribonucleic interference
Robo	roundabout
rpm	revolutions per minute
RT	room temperature
s	seconds
SD	standard deviation
SDS	sodium dodecyl sulphate
SDS-PAGE	sodium sodecyl sulphate polyacrylamide gel electrophoresis
SEM	standard error of the mean
Sema	semaphorin
SHH	sonic Hedgehog
shRNA	short hairpin ribonucleic acid
siRNA	small interfering ribonucleic acid
SOC	super optimal broth with catabolite repression
SSH	slingshot
TAE	tris[hydroxymethyl]-amino-methane-acetate-EDTA
TBS	tris[hydroxymethyl]-amino-methane-buffered saline

TBS-T	tris[hydroxymethyl]-amino-methane-buffered saline + Tween-20
TEMED	N,N,N',N'-tetramethylethane-1,2-diamine
TESK	testicular protein kinase
TIRF	total internal reflection fluorescence
Tris	tris[hydroxymethyl]-amino-methane
U	units
V	volts
v/v	volume/volume
w/v	weight/volume
WB	Western blotting
WD repeat	tryptophan-aspartic acid repeat
WDR-1	WD repeat-containing protein 1
YFP	yellow fluorescent protein
µg	micrograms
µl	microlitres
µm	micrometers
µM	micromolar

CHAPTER 1
INTRODUCTION

CHAPTER 1
INTRODUCTION

1.1 The neuronal cytoskeleton

The brain is the most intricate organ in the human body and is responsible for the way in which we experience the world. From our thoughts to our behaviours, roughly 86 billion neurons form a staggering number of precise connections that are constantly remodelled to allow us to adapt and respond to our environment through our cognitive abilities, the creation and recollection of memories, and to experience emotions. It is essentially how our brains are wired up that makes us who we are as individuals.

To accommodate this exquisite complexity in connectivity, the leading processes of neurons must be able to sense cues in their environment to make navigational decisions in order to synapse with their intended targets. These extracellular signals are sensed by a dynamic structure at the highly motile tip of the growing axon called the growth cone. Receptors residing at the growth cone's plasma membrane transduce the cues and invoke chemotropic responses to chemical gradients. This requires neurons to be able to make profound alterations to their morphology, a process that is facilitated by dynamic rearrangements to the intracellular network of interlinking elements of the cytoskeleton.

With such a complex system, it is unsurprising that cytoskeletal disruptions causing errors in wiring can lead to severely detrimental impairments to the growth, maintenance and function of the brain. This can ultimately result in wide-ranging impacts on a person's quality of life and wellbeing that ripple out into costly social and economic aspects in society. Several neurodevelopmental

disorders have been strongly linked to genes that code for elements of the cytoskeleton. A commonly referenced example is periventricular heterotopia, a migration defect that causes ectopic nodules to form in the ventricles of the brain and manifests in epileptic seizures and strabismus. A percentage of cases are linked to variants in *FLNA,* the gene for a protein pivotal in the reorganisation of the actin cytoskeleton through interactions with the plasma membrane (Parrini et al., 2006). More recently, mutations in SHANK3 identified in autism affect the morphology of dendritic spines, small membranous protrusions that are necessary for synaptic formation in the brain (Durand et al., 2012). Turning to the other end of life, elements of the cytoskeleton are thought to be susceptible to the effects of ageing and the resulting decline in homeostatic regulation within neurons are likely to contribute to the development and progression of proteinopathies.

Despite our understanding of the guidance choices neurons can make *in vivo* during development and the plastic changes that occur through life, fundamental questions about how elements of the cytoskeleton interact at a molecular level remain unanswered, particularly those concerned with disease progression and maintenance of life-long neuronal health during ageing. Understanding how co-ordination of the actin cytoskeleton functions at the cellular level will provide insights to the general mechanisms that underlie the development of the nervous system and lay foundations for the development of much-needed clinical strategies to improve the consequence of neurodevelopmental disorders, lessen the burden of poor mental health and promote life-long brain health of our ageing population.

In the rest of this chapter I will initially outline the key cellular processes in the development of the nervous system. This will be followed by a description of the neuronal cytoskeleton, specifically the actin entity and key regulatory proteins that bind and modulate the actin cytoskeleton. I will then discuss the evidence that implicates the actin binding proteins drebrin and cofilin in disease, following with what is currently known about actin-interacting protein-1 (AIP-1) and why it has potential for therapeutic exploitation in cofilin-induced cytoskeletal abnormalities. I will finish with the aims of this body of work which will provide a deeper understanding of the neuronal cytoskeleton in health and disease.

1.2 Fundamental principles of nervous system formation

The nervous system is a complex network of highly specialised cells and organs that are responsible for transmitting signals and coordinating the body's internal functions as well as processing information from the external environment and generating responses. The system is broadly divided into two functional zones: the central nervous system (CNS) which comprises the brain and spinal cord; and the peripheral nervous system (PNS) which refers to all neurons and glial cells outside of the brain and spinal cord. This division can be further segregated into the sensory division that carries information from the sensory organs derived from external and internal stimuli, and the motor division which is responsible for carrying voluntary and automatic commands from the brain.

It is one of the first systems to form during embryogenesis and continues to develop throughout life resulting in a highly organised and complex structure. Around two weeks post conception, the blastula undergoes substantial reorganisation during the process of gastrulation to become a multilaminar

structure formed of three germ layers. The nervous tissues arise entirely from the most exterior layer, the ectoderm, a region of which partly thickens and differentiates into the self-renewing neuroepithelium, creating the neural plate juxtaposed by the remaining ectoderm. This structure forms the neural groove and the opposing edges of the developing neural tube fold, inducing neural crest formation where the tips of the neural fold meet the overlying ectoderm. The folds then begin to converge along the midline beginning from the future neck area and the neural crest cells migrate out from the region between the newly formed neural tube and the overlying ectoderm. The neural crest cells continue to differentiate and form components of the PNS.

Diffusible sonic hedgehog (SHH) is one of the primary morphogens to form a dorsoventral gradient in developing neural tube. In amniotes, the notochord, a rod of mesenchymal cells underlying the neural tube, triggers the process by secreting SHH initially (Dessaud et al., 2008). In the dorsal region, the overlying ectoderm secretes Bone Morphogenic Protein (BMP) and subsequently induces production of BMP from the roof plate. In combination, the two gradients establish differential expression of transcription factors that define cell fate along the dorsal-ventral axis, and repressive interactions further refine borders (Wilson and Maden, 2005).

The population of cells that form the brain are almost exclusively derived from precursors residing in the neuroepithelium of the ventricular zone adjacent to the lumen of the rostral neural tube (Stiles and Jernigan, 2010). As fusion of the neural tube continues, neural stem cells rapidly proliferate creating new stem cells or post-mitotic neuroblasts which undergo further differentiation after

migrating to their final positions. This proliferation results in additional layers that form rudimentary structures of the brain called the primary brain vesicles. These then form further subdivisions —the secondary brain vesicles— containing zones of cellular proliferation from where neurons, astrocytes and oligodendrocytes emerge from their progenitors through asymmetric cell division (Stiles and Jernigan, 2010). These immature neurons migrate to their final positions and once *in situ* start to form crude networks by extending axonal processes. The initiation of axonal outgrowth and dendrite formation within the brain as well as the long-distance guidance of neuronal process out into the periphery of the embryo are key milestones for neural development (Stiles and Jernigan, 2010).

1.3 Axon guidance and the growth cone

Axons often extend over tremendous distances to make precise, functional connections with their targets; how they are guided has been of intense interest since before the turn of the 20th century. Seminal neuroanatomist Santiago Ramón y Cajal observed that the cellular organisation of embryonic chick nervous tissue behaved in a stereotypical manner (Cajal, 1890). He observed a “cone-like lump”, which he later termed the growth cone, projecting from the end of extending axons which could excavate its way through the tissues of the developing embryo to innervate the body (Cajal, 1890). He astutely postulated the motility and responsiveness of the growth cone resulted from the interaction with diffusible attractive and repulsive signals which determined the route an axon would take (Caja, 1899). However, until late in the 20th century it was believed guidance depended upon cell-surface and extracellular matrix interactions along defined pathways routing the axon to the final target. Cell adhesion molecules such as integrins and neuronal cell adhesion molecules (NCAMs) interact in

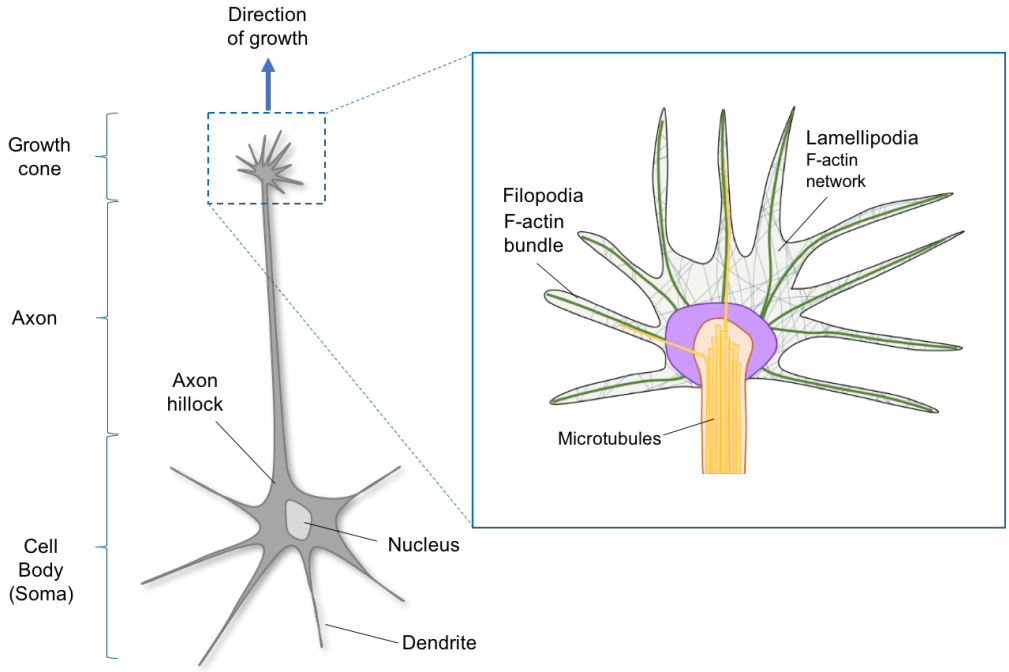

Figure 1-1. Classic growth cone structure displaying cytoskeletal components. *A typical neuron is formed of a cell body (soma), and several processes called neurites. Neurites are further discriminated into multiple dendrites and a single axon. The axon originates from the axon hillock and extends into the periphery, allowing signals to be carried over long distances. The end of the axon usually forms connections called synapses with neurites or soma of other neurons, as well as muscle or gland cells.*

The growth cone is a highly dynamic structure found at the tip of the growing axon. This structure is largely defined by the morphology of the underlying cytoskeleton which is formed of filamentous (F-) actin that make up two key actin structures at the leading edge: Filopodia formed from bundled F-actin and the dense meshwork of F-actin called lamellipodia. These structures reside in the outermost portion of the growth cone, called the peripheral zone (green). Whilst the central domain (yellow) is microtubule rich. The transition zone sits between the two domains. Individual microtubules extend into the transition zone during elongation and can preferentially enter the peripheral zone during turning (Kahn and Baas, 2016).

combination with other adhesion molecules residing on the surface of neighbouring cell membranes and elements of the extracellular matrix (Francavilla et al., 2007; Hinsby et al., 2004). Whilst these interactions influence intercellular adhesion and outgrowth, there is little evidence to support their orchestration of growth cone turning (Lilienbaum et al., 1995). In 1963, Sperry proposed that growth cones carried molecular identification tags which allowed growth towards chemoattractive gradients and away from repellent ones (Sperry, 1963). This hypothesis formed the basis of modern axon guidance models (*Fig. 1-2*), and in combination, technological advances in culturing nervous tissue, biochemistry, and molecular biology led to a productive period of guidance cue discovery in the following decades.

However, the complexity of how these cues interacted with the developing nervous system was slower to clarify. Explanted embryonic trigeminal ganglia and geniculate ganglia co-cultured with age-matched isolated layers of their target tissues in collagen matrices only grew directed processes to particular components demonstrating the level of specificity produced through a combination of fixed cues and gradients generated at relatively long distances (Lumsden and Davies, 1986). Diffusible factors were also shown to emanate from isolated regions of rat spinal cord using conditioned media (Tessier-Lavigne et al., 1988). The molecular basis of axon guidance relies upon the convergence of fixed and diffusible cues that can be permissive and attractive or repulsive and inhibitory (Tessier-Lavigne et al., 1988; Tessier-Lavigne and Goodman, 1996). The simultaneous effects of these guidance forces result in highly robust patterning of the nervous system. Many ligands do not seem to act as exclusively

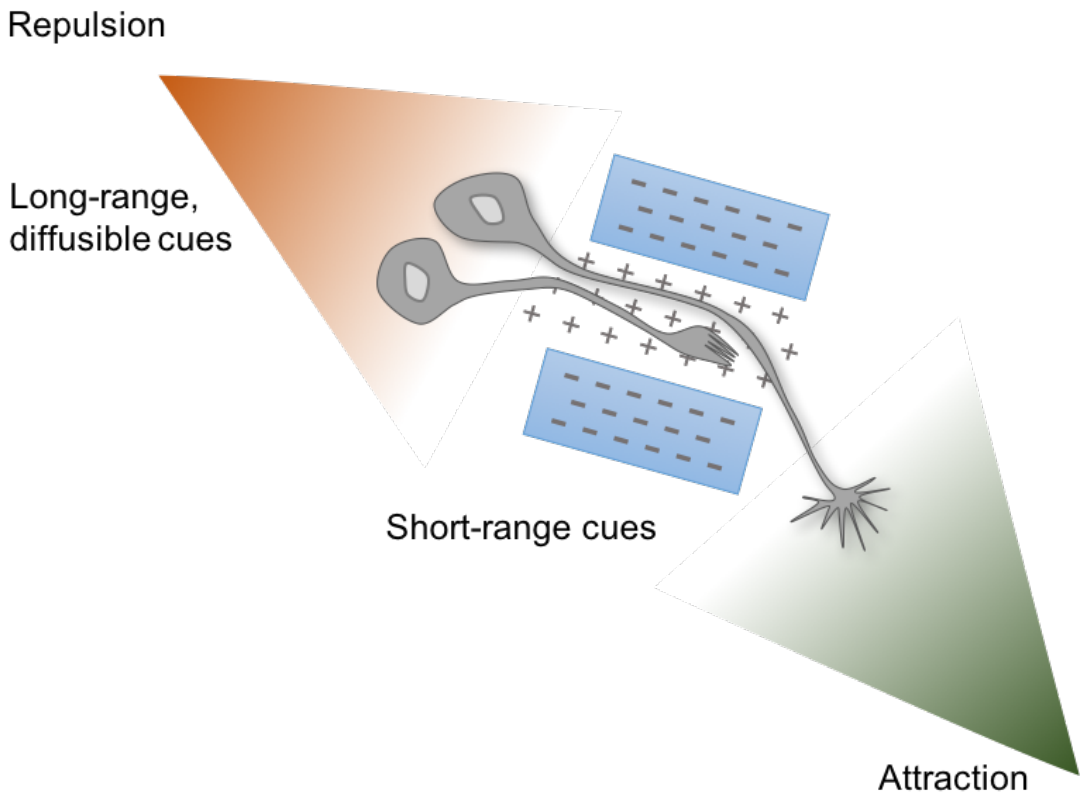

Figure 1-2. Molecular mechanisms underlying axon guidance. *Long-range diffusible cues (orange, repulsive; green, attractive) and short-range contact cues (-, repulsive; +, attractive) combine to guide axon trajectories. Many successive axons follow the paths of pre-existing axon tracts formed by pioneer axons in a process called selective fasciculation. Adapted from (Tessier-Lavigne and Goodman, 1996).*

attractive or repulsive but instead can display dual functionality in guidance and navigation (Baier and Bonhoeffer, 1994).

Cell adhesion molecules (CAMs) not only mediate attachment between cell surfaces but can also generate instructional intracellular signalling cascades that result in changes to directionality and motility. In neurons, NCAMs (neuronal cell adhesion molecules) can mediate side-to-side adhesion of axons to other preexisting axons in a process called selective fasciculation (Grenningloh et al., 1991; Harrelson and Goodman, 1988). Neural cell adhesion molecule L1CAM can recruit signalling-capable co-receptors such as integrins to induce axon growth through Rac, PI3 kinase and ERK (Lemmon et al., 1989; Kamiguchi and Lemmon, 1997; Maness and Schachner, 2007).

Elements of the extracellular matrix, such as fibronectin, laminin and collagen, bind integrin receptors which activate the recruitment of scaffolding proteins including paxillin, talin and vinculin on the cytoplasmic side of the adhesion complex (Letourneau et al., 1994). Many of these molecules directly bind actin filaments which can then influence turn over the actin cytoskeleton in addition to the crosstalk of activated signalling cascades (Myers et al., 2011).

There are several key conserved families of axon guidance molecules, notable examples of these are the netrins, Slits, ephrins and semaphorins. Whilst not the only known guidance molecules, these are the most well studied and understood. Netrins were initially described in the search for the chemoattractants responsible for directing vertebrate commissural neurons in the spinal cord (Kennedy et al., 1994; Serafini et al., 1994). Netrin responses are facilitated by Deleted in

Colorectal Carcinoma (DCC) and UNC-5 transmembrane proteins, often with the former associated with attraction and the latter repulsion. However, DCC is also thought to participate in UNC-5 mediated repulsion where netrin concentrations are lower (Keleman and Dickson, 2001). The Slits were identified after their counterpart receptor, Roundabout (Robo), was discovered in a genetic screen of *Drosophila* midline guidance defects (Kidd et al., 1999). Slit is normally secreted by glia residing in the midline and acts as a repulsive cue preventing axons from crossing. *Drosophila* embryos lacking *Slit* display ectopic trajectories of longitudinal and commissural axons in the mutant nerve cord (Battye et al., 1999). Conversely, Slit has been shown to act as a positive regulator of axonal branching in sensory axons and in the formation of growth cone protrusions (McConnell et al., 2016; Wang et al., 1999).

The ephrins are a key family of guidance molecules that mediate development of the nervous system in conjunction with their counterpart tyrosine receptor kinases, the Ephs (Kania and Klein, 2016). Ephrin-Eph interactions facilitate bidirectional signalling that affects both receptor and ligand expressing cells, constraining cell movements during tissue patterning (Drescher et al., 1997; Lisabeth et al., 2013). This is particularly apparent in the development of the corticospinal tract – the wiring between the brain and the limbs. Many of these connections cross the midline to carry information from the brain to motor neurons that control movements on the opposite sides of the body whilst some remain ipsilateral. Without this wiring strategy, accurate processing of information in three dimensions which allows for asymmetrical movement becomes problematic (Shinbrot and Young, 2008). Individuals with achiasmatic syndrome, a rare genetic condition, display disrupted oculomotor function and stereopsis (Larsson,

2013). In mice, knockout of *EphA4* results in hopping locomotion where the back feet always move in the same direction at the same time. Anterograde axonal tracing demonstrated that axons did not respect their normal midline boundary and many aberrantly terminated to innervate both sides of the spinal column (Dottori et al., 1998). Similar defects in locomotion and wiring were observed in a mouse knockout of ephrin-B3, a ligand of EphA4, which suggests that the signalling between the two acts as a midline barrier. Analysis of expression patterns showed ephrinB3 was concentrated at the midline whilst EphA4 was localised to the surface of migrating axons (Kullander et al., 2001). For the corticospinal tract, the importance of Eph-ephrin signalling only becomes significant once growth cones have crossed the midline where the signal appears to prevent any further crossing (Yokoyama et al., 2001).

The development of visual pathways also requires Eph-ephrin signalling and, crucially, highlights the diversity of these molecules. Retinal ganglion cell (RGC) axons from the retina carry spatial visual information captured by the eye and must be precisely spatially wired within the brain for processing (Sernagor et al., 2001). RGC must make several navigation decisions along their route, the first of which occurs as the optic nerve forms by RGC axons that exit through the optic disc at the rear of the eye. Axons continue to migrate towards the midline of the brain where some will choose to cross at the optic chiasm and others will remain ipsilateral along the optic tract (Petros et al., 2008). This highly reproducible process results in spatial fidelity between specific fields within the retina and zones of the superior colliculus which integrates visual information and controls eye movement (Kolodkin and Hiesinger, 2017). Complementary gradients of both EphB receptors and ephrinB expression, as shown by *in situ* mRNA hybridisation

and immunolabelling, suggested the two molecules work to prevent erroneous migration of RGC axons at specific time points during development (Birgbauer et al., 2001; Henkemeyer et al., 1996). RGC tracing in *EphB2 and EphB3* null mice demonstrated that dorsal axons overshot the optic disk more severely than the ventral counterparts, indicating the proteins may affect discrete populations of neurons differently (Birgbauer et al., 2001).

The semaphorins are another family of highly conserved proteins with multiple roles in regulating the development of the nervous system (Pasterkamp, 2012). An important function of the semaphorins is to provide a molecular barrier that repels growing axons and prevents their entering of inappropriate areas. Collapsin1 (now called sema 3A) was the first semaphorin found in vertebrates, so named owing to its ability to induce growth cone collapse *in vitro* (Luo et al., 1993; Luo et al., 1995). The subsequent discovery of more members with a characteristic stretch of 500 amino acids at their N-terminal end necessitated systematic categorising based on their sequence homology (Goodman et al., 1999). Class 1 and 2 are found in invertebrates, whilst 3-7 are vertebrate and class 8 belongs to viruses. They can be secreted (classes 2, 3 and 8), transmembrane (1, 4, 5 and 6), or membrane anchored (class 7). Most semaphorins act through the plexin family of transmembrane receptors which are largely associated with regulation of Rho-family GTPases (*Fig 1-3*). Class 3 semaphorins also require the presence of neuropilins which have short cytoplasmic tails and are thought to contribute to ligand binding specificity rather than signaling (Dickson, 2002; Takahashi et al., 1999). However, *Neuropilin1* deficient mutant mice display severely aberrant axonal outgrowth in spinal and cranial sensory neurons, and cultured neurons from these animals are no longer

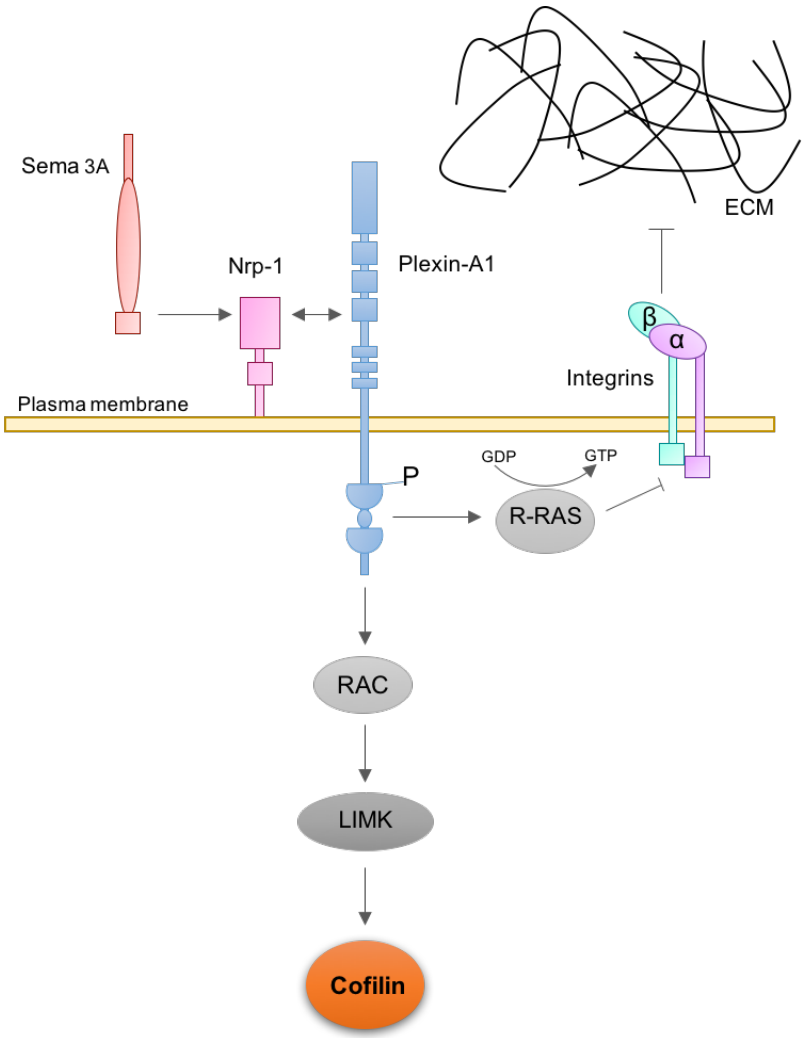

Figure 1-3. Model of Sema 3A signalling through Plexin-A. *Sema 3A binds to neuropilin-1 (Nrp-1) and associates with plexin-A1 which becomes phosphorylated on tyrosine residues on the cytoplasmic domains. The resultant activation of intracellular signalling cascades leads to the eventual triggering of cofilin activity and the cytoskeletal collapse associated with a repulsive response. Several protein kinases including Fes, Cdk-5 and GSK3β (not shown) are also activated by sema 3A which can result in Collapse Response Mediator Protein (CRMP) -2 activation and microtubule reorganisation associated with sema 3A-induced collapse. Plexin signalling also mediates attachment of integrins to the extracellular matrix (ECM). An increase in the GTP bound (inactive) form of R-Ras increases via Sema3A-induced plexin activation, leading to decreased attachment of integrins to the ECM. Adapted from (Kruger et al., 2005; Negishi et al., 2005).*

sensitive to sema 3A induced collapse (Kitsukawa et al., 1997). This phenotype is mirrored in the *sema 3A* knockout and provided strong evidence that the ligand receptor pairing is required for sema 3A to exert its repellent effects (Kolodkin et al., 1997; Taniguchi et al., 1997). Similar phenotypes were characterised in the *Neuropilin2* knockout mouse, however neuropilin-2 is necessary for sema 3F facilitated repulsion rather than sema 3A again highlighting regulation through subunit combinations of the heteroreceptor complexes (Giger et al., 2000).

Sema 3A is one of the most experimentally well utilised of the class 3 semaphorins, and its ability to induce collapse can be observed over time or used spatially to prompt turning of growth cones away from a source *in vitro* (Fan and Raper, 1995; Raper and Kapfhammer, 1990). *Xenopus* RGC growth cones display age-dependent responsiveness to sema 3A which is reliant on the emergence of neuropilin-1 expression at specific time points during development. Growth cones from older retinal explants (around stage 35) rapidly collapsed in response to acute sema 3A treatment whereas those at around stage 24 did not. These younger growth cones displayed sema 3A sensitivity when neuropilin-1 was expressed. Sema 3A-induced collapse response was transient, with 30% of growth cones extending new branches after an hour of recovery (Campbell et al., 2001). It is also likely that the concentration of sema 3A and cellular context play a role in the mode of responsiveness. High concentration, greater than 500ng/ml, induced maximal collapse levels in E7.5 chick dorsal root ganglia (DRG) explants, whilst responses to concentrations lower than 100ng/ml were dependent on local protein-synthesis status (Manns et al., 2012). Different types of neurons may also show different responses to guidance cues. Pyramidal neurons are highly abundant in the CNS, but primarily in brain structures

associated with sophisticated cognitive functions. They are characterised by a highly branched apical dendrite that extends towards the pial surface. This structure integrates inputs from the superficial cortical layers and is thought to play a key role in information processing. The pyramidal neurons of *sema 3A* null mice display abnormal morphologies, suggesting that sema 3A plays a role in regulating their shape (Behar et al., 1996; Polleux, 1998). Further examination *in vivo* showed only dendrites of these cells were not orientated to the pial surface correctly. To test the extent of this regulation, green fluorescent protein (GFP)-expressing cortical neurons were differentiated into pyramidal neurons in culture. The newly differentiated cells were plated on to cortical slices with human embryonic kidney (HEK) 293T cells expressing recombinant sema 3A at the base. The localised source of sema 3A was able redirect dendrite growth demonstrating that sema 3A could act attractively in these cells (Polleux et al., 2000).

1.4 Actin cytoskeleton

Whilst the full mechanism of action of these axon guidance molecules is still not understood, the common underlying consequence of their interaction with neurons is that they initiate modification of the cytoskeleton at the growing tips of axons. The cytoskeleton is a dynamic network of interacting filamentous proteins present in all cells in one form or another. The framework provides three-dimensional structural support, allows for internal organisation and transport of vesicles and organelles as well as providing a system for force generation and resistance to mechanical influences (Fletcher and Mullins, 2010).

Within eukaryotes there are three major cytoskeletal components: microfilaments, intermediate filaments and microtubules, which are each able to rapidly polymerise from subunits and disassemble to provide prompt responsiveness to different stimuli (Fletcher and Mullins, 2010). The actin compartment acts as a major signal transducer forming two main structures required for motility and sensing the environment: filopodia and lamellipodia. Filopodia, thin membrane protrusions, are around 60-200nm in diameter and contain parallel bundles of 10-30 actin filaments with their barbed end directed towards the protruding edge (Medalia et al., 2007). In contrast, lamellipodia are flattened, sheet-like extensions formed from a cross-linked orthogonal network of filamentous (F-) actin. A second population of bundled filaments, 40-100nm wide, is also found in the lamella (Lewis and Bridgman, 1992). The difference in actin architecture is likely to confer different levels of stabilisation of the underlying structures. Shorter filaments in the lamellipodia act as scaffolding maintaining volume at the leading edge which is constantly being remodeled as the structure pushes forward (Lewis and Bridgman, 1992). Those that are longer may be involved in extended substrate interactions. *In vitro*, longer filaments are more stable than shorter filaments and the combination of the two in the lamellipodia may allow for rapid remodeling whilst maintaining adhesive contacts (Cooper, 1991; Small et al., 2008).

1.5 Neuronal growth cone actin

Within the growth cone, the primary cytoskeletal components are the neurofilaments which facilitate axonal transport and regulate axonal diameter; and actin and tubulin which interact to induce axon extension and turning (Yuan et al., 2012). The actin compartment of the neuronal growth cone is of great

interest because it acts as a major signal transducer and forms structures associated with sensing of the local environment and motility. The F-actin network forms the lamellipodium and F-actin bundles form the filopodia whilst microtubules are largely restricted to the central zone of the growth cone (Dent et al., 2011). Signalling cascades converge in reorganisation of the cytoskeleton and change the adhesive qualities of the growth cone (*Fig. 1.4*). Actin polymerisation occurs at the tip, driving the leading edge forward. Forces generated by myosin II push backward where actin filaments are disassembled. Interactions between growth cone receptors and adhesive contacts can act as a molecular clutch slowing retrograde flow. F-actin provides a substrate for invasion of microtubules and transport of organelles resulting in directed axonal elongation toward the source of the guidance cue. With the fundamental dependence of the actin cytoskeleton and associated mediators for basic cell processes, it is of little surprise that many have been implicated in a wide range of disease including neurodevelopmental and neurodegenerative disorders.

The internal environment of a developing embryo is constantly undergoing rapid change as cells proliferate and migrate to form tissues and organs. In turn the cells of the nervous system must be equally dynamic in order to respond to this rapidly remodelling environment and still allow for the precision of neuronal connectivity. Neuronal growth cones navigate this milieu through a series of decision points (Stoeckli and Landmesser, 1998). Early experiments examining the interaction between cell adhesions and nerve fibre elongation yielded the hypothesis that axonal structures were stabilised or promoted by adhesive contacts. Simple comparisons of the number and length of microspikes in growth

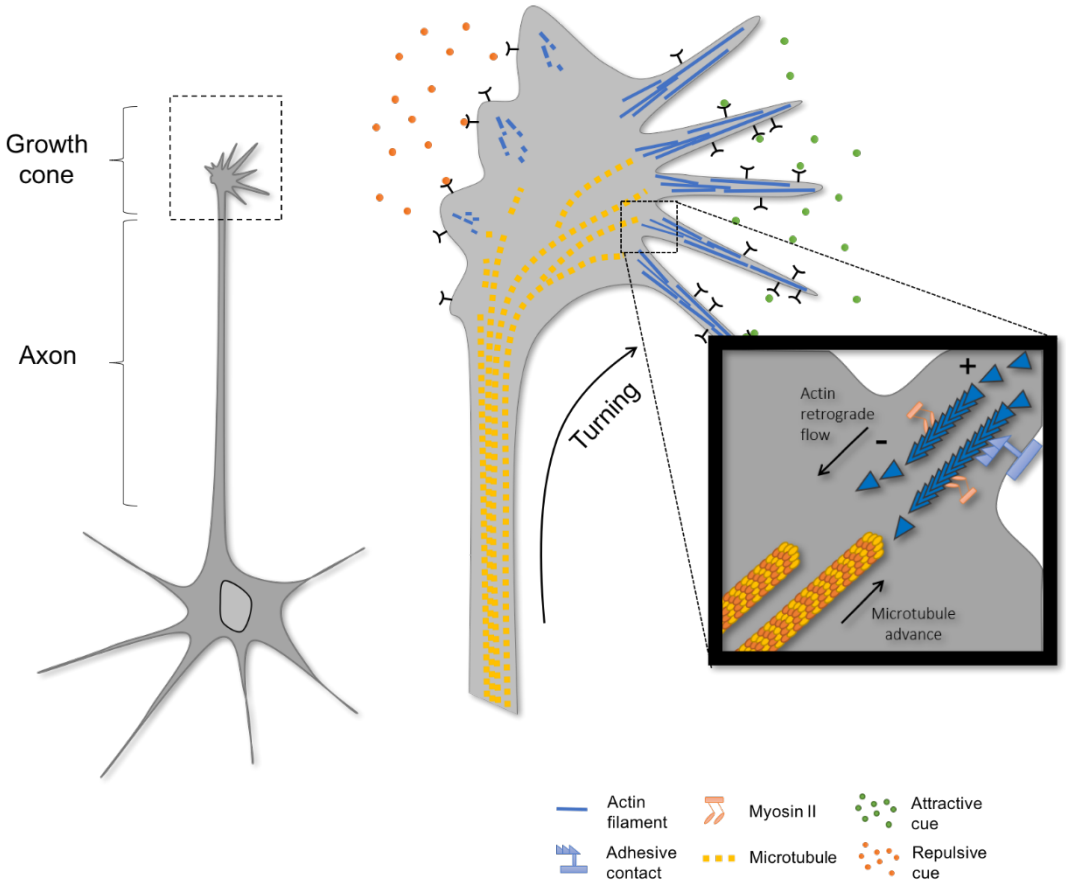

Figure 1-4. The growth cone interprets cues in the extracellular environment which generate directional movements*. Activation of signalling cascades converge to direct changes to the cytoskeleton directly or indirectly via cytoskeletal-associated proteins.*

Inset: *Actin polymerisation pushes the leading edge forward. Forces generated by myosin 2 push backward where actin filaments are disassembled. Interactions between growth cone receptors and adhesive contacts can act as a molecular clutch slowing retrograde flow. This allows advance of microtubules and organelles resulting in axonal elongation. Intracellular signals generated by attractive and repulsive cues interact with these mechanisms regulating navigation*.

cones grown *in vitro* on different substrata showed growth cones would display altered connectivity. Filopodia were longer and more numerous when grown on poly-D-lysine (PDL) coated glass than untreated counterparts (Letourneau, 1975). Further study using interference reflection microscopy highlighted this effect was provoked by increased area of substratum adhesion particularly at the rear of the growth cone. The lamella at the leading edge of the growth cone did not contact the surface, whilst microspikes were in close contact and, interestingly, this interaction continued back along the structure toward the central region. Whole-mount electron microscopy revealed these adhesive sites tracked along actin filaments (Letourneau, 1975). As previously described, a number of guidance cues within the extracellular environment are now known to govern navigation however, a growth cone is able to modulate its response at two key levels: the combination and spatial-temporal organisation of receptors expressed at the plasma membrane of growth cone filopodia; and in downstream signalling components that regulate the cytoskeleton including the actin binding proteins.

1.6 Filopodia in synaptogenesis

In addition to their sensing role in the wiring of the peripheral nervous system in development, filopodia are thought to be the first phase in the generation of synapses both during development and potentially in the remodelling of mature neural circuits. Early observations of synapse formation revealed that developing neurons transiently form many filopodium-like dendritic protrusions (Saito et al., 1992). Time-lapse confocal microscopy of cultured early post-natal rat hippocampal tissue slices showed that fine filopodial protrusions on dendrite shafts rapidly extended and retracted. Some filopodia changed into growth cones

or dendrite branches. As branches matured, dendrites extended fewer, less dynamic filopodia that were replaced by a population of stable, spine-like structures that were able to interact with nearby axons where they became stabilized (Dailey and Smith, 1996; Konur and Yuste, 2004; Ziv and Smith, 1996). These protospines can receive synaptic input, and are thought to develop into mature dendritic spines, forming connections with nearby axonal terminals through further elongation of the spine neck. The spine head is the site of numerous biochemical reactions that are largely isolated from the rest of the dendrite (Araya et al., 2014; Fiala et al., 1998).

The morphological plasticity of these structures is dependent on the actin cytoskeleton. Spine heads contain actin filaments that can interact with the plasma membrane and provide scaffolding for proteins within the postsynaptic density (Fifkova and Delay, 1982). A dynamic pool of actin resides within the spine head and can be quickly remodelled to generate force required for spine expansion associated with activity dependent synaptic strengthening known as long-term potentiation (Honkura et al., 2008). With such a fundamental reliance upon the cytoskeleton, it is unsurprising that disruption to its function is associated with altered dendritic spine morphology that accompanies neurological disorder and disease.

1.7 Actin binding proteins

Under physiological ion conditions, pure actin spontaneously self-aggregates. However, until the initiating oligomer reaches the critical number of three subunits, the resulting microfilament is inherently unstable and disassembly is more favourable. Due to the low probability of a trimer forming, actin

polymerisation is described as multiphasic with an initial lag phase as the reaction speed increases (Pollard and Borisy, 2003). Once this phase is passed, polymerisation becomes the favourable state and extension is rapid, only limited by the pool of free, globular (G-) actin subunits. As the pool decreases, so does the rate of polymerisation until the number of monomers disassociating from the filament equals the number joining, reaching equilibrium (Pollard and Borisy, 2003; Blanchoin et al., 2014).

This phenomenon of treadmilling occurs in the presence of adenosine triphosphate (ATP). Monomers are free to join and leave the filament from both ends but ATP-bound G-actin binds more readily at one end (plus end) which can grow five to ten times faster than the other (minus end). As ATP is slowly hydrolysed to adenosine diphosphate (ADP) towards the minus end, the interaction with the other actin monomers becomes less stable resulting in dissociation from the rest of the filament. This process also acts as a timer for the half-life of the filament where ATP hydrolysis occurs in around 2 seconds and complete phosphate dissociation at 150 times slower (*Fig. 1-2*) (Pollard and Borisy, 2003). Under these purified conditions polymerisation of filaments equates to around 0.4 μm/min which falls short of the 10 μm/min keratocytes can be observed moving at (Fuhs et al., 2014). Actin behaviour is strikingly more complex within cells where around 50% of actin is maintained as a monomeric pool and the turnover of filaments is 100 times faster than in biochemically pure assays (Dominguez and Holmes, 2011). This behaviour of actin is orchestrated by dozens of regulatory proteins that permit cells to perform crucial processes such as manipulation and maintenance of cell shape and cell junctions, cell

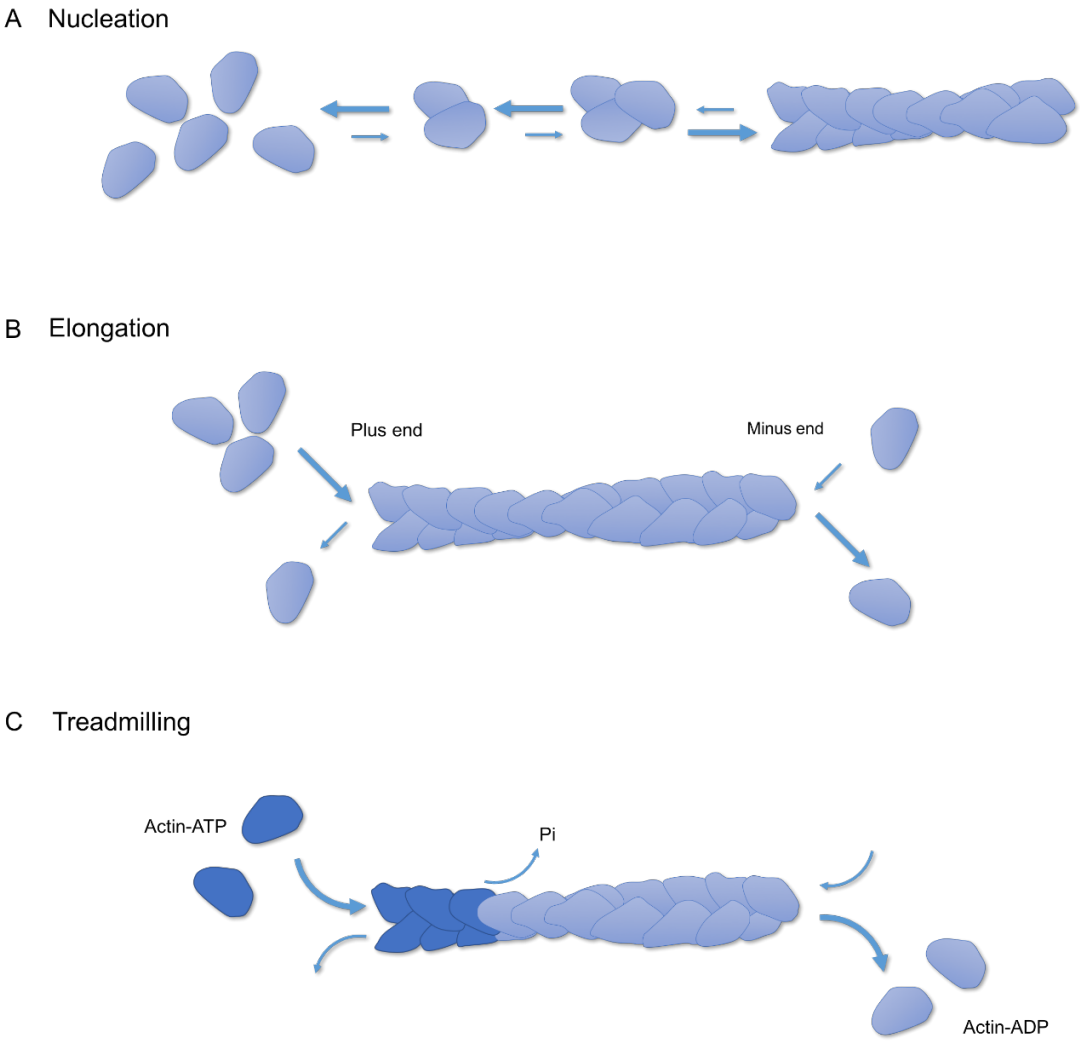

Figure 1-5. Actin self-assembly and the dynamic structure of filaments. ***(A)*** *Nucleation is rate limiting step in polymer formation. Short polymers can spontaneously assemble, but are highly unstable and can disassociate easily. Over time, the aggregation of several subunits can form a stable nucleus which is more favourable for elongation.*
(B) *Elongation phase follows where monomers are rapidly added to the filament. Filaments show structural polarity, with "plus" ends more readily gaining actin monomers and "minus" ends more likely to lose monomers.*
(C) *Treadmilling occurs when a steady state is reached. On and off rates are equivalent and there is no net change in filament length, however monomers appear to move through the filament until they reach the minus end where they dissociate. Actin can associate with ATP which increases the probability of binding at the plus end. Hydrolysis of ATP and phosphate dissociation increases the half-life of the filament compared to when ATP is absent or a non-hydrolysable ATP analogue.*

division and cytokinesis, cell motility and migration, internal transport and endocytosis. A large number of actin binding proteins (ABPs) have been identified (Pollard and Cooper, 1986) with Dos Remedios et al., having reported 162 discrete proteins, excluding synonyms and isoforms (dos Remedios et al., 2003). Many of these bind the same site of actin's surface and are therefore likely to compete. Whilst grouping many of the nearly 200 reported interactors is somewhat arbitrary, ABPs that facilitate the assembly and disassembly of actin can be classified into several functional groups: monomer binding proteins which sequester subunits and maintain a pool of free actin; nucleating proteins that promote polymerisation; capping proteins that halt the addition or loss of subunits from filaments; those that sever and depolymerize drive disassembly; actin-cross linking proteins form complexes to create orthogonal networks; and bundling proteins organise filaments into parallel arrangements (*Fig. 1-6*).

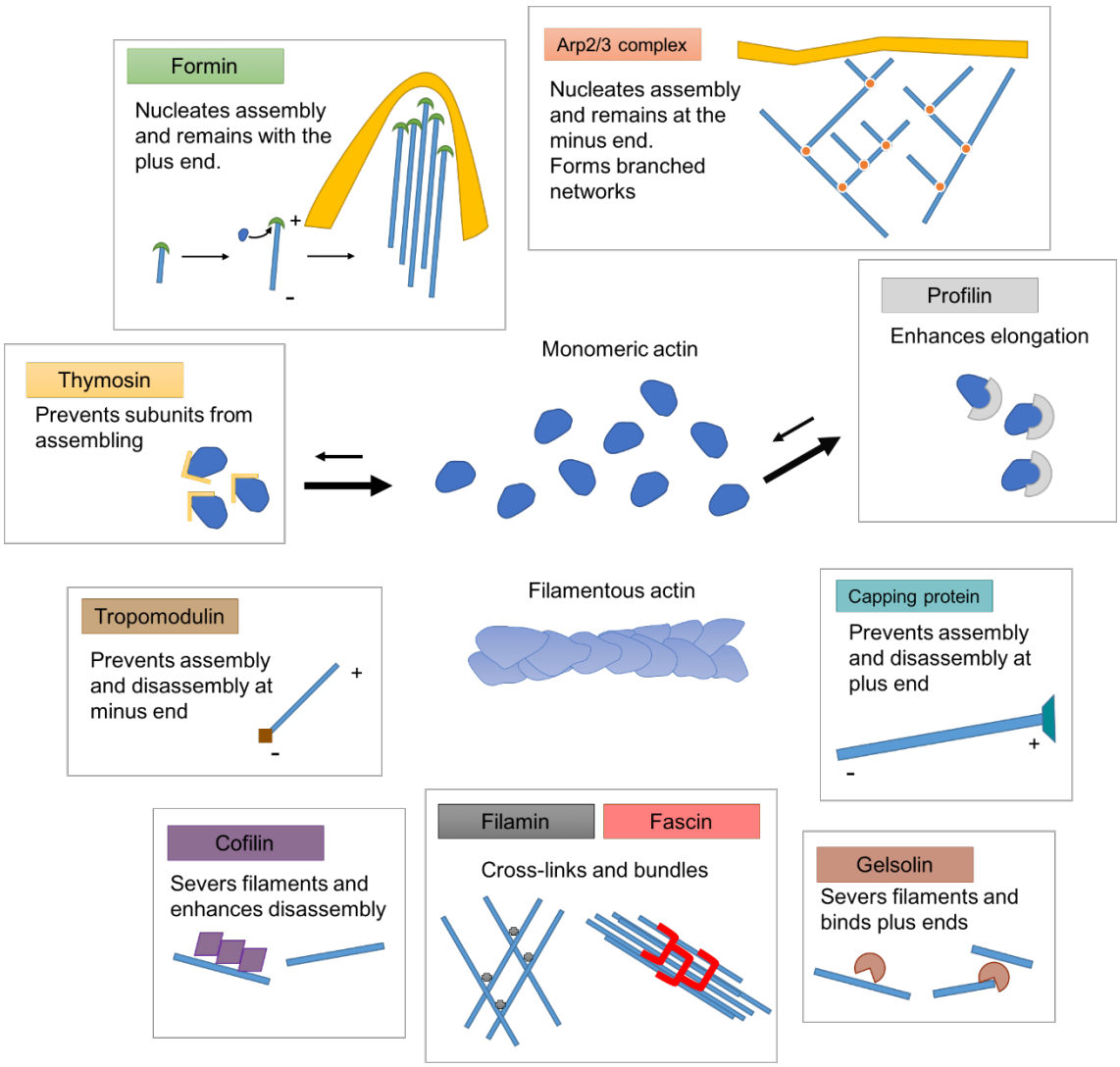

Figure 1-6. Actin architecture and function is governed by actin binding proteins. *An example of each major group is shown, except for the myosins.*

Several of these proteins play indirect regulatory roles, whilst some are completely essential. It is therefore expected that many may be linked to the development of human disease. The protein filamin A promotes orthogonal branching of actin filaments which are required for the formation of filopodia and lamellipodia at the leading edge of motile cells (Fox and Walsh, 1999). It also anchors F-actin to transmembrane proteins, providing scaffolding for signalling processes. Many *FLNA* gene mutations have been linked a group of related conditions, including frontmetaphyseal dysplasia and Melnick-Needles syndrome, caused by disruption to skeletal development (Robertson, 2007; Robertson et al., 2003). More than 120 mutations in this gene have been identified in individuals with periventricular heterotopia – a rare condition in which neurons fail to migrate normally from the lateral ventricular proliferative zone during early foetal brain development causing nodules to form within the walls of the ventricles. The presence of the disease is usually indicated by the onset of seizures during the teenage years. Many individuals display normal cognitive ability; however, some have mild intellectual deficits. The severity of the phenotype is dependent on the loci of the mutation (Parrini et al., 2006).

Profilin 1 is another example of an ABP that is genetically linked to disease. Several mutations in *PFN1* associated with amyotrophic lateral sclerosis (ALS) cause impaired actin binding, whereas many have no effect on actin binding. Profilin 1 was originally described as an actin-monomer sequestering protein that inhibited formation of filamentous actin (Carlsson et al., 1977; Wu et al., 2012). By binding G-actin, profilin changes the G-actin:F-actin ratio, increasing the critical concentration for filament growth. This could either drive the disassembly of filaments or halt further polymerisation. Since its discovery there have been

contradictory reports that profilin can in fact promote F-actin assembly in cells, indicating profilin's complex nature (Schlüter et al., 1997). Yarmola and Bubb attempted to mathematically assess the theoretical reasons why this may be the case. The authors suggested that the profilin-actin complex changes polymerization and depolymerisation rates by modulating the critical concentration of actin monomers. (Yarmola and Bubb, 2006). However, the exact mechanism of function remains elusive. It should be noted that whilst the actin binding impairment in some mutated forms of profilin go some way to explain the mechanism of ALS the other mutations are likely to disrupt signalling pathways that ultimately lead to the demise of the motor neuron (Freischmidt et al., 2015). Again, this example helps to highlight the complexity and pleiotropic nature of actin binding proteins.

The three actin binding proteins this thesis focuses on are now described in detail.

1.8 Cofilin

The discovery of actin depolymerising factors answered the puzzling question of how actin remained monomeric under filament-assembly favouring conditions. Within the brain nearly 50% of actin is found in a non-filamentous form, and prior to the discovery of the ADF/cofilin family, the only proteins known at the time to affect actin turnover (profilin and myosin II) were not found at high enough concentrations to account for the size of the monomer pool. Cofilin was first isolated from chick embryo brain and was originally shown to promote the disassembly of F-actin in a series of biochemical assays (Bamburg et al., 1980). Initially termed actin depolymerising factor (ADF), modern single-molecule studies of actin networks have demonstrated cofilin severs actin filaments in

contrast to myosin II which increases the removal rate of actin subunits at the end of filaments (Smith et al., 2014). The Weeds group also reported a second isoform within blood plasma with similar physical characteristics but possessing a significantly increased rate of depolymerisation (Harris et al., 1980). These studies were the first hints of overlapping roles and discrete spatial and cell specific functionality for the otherwise unclassified protein family. Similar proteins were concurrently discovered in multiple model organisms and named independently, generating some confusion around nomenclature. Phylogenetic studies now show all eukaryotes are likely to express at least one protein containing an ADF domain, all of which are generally considered to reside within the ADF/cofilin family (Maciver and Hussey, 2002). Conformation of the orthologous proteins remains consistent despite wide variation in sequence – most disparities are located outside of the actin binding pocket indicating evolution of ADF/cofilin centered on high conservation of actin across different phyla (Hightower and Meagher, 1986).

Humans express one ADF and two cofilin genes; destrin (also known as ADF), cofilin-1 (non-muscle) and cofilin-2 (muscle) which share around 82% sequence homology (*Fig. 1-7*). All three members are found at varying levels in the same organs by northern blot analysis and are thought to have evolved biochemically distinct actin-binding affinities to meet cell-specific requirements for actin dynamics (Vartiainen et al., 2002). *In situ* mRNA hybridisation indicates cell-type specific restriction; destrin is largely confined to the epithelia and endothelia

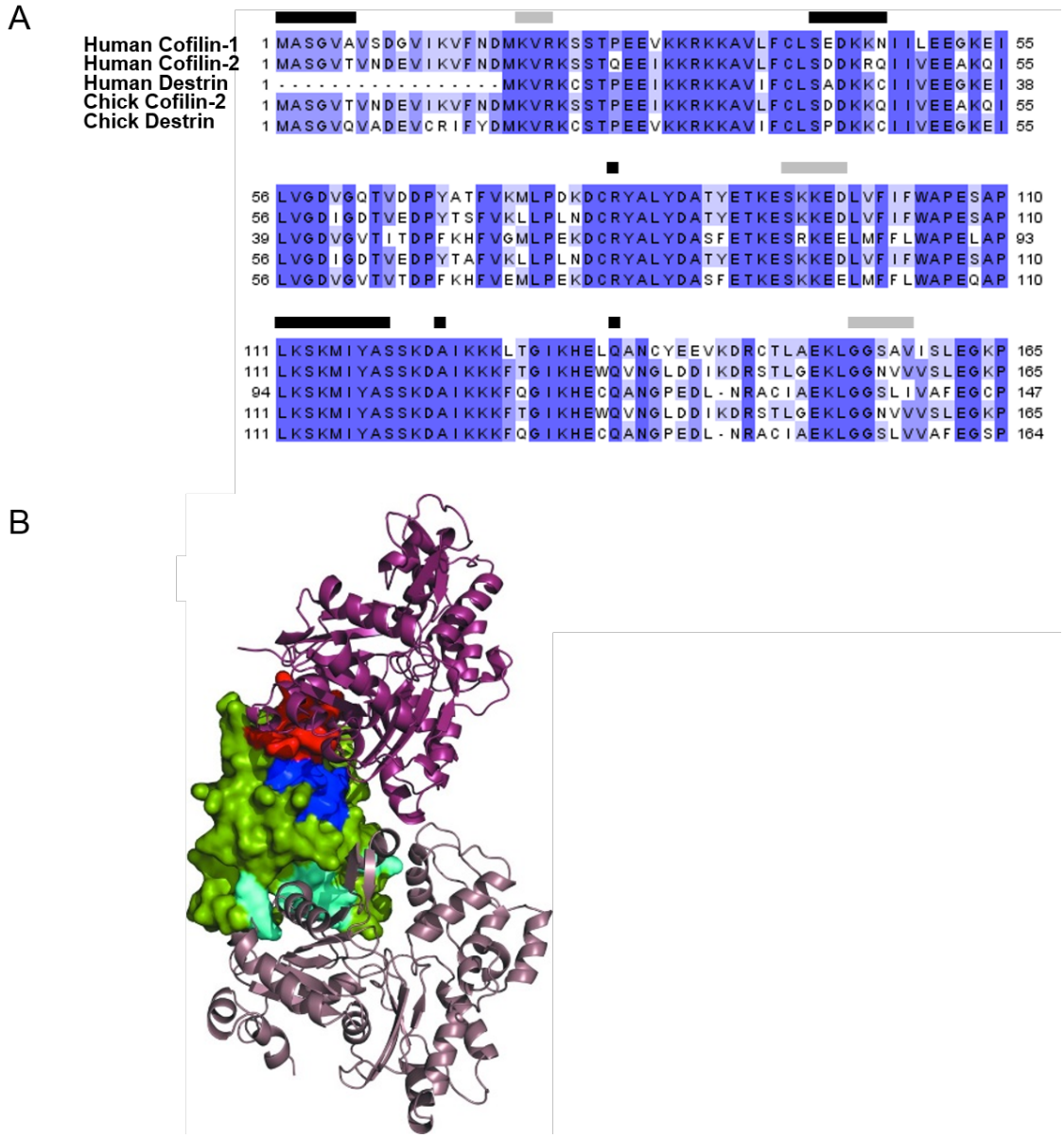

Figure 1-7. Sequences of Human cofilin/AFD family: human cofilin 1 (P23528) and 2 (Q9Y281), Destrin (P60981-2), and Chick cofilin 2 (P21566 and Chick Destrin (P18359). *Human cofilin 1 and 2 share 80% of their sequence identity whilst chick cofilin-2 is most akin to human cofilin-1 with 73% conserved sequence identity.* ***(A)*** *Black bars above indicate residues involved in Cofilin-1 G-actin binding, Grey bars, F-actin binding (Yehl et al., 2017). Purple gradient denotes percentage of residues that are conserved within that column between sequences: darkest mauve = >80%, White = <40%.* ***(B)*** *Human cofilin (surface render) interacting with G-actin (purple) and F-actin (beige). Red shows where G and F actin are able to bind, with blue and cyan thought to be exclusive to G and F actin respectively (Chao, 2003; Klejnot et al., 2013; Lemmon and Schlessinger, 2010).*

and cofilin-1 is ubiquitously expressed and highly enriched in the brain, found at up to 10 times the level of destrin depending on the developmental stage (Bellenchi et al., 2007). Cofilin-2 has two splice variants in humans: CFL2a transcripts found at relatively low levels in most tissues including brain with CFL2b predominantly restricted to heart, skeletal muscle and testes (Thirion et al., 2001).

Despite the overlap in expression, genetic manipulation in mouse models has provided further evidence for differential functionality. The destrin knockout mouse displays the least severe phenotype out of the three, seemingly restricted to the accumulation of F-actin in corneal epithelial cells. Here the authors speculated cofilin-1 could compensate for the loss in other tissues. The cofilin-2 deficient mice were significantly smaller than their wild-type littermates and died by postnatal day 8. Analysis of skeletal muscle showed F-actin inclusions caused severe disruption to the sarcomere indicating cofilin-2 is fundamental to muscle maintenance but not myogenesis. Again, the authors speculated that cofilin-1 could compensate for cofilin-2 loss during development allowing skeletal muscle to form (Agrawal et al., 2012; Obinata et al., 1997). Only loss of cofilin-1 is embryonic lethal in mice, however, until E9.5 embryos were indistinguishable from their wild-type counterparts suggesting cofilin-1 is not obligatory for mass cellular reorganisation during gastrulation. ADF was strongly upregulated in these embryos and may compensate for early cell migration but is not adequate for the neuronal development that occurs after E9.5 (Gurniak et al., 2005).

To further explore the roles of the cofilins in brain development postnatally, Zimmermann et al (2015) developed a conditional double knockout mouse by

intercrossing mutants with a single ADF allele and single floxed cofilin-1 allele. One of the breeding pair additionally expressed cre-recombinase under control of the CaMKIIa promoter. The phenotype of these mice was akin to attention deficit disorder in humans which included behaviours such as hyperlocomotion impulsivity and impaired memory. In comparison, the single mutants appeared normal. Further assessment of synaptic structure by electron microscopy showed altered synaptic morphology in the neurons of the striatum, an area of the brain that plays a key role in controlling locomotion. Excitatory synapses in this area were less dense whilst the presynaptic bouton area, dendritic spine area and post synaptic density were significantly increased. The number of synapses remained the same in the single mutants (Zimmermann et al., 2015). A similar effect was observed in the hippocampus (Wolf et al., 2015). Synaptic vesical exocytosis was increased in hippocampal synapse which mirrored upregulated glutamate release in the striatum (Wolf et al., 2015; Zimmermann et al., 2015). Together, this suggests that ADF and cofilin together are crucial for maintaining synaptic ultrastructure as well as a novel function in neurotransmitter release through cytoskeletal regulation (Wolf et al., 2015)

Cofilin's emerging central role in actin dynamics led to a flurry of reports on its biochemistry after its initial discovery. Using bacterially expressed human cofilin and purified rabbit actin, cofilin was shown to bind F-actin between subunits which results in a change to the helical twist of the filament causing fragmentation (McGough et al., 1997). Reconstructions of cofilin-decorated filaments observed by cryoelectron microscopy reveal a 25% reduction in crossover compared to undecorated counterparts. This is believed to be due to the cooperative nature of

cofilin binding where the affinity for binding increases in the remaining available sites.

However, the intracellular environment is far more complex than within biochemically pure assays and it had been long hypothesised that a cellular factor must be involved in filament turnover within cells. (Carlier et al., 1997) used bacterially expressed ADF-1 from *Arabidopsis thaliana*, which whilst only sharing 30% amino acid sequence homology with the vertebrate family members (including cofilin), has similar actin binding and depolymerising activity (Carlier et al., 1997). The group showed that ADF-1 accelerated the subunit off-rate at the barbed end of the filament by 22-fold which is the rate-limiting step for steady-state cycling. Using fluorescently labelled nucleotide in a pulse-chase experiment, the group demonstrated that this effect enhanced treadmilling of filaments to a level that matched observations in the lamellipodia of motile cells. Interestingly, the group noted the association rate at the barbed end of the filament was approximately 12 times greater than that of G-actin alone. The authors speculated that upon binding G-actin, ADF induces a dipole moment in the monomer which modifies the charge distribution on the surface of the molecule increasing the long range attractive electrostatic interactions with the barbed end. This conclusion was controversial and Theriot noted in a mini-review in response to the paper that another plausible explanation could be that severing enhanced the number of filament ends in the reaction (Theriot, 1997).

Concurrently, Rosenblatt reported the effect of modulating cofilin concentrations in *Xenopus* egg extracts on *Listeria monocytogenes* motility. This intracellular bacterial pathogen hijacks host actin to drive motility through crosslinking of actin

filaments at the surface immediately next to the bacterium resulting in propulsion and the formation of comet tails. The loss of filaments from the tail occurs at a uniform rate and is largely controlled by host factors. This model has been widely used to examine the functional properties of many actin binding factors – changes in the rate of actin-filament turnover, and therefore the speed of movement and length of the tail, can help elucidate the ABP behaviour in a cytoplasmic context (Lambrechts et al., 2008). This assay showed that depletion of *Xenopus* ADF/cofilin resulted in comet tails five times longer than the controls. This effect was rescued by the addition of recombinant *Xenopus* ADF/cofilin and chick ADF. In excess, the *Listeria* tails were shortened, to a limit. The phosphomimetic, inactive, Ser-3 to Glu (S3E) mutant ADF was unable to decrease tail length. Using a slowly hydrolysing analogue of ATP, the group showed *Xenopus* ADF/cofilin could only effectively depolymerise ADP-bound actin, suggesting a substrate preference for ADF/cofilin (Rosenblatt et al., 1997).

Cofilin is negatively regulated through phosphorylation at Ser-3 (Agnew et al., 1995; Moriyama et al., 1996) by direct interaction with two major kinase families: the LIM-kinases (LIMKs) and the closely related testicular protein kinases (TESKs) (Arber et al., 1998; Toshima, 2001; Toshima et al., 1995; Toshima et al., 2001). The LIMKs are modulated through small Guanosine-5'-triphosphate (GTP)ases of the Rho family which in turn decode incoming extracellular signals (*Fig. 1-8*). Cofilin is rapidly dephosphorylated for reactivation by the Slingshot family of phosphatases which has been shown to be activated by receptor tyrosine kinase clustering (Niwa et al., 2002; Rogers et al., 2005). This phenomenon is thought to allow sensing of and response to low levels of ligands (Bray et al., 1998). Chronophin is another phosphatase that reactivates

phosphorylated cofilin through ATP-sensing in conjunction with the chaperone protein, heat shock protein 90 (Gohla et al., 2005; Huang et al., 2008).

Regulation by phosphatidylinositol 4,5-bisphosphate (PIP_2) is arguably the most interesting form of modulation because it is able to sequester cofilin at the plasma membrane preventing it from severing actin, despite spatial proximity, in a LIMK-independent manner (Song et al., 2006; Yonezawa et al., 1990). Activation by chemoattractants, such as epidermal growth factor, allows release following PIP_2 hydrolysis (*Fig. 1-9*) by phospholipase C where local activation results in formation of directional protrusions during chemotaxis (van Rheenen et al., 2007; Zhao et al., 2010).

Changes in pH can modulate the activity of cofilin. At pH greater than 7.3, depolymerisation of F-actin occurs proportionally by the addition of excess cofilin (Yonezawa et al., 1985). Mutation of specific residues demonstrated that His133 and Asp98 were likely to confer pH sensitivity that modifies cofilin binding to actin filaments (Pope et al., 2004). Cofilin distribution remains unchanged by variation in pH and therefore pH sensitivity may allow for regulation of cofilin activity in specific cellular locations (Bamburg, 1999). Filaments that reside under the membrane in regions of ion exchange may experience transient changes in pH that result in localised actin remodeling.

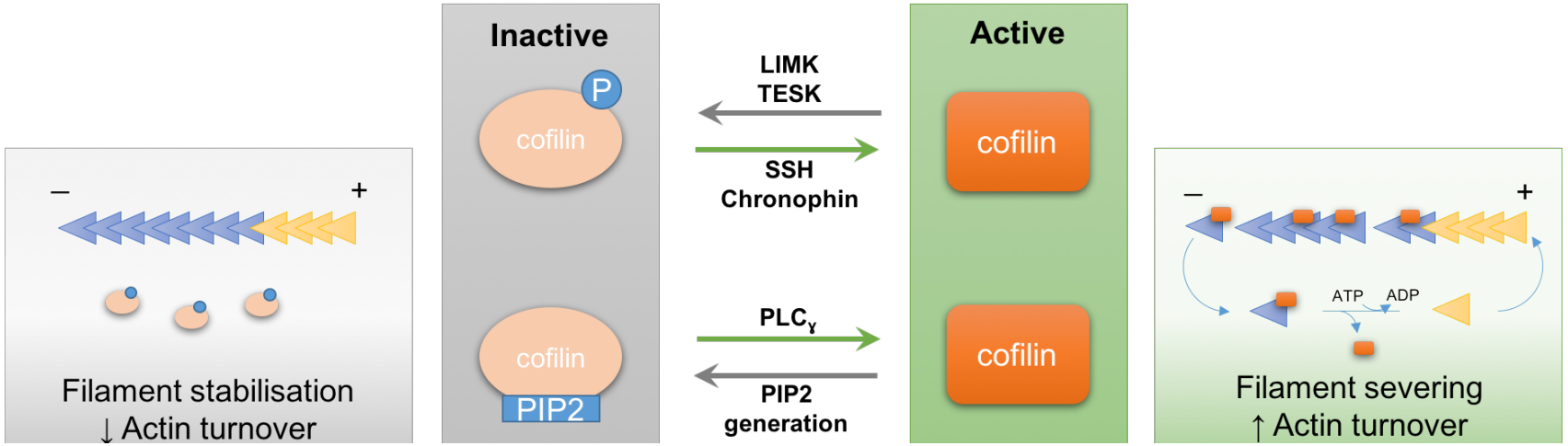

Figure 1-8. Canonical cofilin regulation. *Cofilin is deactivated by phosphorylation (P) of the serine residue at position 3 by LIM-kinases (LIMKs) and testicular protein kinases (TESKs). Slingshot (SSH) and chronophin, activated by ATP depletion (Huang et al., 2008), activate cofilin through their phosphatase activity. Non-phosphorylated cofilin is also sequestered at the membrane by phosphatidylinositol 4,5-bisphosphate (PIP_2). Phospholipase C activation (PLC) leads to PIP_2 hydrolysis and subsequent release of cofilin that can then sever actin filaments.*

Recently, cofilin has been shown to have a synergistic relationship with the actin-oxidising enzyme Mical. Mical is activated in the presence of F-actin which drives oxidation of actin's Met44 and Met47 residues inducing F-actin disassembly (Hung et al., 2011). However, when cofilin is present, oxidation of F-actin is reduced but filament disassembly is enhanced. Time-lapse TIRF analysis of filament dynamics showed that Mical-oxidised F-actin was more susceptible to cofilin binding and subsequent severing (Grintsevich et al., 2016). To test this *in vivo*, *Drosophila* bristle cells were used as they cells form large, stable extensions of crosslinked F-actin bundles and provide a system for examining actin remodelling (Guild et al., 2002). Elevating cofilin and Mical levels in bristle cells resulted in F-actin disassembly and increased bristle branching. This suggested that Mical-oxidised F-actin is vulnerable to cofilin-mediated severing and may therefore have different properties to unoxidised filaments. These two populations may consequently also possess different actin remodelling properties (Grintsevich et al., 2016).

Although cofilin has recently been implicated in novel cellular functions such as lipid metabolism and apoptosis, its canonical role is asymmetrical remodelling of the cytoskeleton in locomotion and motility (Kanellos and Frame, 2016). For migration to occur, cells become polarised in the direction of migration and form a protrusion in response to chemotaxic stimuli. Cofilin-mediated actin filament disassembly is required for lamellipodium protrusion in migrating fibroblasts. However, this activity must be tightly regulated spatially and temporally.

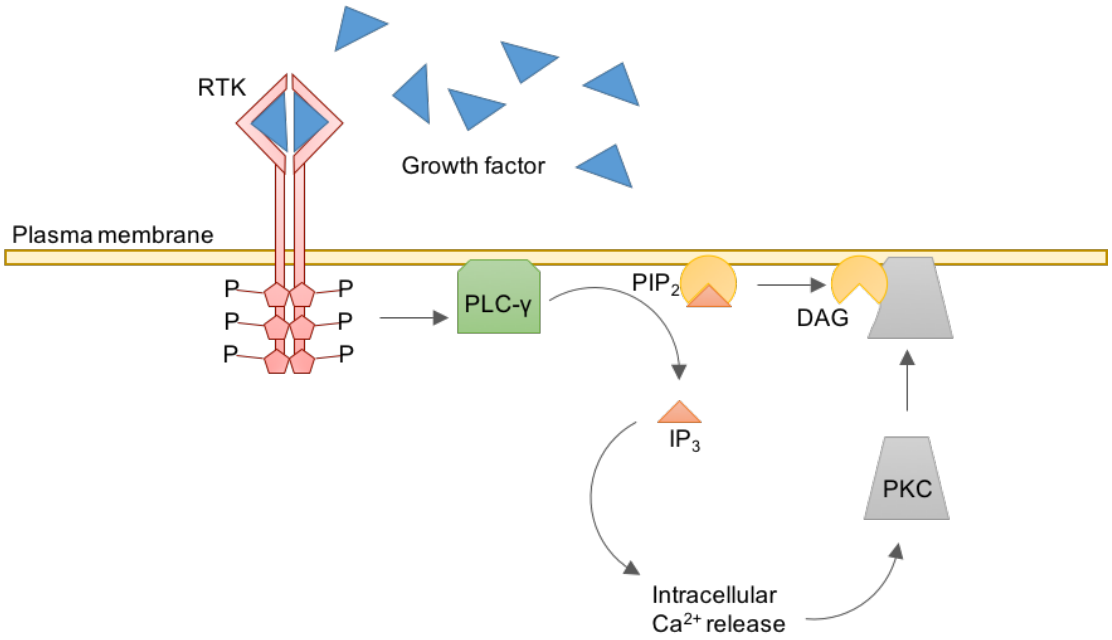

Figure 1-9. Phosphatidylinositol 4,5-bisphosphate signalling downstream of receptor tyrosine kinases. *The hydrolysis of phosphatidylinositol 4,5-bisphosphate (PIP_2) is mediated by the activation of phospholipase-C (PLC-γ) downstream of receptor tyrosine kinase (RTK) dimerisation triggered by neurotrophins including nerve growth factor and epidermal growth factor. This interaction drives the formation of the second messengers: inositol 1,4,5-triphosphate (IP_3) which triggers calcium (Ca2+) release; and diacylglycerol (DAG) which binds protein kinase C (PKC). The two-part signalling cascade is required for a range of cellular activities including cytoskeletal changes and neurite outgrowth. Adapted from (Schlessinger and Ullrich, 1992).*

A study in chick embryo heart fibroblasts showed that only active cofilin (non-phosphorylated form) was localised to the lamellipodium (Dawe et al., 2003). To further test this, expression of constitutively active LIM-kinase resulted in the formation of multiple non-polarised protrusions in almost 90% of cells. Polarity was rescued by coexpression with a non-phosphorylatable form of *Xenopus* cofilin. Local activation of cofilin in uncaging experiments showed cofilin initiates formation of free barbed ends, potentially orchestrating new sites of actin polymerisation (Ghosh et al., 2004).

Analysis of breast cancer expression profiles identified the cofilin pathway as a major determinant of metastasis and invasiveness (Wang et al., 2007). Whilst no single gene in the pathway has been singled out, *in vivo* studies in metastatic tumour cells showed that cofilin and phospholipase C were required for epidermal growth factor (EGF) mediated-chemotaxis (Mouneimne et al., 2004). Mutations in EGF receptors are thought to be a key contributing factor in the development of many human cancers and makes the cofilin pathway an attractive therapeutic target as an effector of faulty signaling (Henson and Gibson, 2006). Interestingly, in some cancer cell types cofilin knockdown increases directionality, and reduces turning frequency (Sidani et al., 2007), which may seem contrary to results in non-cancerous migratory cell types (Dawe et al., 2003). It is likely that the payoff for loss of directionality maintenance is to allow for multiple protrusive structures and increased turning frequency, a beneficial strategy in metastasis.

Specific deletion of *cofilin-1* in mouse embryos results in impaired neural crest cell migration and is ultimately embryonic lethal. These cells cannot polarise and F-actin bundles and fibres are absent. As a result, the apical actin fibres are

constricted and the neural tube fails to close and the development of neural crest derived tissues is disrupted (Gurniak et al., 2005). In humans, single nucleotide polymorphisms in cofilin-1 have been linked to increased spina bifida risk, however the study was underpowered and the finding did not reach significance (Zhu et al., 2007).

To further examine the role of cofilin-1 in the brain where it is most highly expressed, Bellenchi et al., developed a brain-specific conditional knockout mouse by crossing n-cof^{fl} allele with a transgenic Cre-expressing line, driven by the nestin promoter (Bellenchi et al., 2007). Over 90% of homozygous cofilin-1 mutants died between post-natal days 1-3, with a small proportion surviving up to 30 days but with growth retardation, ataxia and seizures. Analysis of embryonic mutant brains revealed largely normal gross anatomy, however the cerebral cortex appeared thinner and ventricles enlarged in comparison to wild-type litter mates. Closer inspection revealed layers of the cortex were missing indicating failure of neuronal progenitor migration which was confirmed by tracing of mitotically active cells in the cortical plate. Cultured cortical neurons from these animals displayed accumulation of F-actin and impaired neurite outgrowth. Cell cycle progression was also impaired, along with the interkinetic nuclear migration, the vertical movement of the nucleus within the cell which correlates to phases of the cell cycle. This process is thought to allow unrestricted cell proliferation whilst maintaining dense packing within the cortex. It is plausible that lack of cofilin-1 results in disruption to cytoskeletal-dependent remodelling of the intracellular environment required for this process (Bellenchi et al., 2007).

It has been known for some time that cytoskeletal components are found in protein aggregations correlated with neurodegeneration. Hirano bodies are small, ovoid, intracellular inclusions first observed by Asao Hirano in 1965 in patients with ALS. These structures are often associated with ageing but are found in significantly greater numbers in patients with Alzheimer's disease making them a clinically relevant marker (Hirano, 1994). The inclusions display sets of parallel actin filaments that are resistant to normal actin turnover and pharmacologically induced disassembly (Galloway et al., 1987; Griffin et al., 2014). Vinculin and tropomyosin were the first ABPs to be found in Hirano bodies (Galloway et al., 1987). Later, Maciver and Harrington (1995) discovered cofilin is a major component of these structures (Maciver and Harrington, 1995).

To assess whether these or similar structures contributed to other neuropathology, Minamide and colleagues performed immunohistochemistry on post-mortem Alzheimer and normal brains. They found cofilin inclusions were present in the hippocampus of Alzheimer brains and were shown to co-occur with amyloid plaques but not in the controls. The group turned to *in vitro* experiments to examine the cause of aggregate formation. Cultured rat hippocampal or cortical neurons were subjected to cellular stress through ATP-depletion, or treatment with glutamate and peroxide. Rods were characterised as "straight spindle" shaped inclusions with intense immunostaining for cofilin but negative for phalloidin derivatives. Rods formed within 5-10 minutes on ATP-depletion and continued to grow over 30 minutes, which was shown to be reversible during that time if washout was performed. Neurons proved particularly sensitive to hydrogen peroxide even with antioxidants present in the media, however, only 7% of neurons that survived the treatment displayed rods. Neither nitric-oxide

generating agents used (diethylamine or spermine) could produce persistent rods (defined as rods present after 24hours after washout), but glutamate treatment could. The group also showed that rods formed in neurites without active mitochondria. On washout of ATP-depletion media, mitochondria were only able to recover on the proximal side of the rod suggesting that persistent rods spanned the diameter of the neurite. Microtubules were also disrupted which, in combination with mitochondria dysfunction, could result in degradation of the neurite and synaptic structure without killing the neuron (Minamide et al., 2010; Minamide et al., 2000).

Cofilin-actin rods are different to Hirano bodies as they largely comprise actin and cofilin in a 1:1 ratio, which was initially shown to be true during all phases of formation. Mass spectroscopic analysis of isolated rods from an ATP-depleted cell line (A431) concluded that the aggregations also contained peroxiredoxin 1, an antioxidant enzyme; annexin A2, an actin- and phospholipid-binding protein; heat shock protein 60, a folding and stress response protein; and several isoforms of 14-3-3 protein. Out of the mass spectrometry candidates, 14-3-3 was the only protein confirmed by immunofluorescence in neurons and appeared in only some of the rods examined which seemed to accumulate over time suggesting 14-3-3 was not a core component (Minamide et al., 2010). The 14-3-3 protein family play a key role in the regulation of many cellular processes such as signal transduction and cell cycle control but had not been linked to the cytoskeleton until 2002. Pull down assays showed a strong interaction between phosphocofilin and 14-3-3-ζ, and expression of 14-3-3-ζ increased phosphocofilin levels. This was thought to occur by protecting phosphocofilin from phosphatase activity and independently of regulating LIMK activity (Gohla and Bokoch, 2002).

Phosphorylated microtubule-associated protein (pMAP) was also shown to colocalise with rods suggesting the inclusions could recruit other elements that are observed in neurofibrillary tangles, a primary marker of Alzheimer's disease. Further investigation assessing cofilin knockdown and actin modifying drugs in primary neurons showed that rod formation was required for subsequent inclusion of pMAP. Rods positive for pMAP were also triggered by amyloid beta peptide treatment indicating there may be a unified pathway for the accumulation of both proteins (Whiteman et al., 2009). However, purified actin and cofilin at physiological concentrations display rapid rod assembly *in vitro* indicating that cofilin and actin are the core elements required for their formation. Time lapse imaging also demonstrated rods aggregate over time, with lengths ranging from 22 to 1480 nm as determined by ultrastructural tomography (Minamide et al., 2010).

Transgenic mouse models of Alzheimer's disease could prove useful in understanding the mechanisms underlying rod formation and the pathological consequence of their presence. Cofilin levels are significantly increased in amyloid precursor protein (APP) transgenic mouse brains compared to wildtype litter mates. This was found to be due to a reduction of post-transcriptional regulation by a decrease in microRNA 103 and 107 levels (Yao et al., 2010). However, the exact reason this may occur is still unknown.

1.9 Actin interacting protein-1

Actin interacting protein-1 (AIP-1) is a 66kDa protein that is also known as Flare in *Drosophila melanogaster*, Unc-78 in *Caenorhabditis elegans*. In humans and other mammals, the term WD repeat-containing protein-1 (WDR-1) is used as the

protein is designated to the WD-repeat family of proteins which are thought to be involved in protein-protein interactions (Li and Roberts, 2001). For clarity, the term AIP-1 will only be used from here on as AIP-1 is more descriptive of its function.

The crystal structure of AIP-1 protein from *Saccharomyces cerevisiae* was initially surprising as it was the first crystal structure to contain more than 8 WD repeats. These structural motifs are homologous sequences of 40 amino acids terminating in tryptophan-aspartic acid at the carboxyl end and are thought to be involved in reversible binding and regulation of protein interactions (Stirnimann et al., 2010). AIP-1 has 10 of these repeats which form two connected seven-bladed ß-propellers. The two propellers are similar in size; the first propeller is formed by residues 20-335, the second of residues 4-10 and 340-613 (Voegtli et al., 2003). This arrangement helps to keep the structure stable; the overall fold resembles an open clamshell (*Fig. 1-10*). Two patches of densely conserved residues on each propeller were suggested as potential binding sites for F-actin and cofilin; the orientation of the two propellers in relation to one another may mediate actin-cofilin complex formation. Furthermore, the interaction between the domains is thought to confer rigidity preventing conformational changes occurring during interaction with a large substrate (Voegtli et al., 2003).

AIP-1 was first discovered in a two-hybrid, actin mutant-based yeast screen to assess conserved components of the actin cytoskeleton and was the third protein, after LIMK and actin, found to directly bind cofilin (Amberg et al., 1995). The same mutagenesis approach was utilised to confirm the residues required for interaction with both actin and cofilin. Deletion of AIP-1 was found to be lethal

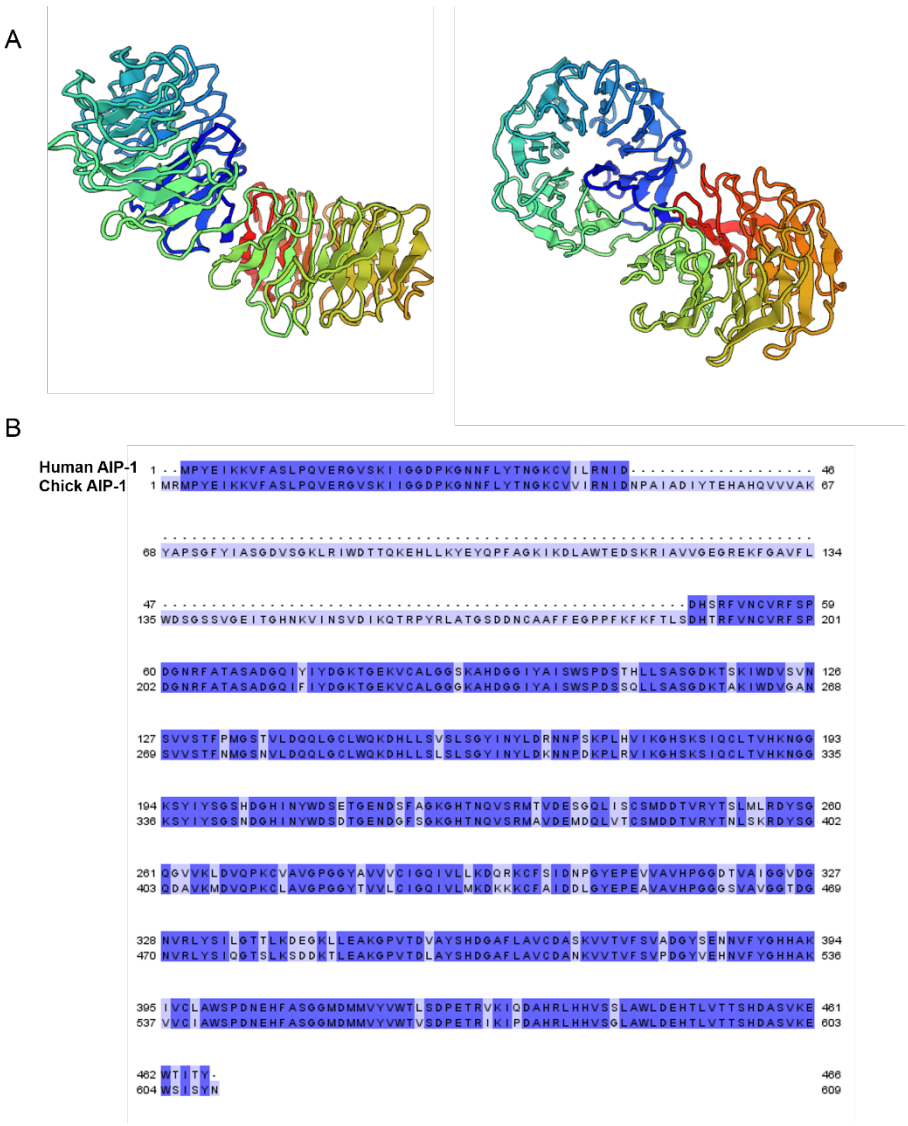

Figure 1-10. AIP-1 structure, and comparative sequences of Human AIP-1 (O75083) and Chick AIP-1 (O93277). ***(A)*** *The ribbon diagram is rainbow-coloured, beginning with dark blue at the NH_2 terminus and ending with red at the COOH terminus. Propeller 1, comprising blades 1-7, is at the top of the diagram. Propeller 2, blades 8-14, is at the bottom. AIP-1 is rotated -90^O in the Y axis (right) relative to the orientation left. The three-dimensional domains of AIP-1 were structurally modelled in silico using http://www.proteinmodelportal.org/ (Haas et al., 2013) The Protein Model Portal - a comprehensive resource for protein structure and model information. Database bat031), with human WDR-1 (UniProtKB-O75083/WDR1_HUMAN) used as input.* ***(B)*** *Aligned sequences for Human and Chick AIP-1 display 86% homology. Purple gradient denotes percentage of residues that are conserved within that column between sequences: darkest mauve = >80%, White = <40%.*

in combination with a specific actin mutant that slows the rate of filament disassembly or cofilin mutants, further supporting the hypothesis that AIP-1, actin and cofilin form a triad complex (Iida and Yahara, 1999; Rodal et al., 1999). In yeast, AIP-1 localises to cortical actin patches; in the mutants, localisation was perturbed indicating that AIP-1 has a direct role in restricting cofilin localisation. Biochemical investigation demonstrated AIP-1 enhances cofilin activity and that cofilin itself enhances AIP-1 binding to actin reciprocally to regulate actin dynamics (Clark et al., 2006; Rodal et al., 1999). Systematic mutagenesis of AIP-1 residues provided the first evidence that AIP-1 promotes rapid turnover of actin in living cells (Okada et al., 2006). However, this work also perpetuated the hypothesis that AIP-1 directly capped actin which has since been challenged (Jansen et al., 2015). Experiments using synthetically formed actin architectures showed that AIP-1 must be present with cofilin to completely and rapidly disassemble F-actin networks compared to cofilin alone. At the single molecule level, the optimal threshold is above 23 cofilin molecules decorated along an actin filament to trigger full disassembly most rapidly which suggests cofilin saturation may act as a marker for targeted dismantling (Gressin et al., 2015).

Whilst most of what is known about AIP-1 has been inferred from yeast-based biochemical investigation, several other model organisms have revealed some of the cellular functions of the protein. In *Dictyostelium discoideum* the orthologue of AIP-1 is enriched in higher order actin structures including phagocytic cups, macropinosomes and lamellipodia. Observation of GFP-tagged AIP-1 showed the protein rapidly redistributes into newly formed cortical protrusions (Konzok et al., 1999). Null mutations in *C. elegans AIP-1* causes disrupted filament organisation in muscle, in combination with impaired muscular contractility (Mohri

et al., 2006; Ono, 2001, 2014). Drosophila *AIP-1* mutants display actin aggregations and grossly altered bristle morphology, the development of which is heavily reliant on ordered actin regulation (Ren et al., 2007).

As the *AIP-1* knockout is embryonic lethal, alternative strategies have been created to examine a loss of the protein. Single point *AIP-1* mutations were specifically made to produce mutant transcripts which in turn resulted in an incorrectly folded protein, reducing its half-life. The severity of the reduced dose of the protein caused a range of phenotypes, from embryonic lethality to defects in neutrophil migration and megakaryocyte maturation (Kile et al., 2007). Xiao and colleagues created AIP-1 depleted zygotes and identified that the time point of lethality occurred pre-implantation (Xiao et al., 2017). Interestingly, they also showed that *AIP-1* knockout resulted in reduced cofilin phosphorylation in both mouse embryonic fibroblasts (MEF) and an embryonic stem cell line established from their knockout embryos. Immunoprecipitation experiments showed AIP-1 interacted with LIMK which the authors speculated may be responsible for the cofilin phosphorylation, and observation of myc-tagged LIMK showed clustering around microtubules in the AIP-1 knockout MEF (Xiao et al., 2017). The authors speculated that AIP-1 presence inhibits LIMK binding microtubules, potentially contributing to cytoskeletal regulation and microtubule stabilisation. Here, unbound LIMK is free to translocate to the cytoplasm and phosphorylate cofilin (Edwards and Gill, 1999; Gorovoy et al., 2005).

In vitro, knockdown of AIP-1 in HeLa cells causes F-actin accumulation around the contractile ring in telophase, impairing cytokinesis which results in formation of multinucleate cells (Kato et al., 2008). This is further supported by more recent

evidence demonstrating contractile ring dysfunction in fission yeast (Chen et al., 2015). Conditional knockout in mouse heart tissue results in hypertrophy, impaired heart function and early lethality. Analysis at the cellular level by immunofluorescence showed F-actin accumulation in the myocardium during the life of the mice. These accumulations disrupted the typical organisation of the muscle structure leading to its dysfunction (Yuan et al., 2014). AIP-1 messenger RNA transcripts have been shown to be upregulated in the noise damaged chick cochlea which the authors speculate may be important in the reinstatement of the cytoskeleton and repair of the damaged cells, potentially playing a signalling role (Oh et al., 2002).

1.10 Drebrin

Drebrin was first discovered by Shirao and colleagues in 1985 in the chick optic tectum, subsequently, the presence of isoforms in other mammals, including humans, was confirmed (Shirao et al., 1987; Shirao et al., 1989; Shirao and Obata, 1985; Toda et al., 1993). In humans, two isoforms, E and A, are produced by alternative splicing and are differentially expressed during development. Drebrin E is found widely in the developing embryo, whilst drebrin A is restricted to neurons in the adult, particularly in dendritic spines. In chick, two embryonic types (E1 and E2) and an adult type (A) exist (Toda et al., 1993). Isoform E1 dominates prior to embryonic day (E) 5, and by E9, E2 is the major isoform (*Fig. 1-11*). (Ketschek et al., 2016). Although only one drebrin E isoform has been isolated in humans, rats and mice, it is regarded as orthologous to chick E2 (Dun et al., 2012).

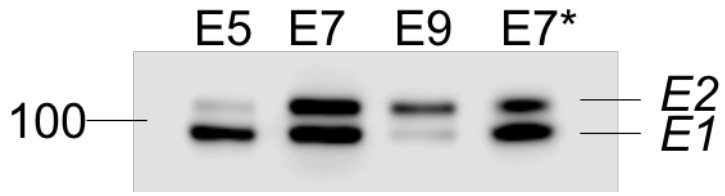

Figure 1-11. Switching of drebrin E isoform expression occurs between E5-9 in chick neural tube. *Chick neural tubes were taken from each embryonic stage, lysed and clarified before isoforms were separated by SDS-PAGE under denaturing conditions. Membranes were probed with an anti-drebrin antibody. Lower band is the drebrin E1. The difference in the size of the detected band (~100 kDa) and in the predicted (~65 kDa) is due to the large number of negatively charged residues in this protein. This is consistent in the literature (Hayashi et al., 1999; Rehm et al., 2013). Protein sizes are in kDA. * = hindbrain lysate control.*

In an attempt to understand the roles of the adult and embryonic form, Kojima et al (2010) produced a knockout mouse that targeted exon 11 which is required to produce the adult form of the protein (Kojima et al., 2010). They reported no defects in gross morphology of the brain or any abnormalities in typical behaviour suggesting that the embryonic form is able to compensate, at least during development. The adult isoform of drebrin is strongly linked to the regulation of dendritic spine morphology through rearrangement of the cytoskeleton (Koganezawa et al., 2017). These structures are small membranous protrusions that receive and respond to synaptic input. The ability of dendritic spines to rapidly modify their morphology relies heavily upon the actin cytoskeleton, and regulation is crucial for synaptic function in higher brain function such as memory and learning.

Deletion of the actin binding domain of drebrin results in redistribution of drebrin into both spines and shafts indicating that actin binding activity is crucial for its localisation. Overexpression of drebrin A causes spines to become significantly elongated in primary cortical neurons (Hayashi and Shirao, 1999). Further immunocytochemical examination of spines treated with antisense oligonucleotides revealed attenuated clustering of post-synaptic density (PSD)-95, a key marker of the post synaptic signalling complex. Reintroduction of exogenous drebrin rescued this effect (Takahashi et al., 2003).

Altered spine morphology is seen in the brains of many neurological disorders associated with cognitive defects such as Alzheimer's disease, Down syndrome and Fragile X syndrome (Fiala et al., 2002; Purpura, 1974). Drebrin levels are reduced in the brains of Down syndrome patients and in those with Alzheimer's

disease (Kojima and Shirao, 2007; Shim and Lubec, 2002). Whether abnormalities in spine morphology cause neurological disturbances or are a consequence of disruption to incoming excitation remains largely unanswered, however, in the case of Alzheimer's disease, downregulation of drebrin precedes the loss of the synapse (Harigaya et al., 1996). Understanding the role of drebrin in organising the cytoskeleton has drawn attention to it as a potential therapeutic target in synaptic dysfunction.

Surprisingly, genetic knockout of drebrin has not clarified this problem. The first drebrin knockout mouse generated was specific for drebrin A to assess its role in synaptic plasticity. Drebrin A is thought to be the only F-actin binding protein that is exclusively localised to post-synaptic submembranous surface and therefore may have an important function, specifically at the post-synaptic membrane (Aoki et al., 2005). Electron microscopy analysis of cortex slices showed no gross changes to synapse morphology or number, and resting synaptic density appeared normal. A pharmacological N-methyl-D-aspartate (NMDA) receptor blockade, was used to examine the functional effects of drebrin A knockout. The blockade induced a dysregulation of the NR2A subunit of the NMDA receptor in wild type animals but not in the drebrin A knockouts. The authors concluded that drebrin E was able to partially compensate for the loss of the adult isoform but not in activity-dependent processes. They also noted some inter-animal differences in basal levels of NR2A, which the authors believe could arise from rearing methods and inter-continental shipment (Aoki et al., 2009).

To completely knock out *drebrin*, exons 4-7 were flanked with LoxP for cre-mediated recombination to generate a frameshift mutation. The hippocampal

dendritic spines of these animals were reduced in number, had significantly altered morphology and reduced levels of receptor complexes for dopamine. Electrophysiological analysis of hippocampal slices from these animals showed alterations in memory-related synaptic changes (Jung et al., 2015).

Recently, a novel *drebrin* knockout mouse was created by excising the first 6 exons of the *drebrin* gene, a strategy in contrast to previously existing knockout models. The animals developed normally and displayed no obvious neurological deformity. Hippocampal synapse activity and activity-dependent plasticity remained unaltered. Synaptic markers, such as PSD-95 and synaptophysin, analysed by Western blotting also remained consistent between the *drebrin -/-* mice and their WT littermates. This suggests drebrin does not have a key role in synaptic regulation within the brains in healthy young adult mice and that the network of actin binding proteins is robust enough to compensate (Willmes et al., 2017). The authors speculate that certain disease conditions, such as cellular stress or ageing, may leave dendritic spines susceptible to drebrin loss. The presenilin conditional knockout mouse, commonly used to model the development of Alzheimer disease, is an example that may underscore these findings. These mice display over 50% decrease in drebrin A at the synapses in the CA1 region of the hippocampus, a region important for memory retrieval (Lee and Aoki, 2012).

In the chick, drebrin has been shown to play a key role in the generation of the leading process in oculomotor neurons. Dun et al., (2012) used short hairpin RNA to block drebrin expression from Hamburger Hamilton (HH) stage 10-12 and embryos were analysed at HH25-27 when oculomotor neurons would normally

reach the midline (Dun et al., 2012). The leading process was absent and migrating cells were not seen in any of the embryos which contrasted with the normal behaviour displayed by controls. The key features of overexpression were misdirected migration, where cells remained motile but were unresponsive to guidance cues. The authors suggest the two forms influence distinct aspects of migration such as initiation or directionality. It is likely these processes require differential modifications of the actin network.

Little is known about drebrin regulation, however there are a number of residues that could undergo phosphorylation. Serine 142 and serine 342 are phosphorylated by a neuron specific variant of cyclin-dependent kinase 5 (cdk-5). Drebrin phosphorylation at these sites has not been shown to affect neurite or spine formation, however, radial migration of cortical neurons is suppressed when expressing drebrin mutants at cdk-5 phosphorylation sites (Tanabe et al., 2014). Cdk-5 appears to play an important role in proper brain development as cdk-5 null mice show disrupted lamination of the brain and perinatal lethality (Ohshima et al., 1996). A similar phenotype is seen in mice lacking the neuronal specific activator of cdk-5, p38 (Chae et al., 1997). However, cdk-5 bound to p38 phosphorylates many cytoskeletal proteins and the deleterious effects are unlikely to be solely caused by absence of drebrin phosphorylation (Zhu et al., 2011). Phosphatase and tensin homologue (PTEN) is a regulator of the phosphatidylinositol 3-kinase (PI3K) pathway and can dephosphorylate drebrin at serine 647. Immunolabelling showed PTEN was largely absent from growth cones and dendritic spines but present in axons and dendrites, suggesting a level of spatial segregation of phosphorylated drebrin was occurring in locations of actin turnover (Kreis et al., 2013). Localised PI3K signaling domains along axons

appear to dictate the formation and longevity of actin patches – precursors of filopodial extension. Aligned and bundled actin filaments that form the shafts of filopodia emerge from these structures (Ketschek and Gallo, 2010; Spillane et al., 2011). Drebrin has been shown to interact with these actin patches to coordinate the actin and microtubule cytoskeleton during the initial stages of axon branching (Ketschek et al., 2016).

High resolution atomic force microscopy analysis of drebrin binding showed significant changes to the helical twist and stiffness of actin filaments that conferred stability (Sharma et al., 2011). This was the first direct evidence that drebrin mechanically remodelled F-actin in a long-range manner that could affect the binding of other ABPs. Drebrin has been indirectly shown to compete with other cytoskeletal proteins. Early biochemical assays demonstrated that drebrin could inhibit tropomyosin association and prevent α-actinin binding and crosslinking of actin. This finding lead to the authors hypothesising that drebrin was involved in destabilising actin filaments (Ishikawa et al., 1994). Later, drebrin was shown to inhibit actomyosin interactions by a reduction in actin-activated ATPase activity of myosin. A further sliding assay which utilised immobilised myosin showed a decrease in filament velocity in the presence of drebrin (Hayashi et al., 1999). Higher resolution analysis of this inhibition revealed drebrin decoration delayed the attachment of myosin leading head, but no reduction in filament velocity was observed (Kubota et al., 2010).

In neuronal growth cones, drebrin is thought to couple microtubules and actin filaments in neuritogenesis and pathfinding via the microtubule plus tip protein, end-binding protein-3 (EB3) (Geraldo et al., 2008). Drebrin has been shown to

interact with actin patches to coordinate the actin and microtubule cytoskeleton during the initial stages of axon branching. In this model, drebrin contributes to actin patch formation and development. Filopodia containing drebrin-bundled filaments emerge from these patches, and drebrin can the permit the entry of microtubule plus tips in preparation of collateral branch formation (Ketschek et al., 2016). Microtubule targeting via drebrin has also been observed in dendritic spines which suggests a central underlying mechanism for protrusion formation (Merriam et al., 2013).

1.11 Identifying the gaps

Despite advances in our understanding of how the neuronal cytoskeleton is regulated by actin binding proteins, basic questions about how these elements interact within a cellular context remain unanswered. This study aims to investigate the relationship between drebrin and cofilin within neurons during development of the nervous system and reveal whether they act in opposition as biochemical data predicts they might. This could shed light on the neurological disorders in which they have been implicated.

We still lack adequate therapies for neurodegenerative diseases and neurological traumatic injury. In combination with an ageing population, many neurodegenerative diseases are late on-set with slow progression, providing an opportunity for preventative measures prior to the onset of symptoms. It is vitally important that we understand the factors that contribute to the development and progression of such profoundly life changing diseases. The work presented here provides evidence that AIP-1 could represent a strong candidate for therapeutic augmentation that is not only limited to diseases of neuronal origin, but also where cellular stress is a central contributing factor to the development of disease.

CHAPTER 2

MATERIALS AND METHODS

CHAPTER 2
MATERIALS AND METHODS

2.1 Buffers, reagents and stock materials

All general-purpose chemicals were acquired from Sigma-Aldrich, with the exception of alcohols which were purchased from Fisher Scientific. All solutions for cell culture were supplied by Lonza, except for sera, Neurobasal media and B-27 supplement which were obtained from GIBCO, and penicillin/streptomycin from PAA laboratories.

Plasticware for tissue culture was acquired from Greiner Bio-one, with other general laboratory consumables purchased from Alpha-Labs and Fisher Scientific. Kits for deoxyribonucleic acid (DNA) amplification and gel extraction were purchased from Qiagen, restriction enzymes were supplied by Promega and New England Biolabs.

Specialist kits, antibodies, chemicals and consumables bought from alternate sources are noted in the text where appropriate.

Components of solutions are detailed in *table 2-1*.

Table 2-1. Solutions.

10% APS	10% (w/v) APS
10% SDS	10% (w/v) SDS
100 x SOC	2M glucose, 1M MgCl2, 250 mM KCl, sterilised by push filtration
2X PFA	8% (w/v) paraformaldehyde, in PBS, pH adjusted to 7.4
2X PG	8% (w/v) paraformaldehyde, 0.4% (v/v) glutaraldehyde, in PBS, pH adjusted to 7.4
3T3 medium	10% (v/v) heat-inactivated calf serum, 100 U./ml penicillin, 100ug/ml streptomycin, in DMEM
3X Laemmli sample buffer	10% (v/v) glycerol, 2% (w/v) SDS, 5% (v/v) β-2 mercaptoethanol, 0.002% (w/v) bromophenol blue, 0.125M Tris-Cl (pH 6.8)
Ampicillin	100 U./ml
Destain	40% (v/v) MeOH, 10% (v/v) acetic acid, in dd.H_20
DMEM 10 % serum (HEK, DF-1)	10% (v/v) heat-inactivated FBS, 100 U./ml penicillin, 100ug/ml streptomycin, in DMEM
6X DNA loading buffer	30% (v/v) glycerol, 0.25% (w/v) bromophenol blue, 0.25% (w/v) xylene cyanol
Filming medium	10% (v/v) heat-inactivated FBS, 4 mM L-glutamine, 100 U./ml penicillin, 100 µg/ml streptomycin, in Phenol Red-free DMEM
HE lysis buffer	25 mM HEPES, 5 mM EDTA, 1 mM MgCl2, 10% (v/v) Glycerol, 1% (v/v) Triton-X100, 100 µM PMSF
Kanamycin	50 µg/ml
LB agar	15 g/L agar, 10 g/L tryptone, 10 g/L NaCl, 5 g/L yeast extract
Luria Bertani Broth	10 g/L tryptone, 10 g/L NaCl, 5 g/L yeast extract
Lysine block	5% (v/v) horse serum, 5% (v/v) goat serum, 50 mM poly-D-lysine, 0.2% (v/v) Triton X-100
Primary neuronal culture medium	180 µM HEPES, 0.5 mM l-glutamine, 10 U/ml penicillin/streptomycin, 2% (v/v) B27 supplement, in Neurobasal media, Phenol Red-free, glutamine-free (GIBCO)
Quenching media	10% (v/v) heat inactivated chick serum, in DMEM
Running buffer	25 mM Tris-base, 192 mM glycine, 0.1% (w/v) SDS
TAE	40 mM Tris-base (pH 7.6), 20 mM acetic acid, 1 mM EDTA
TBS	20mM Tris-Cl, 150mM NaCl
TBS-T	20mM Tris-Cl, 150mM NaCl, 0.1% (v/v) Tween-20
Transfer buffer	25mM Tris-base, 192mM glycine, 0.1% (w/v) SDS, 20% (v/v) MeOH

2.2 Constructs

Plasmids for expression studies were purchased from Addgene unless otherwise noted and are detailed in *Table 2-2*. Cofilin fusion genes were subcloned by polymerase chain reaction (PCR) from their original cytomegalovirus (CMV) vectors, and AIP-1 was cloned by PCR directly from chicken complementary (c)DNA, details of which are found in *Table 2-2*.

For expression in primary neurons, all fusion genes were subcloned into a backbone containing the chick β-actin promoter, pCAβ, which has increased expression efficiency in chick neurons (gift of Dr. J. Chilton). This was facilitated by an intermediate step using the shuttle vector, pILES which is based upon pBlueScript, to add restriction sites for convenient cloning into pCAβ. Maps for key expression vectors and cloning schemes can be found in supplementary material Appendix F.

Constructs were checked at all steps by restriction enzyme digest using unique sites within the inserts and analysis by agarose gel electrophoresis before being confirmed by sequencing by Eurofins, TubeSeq service.

Table 2-2. Constructs. *All fluorescent proteins were fused to the C terminus of the protein of interest except where an asterisk (*) indicates fusion to the N terminus. SC= subcloned in-house. CMV = cytomegalovirus. CAG = (C) Cytomegalovirus early enhancer, (A) promoter first exon and intron of chicken beta-actin gene, (G) splice acceptor of the rabbit beta-globin gene. N= N terminus. C = C terminus.*

Origin	Cat. #	Gene	Fusion protein	Promoter	Bacterial resistance
Addgene	50859	Human cofilin 1	eGFP	CMV	Kanamycin
Addgene	51279	Human cofilin 1 R21Q	mRFP	CMV	Kanamycin
Addgene	50861	Human cofilin 1 S3E	eGFP	CMV	Kanamycin
Addgene	50860	Human cofilin 1 S3A	eGFP	CMV	Kanamycin
Addgene	17275	R-pre	mRFP *	CMV	Kanamycin
SC		Human cofilin 1	eGFP	CAG	Ampicillin
SC		Human cofilin 1 R21Q	eGFP	CAG	Ampicillin
SC		Human cofilin 1 S3E	eGFP	CAG	Ampicillin
SC		Human cofilin 1 S3A	eGFP	CAG	Ampicillin
SC		Human cofilin 1	mRFP	CAG	Ampicillin
SC		Human cofilin 1 R21Q	mRFP	CAG	Ampicillin
SC		Human cofilin 1 S3E	mRFP	CAG	Ampicillin
SC		Human cofilin 1 S3A	mRFP	CAG	Ampicillin
SC		Chick Drebrin E1	eYFP	CAG	Ampicillin
SC		Chick Drebrin E1 C	eYFP	CAG	Ampicillin
SC		Chick Drebrin E1 N	eYFP	CAG	Ampicillin
SC		Chick Drebrin E1	Cardinal	CAG	Ampicillin
SC		Chick Drebrin E1 C	Cardinal	CAG	Ampicillin
SC		Chick Drebrin E1 N	Cardinal	CAG	Ampicillin
SC		Chick Drebrin E1	cherryRFP	CAG	Ampicillin
SC		R-pre	mRFP*	CAG	Ampicillin
SC		R-pre	YFP*	CAG	Ampicillin
SC		R-pre	Cardinal*	CAG	Ampicillin
SC		-	eGFP	CAG	Ampicillin
SC		-	eYFP	CAG	Ampicillin
SC		-	cherryRFP	CAG	Ampicillin
SC		-	Cardinal	CAG	Ampicillin
SC		AIP-1	YFP	CAG	Ampicillin
SC		AIP-1	RFP	CAG	Ampicillin
SC		AIP-1	Cardinal	CAG	Ampicillin
SC		AIP-1	Cardinal*	CAG	Ampicillin

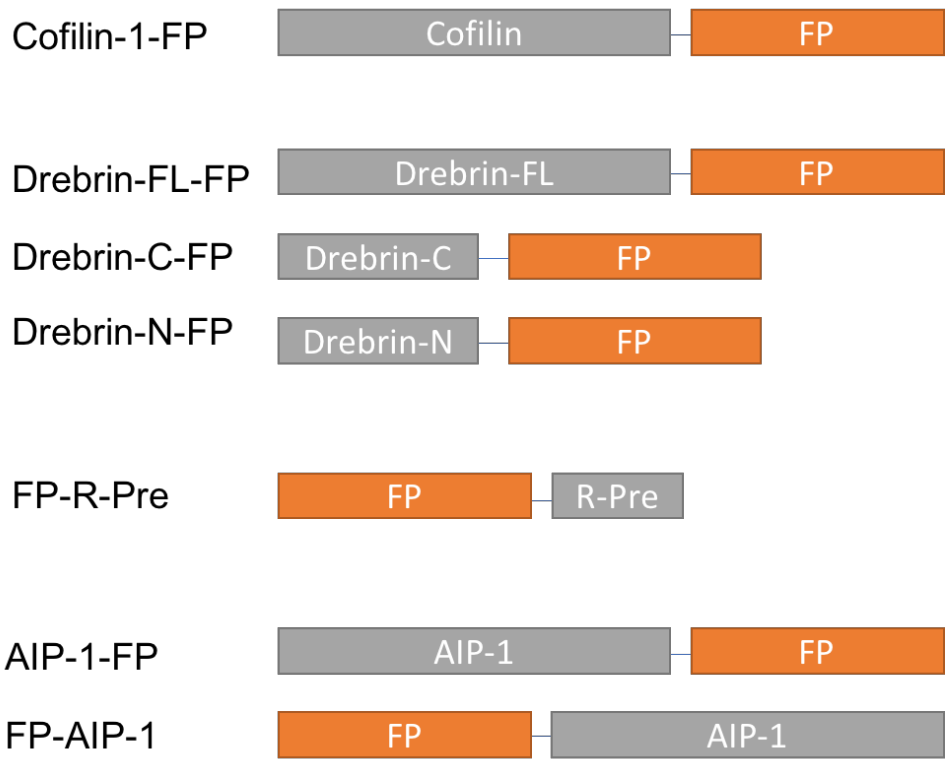

Figure 2-1 Schematics of fusion proteins detailed in Table 2-2. *FP= fluorescent protein.*

2.3 Generation of specific chick Cofilin-1 and WDR-1 hairpins

Target sequences for short hairpin RNA specific for chick cofilin-2 and chick AIP-1 were designed using an online tool (*Table 2-3*) and were the candidates were checked for specific target sequence homology by BLAST.

The target sequences were designed to sit between common sequences which comprise part of the miRNA flanking sequences. The sense and antisense oligomers are designed to overlap in the middle and are used together with the common flanking oligomers in a PCR to generate the miR30 like hairpin and chicken miRNA flanking sequences. The 5' base of the sense strand is changed to create a mismatch with the antisense sequence, mimicking miRNA30. The products were then then digested with NheI and MluI before subcloning into the vector digested with the same enzymes. The custom oligomers containing the target sequences were inserted into the first hairpin site of the RNA cassette within pRFPRNAiC vector (*Fig. 2-2*).

Table 2-3. Sequences for hairpin primers. *The target sequences are uppercase and sit between the flanking sequences (lower case).*

Target	Candidate ID	Sense	Antisense
Cofilin-2	285	gagaggtgctgctgagcgcGA AGGAAGACCTGGTATT TATtagtgaagccacagatgta	attcaccaccactaggcaAGA AGGAAGACCTGGTAT TTATtacatctgtggcttcact
Cofilin-2	355	gagaggtgctgctgagcgcAG CTCTAAAGATGCCATT AAAtagtgaagccacagatgta	attcaccaccactaggcaAAG CTCTAAAGATGCCATT AAAtacatctgtggcttcact
AIP-1	1000	gagaggtgctgctgagcggGG TGGAAAGTCCTATATT TATtagtgaagccacagatgta	attcaccaccactaggcaTGG TGGAAAGTCCTATATT TATtacatctgtggcttcact
AIP-1	1025	gagaggtgctgctgagcgtGC AGTAACGATGGTCATA TTAtagtgaagccacagatgta	attcaccaccactaggcaGG CAGTAACGATGGTCA TATTAtacatctgtggcttcact

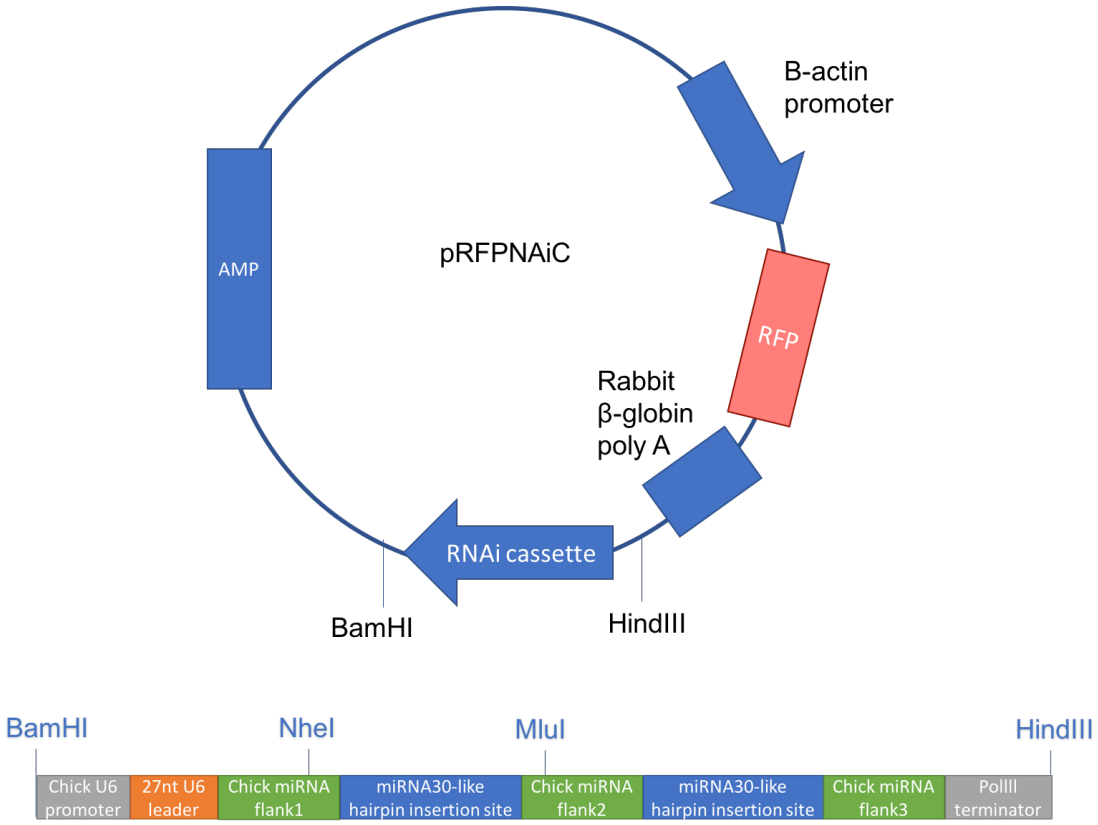

Figure 2-2 Schematic of pRFPRNAiC vector used for hairpin expression. *Specific oligomers for target sequences are used together with the common flanking sites in a PCR reaction to generate the miR30 like hairpin and chicken miRNA flanking sequences. The product is then digested with NheI and MluI, and subcloned into the vector digested with the same enzymes.*

2.4 DNA Plasmid preparation

2.4.1 Streaking out of bacterial stab cultures

Plasmids ordered from Addgene (*Table 2-2*) arrived as live bacterial stab cultures. Using standard sterile technique within a category 2 laminar flow containment hood, cultures were streaked out onto Luria-Bertani (LB) agar plates containing the appropriate selection antibiotic. Plates were then incubated for 12-16 hours at 37 °C to allow colonies to form.

2.4.2 Micropreps

Micropreps were used to quickly identify recombinants by sampling colonies directly from agar plates.

Standard aseptic technique was used within a category 2 laminar flow hood up until cell lysis. Colonies were selected from agar plates using a sterile pipette tip and placed in a 20 ml sterile bacterial culture tube (VWR) containing 5ml LB medium in addition to appropriate selection antibiotic and then shaken at 200 rpm for 12-16 hours at 37 °C.

One ml of culture medium was centrifuged at 4000 rpm for 2 minutes in a 1.5 ml microfuge tube and the supernatant discarded. The remaining culture was stored sealed, at 4 °C for future use. The plasmids where then extracted using the supplied solutions, Buffer P1 – resuspension buffer (50 mM Tris-Cl, pH 8.0, 10 mM EDTA, 100 µg/mL RNase A, excluding LyseBlue reagent), Buffer P2 – lysis buffer (200 mM NaOH, 1% w/v SDS), Buffer P3 – neutralising buffer (proprietary acetate-buffered solution containing the chaotropic salt guanidine hydrochloride),

EB – elution buffer (10 mM Tris-Cl, pH 8.5), from QIAprep Spin Miniprep Kit with the following modifications: The bacterial pellet was resuspended in 100 µl of Buffer P1. The bacteria were then ruptured by alkaline lysis in 100 µl of Buffer P2 and the tube was inverted 4-6 times until the suspension was clear. Cellular debris was precipitated by addition of 100 µl of buffer P3 and a further 4-6 inversions until flocculent matter was evenly dispersed. The solution was then centrifuged at 13,000 RPM for 6 minutes. The clarified supernatant was then combined with 600 µl 95% molecular biology grade ethanol to precipitate the DNA and centrifuged at 13,000 RPM for 6 minutes. The supernatant was gently removed to leave the glossy off-white pellet of DNA intact which was then allowed to air dry. Once dry, the pellet was reconstituted in 10 µl of buffer EB.

To visualise potential recombinants, the eluted DNA was combined with DNA loading buffer and run on a 0.8% w/v agarose tris-acetate-EDTA (TAE) gel alongside 1 Kb Plus DNA ladder (Thermo Fisher Scientific) and 100 ng of supercoiled backbone to easily identify recombinants after electrophoresis.

2.4.3 Minipreps

Minipreps were used to extract small amounts of plasmid DNA, usually around 10 µg per ml of bacterial culture that had been previously identified as containing a potentially correct recombinant clone after Microprep, using QIAprep Spin Miniprep Kit. These plasmids were used for DNA sequencing, restriction mapping, ligations and transient transfections to confirm fluorescence for fluorescent protein-tagged plasmids.

A 5 ml culture of bacteria was grown overnight in LB broth (Sigma) with the appropriate selective antibiotic. A 1.5 ml aliquot was removed and centrifuged at 8,000 rpm for 3 min, the supernatant was discarded and the pellet resuspended in 250 µl of Buffer P1 (50 mM Tris.HCl, pH 8.0; 10 mM EDTA; 100 µg/ml RNAse A, without LyseBlue reagent). The bacteria were ruptured by alkaline lysis in 250 µl of Buffer P2 (200 mM NaOH; 1% w/v SDS) with 4-6 inversions until the suspension had cleared. Cellular debris was precipitated by addition of 350 µl Buffer N3 (a proprietary acetate-buffered solution containing chaotropic salt) and a further 4-6 inversions until the flocculent precipitate was evenly dispersed. This was centrifuged at 13,000 rpm for 10 min, the supernatant removed to a fresh tube and spun at 13,000 rpm for a further 10 min the supernatant was added to a QIAprep spin column and centrifuged at 13,000 rpm for 1 min. The column was washed by the addition of 750 µl Buffer PE (a low salt, high ethanol proprietary solution) to the column which was then centrifuged at 13,000 rpm for 1 min, the flow through was discarded and the column centrifuged for a further 1 min at 13,000 rpm to remove residual ethanol. The column was transferred to a fresh microfuge tube and 30µl of molecular biology grade water was added to the column, then incubated for 1 minute before a final spin at 13,000 rpm for 1 min to elute the DNA.

2.4.4 Midipreps

Midipreps were used in the purification of up to 300 µg of plasmid DNA using HiSpeed Midi Prep Kit (Qiagen) which was then used for expression and functional studies.

A 5 ml starter culture was grown overnight in LB broth with the appropriate selective antibiotic. This was then diluted 1:1000 in 50 ml of LB broth with the appropriate selective antibiotic and grown overnight. The bacteria were harvested by centrifugation at 4,500 rpm for 15 min at 4°C and resuspended in 6 ml of Buffer P1 (without LyseBlue added). The bacteria were lysed by the addition of 6 ml of Buffer P2, mixed thoroughly by 4-6 inversions and incubated at room temperature for 5 min. Cellular debris was precipitated by the addition of 6 ml of Buffer P3 (3 M potassium acetate, pH 5.5) and 4-6 inversions, this was then added to a QIAfilter Midi Cartridge and incubated at room temperature for 10 min. Meanwhile an anion-exchange resin column (Qiagen HiSpeed Midi Tip) was prepared by the addition of 4 ml Buffer QBT (750 mM NaCl; 50 mM MOPS, pH 7.0; 15% v/v isopropanol; 0.15% v/v Triton X-100) which was allowed to empty under gravity. The cell lysate was push filtered in to the column and allowed to move through under gravity. The column was washed by the addition of 20 ml Buffer QC (1 M NaCl; 50 mM MOPS, pH 7.0; 15% v/v isopropanol). The DNA was eluted by addition of 5 ml Buffer QF (1.25 M NaCl; 50 mM Tris.HCl, pH 8.5; 15% v/v isopropanol) and precipitated by the addition of 0.7 volumes of isopropanol, inverted 4-6 times and incubated at room temperature for 5 min. Precipitated DNA was bound to a QIAprecipitator module, washed with 2 ml 70% v/v ethanol and dried by pushing air through the module. DNA was recovered by the addition of 350 µl of Buffer TE (10 mM Tris.HCl, pH 8.0; 1 mM EDTA).

The mass of DNA recovered was quantified using a NanoDropp 2000c UV-Vis Spectrophotometer (Thermo Scientific) by measuring absorption at 260 nm (A_{260}) in undiluted microvolumes of the samples. The proprietary software automatically calculates the concentration by multiplying the value by a factor of 50 (the µg/ml

of pure double stranded DNA). DNA purity was assessed simultaneously by measuring absorption at 280 nm (A_{280}). A ratio of A_{260} to A_{280} of 1.8 to 2.0 indicates “pure” DNA. A secondary measure of absorbance at 230nm (A_{230}) was also taken, where A_{260} to A_{230} ratios of lower than 1.5 indicate salt contamination.

2.4.5 Maxipreps

Maxipreps were used in the purification of up to 600 µg of ultrapure plasmid DNA using EndoFree Plasmid Maxi Prep Kit for endotoxin removal to promote neuronal survival in expression and functional studies.

A 5 ml starter culture was grown overnight in LB broth with the appropriate selective antibiotic. This was then diluted 1:1000 in 100 ml of LB broth with the appropriate selective antibiotic and grown overnight. The bacteria were harvested by centrifugation at 4,500 rpm for 15 min at 4°C and resuspended in 10 ml of Buffer P1 (without LyseBlue added). Cells were lysed by the addition of Buffer P2, 4-6 inversions and incubating for 5 min at room temperature. Cellular debris was precipitated by the addition of Buffer P3, 4-6 inversions and 10 min incubation at room temperature. The lysate was push filtered and any residual endotoxins removed by the addition of 2.5 ml Buffer ER (a proprietary solution contain isopropanol and polyethylene glycol octylphenyl ether), 10-15 inversions and incubation on ice for 30 min. Meanwhile an anion-exchange resin column (Qiagen-Tip 500) was prepared by the addition of 10 ml Buffer QBT which was allowed to empty under gravity. The cell lysate was added to the column and allowed to flow through under gravity. The column was washed by two separate additions of 30 ml Buffer QC. The DNA was eluted by the addition of 15 ml of Buffer QN (1.6 M NaCl; 50 mM MOPS, pH 7.0; 15% v/v isopropanol) then

precipitated by the addition of 0.7 volumes of room temperature isopropanol and centrifuged at 6,000 rpm for 1 hr at 4°C. The supernatant was discarded, the DNA pellet transferred to a fresh microcentrifuge tube and washed by two separate additions of 400 µl of 70% v/v ethanol. Finally, the DNA was dissolved in 500 µl Buffer TE.

The mass and purity of DNA recovered was quantified as described in 2.3.4.

2.5 Glycerol stocks

Once plasmids had been confirmed by restriction digest and sequence verification, glycerol stocks were made using standard aseptic technique within a category 2 laminar flow hood as follows: in a sterile microfuge tube 800µl of bacterial culture was thoroughly combined with 200 µl of sterile glycerol and placed at -80°C for long term storage.

2.6 Primer design

Due to incompatible flanking restrictions sites for cofilin and the mutant gene variants, the inserts were cloned by PCR. Primers were designed to include compatible sites for subcloning into the pclink vector.

Due to the small size of the R-pre sequence, PCR was used for cloning to reduce the risk of subcloning the wrong section of the plasmid.

AIP-1 was directly cloned by PCR from chick cDNA.

All primers were designed to have flanking sequences containing convenient sites for restriction digest whilst following the general rules of primer design that have previously been described (Dieffenbach, Lowe and Dveksler., 1993).

Eurofins was used to synthesize the custom primers, described in *Table 2-4*, and were reconstituted in molecular biology grade water to give a final concentration of 100 µM.

Table 2.4. Custom designed primers.

Sequence (5'-3)	Forward	Reverse complement	Restriction site	Gene
aattagatct ATG GCC TCC GGT GTG GCTG	✔		Bgl II	Human cofilin, Human cofilin R21Q
aattagatct ATG GCC GCC GGT GTG GCTG	✔		Bgl II	Human cofilin S3A
aattagatct ATG GCC GAA GGT GTG GCTG	✔		Bgl II	Human cofilin S3E
atataagctt CAA AGG CTT GCC CTC GCTG		✔	Hind III	Human cofilin, Human cofilin S3A, Human cofilin S3E
atatctcgag TTA CTT GTA CAG CTC GTC CATG		✔	Xho I	Human cofilin-GFP, Human cofilin S3A-GFP, Human cofilin S3E-GFP, Human cofilin R21Q -GFP
aattggatcc ATG GCC TCC TCC GAG GAC GT	✔		Bam HI	R-pre
atatgtcgac TTA CAT ATT ACA CAT CTG GC		✔	Sal I	R-pre
attaggatcc ATG AGG ATG CCG TAC GAG ATC	✔		Bam HI	AIP-1
atgtaagctt ATT GTA GGA AAT AGA CCA TTC		✔	Hind III	AIP-1

2.7 Polymerase chain reaction

Genes were cloned using PCR. The reaction mixture was made in molecular biology grade water (Sigma) to a total volume of 50 µl as follows: 0.1 µg template DNA; 1x manufacturer's polymerase buffer (Promega); 10 nmol dNTPs; 25 pmol of each primer; appropriate units of *Pfu* DNA Polymerase (Promega) used according to manufacturer's instructions. The mixture was gently mixed then placed into a programmable heat cycling block (SimpliAmp Thermal Cycler, Applied Biosystems by Life Technologies) and initially heated to 94°C for two minutes. A 30 second (sec) DNA strand melting step was followed by a 45 sec annealing step at 50°C. This was followed by an extension step which lasted 1 min per kilobase (Kb) of final PCR product. Melting, annealing and extension steps were repeated a further 34 times, followed by a final heating to 72 °C for 10 min and then cooled to 4°C until the tube was collected. A 5 µl aliquot was taken from the tube, combined with DNA loading buffer and subjected to electrophoresis on a 0.8 % w/v agarose gel to verify that the amplicon was of the predicted size.

2.8 PCR product purification

QIAquick PCR Purification Kit was used to remove unwanted primers and impurities such as salts, unincorporated nucleotides, agarose, or dyes, any of which can affect subsequent processing. Purified PCR products were then digested with the appropriate restriction enzymes at 37 °C, overnight. Digested products were then combined with DNA loading buffer and subjected to electrophoresis on a 0.8 % w/v agarose gel and gel purified to remove enzymatic contamination.

2.9 Gel purification of DNA

QIAquick Gel Extraction Kit was used to clean the DNA fragments from enzymatic reactions, and remove unwanted impurities such as salts, agarose, or dyes, any of which can affect subsequent processing.

After suitable restriction digestion, DNA was electrophoresed at 100V on a 0.8% w/v agarose gel in TAE buffer containing 1:20,000 Sybr Safe (Life Technologies) until DNA bands could be resolved and the appropriate fragment excised and placed into a microfuge tube. The DNA was purified using a QIAquick Gel Extraction Kit.

The volume of gel was estimated by weight, with 100 mg ≈ 100 µl. Three volumes of buffer QG (a proprietary chaotropic salt solution, containing an integrated pH indicator that enhances DNA binding to the silica membrane) were added and incubated at 50°C for 10 minutes, vortexing every 3 minutes. If the color of the mixture is orange or violet, then 10 µl of 3M sodium acetate was added to the dissolved gel solution to ensure the correct pH as indicated by a yellow colour. The solution was then added to a QIAquick column and spun at 13,000 rpm for 1 min. The column was washed with 750 µl buffer PE (a low salt, high ethanol proprietary solution) and the column centrifuged at 13,000 rpm for 1 min. The flow through was discarded and the column was spun for a further 1 min at 13,000 rpm to remove residual ethanol. The column was transferred to a fresh microfuge tube and 30 µl of molecular biology grade water was added to the column, then incubated for 1 minute before a final spin at 13,000 rpm for 1 min to elute the DNA.

2.10 Ligation

The following reaction mixture was made up to a total of 10 µl in molecular biology grade water: 1 µl 10X T4 ligase buffer (300 mM Tris.HCl, pH 7.8; 100 mM MgCl2; 100 mM DTT and 10 mM ATP; Promega); approximately 80 ng restriction digested backbone; approximately 240 ng restriction digested insert; a minimum of 2 U T4 DNA ligase (Promega).

The amount of cDNA was estimated by comparison to known amounts of DNA in standard size marker ladders in an agarose gel. The mixture was incubated overnight at 14°C. 1 µl of ligation product was used to transform bacteria.

2.11 Bacterial transformation

The following was carried out using standard sterile practice. A 40 µl aliquot of competent DH5α *Escherichia coli* (NEB) was allowed to thaw on wet ice. To this, 1 µl of plasmid DNA was added and the tube tapped gently to mix. The bacteria were left on ice for a further 15 min. They were heat shocked by being placed at 42°C for 45 seconds and then returned to the ice for a further 2 min. Following this, the bacteria were added to 1 ml of SOC (LB containing 20 mM glucose, 10 mM $MgCl_2$ and 2.5 mM KCl) and placed in a shaker at 37°C for 1 hour to allow expression of antibiotic resistance proteins. The bacteria were harvested by centrifugation at 4,000 rpm for 2 min at 4°C, 800 µl of the supernatant was removed and the bacteria gently resuspended in the remaining liquid then plated out on an agar culture plate containing the appropriate selection antibiotic.

2.12 Primary cell culture techniques

Primary neurons do not grow and divide in culture like cell lines and have a limited period of use during which axonal growth cones can be observed in isolation. Therefore, it was necessary to prepare freshly isolated dorsal root ganglia (DRG) neurons for each experiment.

2.12.1 Isolation and embryonic chick dorsal root ganglia

Fertilised brown chicken eggs were obtained from Henry Stewart and Co. Ltd (Lincolnshire. UK) and incubated pointed end down in a humidified, forced-draft incubator (Lyon, USA) at 38°C. Embryos were staged according to (Hamburger and Hamilton, 1992).

Dorsal root ganglia were dissected from the embryos after 7 days of incubation. Eggs were swabbed with 70% ethanol and a small hole was made off centre of the shell and the top cut off. The chicken embryo was separated from other contents with sterile forceps and scissors, placed into a sterile dish containing Leibovitz's L-15 medium (L-15; Gibco) and the head removed. The head, eyes, limbs and tail were checked for normal anatomy. After 2-4 min allowing for the blood to drain, the rest of the embryo was transferred to a fresh sterile petri dish containing ice-cold L-15 under a dissecting microscope, with the dorsal side facing up.

Forceps were used to gently immobilise the body and micro dissecting scissors used to cut through the skin muscle of the chest wall parallel to the spinal column. Organs in the chest and abdomen were carefully removed with forceps, the tail

cut off and the skin peeled away from the dorsal side, with care taken not to damage the spinal column.

The spinal column was cut along the length of the dorsal side to expose the neural tube which was gently peeled out of the spinal canal. The magnification was increased to better view the DRG that sit in a chain linked by connective tissue along the lateral sides of the spinal column. The chain of DRG were gently teased out of the vertebrae from the inside of the spinal canal. The newly freed DRG were then separated from any residual spinal nerves and connective tissues, and placed in a 15ml falcon tube, covered with a little L-15 medium. Typically, 10-15 DRG were obtained from each side of the embryo.

DRG were either prepared for culturing as explants or dissociated cells.

2.12.2 Preparation of explant cultures

Explants are ideally suited to optimising drug concentrations and immunochemical conditions or examining endogenous protein levels by immunochemistry. Axons grow out radially from the cell body mass forming a “halo” with numerous growth cones at the distal end of the axons.

After dissection, 4 or 5 clean whole DRG were seeded directly on 13mm diameter glass coverslips (Karl Hecht , Thermo Fisher) that had been acid etched (1M HCl, 1 hour at 65 °C), ethanol sterilised, coated with poly-D-lysine (20 µg/ml, 1hour, RT) and laminin (20 µg/ml, at least 1 hour, 37°C).

Explant cultures were maintained in Neurobasal media supplemented with 180 mM HEPES, 0.5mM GlutaMAX (Gibco), 100 U/ml penicillin, 100 µg/ml streptomycin, 1x B-27 supplement for up to 18 hours before use.

2.12.3 Preparation of dissociated cultures

Dissected DRG were first spun at 800 rpm after dissection, the supernatant was removed and the DRG resuspended in Hanks Balanced Salt Solution without calcium or magnesium (Lonza). A second spin step was performed and the supernatant removed. The DRG were then enzymatically dissociated with 0.5 ml of trypsin. For the trypsin to work efficiently, the DRG were placed at 37°C for approximately 15 min.

After digestion, the trypsin was inhibited by the addition of prewarmed DMEM containing 10% (v/v) chick serum. Dissociation was then aided mechanically by trituration with a fire-polished glass Pasteur pipette. The mechanical dissociation step was kept to 5 or 6 cycles of mild filling and emptying of the pipette at approximately 1 cycle per 2 seconds, avoiding formation of bubbles in the cell suspension.

Cell numbers were then counted using a haemocytometer.

The cell suspension was then spun at 800 rpm, 5 min, RT, to remove the trypsin. The supernatant was discarded and the pellet resuspended in supplemented Neurobasal media for seeding or in P3 solution (Lonza) for nucleofection.

2.12.4 Electroporation

Freshly isolated DRG cells were electroporated using a 4-D Nucleofector Device X Unit (Lonza) with the P3 Primary Cell 4D-Nucleofector X Kit (Lonza) for high transfection efficiency and cell viability.

Dissociated DRG were centrifuged for 5 min, 800 rpm and the pellet was resuspended in P3 Solution (Lonza) with provided supplement added according to manufacturer's guidelines. For smaller Nucleovette strip (Lonza) reactions, $5x10^5$ cells were resuspended in 20 µl supplemented P3 solution and a total of 0.4 µg of DNA was added. For the larger Nucleovette (Lonza), $5x10^6$ cells were resuspended in 100 µl supplemented P3 solution (Lonza) with a total of 2 µg of DNA. If multiple constructs were to be expressed, plasmids were combined prior to addition to the cell suspension to enhance co-expression efficiency.

Once nucleofected, primary neurons were seeded at approximately 8.5 $x10^5$ cells per well on 13mm diameter glass coverslips (Karl Hecht, Thermo Fisher) that had been acid treated (1M HCl, 1 hour at 65°C), ethanol sterilised, coated with poly-D-lysine (20 µg/ml, 1hour, RT) and laminin (20 µg/ml, at least 1 hour, 37°C).

For live cell imaging, cells were seeded at a density of 2.5 x 10^5 cells on to 35mm glass-bottom Fluoro dishes (World Precision Instruments) that had been coated with poly-D-lysine (20 µg/ml, 1hour, RT) and laminin (20 µg/ml, at least 1 hour, 37°C).

Dissociated cultures were maintained in Neurobasal media (Gibco) supplemented with 180mM HEPES, 0.5mM GlutaMAX (Gibco), 100 U/ml

penicillin, 100 µg/ml streptomycin, 1x B-27 supplement (Gibco) for up to 18 hours before use.

2.13 Cell line culture

Unless otherwise stated all, cell lines used were cultured in Dulbecco's Modified Eagle's Medium (DMEM), containing 100 U/ml penicillin and 100 µg/ml streptomycin and 10 % (v/v) foetal calf serum. Cells were incubated at 37°C, 5 % CO_2, and were routinely passaged at 80-90 % confluency.

2.13.1 Transient transfection

Cells were transfected using Lipofectamine LTX (Invitrogen) following the manufacturer's protocol. Cells were grown until 40-80 % confluence was reached. An appropriate amount of sterile DNA was diluted in Optimem (Gibco), to a suitable volume for the size of the culture dish being used. If multiple constructs were to be expressed, plasmids were combined prior to addition to enhance co-expression efficiency. The specified amount of Lipofectamine LTX reagent required was added and the contents mixed by gently tapping the microcentrifuge tube. The transfection mixture was incubated for a minimum of 30 min at room temperature. Following this, the transfection mixture was added to the cell culture medium and the cells returned to the incubator overnight.

2.14 Western blotting

2.14.1 Preparation of cell lysates

To detect and analyse endogenous proteins and expression of fusion protein products from exogenous DNA transiently transfected in cell lines as previously described, the proteins were first extracted.

Cells were typically seeded in 6-well plates one day prior to experimentation. Where appropriate, cells were transfected and allowed to express the exogenous constructs for 18-24 hours, and up to 48 hours for knock down experiments. Growth media was removed from culture vessel prior to being placed on ice. Cells were washed with chilled PBS and 150 µl of HE lysis buffer was added. The dish was swirled to ensure coverage then left on ice for 10 minutes. The bottom of the culture vessel was scraped, the lysates collected in 1.5 ml microfuge tube and then spun at 13,000 rpm for 10 minutes at 4 °C. The supernatant was carefully transferred to a fresh microfuge tube without disturbing the pellet of non-solubilised cellular material. The supernatants were retained for further analysis.

2.14.2 Preparation of embryonic chicken brain lysates

Appropriately staged chicken embryos were removed from eggs and placed in a sterile dish containing chilled Ca^{2+} and Mg^{2+} -free Hanks' Balanced Salt Solution (HBSS) under a dissecting microscope. Embryos were immediately decapitated just above the forelimbs and body discarded. The brain was exposed, firstly by removing the tectum, then cutting along the midline of the face, which allows the head to be opened like a book and exposes blood vessels indicating where the metencephalon and mesencephalon lie. These vessels and overlying tissue were gently pulled away revealing access to the roof of the mesencephalon where the optic lobes are found. A bisection was made along the ridge, termed the tuberculum posterius that indicates the internal boundary between the diencephalon and mesencephalon. The neural tissue below this bisection was transferred to a new sterile dish containing fresh chilled HBSS. The upper spinal cord was removed and the reserved tissue placed into a clean 1.5 ml microfuge

tube. Residual media was removed and the mass of the tissue estimated by weighing. Three to five volumes of chilled HE lysis buffer was added and the tissue-lysis buffer mix was transferred to a borosilicate mini homogeniser (1ml, Fisherbrand). The homogenate was then transferred to a clean 1.5ml microfuge tube incubated at 4 °C for 30 min on a roller. The homogenate was then clarified to remove insoluble cellular contents by centrifugation at 13,000 rpm, for 10 min at 4 °C. The supernatant was retained for further analysis.

2.14.3 Protein quantification

A protein assay was carried out in order to estimate the amount of protein present in clarified lysates using a Pierce bicinchoninic acid (BCA) Protein Assay Kit (Thermo) according to the manufacturer's protocol.

Briefly, working reagent was prepared by combining 50 parts of BCA reagent A with 1 part of BCA reagent B. Bovine serum albumin protein standards (0.2-1.2 µg/ml) were prepared in a 96-well plate by diluting 2 mg/ml stock with the same diluent as the samples. However, as HEPES-EDTA (HE) lysis buffer contains more EGTA than the microplate assay can accommodate, the diluent lysis buffer was first diluted 1:10 with PBS before preparing the standards. The samples were also diluted 1:10 in PBS and 10 µl of both samples and standards were loaded into wells in triplicate.

Following 8 min incubation at RT, shaking on an orbital shaker (LSE Low Speed Orbital Shaker, Corning), absorbance was measured at 562 nm using a PHERAstar FS microplate reader (BMG Labtech) and the concentrations of each sample were calculated against the standard curve. Each sample was then

diluted in lysis buffer and 1x Laemmli sample buffer to give 1 mg/ml. Samples could then be stored at -20°C until required.

Table 2-5. SDS-PAGE gel percentages.

Protein size (kDa)	Gel percentage (%)
4-40	20
12-45	15
10-70	12.5
15-100	10
25-200	8

2.14.4 SDS-PAGE separation of proteins

Sodium dodecyl sulphate polyacrylamide gel electrophoresis (SDS-PAGE) was used to separate proteins according to their molecular weight. SDS was present to confer a negative charge to denatured proteins to maintain the linearised state and therefore, when a voltage was applied, migrate through the acrylamide matrix to the positively charged electrode. The resolution of the gel was adjusted by varying the amount of polyacrylamide (*Table 2-5*) to change the pore size of the acrylamide matrix – better resolution of smaller proteins (4-40 kDa) requires greater acrylamide concentration and vice versa for larger proteins (>200 kDa).

***Table 2-6. Gel recipes**. These volumes (in ml, unless otherwise stated) are for 40% Acrylamide/Bis solution 37.5:1 ratio and makes 2 gels.*

	Stack	*Resolve*				
%	4	7.5	10	12	15	20
40% Acrylamide/Bis	0.7	4.7	6.3	7.5	9.4	12.6
1 M Tris-HCl pH 6.8	0.88	-	-	-	-	-
1.5M Tris-HCl pH 8.8	-	6.25	6.25	6.25	6.25	6.25
10% SDS	0.07	0.25	0.25	0.25	0.25	0.25
10% APS	0.07	0.125	0.125	0.125	0.125	0.125
dd.H_2O	5.28	13.7	12.1	10.9	9.0	5.8
TEMED (µl)	2.5	2.5	2.5	2.5	2.5	2.5
Volume (ml)	7	25	25	25	25	25

SDS-PAGE gels were prepared according to the recipes in *Table 2-6* using the Mini-PROTEAN™ Tetra Handcast System (BioRad). Ammonium persulphate (APS) and N,N,N',N'-tetramethylethane-1,2-diamine (TEMED) were added last to initiate polymerisation of the acrylamide.

Each well was loaded with 25 µg of protein in Laemmli sample buffer and 5 µl BLUeye Prestained Protein Ladder (Gene Flow) was loaded at either end of the gel. The loaded gel was then immediately run at 200 mA on ice for 90 min. The buffers used are detailed in *Table 2-1*.

2.14.5 Membrane transfer

After separation of proteins by SDS-PAGE, gels were incubated in transfer buffer for 10 min to reach stability. This step was required to allow expansion of the gel as the polyacrylamide takes on water; unequilibrated gels can swell during transfer resulting in poor protein resolution. Proteins were then transferred to Immobulon-P polyvinylidene difluoride (PVDF) transfer membrane (Merck) by sandwiching the two together between chromatography-grade blotting filter paper

(GE Healthcare) and applying a constant current of 200 mA over the stack to enable efficient migration of the proteins towards the anode and bind the PVDF membrane.

To check efficient and even transfer, membranes were stained with the reversible dye Ponceau-S Red which non-specifically binds to protein. The dye was then washed off in H_2O without affecting subsequent processing.

2.14.6 Immunodetection and visualisation

After transfer, PVDF membranes were blocked with 5% (w/v) skimmed milk in tris-buffered saline with 0.1% Tween-20 (TBS-T) for one hour at RT to prevent non-specific binding of the detection antibodies. Blocked membranes were then incubated in primary antibody solution according to the details in table 2-6. Membranes were then removed from the primary antibody and washed in TBS-T three times for 5 min. Incubation for 1 hour at RT with appropriate secondary antibody conjugated to horse-radish peroxidase (HRP) followed with another set of washes (*Table 2-8*).

Proteins were visualised using enhanced chemiluminescence (ECL) detection reagent. This method involves the breakdown of the ECL detection reagent by the HRP conjugated to the secondary antibody.

Table 2-7. Primary antibodies.

Cat. #	Clone	Antigen	Host	Supplier	Developer	Application	Dilution
ADI-NBA-110-E	M2F6	Drebrin	Mouse	Enzo		ICC, WB	1:200, 1:1000
ab11062	NA	Cofilin	Rabbit	Abcam		ICC, IHC WB	1:200, 1:1000
		Cofilin	Mouse		J.Bamburg	ICC	
		phospho -cofilin	Rabbit		J.Bamburg	ICC	
ab173574	EPR8793	AIP-1	Rabbit	Abcam		ICC	1:100
PA5-27645		AIP-1	Rabbit	Thermo Fisher		ICC	1:100

Table 2-8. Secondary antibodies.

Cat. #	Target	Host	Conjugate	Supplier	Application	Dilution
A32723	Mouse IgG	Goat	AlexaFluor 488	Invitrogen	ICC	1:400
A-11034	Rabbit IgG	Goat	AlexaFluor 568	Invitrogen	ICC	1:400
A-11004	Mouse IgG	Goat	AlexaFluor 488	Invitrogen	ICC	1:400
A-11036	Rabbit IgG	Goat	AlexaFluor 568	Invitrogen	ICC	1:400
A9044	Mouse IgG	Rabbit	Horseradish peroxidase	Sigma	WB	1:5000
A0545	Rabbit	Goat	Horseradish Peroxidase	Sigma	WB	1:5000

2.15 Immunocytochemistry

Prior to staining, cells were seeded on to coverslips at a density of approximately 1 x 10^4 cells per 13mm diameter coverslip, and cultured for a minimum of two days prior to staining. All washes were carried out at room temperature, unless otherwise stated. Cells were fixed by adding matching volume of 4% w/v paraformaldehyde, prewarmed to 37°C, to the culture medium. This was then removed and replaced with fresh prewarmed paraformaldehyde and the cells fixed for 15 mins at 37°C. Following this, the coverslips were subjected to three

5 min washes with PBS. Non-specific binding was pre-blocked by incubation at room temperature in lysine block for 1 hour. Primary antibodies (*Table 2-7*) were diluted in lysine block and 50 µl applied to each coverslip to cover it completely, and left for one hour at room temperature.

The coverslips were then washed three times for 5 minutes with PBS. The appropriate fluorescently conjugated secondary antibodies (*Table 2-8*) were diluted in lysine block and applied as for the primary antibodies and incubated for a minimum of 1 hour at room temperature. Where required, fluorescently conjugated phalloidin (Molecular Probes) to mark F-actin was added at 1:50 to the secondary antibody solution. Coverslips were then washed three times for 5 minutes with PBS. Where appropriate, to stain nuclei, the final wash was replaced with 4,6- diamidino-2-phenylindole, dihydrochloride (DAPI, Invitrogen) at 1:1000 in PBS. After blotting off excess PBS, coverslips were mounted on Superfrost slides (VWR) in Fluorsave (Calbiochem) and left to cure for 24 hours, in the dark, at room temperature. Images were captured using a Leica SP8 confocal microscope.

2.16 Preparation of J20 mouse brain slices

PFA-perfused whole brains of J20 mice and wild type counterparts were kindly gifted by Tom Ridler (University of Exeter). Brains were equilibrated in 30% sucrose for up to 48 hours prior to snap-freezing and storage at -80°C.

Frozen brains were mounted in Cryo-M-Bed (Bright Instruments) on to a temperature controlled stage (Solid State Freezer, Bright Instruments) set at around -15°C and 30 µm sections were cut using a retracting base sledge

microtome (Bright Instruments). Sections were placed in to PBS before immunohistochemistry.

2.17 Immunohistochemistry

Microtome cut free-floating sections were placed into wells of a 12-well plate and preblocked in lysine block, rocking, for 1 hour at room temperature. Primary antibodies were diluted in lysine block at appropriate concentrations (table 2-6) and sufficient volume (500 µl) applied to each well section to cover it completely for 1 hour, rocking, at room temperature. Sections were washed three times for 15 mins with PBS. The appropriate fluorescently conjugated secondary antibodies were diluted and applied as for the primary antibodies (table 2-7). Sections were then washed for 15 minutes with PBS three times. Sections were then mounted onto Superfrost slides and allowed to air dry. Sections were sealed with Fluorsave under a coverslip and cured for 24 hours in the dark, at room temperature. Images were captured using a Leica SP8 confocal microscope.

2.18 Microscopy

Phase contrast live cell time lapse imaging was performed using a Zeiss Axio Observer Z1 inverted widefield system, fitted with an AxioCam HRm charge-coupled device (CCD) camera, motorized stage, HAL 100 illuminator light source, and Plan-Apochromat x40 (1.3 NA) oil objective, temperature-controlled environmental chamber and CO_2 feed.

Fluorescent live-cell time-lapse imaging was performed using a Leica DMi8 inverted widefield system, fitted with a Hammamatsu digital camera C11440 ORCA-flash 4.0, LED external light source EL600, HC Plan-Apochromat x40 (1.3

NA) oil objective, motorised stage, and temperature-controlled environmental chamber (Pecon).

Fixed samples were imaged using a Leica TCS SP8 inverted confocal laser scanning system fitted with a piezoelectric stage and HC Plan-Apochromat x63 (1.4 NA) oil objective.

Leica Application Suite X was used on the PCs to control both Leica systems and AxioVision LE64 for the Zeiss system.

2.19 Image analysis

Fiji (Schindelin et al., 2012) was used for general manual image analysis.

Matlab and Statistics Toolbox Release 2012b (The Mathworks, Inc., MA, USA) with custom scripts was used for semi-automated image analysis as detailed in relevant results chapters. Scripts can be found in appendix G.

2.20 Statistical analysis

To assess within group differences of groups of three or more, a one-way ANOVA was used with a post-hoc Tukey test to determine where significant differences occurred for data that was normally distributed. For data that was identified as not normally distributed by Shapiro-Wilk normality test, a Kruskal-Wallis test with Dunns post hoc test was used to assess differences. A one sample t-test was used when comparing only two groups of normally distributed data, and the non-parametric counterpart, the Mann-Whitney U test, was used for non-normally distributed data. A *P* value of 0.05 or less was judged to be of statistical

significance. In most cases, medians are presented with interquartile range to provide information on variation within the data set.

CHAPTER 3

Drebrin is required to stabilise and maintain actin filaments during growth cone filopodia formation and maintenance

CHAPTER 3

3.1 Introduction

Drebrin has an established role in controlling morphology and motility in a range of cell types and is known to be essential for the formation and guidance of the leading process in migration of ocular motor neurons (Chilton and Dun, 2010; Dun et al., 2012). Whilst up or down regulation has profound effects on growth cone morphology *in vivo*, existing studies have focussed on drebrin's purported roles in stabilising the actin cytoskeleton to allow microtubule invasion to filopodia for growth cone turning and axonal branching (Geraldo et al., 2008; Ketschek et al., 2016). Crucially, these studies lack data on the fundamental mechanics of how drebrin responds to incoming guidance cues to drive formation of protrusions and allow precise wiring decisions.

The first step to understanding the behaviour of growth cone filopodia is to modulate drebrin and its binding to actin. Currently, very little is known about post-translational regulation of drebrin, which creates difficulty in experimental manipulation. There is some evidence to suggest phosphorylation by PTEN can modulate activity specifically at the synapse, however the exact process of cytoskeletal rearrangement in filopodia formation for direct motility has not been well characterised (Kreis et al., 2013). The CRAC channel inhibitor, BTP2, has been shown to block drebrin induced cytoskeletal rearrangements through a direct interaction at residues K270 and K271 which forms part of the actin-binding domain (Mercer et al., 2010). Conversely, co-localisation with F-actin remains unaffected, and when these residues were mutated, BTP could not bind but drebrin retained its function in protrusion formation, suggesting the mechanism is

not fully elucidated. Additionally, the role of calcium signalling is well known to affect growth cone morphology, and specifically filopodial behaviour (Gasperini et al., 2017; Gomez and Zheng, 2006); therefore, use of BTP2 could obscure direct cytoskeletal effects on filopodial behaviour making it an unfavourable option for drebrin manipulation.

Truncated Drebrin domains have previously been used to study the nuances of the protein's actin-binding and actin-remodelling behaviour (Hayashi et al., 1999), and can be exploited as experimental tools. Dun et al., generated two truncated forms of chick drebrin fused to fluorescent proteins – drebrin-N, including the highly conserved ADF-cofilin homology domain and the coiled-coil and helical regions terminating at amino acid 315; drebrin-C, containing the rest of the protein, which, in chick, shows most divergence and only has homology to the Homer-binding motif (*Fig. 3-1*) (Dun et al., 2012).

Drebrin has 5 potential functional domains that were identified by in silico analysis (Worth et al., 2013). The actin-depolymermising domain factor homology (ADF-H) appears to only interact with F-actin and does promote disassembly domain. Expression of the coiled-coiled (CC) or helical (HEL) domains alone or in conjunction with one another induced formation of F-actin rich filopodia to the same extent as the full-length protein. Interestingly, the increased filopodia formation induced by the HEL domain is suppressed in the HEL-proline rich region-blue box deletion construct (Worth et al., 2013). Further *in vitro* analysis using F-actin co-sedimentation assays showed the presence of separate F-actin binding regions in the CC and HEL domains. Worth et al., proposed that the blue

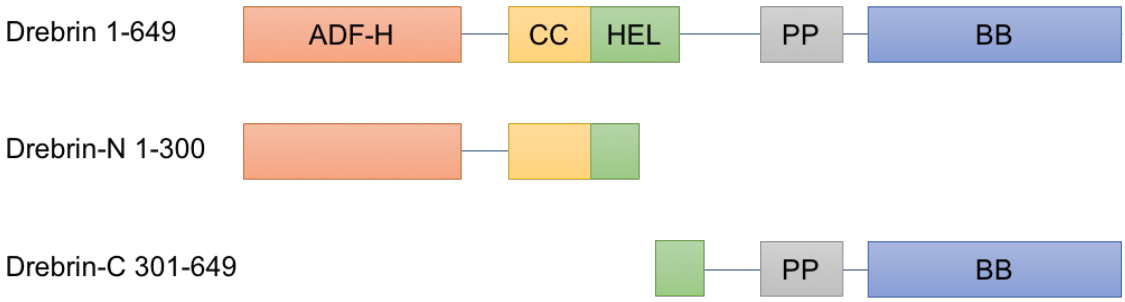

Figure 3-1. Schematic of drebrin protein domains. *Full length drebrin contains the following domains: ADF -H, actin-depolymerising factor homology domain (orange, residues 1-135); CC, coiled-coil domain (yellow, residues 167-256); HEL, helical domain (green, residues 176-355); PP, proline-rich region (grey, residues 364-417); BB, blue-box domain (blue, residues 431-649). Drebrin-N contains all domains between residues 1-300. Drebrin-C starts at 301 and comprises the C-terminus. Characterisation of debrin constructs showed that drebrin 1-300 binds F-actin with a similar affinity to the full length drebrin (Grintsevich et al., 2010). Further analysis demonstrated that the CC and HEL domains alone can induce filopodia, but the BB region is able to repress unless the CC domain is present, too (Worth et al., 2013).*

box (BB) and proline rich (PP) domains partake in an autoregulation by maintaining a ‘closed’ conformation. In this way, drebrin can bind F-actin to stabilise but cannot bundle or straddle adjacent filaments. Only on phosphorylation of S142 by CDK-5 signalling is the repression lifted allowing the CC and HEL domains to bind separate filaments, bundling them together.

Dun et al., (2012) had previously showed that the N-terminus induced formation of numerous filopodia-like protrusions in transiently transfected NIH/3T3 cells whereas the C-terminus significantly supressed spike formation. Drebrin-C also down regulated the effect of full length drebrin when the two were co-expressed suggesting it may have autoregulatory properties. These constructs were then electroporated into the oculomotor nucleus of chick embryos at HH stage 29. Both forms induced changes to the morphology of growth cones: drebrin-N growth cones appeared enlarged and axons displayed significant pathfinding defects, whereas drebrin-C axons grew normally but with varicosities along the length, and importantly, a significant reduction in the number of filopodia compared to controls. Only formation of the leading process was examined when drebrin was knocked down using shRNA and axon guidance was apparently unaffected. This suggests separate regulation of leading process and cell migration in axon guidance (Dun et al., 2012). Major questions remain. How can axons still make their targets with severely reduced numbers of filopodia? Conversely, how do too many filopodia abrogate accurate guidance?

These findings begin to undermine the central dogma that growth cone filopodia are required for pathfinding. Observing the dynamic nature of filopodia led to the suggestion that their primary function was to interpret signals that regulated

growth cone behaviour. Filopodia isolated from their parent growth cone *in vitro* still maintain the ability to transduce incoming signals that allow autonomous responses (Davenport et al., 1993). *In* vivo, the extension of numerous filopodia occurs when a growth cone enters a new area or where a directional choice is required. This behaviour suggests growth cones are actively sampling the local environment for cues that will direct growth (Dent and Gertler, 2003; Gupton and Gertler, 2007). However, a growing body of evidence suggests that under certain conditions, neurons can pathfind without the presence of filopodia (Marsh and Letourneau, 1984). Retinal ganglion cells with suppressed filopodia were able to navigate along the optic pathway without noticeable guidance faults but were unable to branch correctly in the tectum (Dwivedy et al., 2007). This study highlights that filopodia may not be essential for all types of navigation, a phenomenon that extends beyond the development of the nervous system (Wacker et al., 2014).

Whilst it is already well established that the growth cone is highly specialised and has some independent function, a growing body of evidence is beginning to show that growth cone filopodia and those found along the axon fulfil distinctive roles. During the undertaking of this thesis, (Ketschek et al., 2016) demonstrated that drebrin promotes axonal filopodia formation involved in axon branching through the prior development of actin patches (Spillane et al., 2011). Surprisingly, a similar link between filopodia formation and drebrin has yet to be demonstrated for the growth cone.

The following figures will focus on growth cone filopodia by manipulating drebrin using the truncated domains (gifts of Dr J. Chilton). Here, I hypothesise that

drebrin directs motility by stabilising the bases of active filopodia. I will also describe my development of tools for visualising the growth cone and measuring growth cone dynamics.

3.2 Results

3.2.1 Drebrin localisation in fixed and live dorsal root ganglia neuronal growth cones

To assess endogenous drebrin expression, embryonic day 7 dorsal root ganglia were grown as explants before fixation and immunolabelled with drebrin monoclonal antibody (M2F6). Endogenous drebrin mostly localised to the peripheral domain of non-stimulated growth cones (*Fig. 3-2A*). The fluorescence intensity was seen to reduce towards the distal end of filopodia which suggests a concentration gradient and therefore a reducing level of actin stability towards the portion of the growth cone which is under constant morphological change. Greatest overlap with F-actin occurs at the base of filopodia (*Fig. 3-2A*, merge), an area that, during filopodia formation, requires filaments to be bundled and stabilised to support extension of the growing filaments (Sasaki et al., 1996).

To examine the temporal relationship between drebrin localisation and filopodia extension, embryonic day 7 dissociated dorsal root ganglia neurons were nucleofected with full-length (FL) drebrin-YFP and live filmed using 2-channel fluorescence microscopy. Expression of drebrin in live neurons mimicked fixed examples in all growth cones observed (*Fig. 3-2B*), and drebrin enrichment occurred prior to the extension of, or formation of new branches from, existing filopodia and nascent protrusion sites at the edge of the lamella (*Fig. 3-2C*). This enrichment appears to be delivered in discrete puncta in some instances. Puncta of drebrin were seen in all growth cones observed. These structures are likely to be associated with actin patches in a process that has already been documented in axonal filopodia formation (Ketschek et al., 2016), but not in the growth cone.

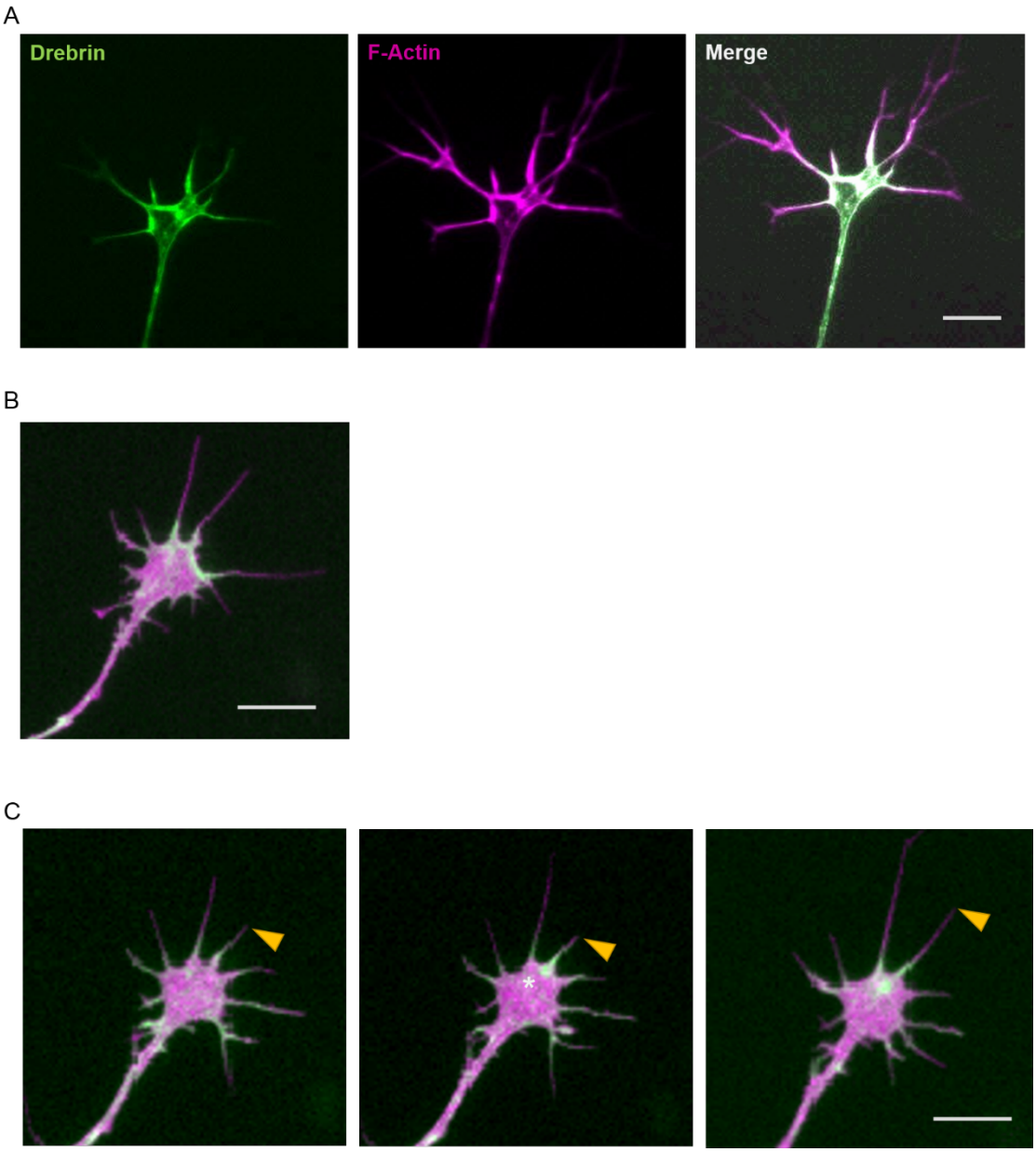

Figure 3-2. Drebrin is largely restricted to the distal area of the growth cone and enriches at the base of extending filopodia. (A) *Drebrin (green) strongly co-localises with F-actin (magenta) at the base of the filopodia with little occurring past the first third of the filopodium. Phalloidin conjugated to a fluorophore has been used as a counterstain to visualise F-actin in fixed DRG explant growth cones.* ***(B)*** *Drebrin localisation is similar in live dissociated DRG neurons co-nucleofected with full-length drebrin-YFP (green) and RFP-R-pre (magenta).* ***(C)*** *Patches of drebrin locates to filopodia base (asterisk) prior to filopodial extension (arrow head) during live cell imaging. Scale bars represent 10 µm. See Appendix A for Supplementary Media File 1.*

3.2.2 Effect of drebrin overexpression on the stability of filopodia

To examine the effect of drebrin at the level of the growth cone, the full-length and truncated forms of the protein were transiently expressed in dissociated dorsal root ganglia growth cones and imaged at 37°C with CO_2 feed. Expression of the constructs was first confirmed by briefly visualising the fluorescence of the cell. Phase-contrast microscopy was selected for continued live cell imaging as drebrin fusion construct products have inherently discrete and restricted expression patterns and fluorescence microscopy would only allow observation of these areas, leaving other details of morphological complexity obscured (Dun et al., 2012). Additionally, endogenous and fluorescent molecules tend to release reactive chemical species when illuminated by an epifluorescent light source or laser, particularly at shorter wavelengths.

Preliminary observations highlighted a clear difference in morphology. Growth cones of drebrin-C expressing neurons were largely collapsed with few axonal filopodia present, some displaying curved tips. Varicosities were also seen along the length of the axon which are likely to be formed from collapse of lamella-like actin structures (*Fig. 3-3A*). Growth cones expressing full-length drebrin showed similar morphology to control counterparts with a more defined growth cone structure and filopodia protruding from the edge of a central lamellum. Drebrin-N expressing neurons displayed a thicker axon, with a 4-fold increase in the mean number of filopodia per 50 μm of cell perimeter when compared to the YFP control, although this did not reach significance ($p=0.0571$, Mann-Whitney U-Test) (*Fig. 3-3A & B*). When the length of the axons was measured, there was a trend toward C-terminus expressing neurons to have longer axons (*Fig. 3-3D*). Measuring the distances growth cones moved forwards or backwards could

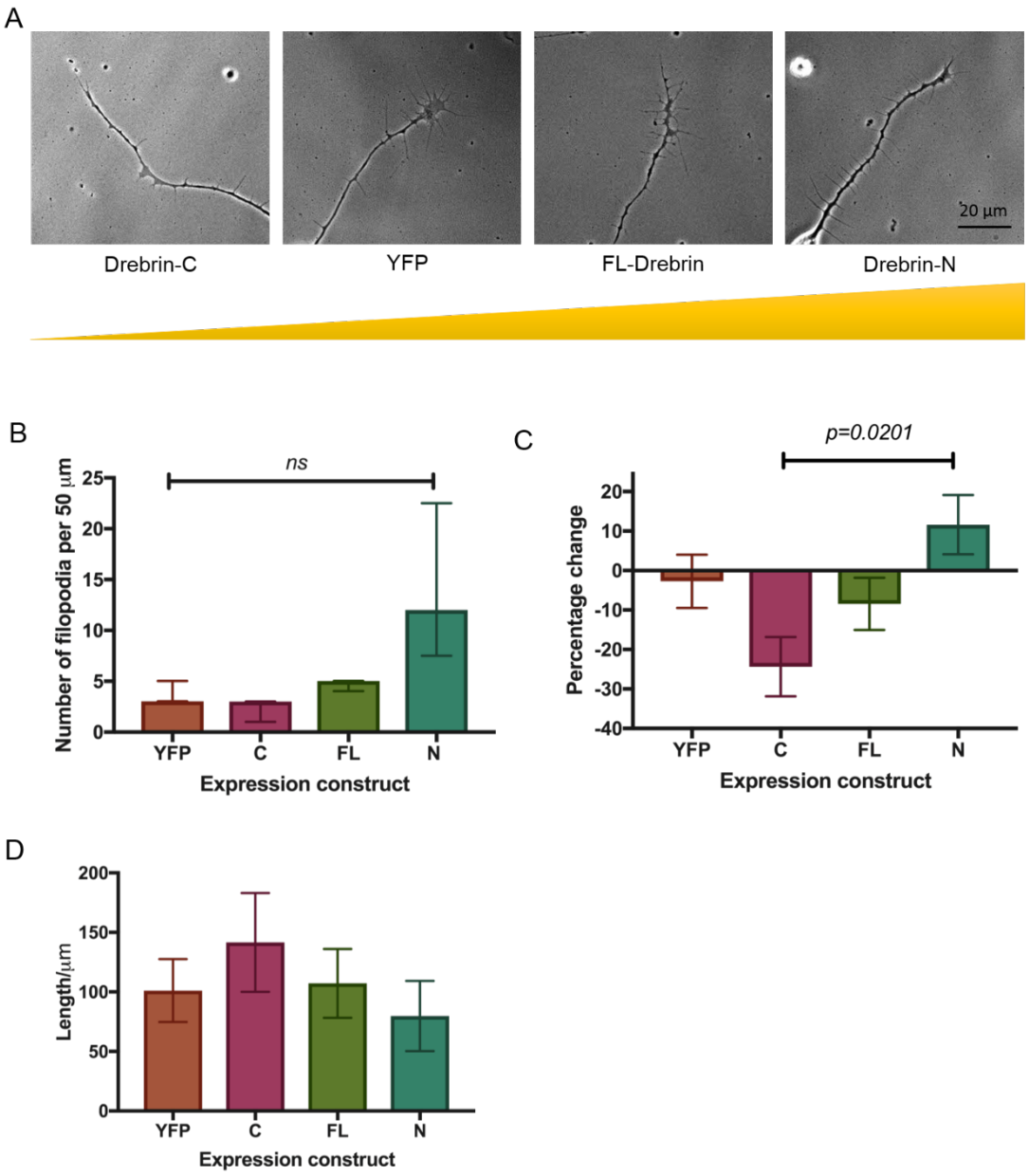

Figure 3-3. Drebrin modifies stability of filopodia. *Overexpression of drebrin constructs in dissociated dorsal root ganglion sensory neurons at E7* ***(A)*** *shows a trend towards an increase in the number of filopodia and increasing drebrin activity* ***(A)****, quantified in* ***(B)*** *displayed as median number of filopodia (+/- IQR), Mann-Whitney U-Test for significance between drebrin-N overexpression and control shows the increase in the number of filopodia does not quite reach significance (p=0.0571). Initial manual analysis shows net mean change in the percentage of filopodia* ***(C)*** *during filming is significantly decreased when drebrin-C is overexpressed compared to drebrin-N overexpression (p=0.0201), Kruskal-Wallis ANOVA with Dunn's post hoc multiple comparison test. Surprisingly, drebrin-C overexpressing neurons trend towards longer axons* ***(D)****. For all, n=>2 on three separate experimental days. Stills are representative of each condition, scale bar in A = 20 µm.*

provide an interesting insight into whether the structures are able to move in the absence of filopodia. However, the period assayed in this experiment was too short to capture any meaningful extension or retraction of the growth cone. The first frame of each phase-contrast film was firstly manually analysed to simulate fixed-cell experiments but abrogate any artefacts incorporated during the fixing process. As an initial assessment of stability, the number of filopodia between the first and the final frame was quantified and presented as percentage net change to show to what level the number of growth cone filopodia persisted. The net change was calculated by subtracting the number of filopodia remaining in the final frame from the original number in the first frame. The difference was converted to a percentage. A reduction was presented as minus (-) percentage and an increase was presented as a positive (+) percentage. This denotes whether the truncation was associated with an increase or reduction in filopodia formation. Drebrin-C expressing growth cones had a mean reduction of 24% of filopodia from beginning to end of the filming period, with an 12% mean increase in filopodia number when expressing drebrin-N which was statistically significant ($p=0.0201$) (*Fig. 3-3C*).

This initial analysis suggested there was a difference in the truncated drebrin domains, therefore parameters of growth cones in every frame of each film were manually extracted by plotting the X and Y coordinates for bases and tips of each filopodia for every frame using the FIJI plugin Manual Tracking. The coordinates were then reconstructed in Matlab using the custom-written script *tipTracks2*, and filopodial lengths were extracted and plotted for each frame.

To assess filopodial dynamics over time, the X, Y co-ordinates of the tip and base of each filopodium was recorded using FIJI, manual tracking plugin. The lengths between corresponding tips and bases were automatically extracted using the custom Matlab script *tipTracks2*. There was a significant difference in filopodial length between full-length drebrin and the truncated proteins compared to the YFP control (*Fig. 3-4*). Filopodia of drebrin-C expressing growth cones had the largest range in length compared to other constructs.

A

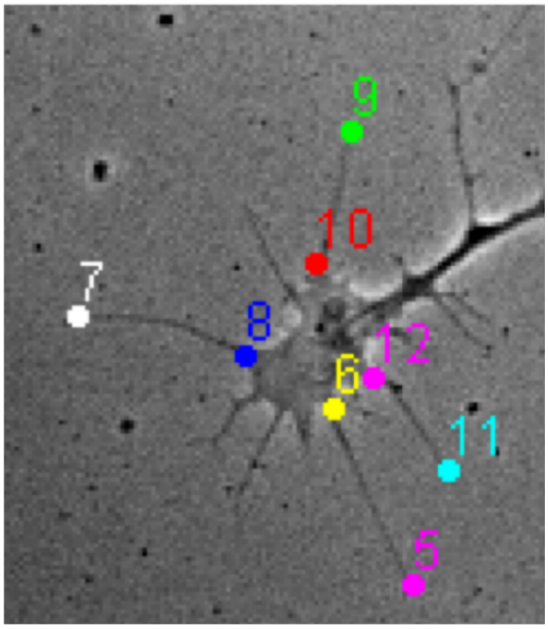

B

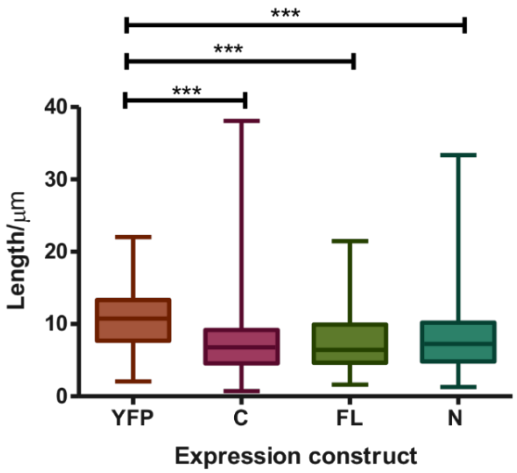

Figure 3-4. Drebrin overexpression results in shorter filopodia.
(A) *Representative image of manual tracking using FIJI. Tips and bases of individual filopodia were traced as separate tracks through each frame of the films. This tracking recorded the X,Y coordinates for each point. A custom* Matlab *script, tipTracks2, was then used to calculate the distance between the corresponding tip and base.* ***(B)*** *Expression of the drebrin constructs resulted in significantly shorter filopodia compared to the YFP control (P<0.001, Kruskal-Wallis test with Dunn's multiple comparison test. Filopodia of at least 3 growth cones measured per condition).*

3.2.3 Growth cone complexity and phasic behaviour visualised by genetic membrane marker

3.2.3.1 Construction of R-pre-mRFP expression vector

As described in 3.2.2, phase-contrast microscopy was used to overcome the effects of phototoxicity and restricted expression patterns. However, an additional and major limitation of the technique is in the speed of extraction of meaningful information from the films. Phase-contrast converts the otherwise invisible phase changes in light passing through the specimen into brightness changes. Whilst these changes in brightness become visible to the human eye, automated image processing and analysis becomes problematic as the first step typically requires thresholding which converts all pixels to either black or white according to whether the grey-scale intensity values fall below or above a predefined constant, respectively. Specimens such as growth cones are typically very thin and thus the brightness changes are minimal in phase contrast images. Bright halos are another troublesome image distortion caused by diffracted light passing through the phase ring, and precise object segmentation becomes difficult to guarantee.

To overcome these confounding factors, R-pre-mRFP fusion construct was used to mark the membrane, a previously described and characterised fluorescent reporter for the plasma membrane originally designed as a probe for assessing membrane surface potential in macrophages (Yeung et al., 2006). R-pre is based on the C-terminus of K-Ras which associates with the plasma membrane in a charge dependent manner, and has been rendered non-phosphorylatable and resistant to ubiquitination by substitution of serine and threonine residues to alanines, and lysines to arginines respectively.

R-pre, from Addgene, was first cloned R-pre-mRFP and the restriction sites HindIII and Xho1 added by PCR. The fragment was then digested and ligated into a backbone containing the chick β- actin promoter, pCAβ, which has increased expression efficiency in chick when compared to the original vector which uses only a CMV promoter (*Appendix F*). The resulting construct was expressed in NIH/3T3 fibroblasts to confirm R-pre-mRFP localised to the plasma membrane as expected. The fluorescent product was bright and appeared to tolerate extended periods of illumination during imaging without significantly noticeable levels of bleaching (*Fig. 3-5A*).

3.2.3.2 R-pre-mRFP expression in neurons

R-pre-mRFP was nucleofected into dissociated E7 dorsal root ganglia neurons which were cultured overnight and fixed the next day. The fixed neurons were counterstained with fluorescently labelled phalloidin to mark F-actin. Under widefield microscopy, R-pre-mRFP appeared to localize to the cytoplasm as well as the plasma membrane of the neuron when compared to expression in NIH/3T3 fibroblasts (*Fig. 3-5*). This disparity is likely a consequence of the relative thinness of a growth cone and the spatial plane in which the filopodia are in focus such that perceived cytoplasmic signal is in fact coming from the basal plasma membrane of the neuron.

Observations by confocal fluorescence microscopy in neurons revealed that F-actin staining decreases in intensity towards the distal end of the filopodium (*Fig. 3-6A*). The contiguous expression of R-pre-mRFP along the membrane made discrimination of the filopodium tip more accurate by eye for data extraction from

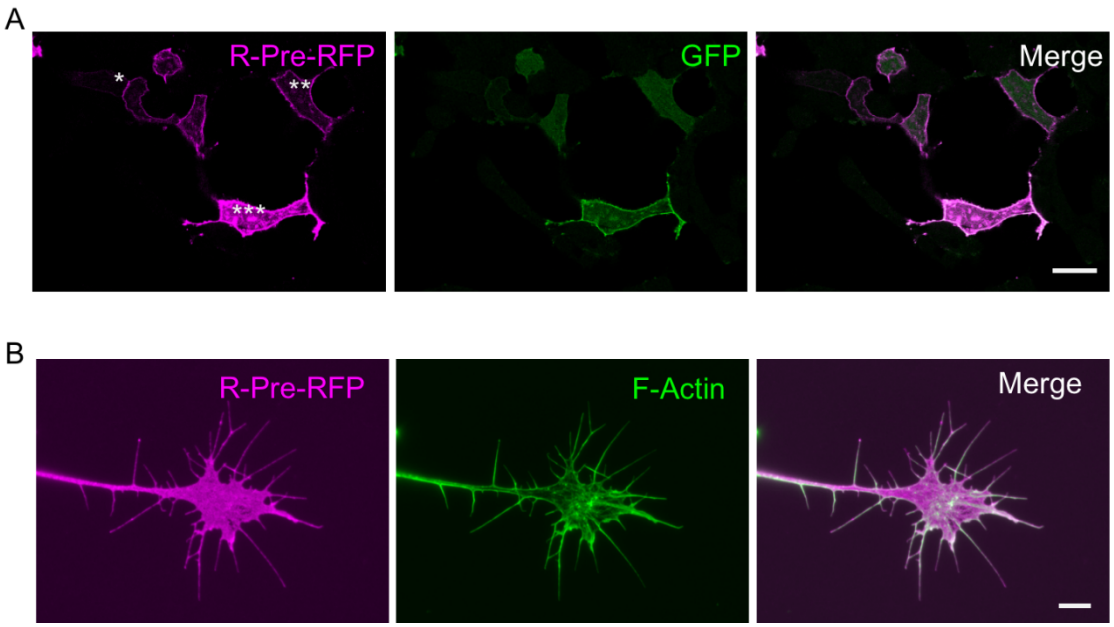

Figure 3-5. R-pre-mRFP expression in 3T3 fibroblasts. (A) *R-pre-mRFP localises to the plasma membrane in transfected 3T3 fibroblasts. Two-channel confocal images at 40x showed relative levels of expression: High = ***; Medium =**; Low =* ; scale bar = 25 μm.* ***(B)*** *Localisation of R-pre-mRFP in neurons initially appeared to localise in the cytoplasm as well as at the membrane, however this is likely a consequence of the thinness of a growth cone and the spatial plane in which the filopodia are in focus. Representative images (A,B) taken using confocal at 63x, scale bar = 7.5 μm.*

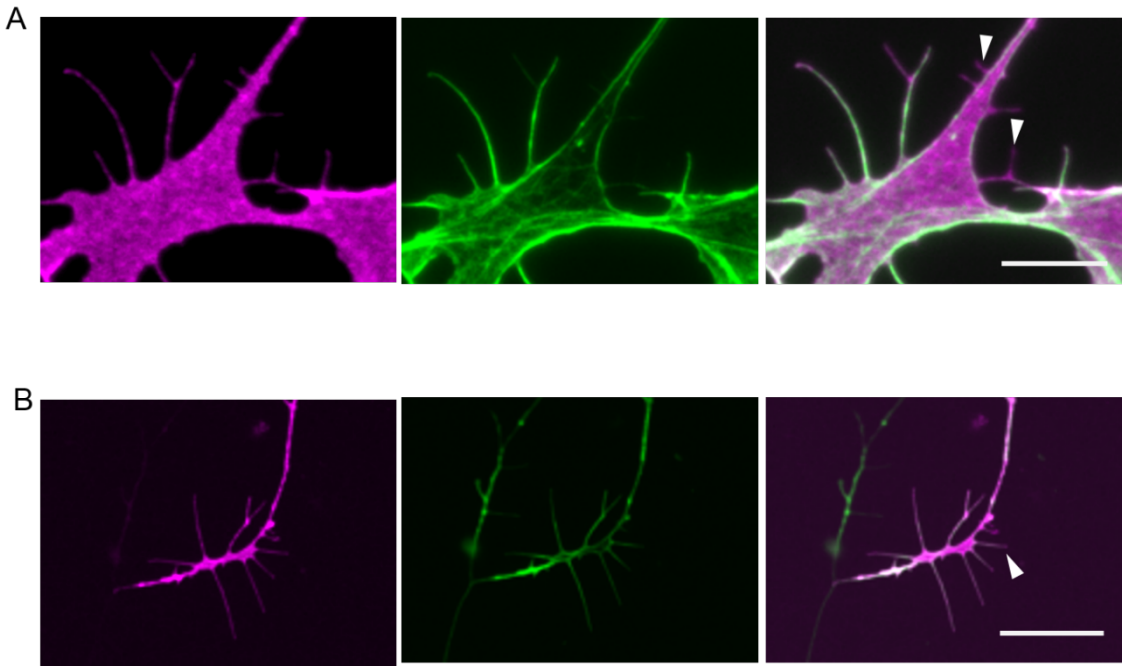

Figure 3-6. R-Pre-mRFP can be used as a marker to highlight membrane complexity *that could otherwise be missed using conventional methods.* ***(A)*** *Dissociated dorsal root ganglion sensory neurons at E7 expressing R-pre-mRFP (magenta) were fixed, co-stained with labelled phalloidin for F-Actin (green) and imaged by confocal microscopy. Filopodial tips were more accurately distinguished (white arrows merge image A) compared to when assessing F-Actin alone. Some protrusions were not detected by labelled phalloidin staining. Representative images taken using confocal at 63x, scale bar = 7.5 μm. White arrow heads in* ***(B)*** *indicate filopodia-like protrusions without detectable F-actin staining. This loss of information is amplified when images are taken at 40x using a widefield epifluorescent microscope and CCD. Representative images, scale bar = 25 μm.*

images. Furthermore, when R-pre-mRFP expressing neurons were imaged by widefield epifluorescence the drop-off in labelled phalloidin fluorescence intensity was even more noticeable (*Fig. 3-6 B*).

For widefield epifluorescent live-cell imaging, R-pre-mRFP nucleofected dissociated E7 dorsal root ganglia neurons were grown on filming dishes overnight and imaged the next day. Exposure time and illumination intensity were lowered to reduce phototoxicity and camera binning increased to 2x2. Binning combines the charges from adjacent CCD pixels which increases signal to noise ratio but reduces spatial resolution. These optimisations allowed imaging of the fluorescent product at relatively short intervals over an extended period with little effect on neuronal viability.

The custom written Matlab script *fILMv5* was used to first manually set the threshold to allow accurate segmentation of the objects to be measured and then automatically extract the number of growth cone filopodia per frame. Manual thresholding was required because automatic estimations tended to lose fine detail of filopodia. As each filopodium was tracked between frames, filopodial life times and rates of extension and retraction could also be extracted.

When average filopodial length was plotted over time (*Fig. 3-7B*), the data revealed a sine-wave like oscillation which is interpreted as global periods of extension and retraction that describe exploratory behaviour in axon outgrowth in which a neuron undergoes substantial and continual morphological changes in stages as it forms new lengths of axon (Goldberg. D and Burmeister D, 1986). Periodic phases of increased activity were consistently observed in growth cones,

however, analysis was performed manually and therefore was challenging to quantify.

A

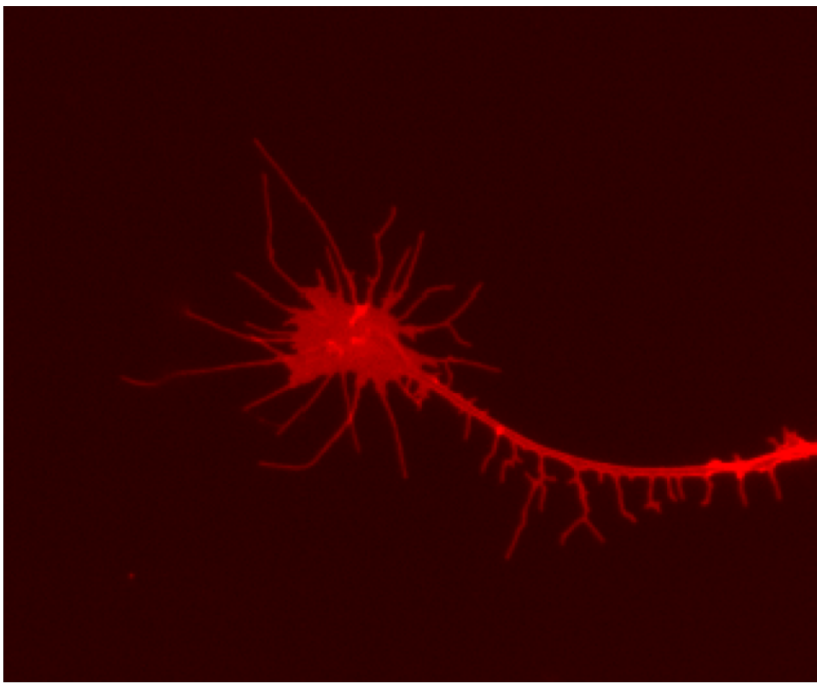

B

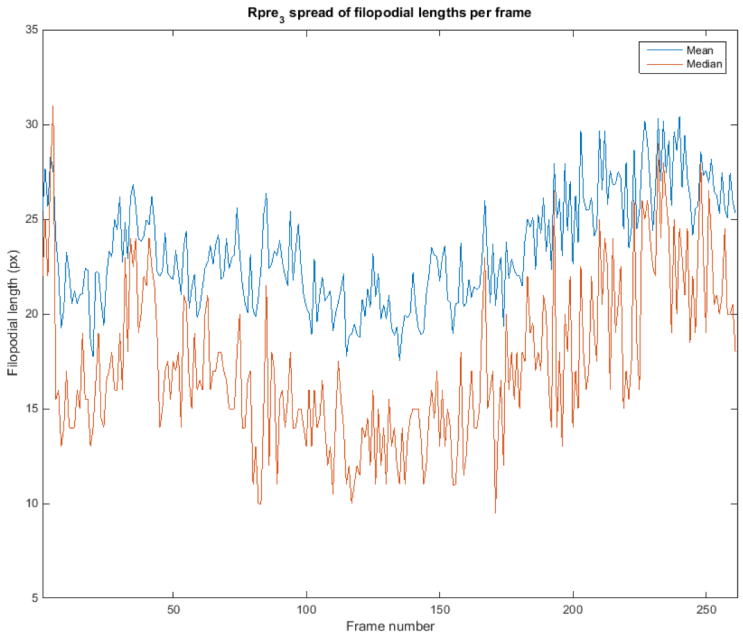

Figure 3-7. Live cell imaging of filopodia demonstrates periodicity of extension and retraction rates. (A) *Dissociated dorsal root ganglion sensory neurons at E7 expressing R-pre-mRFP were imaged every 15 seconds for 65 minutes. The custom written Matlab script fILMv5 was used to identify individual filopodia and measure the lengths every frame and produce graphical output* ***(B)****. The phasic nature of extension and retraction probably linked to growth cone pausing between periods of axonal extension. See Appendix B for Supplementary Media File 2.*

3.3 Discussion

Drebrin is known to be involved with development of the leading process, and that overexpression triggers and an increase in protrusion formation in neurons. It is largely unknown how drebrin is involved in directed motility. Truncated forms of drebrin expressed *in vivo* showed that drebrin-N, containing the actin-binding domain, had the strongest aberrant migration phenotype, whereas drebrin-C axons were correctly orientated but were thin with varicosities (Dun et al., 2012). Axon guidance appears unaffected, therefore separate regulation of leading process and axon guidance in individual cells may exist. The aim of this chapter was to understand how drebrin directs motility of filopodia of the neuronal growth cone. Using truncated drebrin constructs *in vitro,* these results demonstrate a strong trend towards filopodia of growth cones expressing drebrin-N being more persistent and those expressing drebrin-C display unstable, short filopodia. It is likely that the C-terminus plays a regulatory role which allows protrusions to maintain plasticity of the actin cytoskeleton for motility related remodelling. Furthermore, drebrin was observed at the base of filopodia, an area which requires stability to support the rest of the structure as it undergoes continuous extension and retraction during exploration of the environment. In addition, R-pre has been identified as a useful and novel genetic reporter of growth cone morphology and dynamics.

Filopodia are constantly undergoing rearrangement of their comprising actin filaments. This activity must be tightly orchestrated to produce directed motility. Filaments of actin form at the leading edge of a cell, force is exerted on the plasma membrane causing a protrusion to form. However, a filopodium will only extend if it can overcome the rigidity of the membrane. This process requires

filaments to be strong enough to withstand the opposing forces of the membrane. Filament bundling proteins contribute to structural strength by crosslinking filaments to increase the overall stiffness of the structure. There are more than 23 different classes of proteins that crosslink F-actin in a similar manner (Tseng et al., 2005). The extent of redundancy remains controversial, however many of these proteins display discrete subcellular localisation which suggests that each of these proteins has a specialised role in organising the formation and maintenance of filopodia.

Drebrin is enriched in areas of the growth cone that are required to be stable suggesting that increased bundling, and therefore increased stiffness, is required to allow the filopodium to continue to overcome the force of the bounding plasma membrane (Sasaki et al., 1996). More recently, biochemical assays using purified rabbit actin and drebrin showed that drebrin protects filaments from depolymerisation at the barbed end by wrapping around two protofilaments and "stapling" them together (Mikati et al., 2013).

Growth cone filopodia express receptors on their surface in order to probe the local environment and the structures themselves require a certain amount of freedom to explore the surroundings which is a likely explanation why endogenous drebrin is restricted to the proximal third of the filopodium. When the truncated form of drebrin which only includes the C-terminal portion of the protein is mis-expressed in neurons, the filopodia that form are small and unstable. Along the axon, they typically co-exist with large varicosities which are not normally seen in the wild-type axons. This truncated form lacks the "actin binding core" and therefore probably prevents the formation of longitudinal lateral contacts

when interacting with F-actin resulting in less or no bundling (Grintsevich et al., 2010; Mikati et al., 2013). In a functional cellular context, this is likely to prevent structural stabilisation for formation, resulting in filopodia that are more likely to buckle under the counter resistance of the plasma membrane, additionally preventing entry of exploratory microtubules which also provide support (Ketschek et al., 2016). Mathematical modelling of filopodial protrusion physics predicts that at least 10 bundled filaments are required to overcome membrane resistance and 30 or greater are required to resist buckling and allow elongation (Mogilner and Rubinstein, 2005).

Filopodia in live growth cones expressing drebrin-C display a reduced persistence time which also supports previously published biochemical evidence that full length drebrin prevents depolymerisation of filaments. Here, the mis-expressed truncated form of the protein may be outcompeting endogenous full-length drebrin, thereby acting in a regulatory manner. If the hypothesis that drebrin is providing stiffness to the filaments by bundling and thus allowing of elongation of filopodium is correct, we could expect filopodia in growth cones overexpressing drebrin to be longer. However, I have shown that filopodia of FL-drebrin over expressing growth cones do not have significantly longer lengths compared to the wild type counterparts and in fact show a trend towards being shorter. Again, mathematical modelling of protrusion physics predicts there is an inverse relationship between bundle thickness and filament length where more filament tips deplete G-actin (Mogilner and Rubinstein, 2005). If this prediction is applied to the condition of overexpression of FL-length drebrin one could speculate that increased concentration of drebrin would result in increased number of filaments bundled, affecting the balance of F:G actin ratios. This is

particularly apparent in growth cone filopodia expressing drebrin-N (containing the “actin binding core” of drebrin) which appear thicker, more stable and less dynamic in their movement. On the counter side, growth cone filopodia expressing drebrin-C are wavy and flaccid, a phenomenon that has been reported in mutants of other actin crosslinking proteins (Jaiswal et al., 2013; Okenve-Ramos and Llimargas, 2014; Vignjevic et al., 2003).

It is plausible that, if the C-terminus does perform an autoregulatory role, drebrin-N is free of repression normally conferred by the C-terminus and therefore also explains why overexpression of full-length drebrin results in shorter filopodia. Phosphorylation events could also modulate drebrin activity. Drebrin has a number of serine/threonine residues that can be phosphorylated; the majority reside in the C-terminal portion of the protein. Cyclin-dependent kinase 5 (cdk-5) can phosphorylate drebrin at S143 within the N-terminus and enhances its bundling activity (Worth et al., 2013). Mutation of the Cdk-5 phosphorylation site did not have any effect on neurite number or spine morphology, it did suppress radial migration in embryonic cortical neurons *in utero* suggesting it plays a role in directionality (Tanabe et al., 2014). Drebrin can also be phosphorylated at S647 by membrane depolarisation of neurons. Phosphatase and tensin homologue (PTEN) can reverse this phosphorylation and synaptic activity can initiate dissociation of two proteins, resulting in spatial separation, although the functional consequence of this event has not been examined (Kreis et al., 2013). It is possible that the differential phosphorylation of drebrin could result in regulation of its function.

Drebrin has also previously been reported to compete with other actin binding proteins such as α-actinin and fascin which cross-link filaments, and tropomyosin which stabilises filaments and also inhibits the ATPase activity of myosin which has been reported to slow retrograde flow (Hayashi et al., 1996; Ishikawa et al., 1994; Sasaki et al., 1996); the speed by which this actin sliding is decreased still remains to be independently confirmed (Ishikawa et al., 2007)

I further suspect there is an upper limit to which filament stiffness is beneficial for elongation and that actin binding proteins must respond to local structural requirements, however there is a paucity of biomechanical studies which have assayed single filaments and mathematical modelling of filament behaviour to support this theory (Claessens et al., 2006; Howard, 2008).

In a bid to automate quantitation of filopodial dynamics to yield higher throughput, genetic approach was used to mark the plasma membrane of the neuronal growth cone. This work has emphasised the extent of growth cone morphological complexity and it is possible that approaches that do not visualise the plasma membrane could miss detail. Attempts at automation also highlighted the challenges in automating analysis of microscopy images. Two major issues still plague its application to answering biological questions. Firstly, despite technological advances, the contrast between the region of interest to be analysed and the background is still causing issues decades on (Bradbury, 1979). The second setback is the complexity in the nature of biological samples themselves. In the case of the neurons assessed in this chapter, filopodia do not extend at uniform rates, or in a predictable fashion. Often two separate filopodia will come in such close proximity that an algorithm is unable to distinguish two separate structures, despite this being interpreted as so by a human.

Furthermore, filopodia often cross one another and in some cases, appear to merge which again causes issues with tracking movement. Exclusion of these events is particularly ill-advised as branching and merging of filopodia are intrinsic characteristics of their behaviour, especially when assessing the functions of actin-binding proteins that may affect these qualities. Ultimately, successful extraction of accurate information requires a degree of human input that makes the approach labour intensive.

The use of R-pre as a marker of the plasma membrane, combined with high-resolution timelapse imaging, offers a unique opportunity to visualise dynamic shape changes that may otherwise be lost. Marking of the growth cone plasma membrane revealed morphological fluctuations in the growth cone which are associated with pausing and extension of the growing axon. Complex growth cones are consistently found at decision points in the developing nervous system where axons make directional choices, whereas streamlined morphology is found during growth cone advance. The length of advance periods varies, with 100 minutes being the longest stint observed in the retina, and the shortest approximately 15 minutes in the optic chiasm (Erskine et al., 2000). With the use of R-pre, the tempo of advance and the changes in morphology can be readily extracted to give detailed information about the behaviour of the growth cone.

Conventional methods for marking the membrane using lipophilic dyes such as DiI can lead to dye transfer. Some probes can also enhance photo-induced lipid degradation, or be highly susceptible to photobleaching (Jensen, 2012). Imaging of R-pre was well tolerated in growth cones, and the fluorescence intensity did

not diminish during extended periods of imaging with relatively short intervals (15 seconds) between illuminations.

In summary, it is plausible that drebrin localises to areas requiring stability, such as at the base of filopodia. This behaviour may facilitate directed motility by providing a steadied platform firstly for filopodia to extend from and probe the environment but also as an anchor point for navigation. This dual role may explain previous findings where the leading process fails to form but axon guidance is not affected. Exactly how incoming signals spatially control drebrin remains unknown, although PTEN activation may be involved. Furthermore, the use of R-pre as a genetic marker of the membrane is useful for capturing detailed information from highly dynamic neuronal growth cone.

CHAPTER 4

Drebrin and cofilin interact to modulate growth cone dynamics

CHAPTER 4

4.1 Introduction

Investigation of how actin binding proteins contribute to the switching of stable and dynamic states of the cytoskeleton is key to understanding its plastic nature, particularly with structures such as growth cones and dendritic spines which are under constant and rapid remodelling (Okamoto et al., 2004; Star et al., 2002). Maintenance of dendritic spine morphology is crucial for proper function and underlies learning and memory. Dysregulated actin remodelling is thought to be connected to the development and progression of neurological disorders including Alzheimer's disease and Down syndrome (Calon et al., 2004; Kojima and Shirao, 2007). A loss of drebrin at the synapse has been shown to correlate with the severity of cognitive impairment and therefore resides at the centre of a hypothesis proposed by Kojima and Shirao in 2007 (Kojima and Shirao, 2007). Here, synaptic dysfunction was proposed to be caused by imbalanced regulation of elements of the actin cytoskeleton, specifically an increase in cofilin dephosphorylation displacing drebrin. Indeed, cofilin activity has been previously linked to the shrinkage of hippocampal dendritic spines induced by low frequency stimulation in brains of neonatal rats (Zhou et al., 2004). Knock down of either cofilin or drebrin causes disrupted spine morphology and altered synaptic transmission (Hotulainen et al., 2009; Ivanov et al., 2009).

As key regulators of the cytoskeleton, the relationship between cofilin and drebrin has attracted much interest at a molecular level, too. Despite each containing an ADF homology domain they appear to have contrary functionality; where cofilin increases actin turnover, drebrin stabilises filaments. There is strong biochemical

evidence for the roles of the two proteins at a filament level. Drebrin binds and stabilises F-actin and cosedimentation assays show this occurs at a 1:5 molar ratio of drebrin: actin. Atomic force microscopy analysis of drebrin decorated filaments shows drebrin changes the mechanical properties of f-actin at nanoscale resolution. Drebrin binding increases the length of one complete helix turn with regular periodicity. The consequence of this interaction is to increase the stiffness of the filament by 55% (Sharma et al., 2011).

There are few examples of ABPs that modify the helical pitch of actin, cofilin being the most often used as comparison. Cofilin binds cooperatively between two actin subunits and effectively shortens the pitch of the helix (McGough et al., 1997). The result is a dramatic decrease in filament stiffness and consequently results in filament severing (McCullough et al., 2008). These long-range effects on F-actin could affect how each protein may bind further along the filament and therefore interfere with their functioning. Grintsevich and Reisler (2014) hypothesised that cofilin binding to actin filaments would reduce drebrin binding affinity through long-range allosteric changes to the filament's pitch (Grintsevich and Reisler, 2014). Experiments at the single filament level, showed drebrin decoration increased filament length compared to bare F-actin. In the experiment repeated without drebrin-decoration, cofilin presence reduced filament length by 56%. Cofilin-severing activity was halved in the presence of drebrin, suggesting that drebrin binding could inhibit cofilin activity, and therefore binding.

Assessment of binding affinities showed that cofilin could still bind F-actin near bound-drebrin and vice versa. However, the strength of cofilin binding was two times weaker when drebrin was bound. Furthermore, drebrin bound more readily

than cofilin which is potentially because the drebrin binding interface is more exposed than that of cofilin and that the overall twist of the filament when drebrin is bound is less favourable for cofilin binding (Grintsevich and Reisler, 2014). Furthermore, the elongation rate of filaments was increased due to the formation barbed ends on shorter fragments that readily underwent extension. Total internal reflection fluorescence (TIRF) microscopy experiments showed that elongation rates were slightly reduced in drebrin-decorated filaments compared to the bare controls (Grintsevich and Reisler, 2014). It is possible that these fragments act as seeds for further F-actin polymerisation during rapid remodelling.

Despite the contribution of these studies to the understanding of the molecular interactions that occur between drebrin and cofilin, biochemically pure assays can only help in the formation of hypotheses for what occurs within cells. Following on from the theme of the last chapter, the formation of filopodia and filopodia-like protrusions will be used as an output to assess the effect of manipulation of the two proteins. Having confirmed drebrin stabilises filaments and promotes filopodia formation, I tested whether cofilin would compete with drebrin and prevent the filopodia-inducing effects by its ability to sever filaments within primary neurons. As cofilin and drebrin have opposing effects on F-actin, it was hypothesised that cofilin and drebrin would have similarly competing actions on filopodial dynamics (*Fig. 4-1*). I mapped endogenous drebrin and cofilin in the growth cone and then assessed the effect within a cellular context by co-expressing combinations of drebrin truncations and cofilin mutants in a fibroblast cell line and analysing the morphological consequence. Primary embryonic neuronal cultures were used to understand the effects of this relationship in a more physiologically relevant cell type. Knock down experiments

were used to understand the extent of the relationship and sema 3A was used to examine how cofilin and drebrin modulate dynamics from a functional perspective.

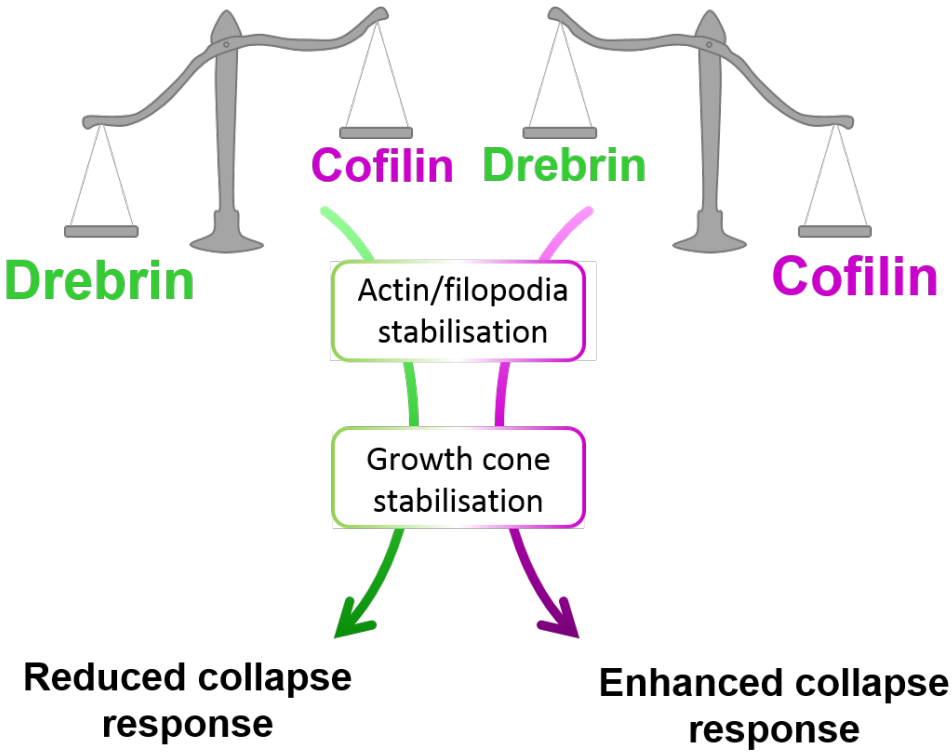

Figure 4-1. Cofilin and drebrin may have opposing effects on filopodial dynamics. *Cofilin and drebrin have competing actions of F-actin, and therefore may display similar behaviour in filopodial dynamics.*

4.2 Results

4.2.1 Drebrin and cofilin increase morphological complexity in fibroblasts

Drebrin has been shown to modify fibroblast morphology and therefore this simple model system was used to determine the effect of competition with cofilin (Dun et al., 2012). To manipulate cofilin activity, three cofilin mutant constructs were utilised: cofilin S3E is a constitutively inactive phosphomimetic and therefore cannot be activated by dephosphorylation; cofilin S3A is constitutively active and cannot be turned off; cofilin R21Q is a non-rod forming mutant which does not form cofilin-expression artefacts (Mi et al., 2013).

Truncated forms of drebrin and cofilin mutants were transiently co-expressed in NIH/3T3 cells, which were then fixed and co-stained with phalloidin-Alexa647 to mark filamentous actin. Changes in cell morphology were quantified by measuring the along the perimeter of the cell and calculating its area. These values were then used to calculate the circularity factor for each cell measured. Circularity (*c*) is a common way to numerically describe changes in cell shape and is function of the perimeter and the area. The circularity of a circle is 1 and values of less than 1 move closer to a star shape. A lower circularity factor value can thus be said to represent an increase in morphological complexity (*Fig. 4-2*).

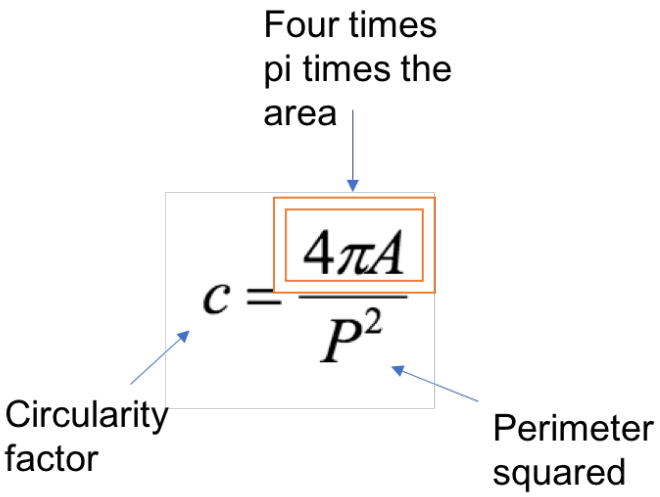

Figure 4-2. Circularity factor equation. *Circularity factor is common method of calculating circularity by comparing the area and radius of a shape regardless of size. This is calculated by four times pi times the area divided by the perimeter squared. For a circle, C = 1. Values for other simple shapes are: 1x2 rectangle, 0.698; equilateral triangle, 0.605; Square, 0.785 and Hexagon, 0.907.*

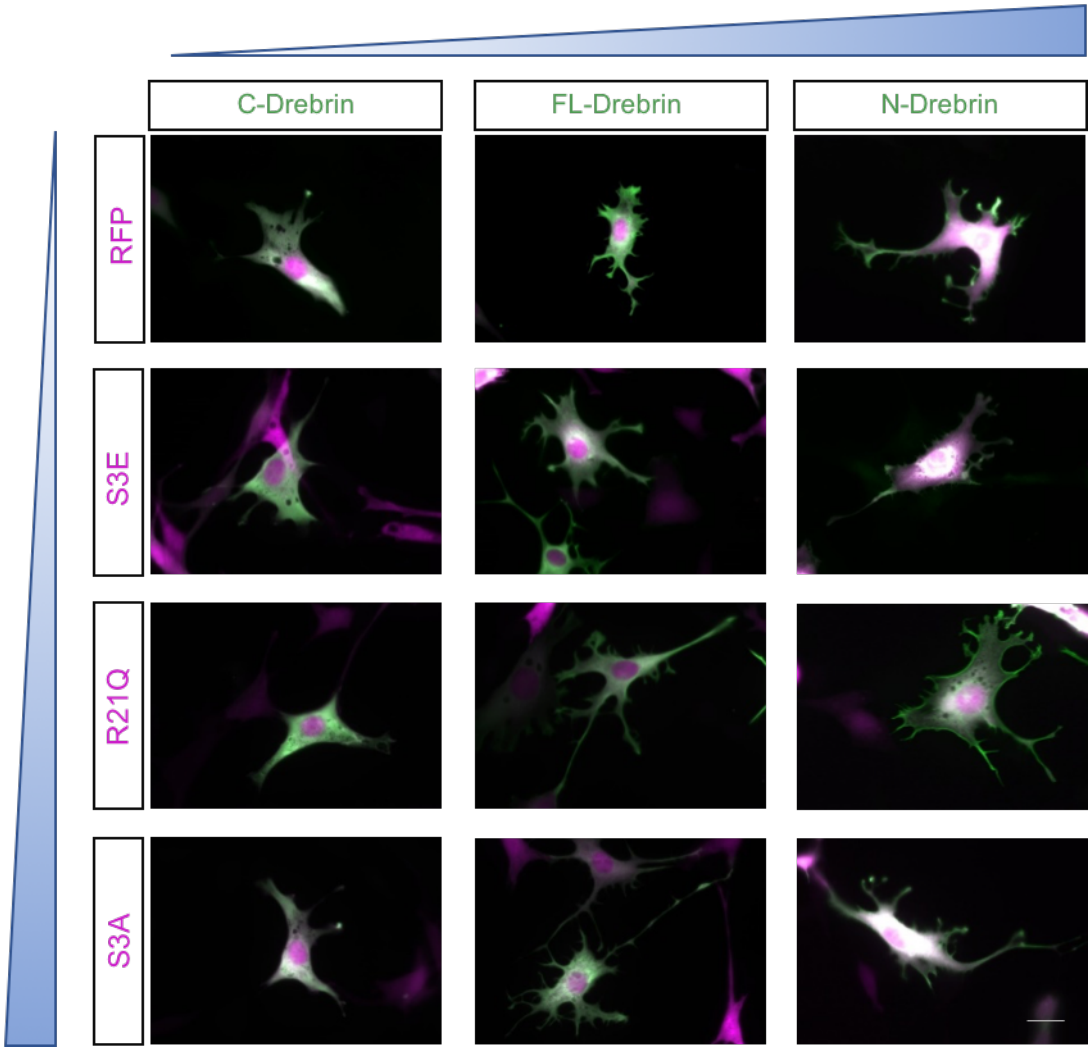

Figure 4-3. Ectopic expression of drebrin and cofilin increases morphological complexity in NIH/3T3 fibroblasts. *Cells were transiently co-transfected with combinations of drebrin and cofilin constructs and fixed 16 hours later. As the activity of drebin and cofilin are increased, cells become increasingly more complex morphologically. Images in are representative. Scale bar = 20 μm. S3E = pseudo-phosphorylated, non-activatable; S3A = constitutively active; WT = Wild Type, normal function; R21Q = does not form overexpression artifacts.*

Each cofilin mutant and drebrin construct was individually co-expressed with RFP to test the morphological effect of the proteins in isolation (*Fig. 4-3*). None of the cofilin constructs alone significantly modified circularity factor when compared to the control (p=0.7591, Kruskal-Wallis ANOVA, *Fig. 4-4D*). Full-length drebrin alone induced a highly significant decrease (p=<0.0001, Kruskal-Wallis ANOVA, Dunn's *post hoc* test) in circularity factor indicating the greatest increase in morphological complexity when compared to drebrin-N and control (*Fig. 4-4E*).

Dun et al., indicated that Drebrin-N had the most extreme effect on cell morphology, however, the group looked specifically at the differences in the number of spikes induced by the truncated forms of drebrin in NIH/3T3 cells (Dun et al., 2012). This type of quantification was deemed unsuitable for this study as I intended to examine the change in the morphology of the growth cone from a global perspective to understand the potential functional consequences of increasing the number of filopodia.

I hypothesised that co-expressing cofilin and drebrin would abrogate the effects of each protein on filopodia formation based on biochemical observations described. Unexpectedly, morphological complexity increased when the two proteins were co-expressed (*Fig. 4-4A*). The effect was highly significant when constitutively active cofilin was expressed with full length drebrin in comparison to the control (p=<0.001, Kruskal-Wallis ANOVA, Dunn's post hoc test). Furthermore, growth cones expressing S3E were significantly less complex than those expressing S3A ($P \leq 0.0001$, Kruskal-Wallis ANOVA, Dunn's post hoc test).

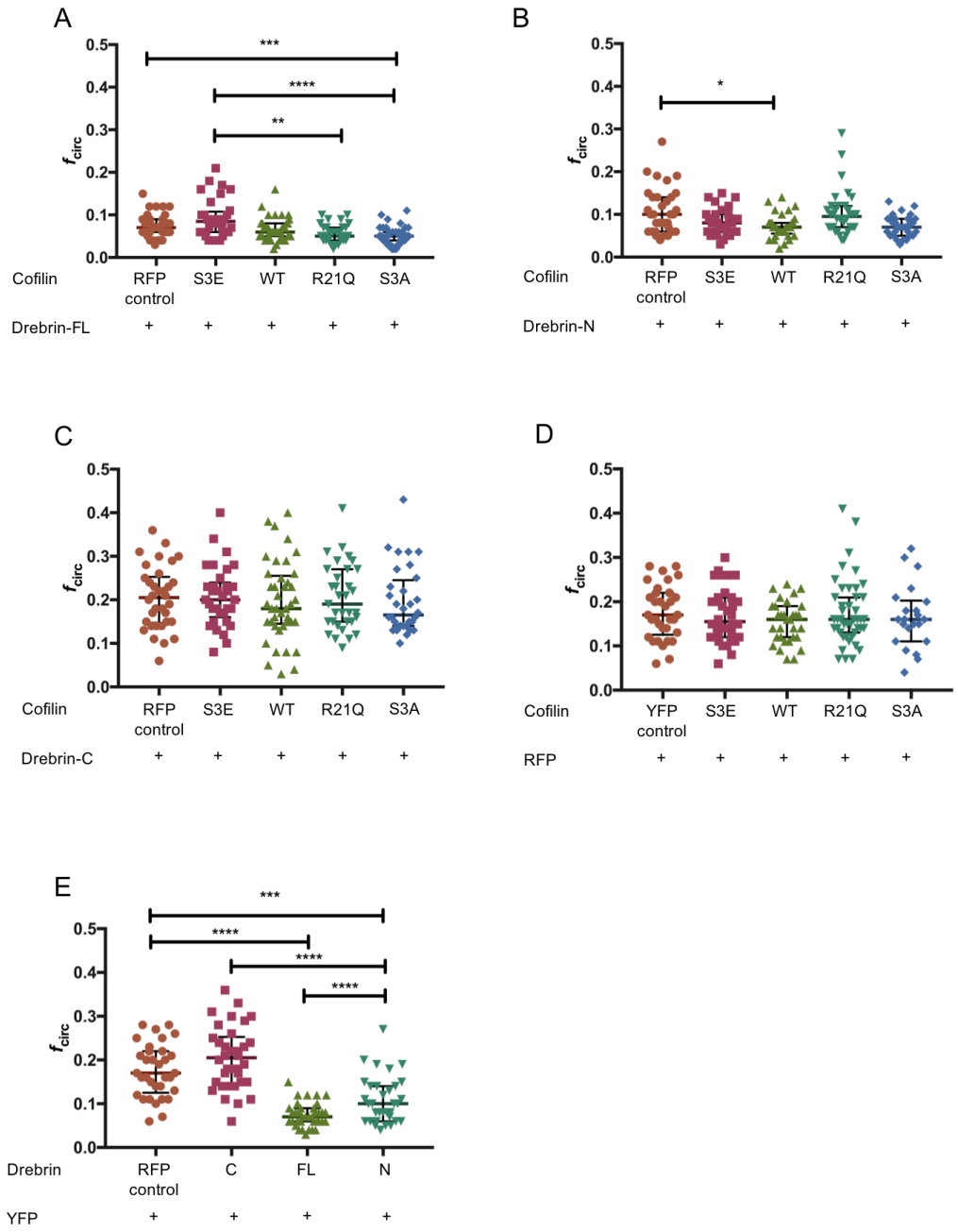

Figure 4-4. Increased cofilin activity drives formation of protrusions when full-length drebrin (A) *or drebrin-N* ***(B)*** *is co-expressed in NIH/3T3 cells. Morphology was assessed on fixed cells by measuring perimeter and area of cells to give circularity factor (f_{circ}) where 1 is a perfect circle. In comparison, drebrin-C* ***(C)*** *Drebrin does not have the same affect, neither does cofilin when co-expressed with RFP as control* ***(D)****. Unsurprisingly, full-length drebrin (FL) and drebrin-N (N), co-expressed with RFP as a control, have a profound effect on cell morphology* ***(E)****. Scatter plots show median with IQR, where n=3 with at least 9 cells per condition per replicate. Kruskall-Wallis ANOVA with Dunn's post hoc multiple comparisons test was used to determine significance, *p=0.05, **p=0.01, ***p=0.001, ****p=0.0001. S3E = psuedo-phosphorylated, non-activatable; S3A = constitutively active; WT = Wild Type, normal function; R21Q = does not form overexpression artifacts.*

For this experiment, it is clear that cofilin activation is required for the increase in morphological complexity to occur. Whilst this suggests the two proteins work somehow synergistically, the result could be a limitation of using a non-neuronal cell line, particularly as NIH/3T3 cells do not express detectable levels of drebrin (Dun et al., 2012). It is plausible that there are otherwise unknown neuron-specific factors required that are not present in the cell line. To investigate this relationship further within a neuronal context, co-expression was performed in chick primary neurons after mapping endogenous cofilin in growth cones and generating cofilin constructs that could be expressed efficiently in chicken cells.

4.2.2 Cofilin is associated with the more dynamic peripheral area of the growth cone.

To assess the endogenous distribution of Cofilin within neuronal growth cones, fixed explants of chick dorsal root ganglia growth cones were probed with anti-cofilin antibody (Abcam, #11062) which has been previously used in immunofluorescence (Ma et al., 2009; Shao et al., 2015); (Reinhard et al., 2016). To allow comparison to drebrin, growth cones were co-stained with drebrin M2F6 antibody. Cofilin was typically found throughout the growth cones of fixed E7 chick dorsal root ganglia neurons (*Fig. 4-5*), which corroborates previously reported findings (Sarmiere and Bamburg, 2004). Whilst the protein extended along the length of filopodia, particularly intense fluorescent rod-shaped structures could be seen at the filopodial base that protrude into the shaft of some filopodia. Circular punctate structures were also observed in the central area of the growth cone. Severing and dismantling of filamentous actin by cofilin is required to enable rapid remodelling of the actin cytoskeleton. These processes also maintain the turnover of local globular actin supplies. The likely reason for

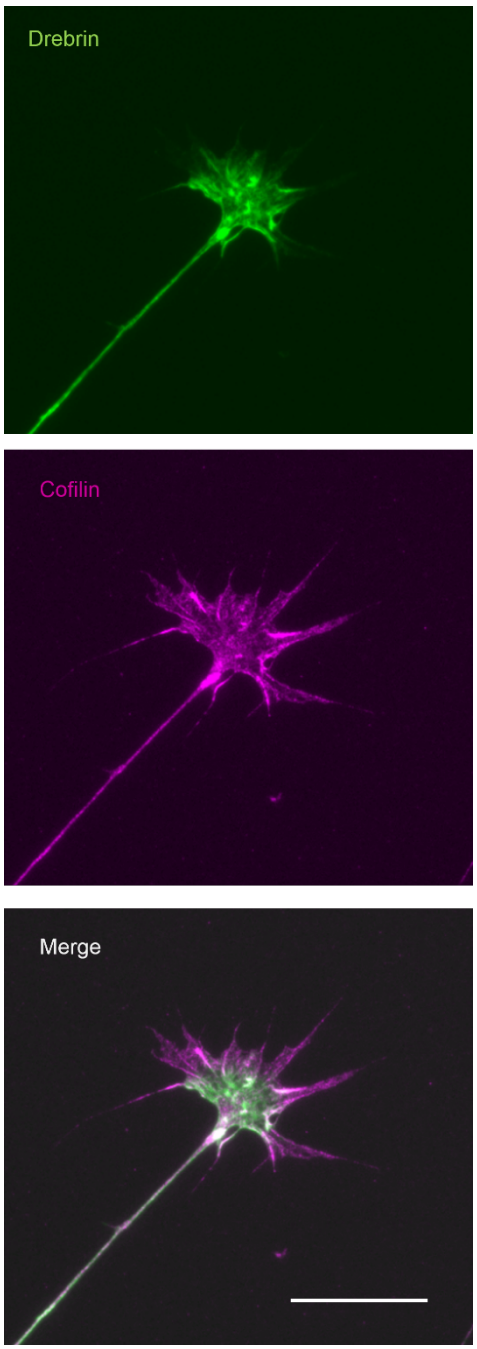

Figure 4-5. Cofilin (magenta) is associated with the more dynamic peripheral area of the growth cone. *Drebrin (green) is largely confined to the transition zone and does not fully extend to the tips of filopodia. Immunocytochemistry staining mirrors expression patterns when tagged cofilin and drebrin are overexpressed (Drebrin, Fig. 3-2; Cofilin, Fig. 5-3). Furthermore, when cofilin is knocked down by siRNA, fluorescence intensity is reduced indicating antibody specificity (Fig. 4-7). Representative image of a fixed neuronal growth cones. Scale bar represents 20µm.*

this distribution pattern is that filopodia extend past the leading edge of the growth cone lamella and undergo constant remodelling as these structures are the first part of the cell to interact with the external microenvironment.

When endogenous drebrin expression was assessed, there was clear overlap between the two proteins that was largely constrained to the base of filopodia with some clear co-localisation along the rod-like cofilin structures mentioned above. Punctate structures were also visible where both proteins were present and some where they were found alone. Why this might be is unclear, however it could be the result of either of the proteins having a preference for a particular type of underlying architecture of the actin cytoskeleton.

4.2.3 Cofilin and drebrin synergistically drive protrusion formation in fixed primary neurons

To examine the relationship between cofilin and drebrin, fluorescently tagged versions were co-expressed to allow for visualisation within live neurons. This was important to assess dynamics of the proteins. For the efficient expression of the cofilin fusion proteins in embryonic chick primary neurons, constructs containing an appropriate expression vector were generated (*Appendix F*). Briefly, plasmids encoding human *CFL1-GFP,* and three mutant forms S3E, S3A and R21Q, were acquired from Addgene and are described by (Garvalov et al., 2007) and (Mi et al., 2013). The genes were amplified by polymerase chain reaction as described in section 2.6 using custom designed primers (*Table 2.3*) to introduce *BglII* and *XhoI* restriction sites at the 5' and 3' ends of *CFL-GFP* respectively. Each product was then digested with *BglII* and *XhoI* and ligated with the pCAβ vector (kind gift of Dr J. Chilton) that had previously been opened with

BamHI and *XhoI,* to give pCAβeGFP-N1Cofilin, the mutants following the same naming convention. The resulting fusion constructs products were then validated by Western blot (*Fig. 4-6*) to check the plasmids were properly expressed. Clean, single bands at around 40 kDa for each cofilin construct indicated the fusion protein was linked to the fluorescent tag. Constructs were systematically co-expressed in dissociated E7 chick dorsal root ganglia neuron which were fixed after 24h in culture.

The length of growth cone filopodia was significantly reduced (p=0.0324) when constitutively inactive phosphomimetic cofilin (S3E) was co-expressed with drebrin compared to the control. Length was significantly longer when cofilin S3E was compared to the non-rod forming mutant, cofilinR21Q (*Fig. 4-8A*). There was no statistically significant difference in the number of filopodia formed however there was a trend towards an increase in the number of filopodia when both constitutively active (S3A) and wild-type cofilin was co-expressed with drebrin (*Fig. 4-8B*). Over expression of cofilin S3E slightly decreased filopodia number when compared to controls.

To measure the effect of co-expression on branching, the tip to base ratio was used where 1= no branching, <1= merging of filopodial tips and >1= increased branching (*Fig. 4-7*). Branching appeared reduced when cofilin S3A mutant was co-expressed (*Fig. 4-8E*). Growth cone complexity was also slightly, but not significantly, reduced (*Fig. 4-8D*) and growth cone spread was confined to a smaller area (*Fig. 4-8C*).

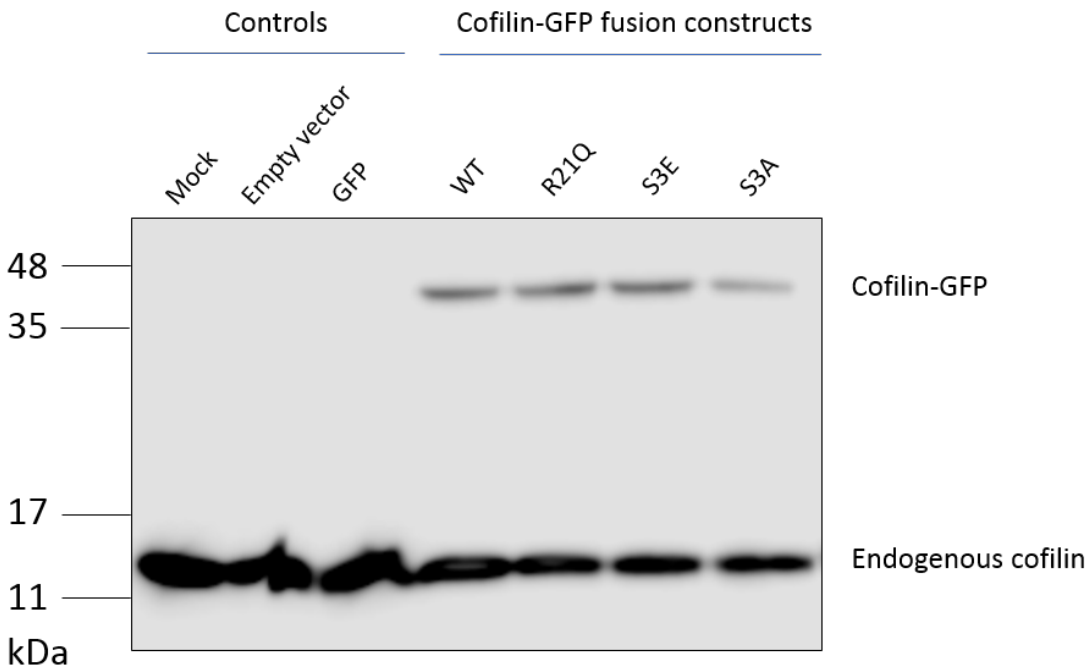

Figure 4-6. Cofilin GFP fusion construct validation by western blot. *Bands present at around 40 kDa indicate presence of cofilin-GFP fusion protein. Predicted size was estimated to be molecular weights of cofilin and GFP combined, 41 kDa. Cos-7 cells were transfected with cofilin-fusion constructs or controls. Total extract was separated by SDS page and probed with a cofilin antibody (ab11062, Abcam) as described in the methods. WT = Wild-type cofilin; R21Q = Non-rod forming cofilin mutant; S3E = Phosphomimetic cofilin mutant; S3A = Constitutively active cofilin mutant; GFP = green fluorescent protein.*

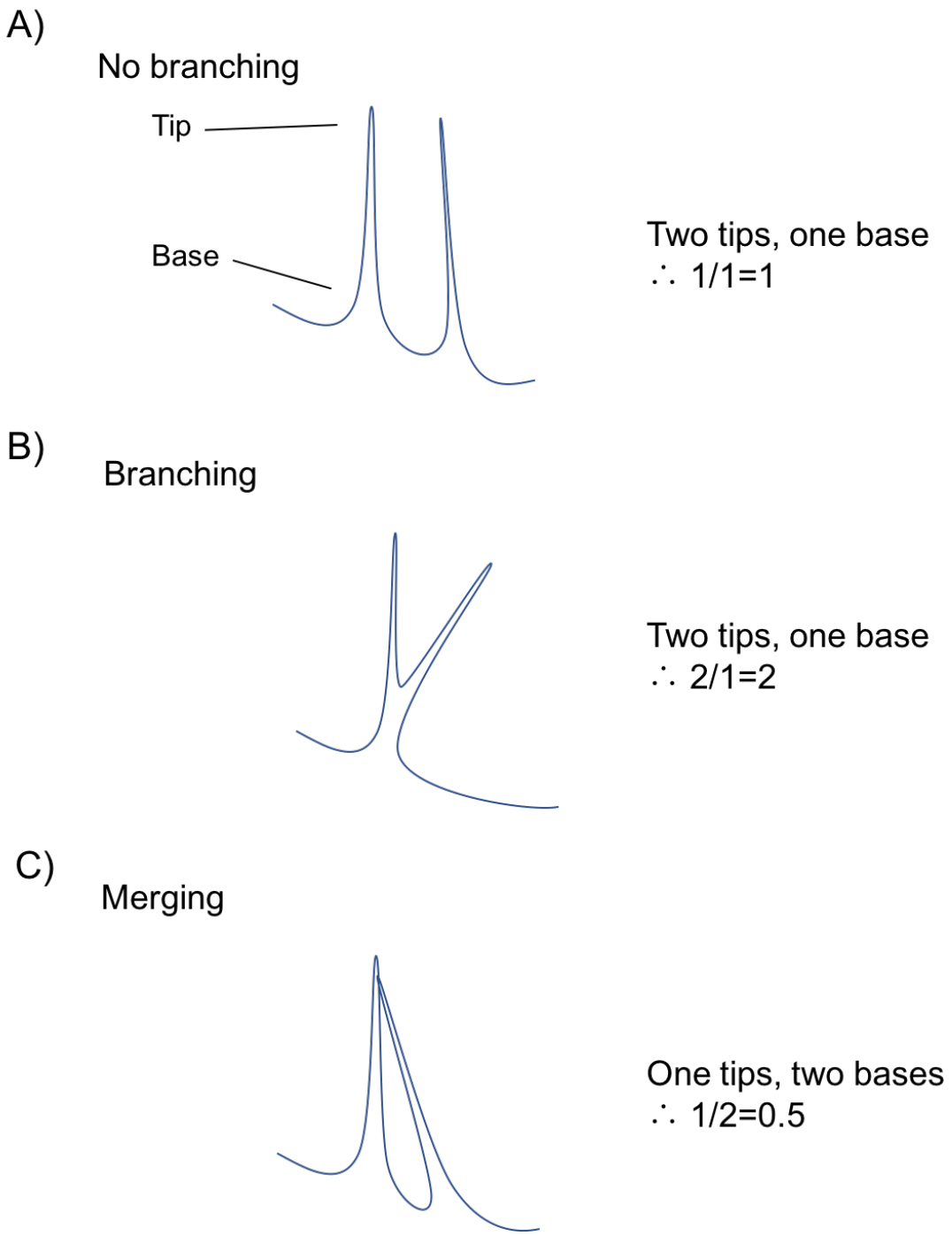

Figure 4-7. Use of tip to base ratio to assess filopodial branching.
In (A) the filopodia display no branching, each tip has its own base and vice versa. Taking the tip to base ratio gives 1, therefore if the tip to base ratio is 1, the filopodia are unbranched. In (B) branching has occurred, where two filopodia emanate from the same base. Here, the tip to base ratio is greater than 1 and therefore, the filopodia can be described as branching. In (C) two filopodial tips have merged with the bases remaining. Here the ratio is less than 1 and the filopodia are therefore described is merging.

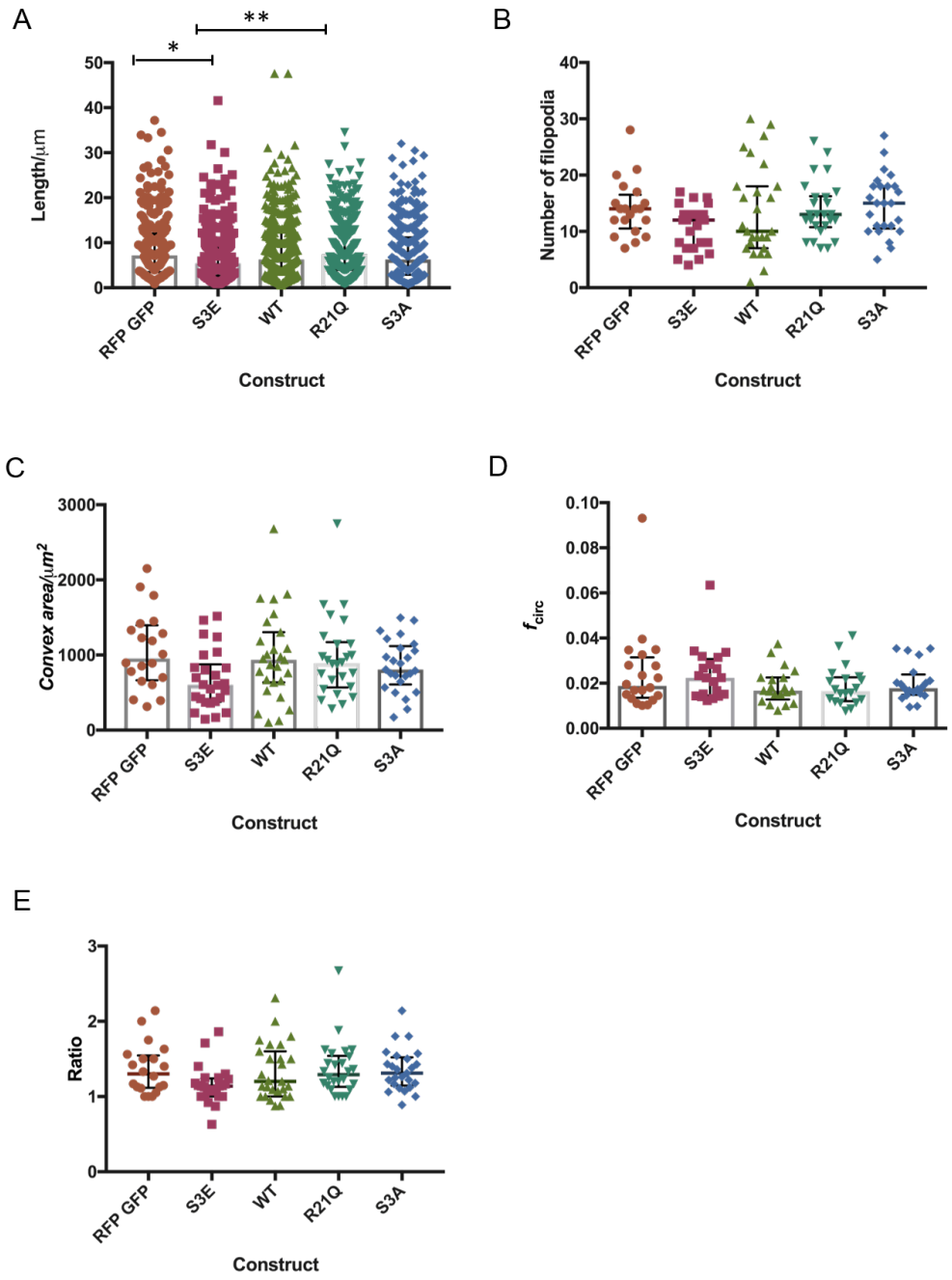

Figure 4-8. Cofilin inactivation results shorter filopodia. *Cofilin inactivation results in significantly shorter filopodia **(A)**, reduced in number **(B)**, and whose growth cones have a reduced spread **(C)** with a slight increase in circularity **(D)** and decrease in branching **(E)**. Dissociated dorsal root ganglion sensory neurons at E7 were co-nucleofected with full-length Drebrin and S3E/WT/S3A/R21Q Cofilin. Cells were fixed, co-stained with phalloidin and imaged at random. Number of filopodia, length, area, perimeter and convex area of growth cone were measured using FIJI. Scatter plots show median with IQR, where n=3 with at least 5 cells per condition per replicate. Kruskal-Wallis ANOVA with Dunn's post hoc multiple comparisons test was used to determine significance, *p=0.05, **p=0.01. S3E = pseudo-phosphorylated, non-activatable; S3A = constitutively active; WT = Wild Type, normal function; R21Q = does not form overexpression artifacts.*

Where cofilin activity was enhanced by expression of the cofilin S3A mutant or total concentration was increased by over-expression of the wild-type there was a trend towards increased morphological complexity globally as denoted by a lower value for circularity. Additionally, there was a marginal decrease in filopodia length. Branching and growth cone spread remained largely unchanged however there was an increase in variation for these parameters. One plausible reason for this is that it is difficult to control for differences in expression levels despite attempting to visually match fluorescence intensity when selecting cells for imaging.

In summary, a reduction in cofilin activity results in fewer filopodia per growth cone, these are shorter in length, less branched and cover a smaller sampling area resulting in a less complex growth cone morphology. When cofilin levels are increased alongside drebrin there is very little difference from the control suggesting the relationship is balanced by feedback mechanisms. Furthermore, these experiments were performed on a background of endogenous proteins levels which may have a compensatory effect.

4.2.4 Cofilin knockdown constrains drebrin-induced growth cone spread

The major limitation of the overexpression system was that the proteins were being expressed against a background of endogenous cofilin and drebrin. Cofilin is ubiquitously expressed in cells and its active form restricted to intracellular locations that undergo constant remodelling of the cytoskeleton (Sarmiere and Bamburg, 2004); the growth cone of embryonic neurons is a prime example.

Therefore, to confirm if cofilin was required for drebrin to induce the formation of spikes its expression was knocked down using Cofilin specific siRNA.

The generation of pRNAiCCofilin utilised the pRFPRNAiC vector (ARKGenomics) as described by (Das et al., 2006). This vector uses the flanking sequence and part of the coding sequence of an endogenous chick micro RNA (miRNA) miRNA30, to produce more efficient processing of the small interfering RNA (siRNA) hairpin sequence and therefore more effectively knockdown expression of the target gene. The vector also encodes RFP to allow visualisation of neurons expressing the hairpins. Overlapping primers were used to generate the siRNA cassette by PCR as described in section 2.6. The product was then cloned into pRFPRNAiC to give pRFPRNAiCCofilin. A scrambled control was also generated. Two candidate siRNA hairpins were generated (gift of Dr J Chilton) and validated by immunofluorescence (*Fig. 4-9*). From immunofluorescence data, candidate 355 appears to reduce the fluorescence intensity when stained with anti-cofilin antibodies, suggesting the candidate is active, compared to candidate 285 which appears inactive. Validation of knockdown by Western blot was attempted, however, it was not technically viable to collect enough neuronal cells expressing the hairpins. A chick derived fibroblast cell line, DF-1 (gift of Dr Joe Rainger, Roslin Institute, Edinburgh) was trialled as a substitute for chick neurons as these cells could be grown in large enough quantities suitable for lysis. As cofilin is ubiquitously expressed, an enrichment of a population of hairpin expressing cells was attempted by fluorescence-activated cell sorting, however all three attempts failed to pool a sample large enough to lyse for Western blotting.

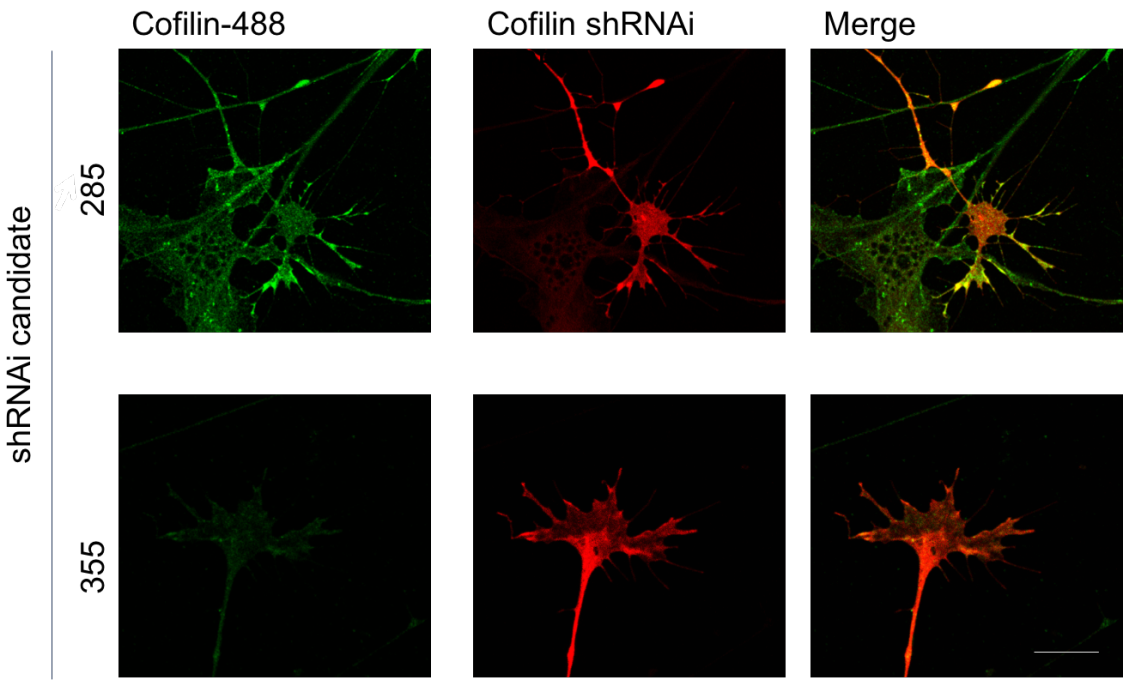

Figure 4-9 Validation of cofilin short hairpin interfering RNA by immunofluorescence. *Dissociated E7 dorsal root ganglia neurons were nucleofected with two candidate hairpins, 285 and 355, for cofilin and cultured for two days. Neurons were fixed and stained for cofilin and imaged using confocal microscopy. Offset and gain settings kept constant to ensure changes in fluorescence were comparative between the two shRNAi candidates. From immunofluorescence data, candidate 355 appears to reduce the fluorescence intensity when stained with anti-cofilin antibodies and is therefore likely to be actively reducing cofilin levels, compared to candidate 285. Images representative, scale bar = 10 μm.*

The dorsal root ganglia of E7 chicken embryos were dissociated and nucleofected with combinations of pRFPRNAiCCofilin and pSilencerDrebrin308 (Dun et al., 2012) or full length drebrin and then fixed 48 hours later (*Fig. 4.10*). To visualise F-actin, fixed cells were stained with conjugated phalloidin. Initial observations of the growth cones over-expressing drebrin showed that there was a large difference in growth cone size when cofilin was knocked down compared to when cofilin was present. To quantify the apparent change in morphology, the convex area was measured. This shape factor was used as a way of expressing the spread of a growth cone numerically. The convex hull of an object is a connected series of straight lines enclosing all the protrusions of the object where the individual interior angle of each connection does not exceed 180 °.

There was no significant difference in convex hull area in growth cones when cofilin was knocked down either alone or co-knocked down with drebrin. There was also no difference when drebrin was knocked down alone. However, there was a dramatic change in average convex hull area when cofilin was present compared to the knock down (1383 μm^2 Vs 512.8 μm^2) in cells overexpressing drebrin (*Fig. 4-10B*). These results suggest that it is the concentration of drebrin that determines the spread of the growth cone. It is likely that the relationship is a temporary association whereby cofilin initially severs existing filaments, creating new barbed ends which are preferential sites for the formation of new filaments that can be extended and bundled to form filopodia. Whether drebrin physically initiates or supports the extension in growth cones is currently unclear. It is plausible that drebrin decorates the base of the growing filament protecting the area from severing by active cofilin, essentially conferring resistance to further cofilin-mediated severing.

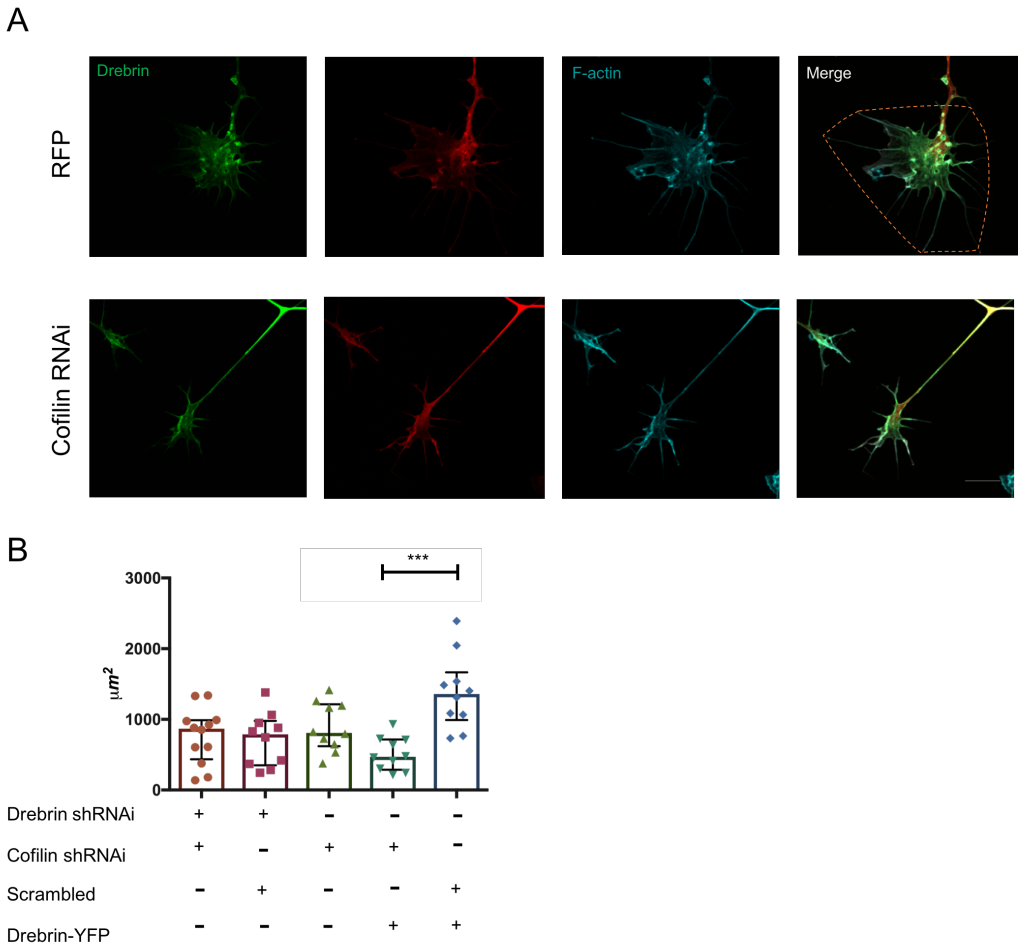

Figure 4-10. Growth cone spread induced by drebrin is constrained when cofilin is knocked down. (A) *Chick dorsal root ganglion neurons co-expressing drebrin-GFP (green) and either cofilin RNAi (red, lower) or RFP (red, upper). Representative images of fixed neuronal growth cones for each condition. Scale bar represents 10µm.* ***(B)*** *Median convex area of growth cones expressing drebrin with cofilin RNAi shows significant difference in spread compared to control growth cones. Convex area is defined as the area bounded by a set of points within the same plane where individual interior angles do not exceed 180º. Statistical test: Kruskal-Wallis 1-way ANOVA, asterisk refer to significance where ***p<0.001 using Dunn's multiple comparison post-hoc test, n>=10 for each condition.*

4.2.5 Cofilin and drebrin display minimal overlap in live neurons

To assess the temporal relationship between drebrin and cofilin, fluorescently labelled versions of the proteins were co-expressed in E7 chick dorsal root ganglia. After 24 hours, growth cones co-expressing drebrin and cofilin were sequentially imaged every 15 seconds for 100 cycles. When films were viewed as overlaid false-colour sequences red (drebrin) and green (cofilin), some areas of the growth cone displayed apparent overlap between the two channels (yellow), particularly at the base of filopodia (*Fig. 4.11*). However, qualitative observation can be easily misinterpreted due to subjective bias.

To further confirm the extent of co-occurrence, the fluorescence intensities for each channel were normalised and expressed as a ratio. A heatmap was applied using the custom Matlab script *showOverlap4* to expose the areas in which both proteins occurred at highest intensities. This showed very little overlap of the two proteins in the growth cone and suggests that cofilin and drebrin work sequentially to drive protrusion formation rather than forming a direct physical complex.

4.2.6 Cofilin drives protrusion formation in the presence of sema 3A

Sema 3A was used to assess the functional outcome of increased cofilin or drebrin in live growth cones. Sema 3A is classically described as a repulsive guidance cue and therefore I hypothesised that increasing drebrin concentration would confer stability and thus growth cones would display less collapse when compared to cofilin which severs filaments. Low doses of sema 3A (100ng/ml)

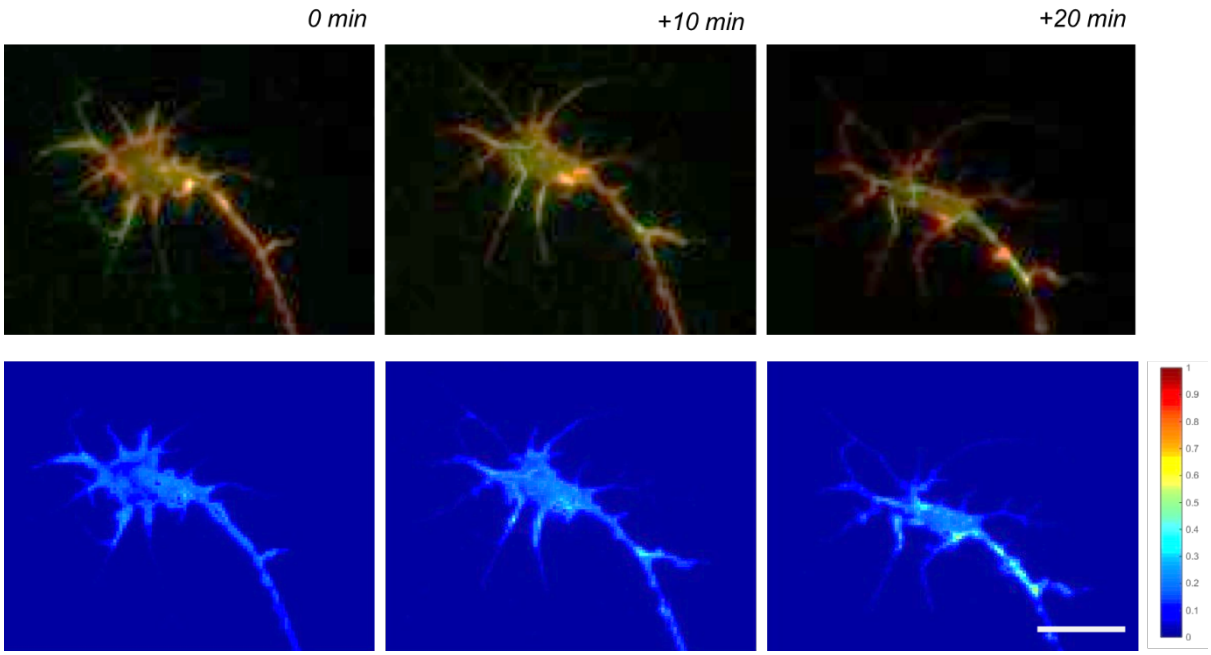

Figure 4-11. Drebin and cofilin overlap minimally which suggests a temporal relationship rather than spatial colocalisation. *Due to cytoplasmic presence of both fluorescent fusion proteins when not active, merged images can obscure true colocalisation (upper panels). To overcome this limitation, fluorescence intensities for both channels were normalized and a heatmap applied to channel ratio using the custom Matlab script showOverlap4 to expose areas of co-occurrence (lower panels). Dissociated DRG neurons co-nucleofected with full-length drebrin (RFP) and wild-type cofilin (GFP) were sequentially imaged every 15 seconds for 100 cycles. Example representative. Scale bar = 10 µm. See Appendix C for Supplementary Media File 3 & 4.*

were used in an attempt to capture subtle changes in morphology rather than complete collapse (Manns et al., 2012). Each batch of sema was tested at collapsing concentrations to confirm the agent was active in advance of experimentation. Sema 3A was added to growth cones expressing drebrin-YFP or cofilin-GFP during widefield fluorescence imaging. Surprisingly, filopodia were more likely to persist longer when expressing cofilin and treated with sema 3A when compared to PBS controls ($p<0.001$, Kruskal-Wallis test, Dunn's multiple comparisons test). This increase in persistence time was significantly greater than growth cones expressing drebrin or the YFP controls. A combination of dynamic behaviour and large data sets created variability that translates as noise in the graphical representation of the data and therefore numbers of filopodia per frame were normalised (*Fig 4.12*). This shows addition of sema 3A increases filopodia formation; the difference between sema 3A and PBS treatments was significant for cofilin, drebrin and YFP (*Fig. 4-12*). Comparison of the normalised mean number of filopodia per frame shows that addition of sema 3A increases filopodia formation. The difference in filopodial longevity between sema 3A and PBS treatments was significant for cofilin, drebrin and YFP. This suggests that sema 3A can drive protrusion formation in growth cones, potentially through cofilin-mediated actin turnover.

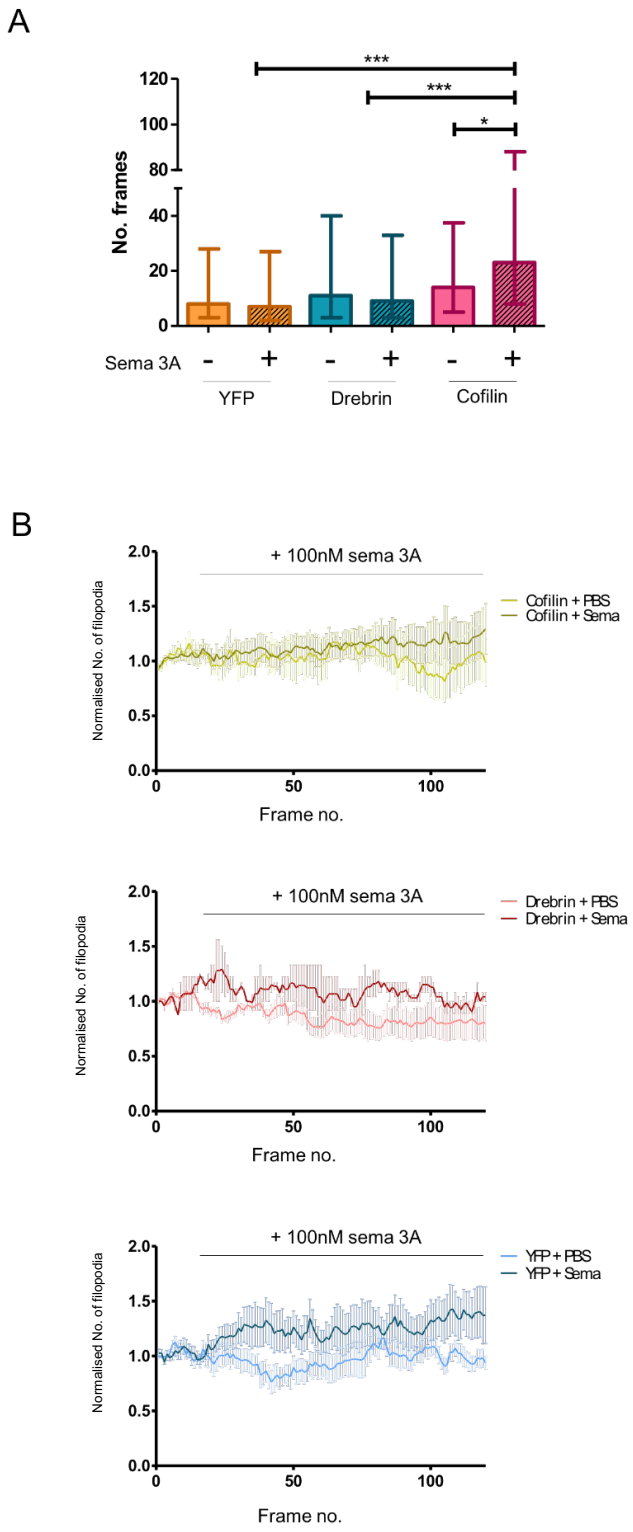

Figure 4-12. Cofilin drives protrusion formation in the presence of sema 3A. (A) *The median number of frames a single filopodium exists for is increased when cofilin is overexpressed. Error bars = IQR.* ***(B)*** *Normalised numbers of filopodia per frame shows addition of sema 3A increases filopodia formation. The difference between sema 3A and PBS treatments was significant for cofilin, drebrin and YFP. At least 3 growth cones were analysed for each condition. The custom Matlab script AUTO was used to analyse the films that produced the data for this figure.*

4.3 Discussion

Cofilin and drebrin are known to induce opposing changes in helical periodicity of F-actin at the molecular level. Cofilin binding promotes the bending of filaments which results in their disassembly, whereas drebrin binding stiffens filaments conferring stability. However, it is not known whether this antagonism of filament twist extends to the dynamics of the filaments that form filopodia. In this chapter, the functional relationship between the two proteins within the neuronal growth cone was assessed in terms of filopodia formation. The data presented here unexpectedly demonstrate that cofilin and drebrin have a synergistic association that drives the formation of actin-based protrusions. Coexpression experiments showed a trend that, together, cofilin and drebrin increase morphological complexity in neuronal growth cones. This effect is dependent on cofilin's activation state as when inactive cofilin was expressed, the number of filopodia was reduced. Each parameter of growth cone morphology measured showed a consistent trend when the cofilin S3E mutant was overexpressed, despite not reaching statistical significance. Furthermore, knock down of cofilin strongly inhibited drebrin-induced growth cone spread. These results contrast with what is known about how cofilin and drebrin change the twist on F-actin – cofilin producing an "under twist" which results in severing, and drebrin binding which confers stability by increasing filament persistence. Immunolabelling of endogenous expression of the two proteins showed that drebrin sits at the base of filopodia which are relatively more stable, and cofilin is associated with more dynamic structures such as the leading edge of the lamellipodium which are undergoing constant actin turnover. Live cell imaging of cofilin and drebrin in real time showed minimal overlap which suggest their activities are sequential.

However, it is likely that these two functions still occur as predicted, but rather in a temporally separate manner.

It is plausible that increased cofilin has a bipartite effect on F-actin assembly. Firstly, cofilin drives actin disassembly and expands the monomeric actin pool available for filament extension; secondly, cofilin-induced severing increases the number of new barbed ends which are thought to preferentially nucleate new barbed ends (Amann and Pollard, 2001). The overall effect may drive localised amplification of filament formation and therefore directed filopodia protrusion. As extension occurs, force is exerted on the plasma membrane. The protruding structure must then be firm enough to overcome the rigidity of the membrane. It is here that the bundling role of drebrin is likely to come into play. It is possible that drebrin localises to the base of the nascent filopodia, bundling adjacent filaments together to increase overall stiffness and allowing continued extension. Knock down experiments confirmed that cofilin is required for drebrin to induce the spread of growth cones. Here, drebrin has a reduced number of filaments to bundle as cofilin-induced actin turn over and barbed end creation is absent. Furthermore, growth cone spread was not significantly decreased when drebrin expression was suppressed suggesting that other actin bundling proteins, such as α-actinin and fascin, may compensate for the loss. However, this substitution may lead to mechanical changes in filopodial function (Tseng et al., 2005; Tseng et al., 2002).

A temporal relationship has been demonstrated between drebrin and cofilin during long term potentiation in individual dendritic spines. Protein translocation was observed in sequential phases. In the initial phase, cofilin rapidly entered the

spine and induced F-actin remodelling allowing spine expansion. A stabilisation phase followed in which cofilin concentration increased and F-actin became stabilised in complex with cofilin. In the final phase, proteins, such as drebrin, entered to stabilise and provide scaffolding for the insertion of receptors at the membrane of the spine (Bosch et al., 2014). It is plausible that a similar process occurs in the growth cones of DRG neurons. Based upon this work, I propose that under temporal regulation, drebrin and cofilin synergistically drive the formation of filopodial protrusions resulting in the more complex morphology required for directed motility of the growth cone (*Fig. 4.13*). Testing this temporal relationship presents a technical challenge as any pharmacological approaches would impact actin dynamics. Optogenetics is one such technique that could control the activity of cofilin and drebrin with spatial and temporal precision. In combination, optogenetic control and genetically encoded biosensors could act as coincidence markers of protrusion formation (Guglielmi et al., 2016). This approach has been successfully used to visualise calcium signalling in filopodial formation and cell migration and therefore represents a viable strategy (Mills et al., 2012).

Rapid remodelling of the actin cytoskeleton in response to guidance cues is crucial for pathfinding of growth cones in the formation of precise neuronal circuits. The complexity and motile behaviours of the actin based structures formed are linked to determination of the navigation decisions made. The application of guidance cues is used to understand this process, however, *in vivo,* axons rarely encounter single cues and are unlikely to experience the high concentrations used experimentally. This results in contradictory reports of the roles of these cues. The developing ocular motor system is an excellent example

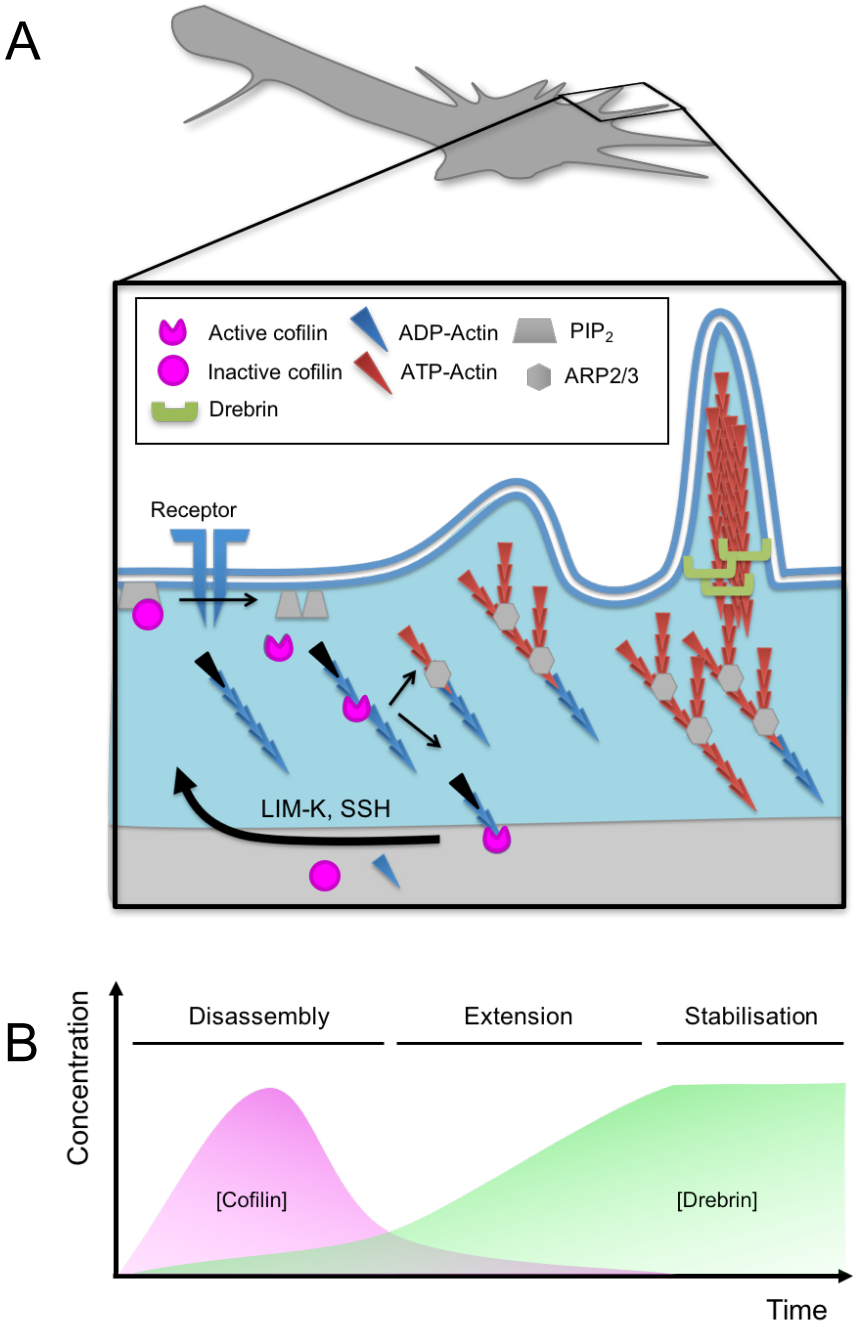

Figure 4-13. Proposed model of cofilin and drebrin synergy in neuronal growth cones. (A) *Active cofilin severs existing filaments to provide new barbed ends for extension of filaments. This also helps maintain a pool of monomeric actin available for assembly. As extension occurs filaments are bundled together by drebrin which stabilizes the bases and allows for further extension of the filopodium past the leading edge. Cofilin can be sequestered at the membrane by PIP_2 in an active state and released on receptor activation which hydrolyses PIP_2. LIM-K phosphorylates cofilin deactivating it and SSH (Slingshot) dephosphorylates cofilin allowing the cycle to begin again.*
(B) *Graphical representation of changes in concentration over time for drebrin (green) and cofilin (purple) during the process described in (A).*

of how repulsive guidance cues, such as sema 3A slow axonal progression but increase growth cone complexity to effectively fine tune navigation (Clark et al., 2013). Sema 3A also plays an important role in promoting branching in dendritic spines. Neurons in brain slices from sema 3A null mice display decreased dentritic branching and length which were rescued by exogenous addition of sema 3A (Fenstermaker et al., 2004). Furthermore, sema 3A can act as a chemoattractant for cortical apical dendrites (Polleux et al., 2000).

Interestingly, Aizawa et al., (2001) reported that sema 3A-induced collapse requires phosphorylation of cofilin by LIM-kinase (Aizawa et al., 2001). The authors speculated that phosphorylation at serine 3 is necessary to initiate release of the cofilin-actin heterodimer after it has dissociated from the filament. This frees the actin monomer for repolymerisation and cofilin is then available for reactivation via phosphatase activity (Aizawa et al., 2001).

Sema 3A was used to determine the functional outcome of increased complexity in growth cone morphology linked to cofilin and drebrin expression. I predicted that presence of sema 3A would lead to increased growth cone collapse when cofilin was overexpressed, and that the inverse would occur for drebrin overexpression. Surprisingly, the filopodia of growth cones overexpressing cofilin were more persistent than those expressing drebrin or the YFP controls. Intriguingly, filopodial number was increased in the presence of sema 3A for drebrin, cofilin and control growth cones when compared to their mock treated counterparts (*Fig 4-12*). This finding is particularly surprising as this guidance cue is typically used in collapse assays to assess the growth cone responses to inhibitory cues (Manns et al., 2012). Low doses of sema 3A (100ng/ml) were used

in an attempt to capture more subtle changes in morphology rather than complete growth cone collapse. It is possible that low dose sema 3A can drive protrusion formation through increased cofilin-mediated actin turnover. Marsick et al., showed that protrusive activity in RGC growth cones was halted by inhibition of cofilin activity by both ephrin-A2 and slit-3, which may seem counter intuitive when considering cofilin's canonical severing role. However, this inhibition is thought to be necessary to prevent actin polymerisation occurring at free-barbed end sites formed by cofilin severing. Furthermore, decreased F-actin turnover may mediate retraction through actomyosin contractility (Marsick et al., 2012). Interestingly, sequential cofilin activation and deactivation was noted when DRG explants were acutely treated with sema 3A (Aizawa et al., 2001). The levels of deactivated cofilin are also seen to drop in attractive growth cone turning mediated by netrin-1 and nerve growth factor. When cofilin activity was reduced, turning responses were disrupted (Marsick et al., 2010). Together, these studies suggest that cofilin activity is required for changes to actin dynamics in response to both attractive and repulsive cues.

The difference in the effect between coexpression in the fibroblast cell line and the primary neurons can be largely explained by the fundamental differences between the cell types. Neurons are highly specialised and will express a specific set of factors that define functions that fibroblast cell lines may not (Santiago and Bashaw, 2014). Neuron-specific binding partners, known and unknown, may be missing within the cellular environment of the fibroblast which results in different function. Similarities will lie within overarching principles that govern activity of the cytoskeleton. The actin cytoskeleton of a neuronal growth cone is constantly being remodelled can be likened to a polarised cell, and this morphology is

maintained even in the absence of stimulation. Conversely, the NIH/3T3 cells were not stimulated and did not display directed polarisation. Polarisation is a complex process that requires the coordinated action of cytoskeletal elements, rearrangement of membranes and organelles, interpretation of extra- and intracellular signalling. It is likely that neurons have regulatory networks that compartmentalise the activation and function of actin binding proteins, such as cofilin and drebrin. Compartmentalisation is not uncommon and allows the formation and maintenance of defined regions of specialised function (Sokac and Wieschaus, 2008). In neurons, this may enable a basal level of remodelling to allow for protrusion formation and continuous searching of the environment.

In summary, the data suggest that cofilin and drebrin may work synergistically in a temporally regulated manner. This supports other data in the literature which adds to our understanding of how the two actin binding proteins contribute to directed motility in neuronal growth cone filopodia. Additionally, this work provides further evidence that sema 3A is important for axonal guidance decisions by signalling pause periods at decision points.

CHAPTER 5

Cofilin Rods

CHAPTER 5

5.1 Introduction

In establishing the link between the cytoskeleton and neurodegeneration, research has focused on genetic mutations that result in the accumulation of faulty gene products such as amyloid plaques and neurofibrillary tangles in Alzheimer's disease or tubulin aggregation in the Lewy bodies of Parkinson's disease (Dickson, 1997; Goldman and Yen, 1986). Mutations that contribute to these diseases are increasingly associated with disruption of the actin cytoskeleton and its function in vesicular biogenesis and organelle trafficking (Bamburg and Bloom, 2009; Bloom and Morgan, 2011; McMurray, 2000). Cofilin-actin rods are one such cytoskeletal abnormality, formed from short stretches of actin that have been severed and then stabilised by the actin-binding protein cofilin. These rods form in response to amyloid beta (-β), energy depletion and oxidative stress; three of the major risk factors for dementia (Bamburg and Bernstein, 2016).

Neurons are particularly prone to developing rods when stressed which may act initially as a protective, homeostatic mechanism. In cell culture experiments, rod formation has been associated with resistance to apoptosis and therefore Huang et al., (2008) hypothesised this process was a protective response which frees a pool of ATP that would normally be tied up in actin filament treadmilling (Huang et al., 2008). By halting this energetically greedy process, energy could then be diverted to other survival activities such as maintenance of ion balance for electrical activity or the function of protein machinery in mechanisms such as the unfolded protein response, a process which is chronically upregulated in neurodegenerative diseases (Bernstein, 2006).

Energetically stressed neurons *in vivo* typically display the three factors required for rod formation: high concentrations of active cofilin, elevated levels of ADP-actin and an oxidative environment. Under these conditions, activated phosphatases dephosphorylate cofilin which then decorates and severs F-actin. These fragments then form rod shaped structures which aggregate (Bamburg and Bernstein, 2016; Bernstein et al., 2012) (*Fig. 5-1*). *S*tudies in hippocampal neurons *in vitro* have since shown that rods form in response to a variety of cellular stress conditions including ATP-depletion, excess glutamate, hypoxia, peroxide treatment and exposure to soluble amyloid-β – the main peptide component of senile plaques associated with Alzheimer's disease (Minamide et al., 2010). Mutant huntingtin, the protein responsible for Huntington's disease, has also been shown to cause rod formation which disrupts cellular function (Munsie et al., 2011). Furthermore parkin, implicated in Parkinson's disease, can interact with LIMK-1 and attenuate cofilin phosphorylation, potentially upregulating activation of cofilin which could saturate actin filaments (Lim et al., 2007). Whether cellular stress is the initiating trigger or a consequence of disease progression is a topic of intense debate, however mice expressing mutant amyloid display disrupted hippocampal activity before the appearance of amyloid deposits (Hsia et al., 1999). With rods found in aged controls, it remains to be answered whether rod-formation could in fact drive the early stages of disease progression.

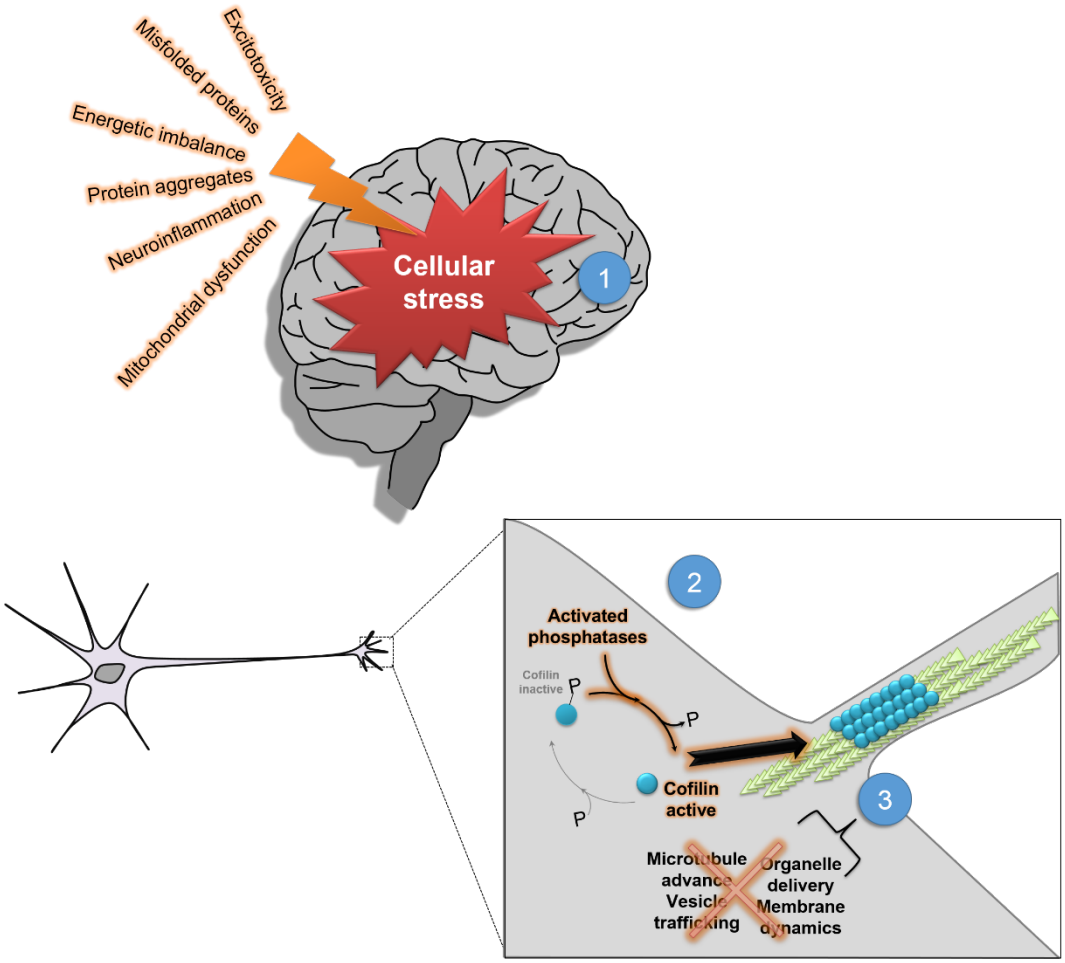

Figure 5-1. Cofilin-actin rod stress response*. **(1)** The onset of cellular stress causes activated phosphatases to dephosphorylate cofilin. **(2)** Activated cofilin saturates actin filaments causing them to bundle into aberrant rod structures. **(3)** These rods block major activities required for synapse formation resulting in the breakdown of synaptic function.*

Rods occur in brains of Alzheimer's disease patients in association with senile plaques suggesting there is a link between their formation and pathogenesis (Minamide et al., 2000). They form in cultured hippocampal neurons exposed to amyloid-β and are also found in the brains of transgenic mouse models of dementia in which amyloid-β is overexpressed (Davis et al., 2009). Cofilin rods may seed the accumulation of amyloid plaques by trapping amyloid-β and its processing machinery leading to a negative cycle of local accumulation of further amyloid-β oligomers and induction of rods in neighbouring neurons (Minamide et al., 2000).

Persistent rods can span the diameter of neurites, disrupting microtubules and delivery of organelles required for neurite maintenance. These rods have increased longevity and are a plausible reason why synapses are lost before neuronal death occurs. Rod formation is reversible and therefore represents a target that could slow or reverse disease progression in its infancy whilst cognitive function is relatively intact (Mi et al., 2013). Current approaches for removing plaques are centred on antibodies, these present serious hurdles for delivery due to their size and possibility of side-effects. Elucidating molecular triggers for rod disassembly could lead to targeted pharmacological compounds that circumvent these problems (Shaw and Bamburg, 2017).

In 2015, Gressin et al., provided new insights into how cofilin could preferentially disassemble F-actin networks with the aid of AIP-1 (Gressin et al., 2015). Using micropatterning, the group created defined fluorescently labelled actin architectures. Cofilin alone decorated the filaments and partially dismantled and debranched the networks, whilst bundled filaments remained stable. In the

presence of AIP-1, disassembly was rapid and complete, with the fastest reaction occurring after cofilin had bound the filaments (*Fig. 5-2*). Based on these findings, the group proposed that parallel or mixed polarity actin filaments in the presence of high cofilin concentration rendered filaments in a stable, pre-disassembly state. When AIP-1 was present, these highly decorated filaments became unstable and vulnerable to stochastic disassembly, thus increasing disassembly rate.

AIP-1 therefore presents a cellular mechanism for cells to switch from stabilisation to rapid disassembly, offering a strategy for modulating rod-formation. Much of the existing focus on AIP-1 has been the result of attempts to understand cofilin's seemingly concentration-dependent contradictory behaviour. FRET-based spectroscopy and single-filament imaging of actin showed that AIP-1 drove rapid severing of cofilin-actin filaments and that AIP-1 could modulate monomer dissociation at either end of the filament (Nadkarni and Brieher, 2014). This disassembly was thought to be rapid and occur in bursts and, unlike severing by cofilin alone, no daughter fragments were detected, suggesting AIP-1 mediated full filament disassembly (Kueh et al., 2008).

Rapid AIP-1 induced actin turnover in living cells was first shown in yeast actin patches and cables by comparing the activities of AIP-1 mutants. Again, the authors of this study suggested that the observed loss of capping activity *in vitro*, correlated with the loss of rapid actin turnover *in vivo* (Okada et al., 2006). This was thought to be due to the presence of another cellular factor and not necessarily AIP-1 directly (Kueh et al., 2008).

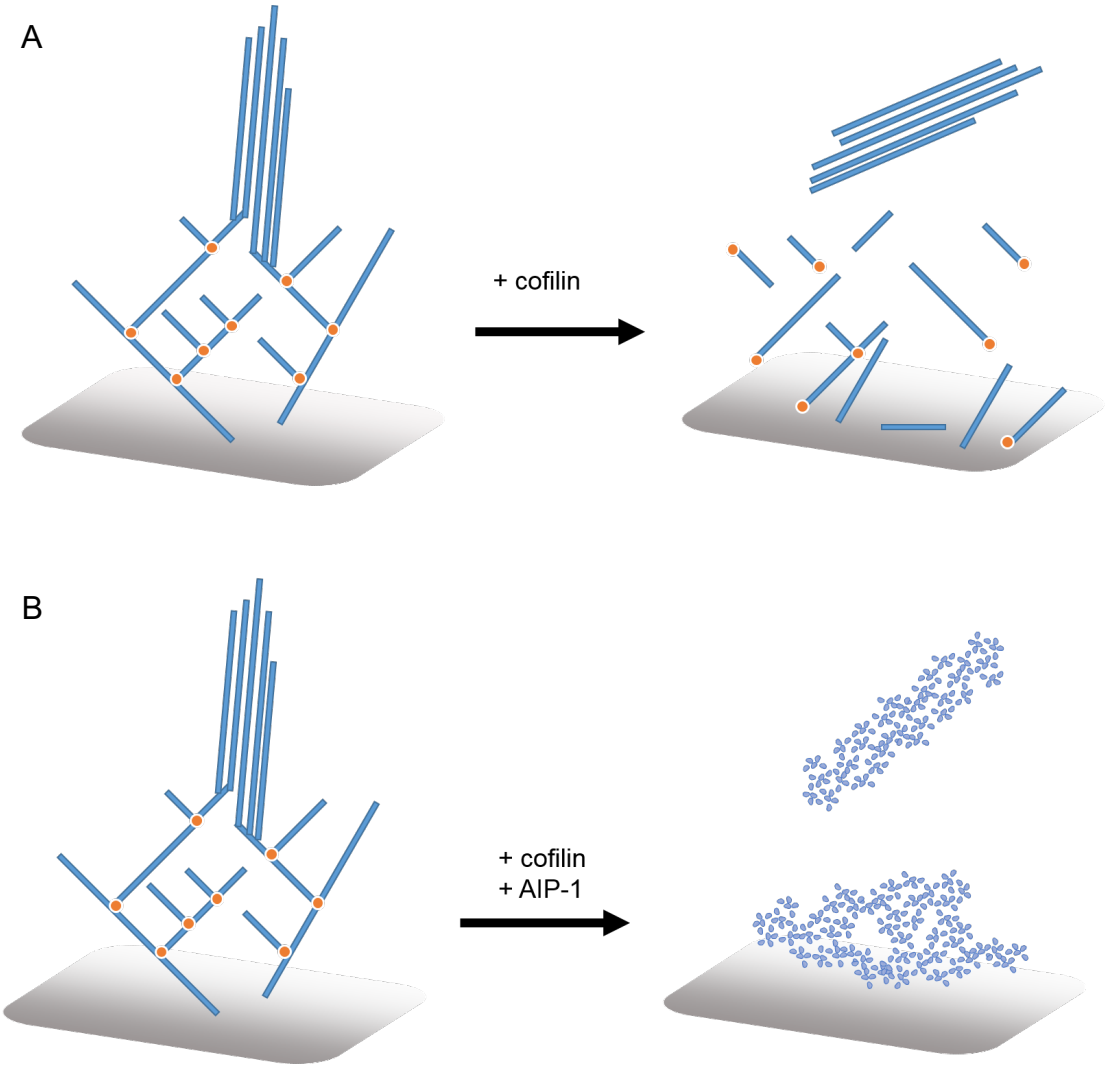

Figure 5-2. Disassembly of actin structures by cofilin and AIP-1.
(A) *Cofilin alone decorates actin filaments and partially dismantles and debranches networks, whilst bundled filaments remained stable.* ***(B)*** *In the presence of AIP-1, disassembly is rapid and complete, with the fastest reaction occurring after cofilin binds filaments (Gressin et al., 2015).*

There are several convincing studies demonstrating that AIP-1 enhances cofilin-severing of actin filaments, and that this additional layer of regulation is important in dynamic cytoskeletal processes such as mammalian cell migration in immune responses and development (Fujibuchi et al., 2005; Gressin et al., 2015; Kato et al., 2008; Kile et al., 2007; Nadkarni and Brieher, 2014; Nomura et al., 2016; Rodal et al., 1999; Yuan et al., 2014). However, a therapeutic role in targeting cytoskeletal abnormalities in neurodegenerative diseases has not been investigated.

In the following chapter, I show that AIP-1 has a potent effect on cofilin-actin rods formed by factors involved in the progression of neurodegeneration. This is of great importance because rod formation may precede neuronal loss and therefore understanding rod formation and disassembly has potential to enable the development of a targeted strategy for enhancing neuronal survival. Neurodegenerative diseases typically only become clinically evident when higher brain functions are affected by neuronal loss. There is a window of opportunity for intervention and this renders rods an attractive therapeutic target for halting or reversing disease progression whilst cognitive function remains intact. If the rod formation can somehow be regulated, neurite function could be protected, potentially preventing loss of brain function at an early stage in neurodegeneration.

5.2 Results

5.2.1 Cofilin-actin rods form when cofilin is over-expressed and in response to energetic stress

Cofilin is known to complex with actin to form aggregates that can hinder cellular function (Minamide et al., 2000). Overexpression of fluorescently tagged wild-type cofilin can lead to the concentration-dependent formation of cofilin-actin rod-shaped complexes (Mi et al., 2013). Obvious rod-shaped structures were observed in the growth cone filopodia of fixed dissociated E7 dorsal root ganglia neurons nucleofected with Cofilin-GFP (*Fig. 5.3A*). These had high expression of cofilin as indicated by relatively high fluorescence intensity compared to growth cones with low fluorescence intensity and no rods. Growth cone rods extended from the transition zone and into the shaft of the host filopodium. Some rods were present in axonal filopodia but did not extend as far into the filopodium. Rods were also seen to spontaneously form over a period of minutes in neurons expressing WT cofilin-GFP during live cell imaging (*Fig. 5-3B*). This is likely due to phototoxicity which can occur when chemically reactive, species such as free radicals, are generated by high-intensity excitation of fluorophores required to detect a recordable signal. Despite attempting to minimize this effect with minimal sample illumination, overexpression of wild-type cofilin was likely to compound the effect.

To examine the effect of energetic stress on rod-formation, E7 dorsal root ganglia explants were treated with 100 mM 2-Deoxy-D-Glucose (2DG), for 10 mins at 37°C. 2-DG is a glucose analogue that cannot undergo metabolism; at 100 mM 2-DG essentially outcompetes the glucose in the media and inhibits glycolysis resulting in cellular ATP depletion.

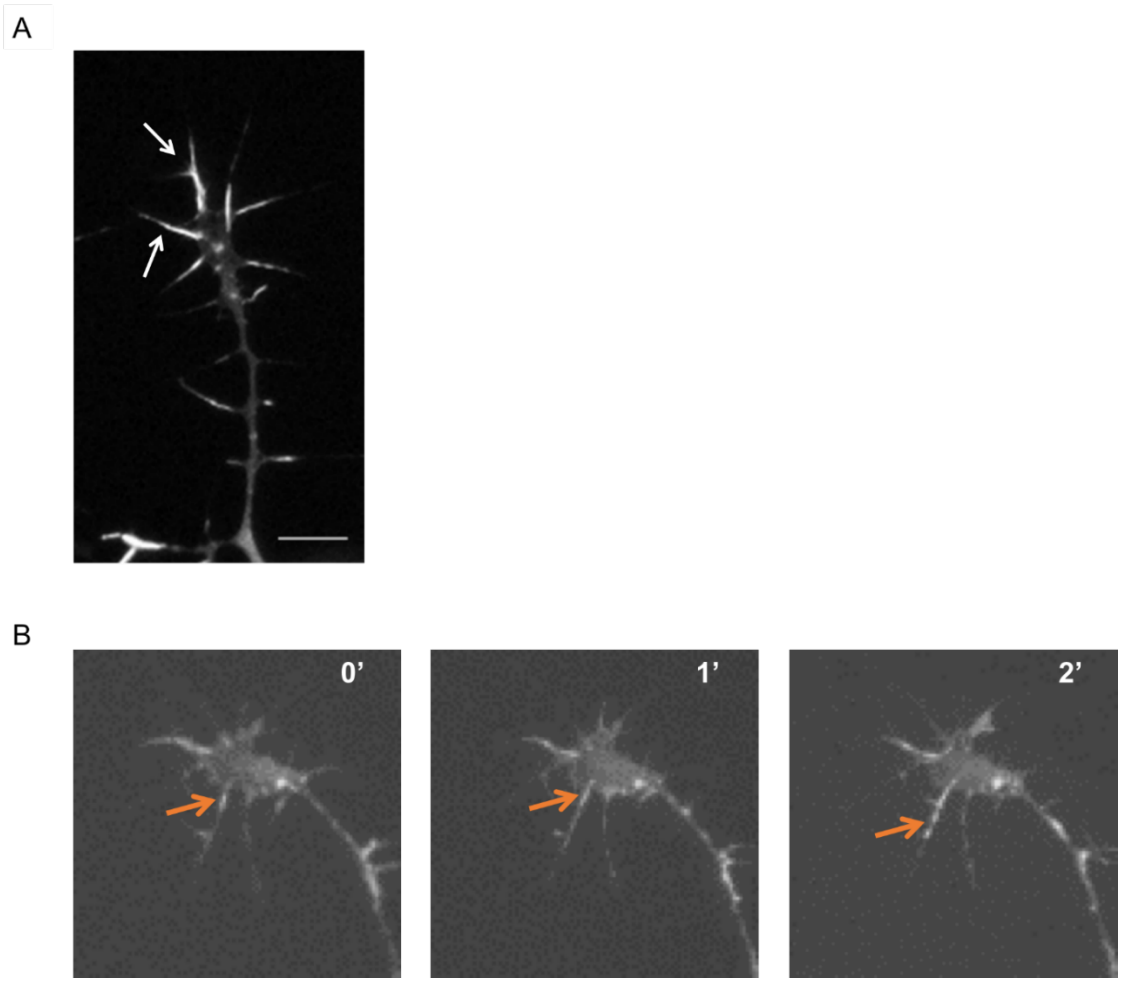

Figure 5-3. Cofilin stabilises actin filaments at high concentrations. *Dissociated E7 dorsal root ganglia neurons were nucleofected with cofilin-GFP.* ***(A)*** *Fixed neurons expressing high levels of cofilin-GFP exhibit bright, rod-shaped structures (white arrows) that extend from the transition zone of the growth cone along the host filopodium. Some rod-like structures are present in the axonal filopodia but shorter.* ***(B)*** *These structures can be seen to form in live neurons (orange arrows). In this film, the length of the structure tripled over approximately 2 minutes. Representative neuron was imaged over a period of 24 minutes at 15 second intervals. Scale bar = 10 μm.*

Rods were identified by staining neuronal growth cones with anti-cofilin antibodies and counterstained with fluorescently conjugated phalloidin. As filaments become saturated with cofilin during rod formation, the phalloidin binding sites become obscured which results in rods that are positive for cofilin staining but phalloidin negative. Unsaturated filaments are still able to bind phalloidin and are not classed as rods and this can therefore be used to robustly distinguish between potentially pathogenic rods and other structures that comprise cofilin and actin (Bamburg and Bernstein, 2016).

Rods clearly formed in response to 2-DG treatment. Rods were seen in both growth cone and axonal filopodia as well as along the axons themselves. In comparison, cofilin remained diffuse in growth cones that had been mock treated with strong cofilin staining accompanied by phalloidin counterstaining (*Fig. 5-4*). In some cases, this is difficult to tell by eye and therefore the custom image analysis Matlab script *Crod* was designed to automatically and consistently detect the presence of rods (*Fig. 5-4*). Briefly, to detect areas enriched in cofilin the script first identifies any pixels representing cofilin signal greater than 1 standard deviation above the background-subtracted global average. This is then checked against the presence of signal in the F-actin channel to verify that the cofilin increase is not simply due to increased F-actin in that area. Confirmed rods will have significant cofilin signal and no F-actin signal. The script then segments these areas of the image to identify rods by using a morphological operation to automatically determine shape. This analysis was used on fixed neurons where this double labeling method could be utilized (*Fig. 5-5*). 2-DG treatment caused a highly significant increase in rod formation in DRG explant growth cones ($p=0.0002$, Mann Whitney U-test, $n=20$, *Fig. 5-6*).

Lamellipodia collapse was a common observation in the growth cones displaying cofilin rods. This suggests that once in a rod, cofilin is sequestered and unable to perform its functions for maintaining lamellipodia. One plausible explanation is based upon the array treadmilling protrusion model (Bravo-Cordero et al., 2013). Here, cofilin severs and depolymerises actin filaments at the base of lamellipodium, maintaining a pool of G-actin for steady-state actin polymerisation in G-actin depleted conditions (Pollard et al., 2000; Pollard and Borisy, 2003). Disrupting this balance can have global effects on actin networks (Carlier and Shekhar, 2017). If cofilin is tied up in rods and not severing and releasing actin monomers for polymerisation, lamellipodia may not be able to spread, resulting in collapse.

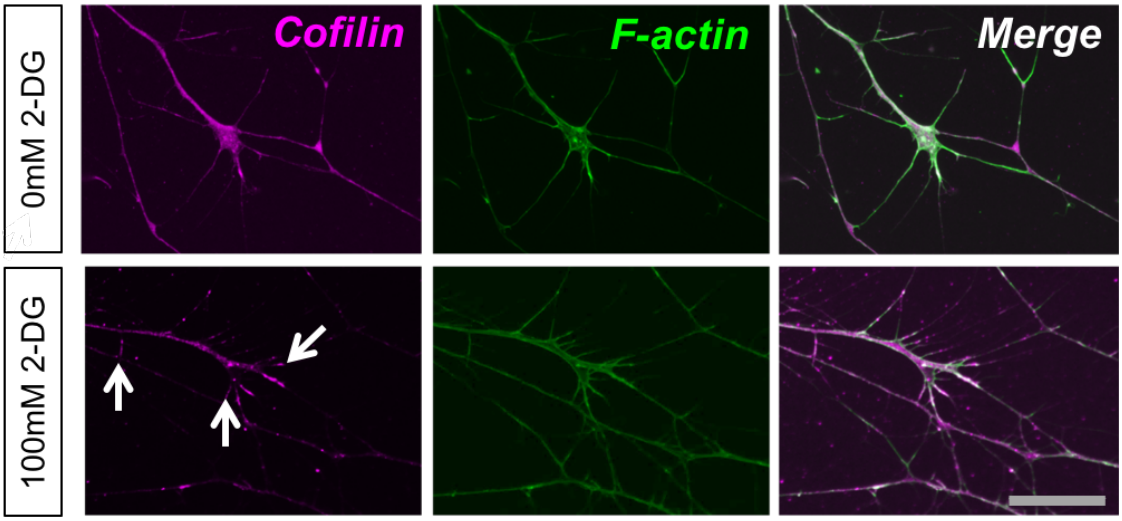

Figure 5-4. Cofilin rods form in neurons in response to acute energetic stress. *Cofilin distribution remains diffuse in growth cones that were mock treated (upper, left) compared to those treated with 2-Deoxy-D-Glucose (2-DG) (lower, left) which show rod-like structures (white arrows) towards the base of the filopodia. The explants were fixed, stained with cofilin (magenta) and counterstained with phalloidin (green) for F-actin. Confocal images representative, scale bar = 20 μm.*

A

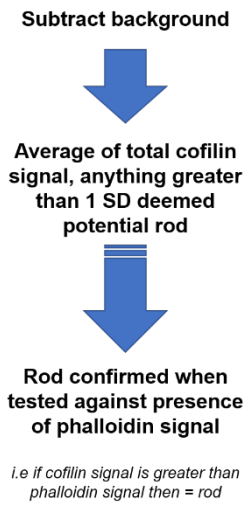

B

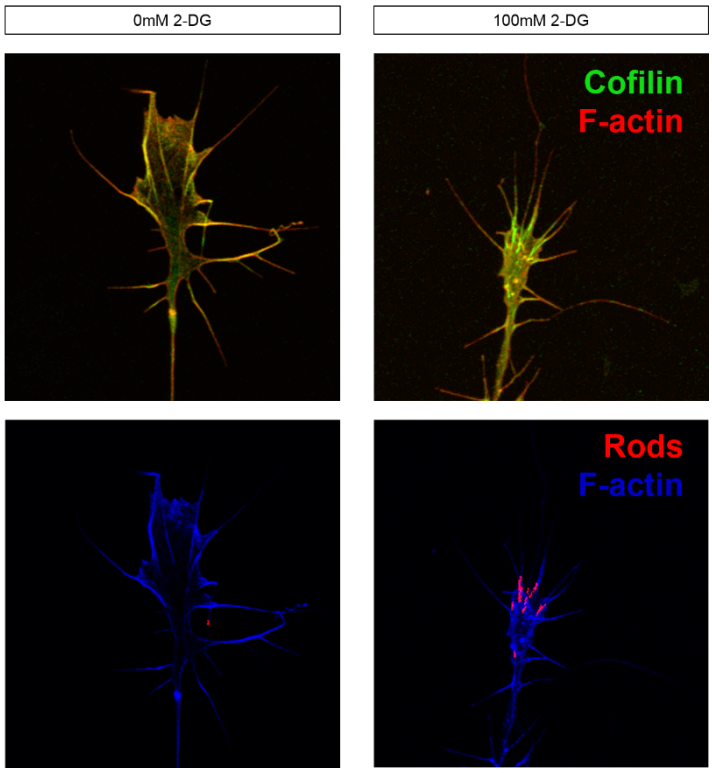

Figure 5-5. Automated analysis of cofilin rods. ***(A)*** *Algorithm used to distinguish rods from other structures containing cofilin and actin.* ***(B)*** *Visual representation of structures identified as rods by the custom image analysis Matlab script Crod.*

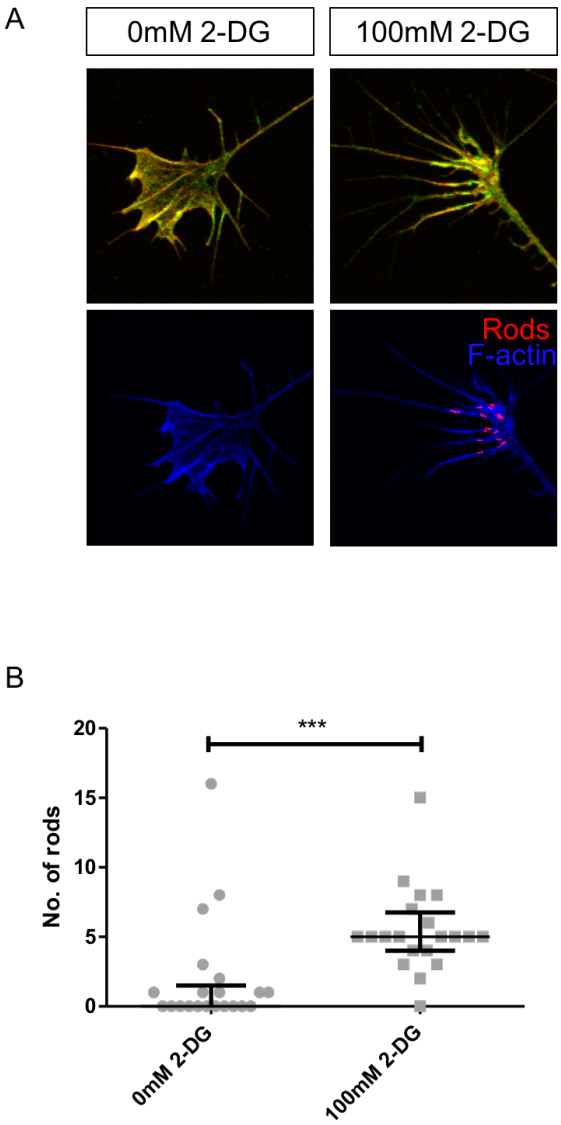

Figure 5-6. 2-DG induces rod formation in DRG. (A) *Rod shaped structures can be seen in both treated and non-treated growth cones (upper). The Matlab script Crod was used to identify individual rod structures that fulfilled the requirements of the algorithm in Fig. 5-3 (lower).* ***(B)*** *2-DG significantly induces rod formation compared to mock treated controls. Algorithm output presented in a scatter plot showing median number of rods and IQR (p=0.0002, Mann Whitney U-test, n=20)*

5.2.2 Rods are formed by endogenous cofilin

The strategy for identifying rods in fixed cells could not be used in live cells. This is because phalloidin interferes with actin dynamics and is not readily permeant to live cells, also expression of cofilin-GFP can cause spontaneous rod formation. Therefore, a genetic reporter for rods was required to assess the dynamics of formation in live neurons. The cofilin mutant, R21Q, made an ideal candidate as it has been shown not to form rods in live cells (Mi et al., 2013). The single amino acid substitution resides outside of the actin binding surface and has a twofold effect on rod formation. Firstly, the type of substitution modifies the level of vulnerability to oxidation, a process thought to be involved in rod formation. Furthermore, the mutant does not bind actin as strongly which may contribute to its reduced ability to form rods, however it is still incorporated into rods (Mi et al., 2013).

To assess the suitability of the cofilin R21Q, the fusion mutant was expressed in dissociated E7 dorsal root ganglia neurons which were then subjected to 2-DG or mock treatment with media not containing 2-DG. Co-staining with anti-cofilin antibodies showed overlap between the brightest cofilin R21Q GFP structures and immunolabelling of total cofilin. However, visualisation of co-occurrence was obscured by back ground signal from the cofilin R21Q-GFP in the cytoplasm of the neuron (*Fig. 5-7A*). To overcome this, relative fluorescence intensities were converted into a heat map where blues were least intense values and yellows represent the greatest values (*Fig. 5-7B*). The most intense pixels from each channel overlapped which showed that cofilin R21Q-GFP signal correlates with immunofluorescent detection of cofilin rods. This validated the use of cofilin R21Q-GFP as a genetic reporter of cofilin rod formation.

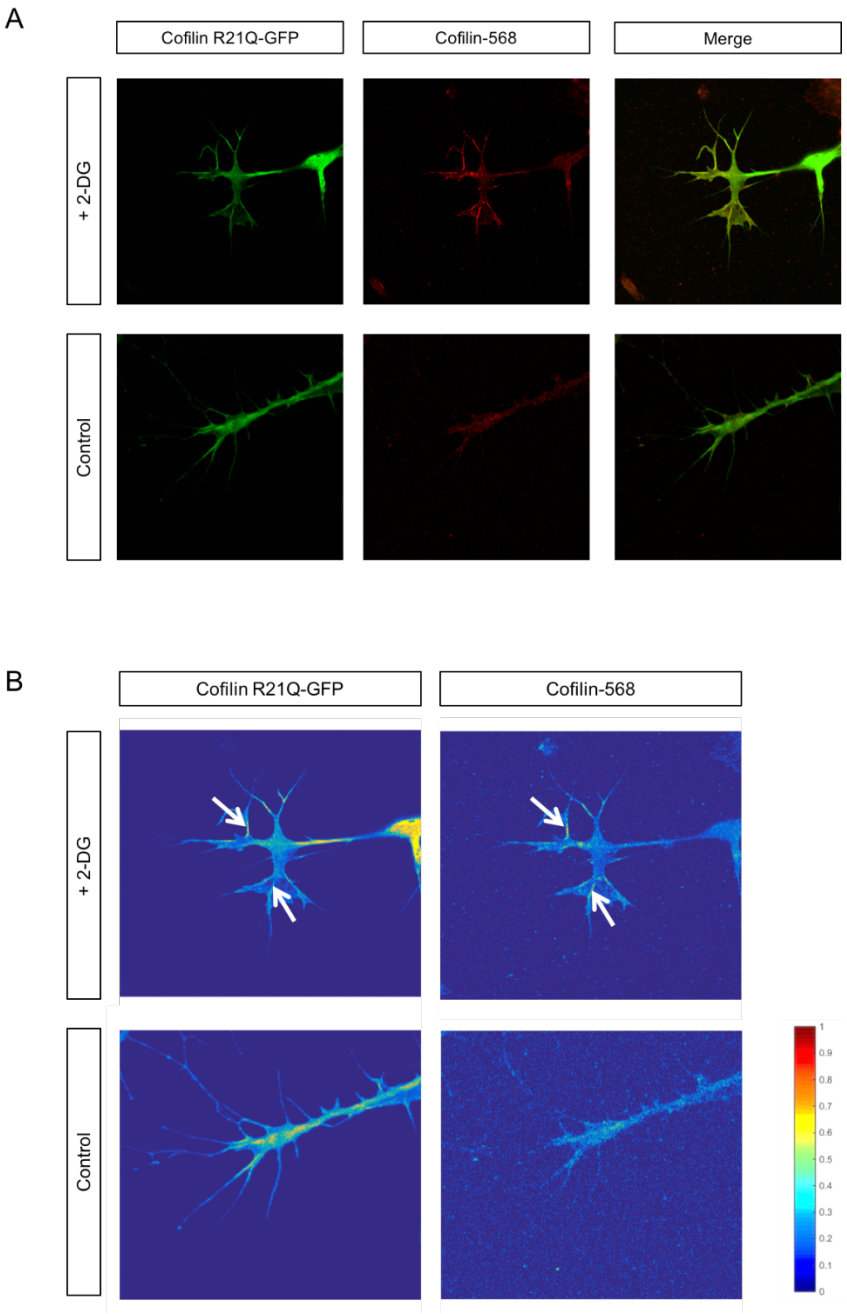

Figure 5-7. R21Q Cofilin mutant can be used as a genetic reporter for rods. *Dissociated E7 dorsal root ganglia neurons were transfected with cofilin R21Q-GFP (green) and cultured for 24 hours prior to acute treatment with 100mM 2-Deoxy-D-Glucose (10 min, 37 °C) before fixation and staining with Cofilin (red).* ***(A)*** *shows rods forming in response to 2-DG treatment, and can be seen by both immunofluorescence (middle, upper) and genetically reported (left, upper). Visualisation of co-localisation is obscured by back ground signal from the cofilin R21Q-GFP in the cytoplasm on the neuron. In* ***(B)****, relative fluorescence intensities have been converted into a heat map where blues are least intense values and yellows represent the greatest values. This confirms that Cofilin R21Q-GFP overlaps with immunofluorescent detection of cofilin rods. Confocal images representative.*

To verify that cofilin R21Q could not form rods itself, the construct was co-expressed with shRNAi specific for cofilin. There was no significant difference in the percentage of neurons with rods after 2-DG treatment compared to the mock control (untreated=33% ± 6.2, treated=42% ± 6.2). Additionally, there was no significant difference in the median number of rods formed in the neurons that did develop rods (median = 0 for both groups, p=0.3097 Mann-Whitney U-test, n=18). This confirms that cofilin R21Q-GFP can only be incorporated into rods formed by endogenous cofilin. Those rods that did form were probably due to incomplete knock down of cofilin (*Fig. 5-8*).

Rod formation was then observed in living neurons by widefield microscopy. Growth cones of DRG neurons were filmed 48 hours after nucleofection with cofilin R21Q-GFP and the shRNAI for cofilin. Transfected cofilin genes were hair-resistant due to species differences. Fluorescence intensity of the human cofilin fusion proteins did not appear reduced when co-expressed with the hairpins for chick cofilin, however it was it was not viable to harvest enough primary neurons to confirm this by Western blot. Rods began to appear in growth cones containing normal levels of cofilin at around 6.5 minutes after addition of 50mM 2-DG and remained for the entirety of the imaging period. These structures were seen to coalesce as imaging continued. In comparison, no rods were seen in growth cones where cofilin was knocked down. Importantly, no rods formed in the mock treated controls which suggests that illumination settings were below the levels required to initiate rod formation by phototoxicity (*Fig. 5-9*).

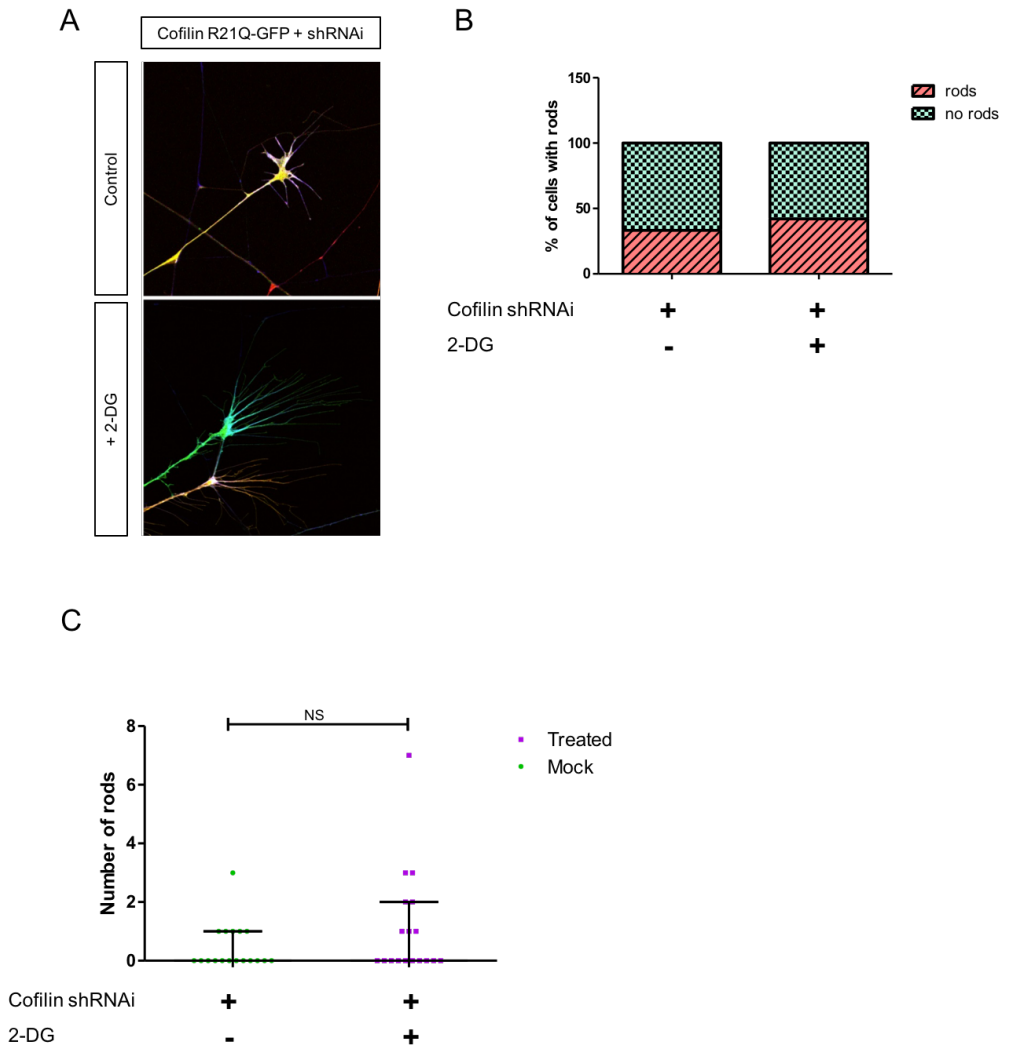

Figure 5-8. R21Q Cofilin mutant is only incorporated into rods formed by endogenous cofilin. (A) *Dissociated E7 dorsal root ganglia neurons were co-nucleofected with cofilin R21Q-GFP and shRNAi construct for Cofilin. Neurons were cultured for 48 hours before treatment with 100 mM 2-DG (10 mins, 37℃), then fixed and stained with phalloidin-647. Confocal images representative.* ***(B)*** *Treatment with 2-DG induced a modest but statistically insignificant increase in the percentage of neurons with rods. Quantification of neurons imaged showing the percentage of growth cones with and without rods where cofilin had been knocked down but cofilin R21Q was present (mock treated=33% ± 6.2, treated=42% ± 6.2).* ***(C)*** *There was no significant difference median in the number of rods formed in neurons displaying rods (p=0.3097 Mann-Whitney U-test, n=18). Scatter plot shows median, error bars indicate interquartile range.*

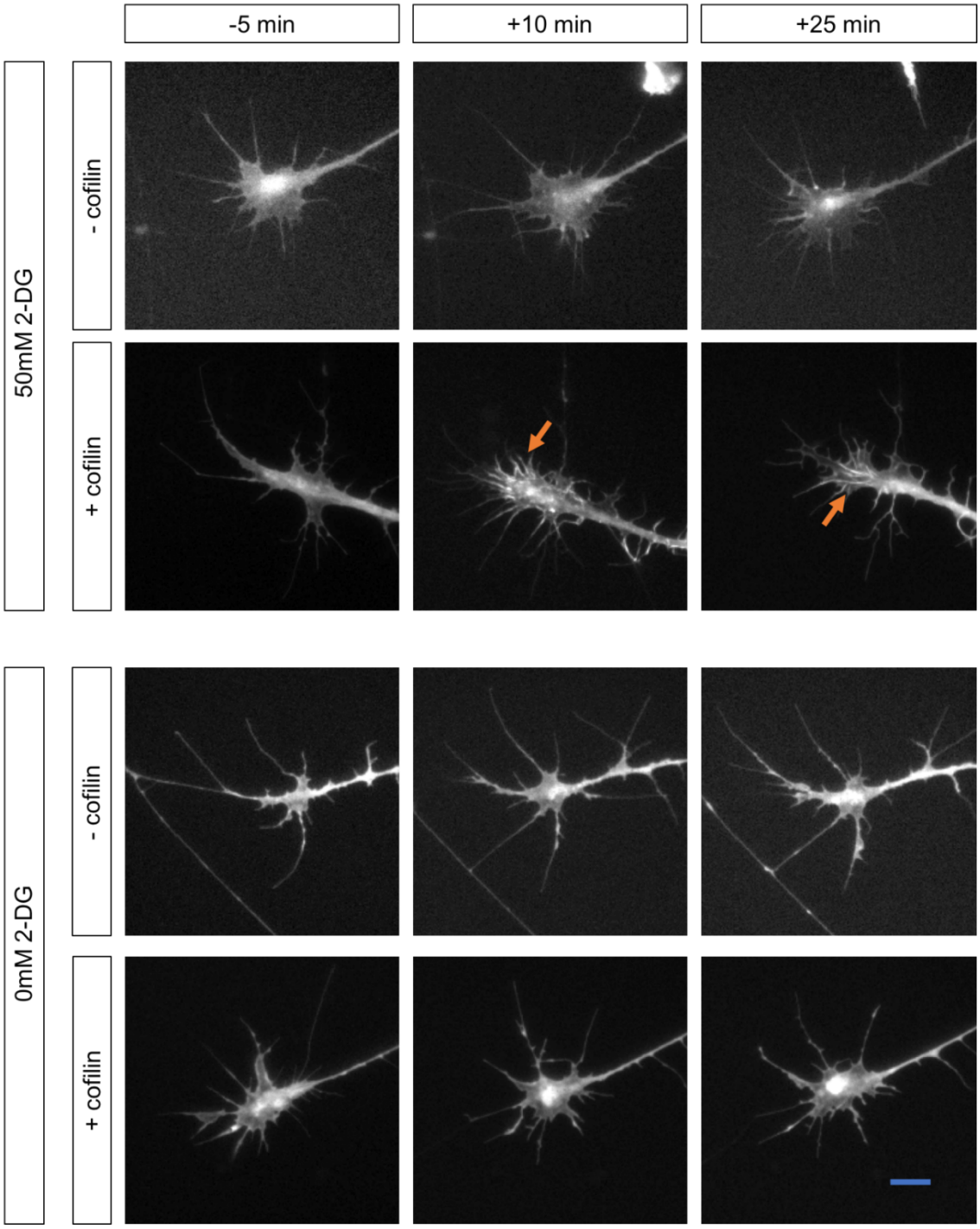

Figure 5-9. Cofilin rod formation in growth cones of live neurons. *Rods only formed when cofilin was present on 2-DG treatment. Rods first emerged at 6.5 minutes post-2-DG treatment and remained for the entirety of the imaging period. Many of those that appeared first coalesced to form larger structures (orange arrows). Rods were not observed in mock treated controls or when cofilin was knocked down. Scale bar = 10 µm. See Appendix D for Supplementary Media File 5, 6, 7 & 8.*

5.2.3 Cofilin must be activated for rods to form

To assess the activity state of cofilin in rod formation, cofilin S3 mutants were expressed with cofilin hair pins in DRG dissociated cultures. Cells were treated with 50 mM 2-DG, 10 min at 37°C before fixing and costaining with fluorescently conjugated phalloidin. Rods formed in response to 50 mM when constitutively active cofilin was present (*Fig. 5-10*). The aggregates formed in these growth cones were large and localised to filopodia and at the neck of the axon. Automated analysis of rod formation was attempted using the automated Matlab script *Crod,* however the contiguous nature of the aggregates prevented an accurate rod count (*Fig. 5-11*).

5.2.4 Cofilin inclusions form in the brains of J20 mice

The J20 mouse model of Alzheimer's disease has been well characterized and frequently used in the examination of pathophysiology of Alzheimer's disease. The mouse line expresses high levels of the human amyloid precursor protein (APP), harbouring two familial mutations (Swedish KM670/671NL and Indiana V717F) under the control of the platelet-derived growth factor (PDGF) promoter, resulting in significant amyloid-β $_{1-42}$ deposition in the brain. This causes age-dependent formation of amyloid plaques, a corresponding decrease in synaptic density and a range of learning and memory deficits which are strongly linked to the amyloid-β based disease progression in humans (Elder et al., 2010; Harris et al., 2010; Mucke et al., 2000). The brain slices of J20 mice were examined by immunohistochemistry to confirm that rod formation was relevant in disease *in vivo*. Cerebral cortex sections of wildtype or J20 +/- mice were labelled with DAPI and anti-cofilin antibodies (*Fig. 5-12*). Cofilin-positive inclusions were small and rare in wildtype but occurred at much higher density in J20 mice, this difference was found to be significant (Mann Whitney U test, ****=$p<0.0001$).

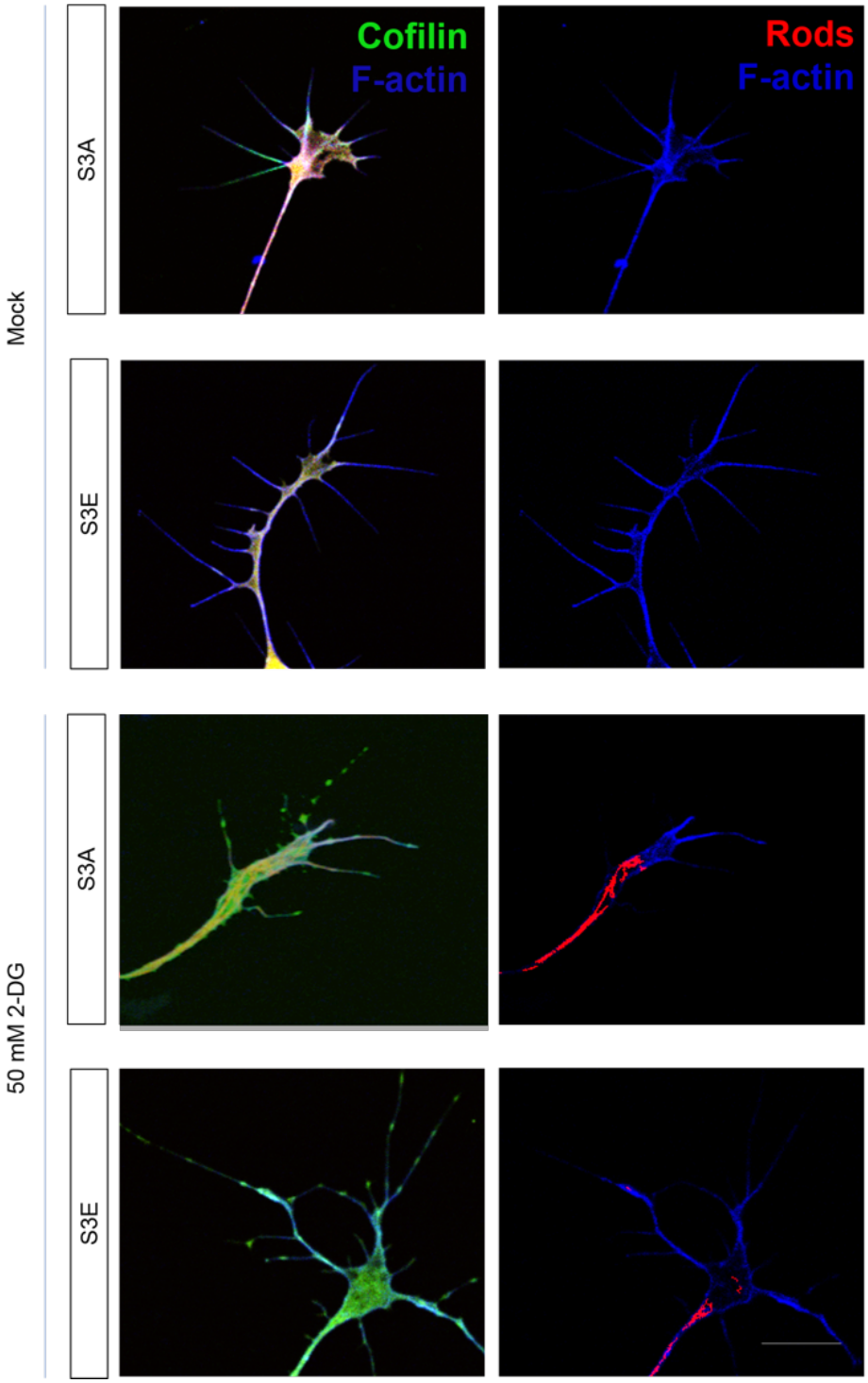

Figure 5-10. Cofilin must be activated to form rods. *Rods form in response to 50 mM 2-DG when cofilin is constitutively active. Rods could be seen to occlude the bases of filopodia and the growth cone itself. S3E = Phosphomimetic cofilin mutant; S3A = Constitutively active cofilin mutant. Images representative of each condition. Scale bar = 10 μm*

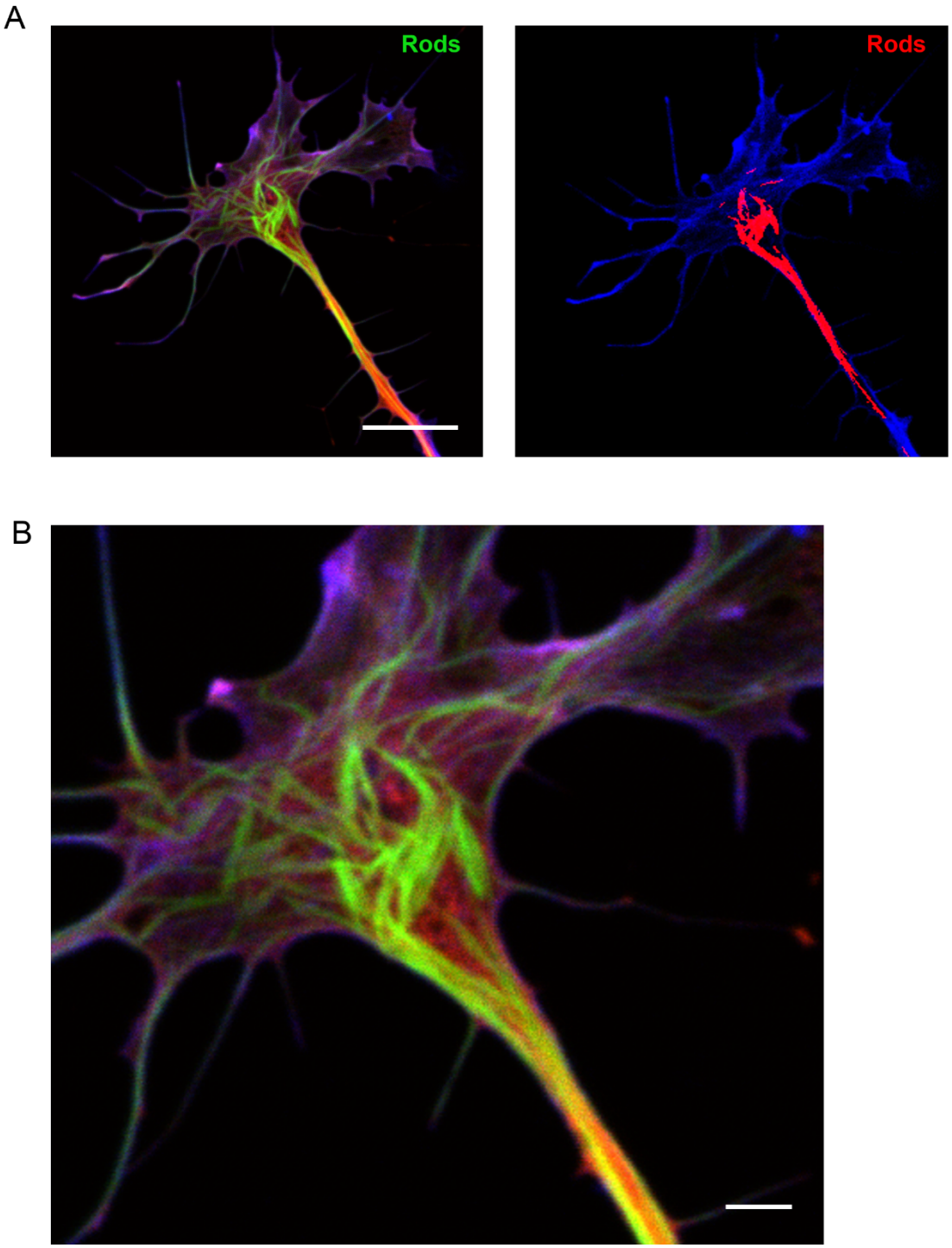

Figure 5-11. Growth cone displaying large rod aggregate. (A) *Example of the large aggregations of rods that can form within the growth cone and how single rods cannot be defined in these mega structures. Scale bar = 10 µm* ***(B)*** *Close up of confocal image in* ***(A)*** *demonstrates the complexity of the coalesced rod aggregates. Scale bar = 2.5 µm.*

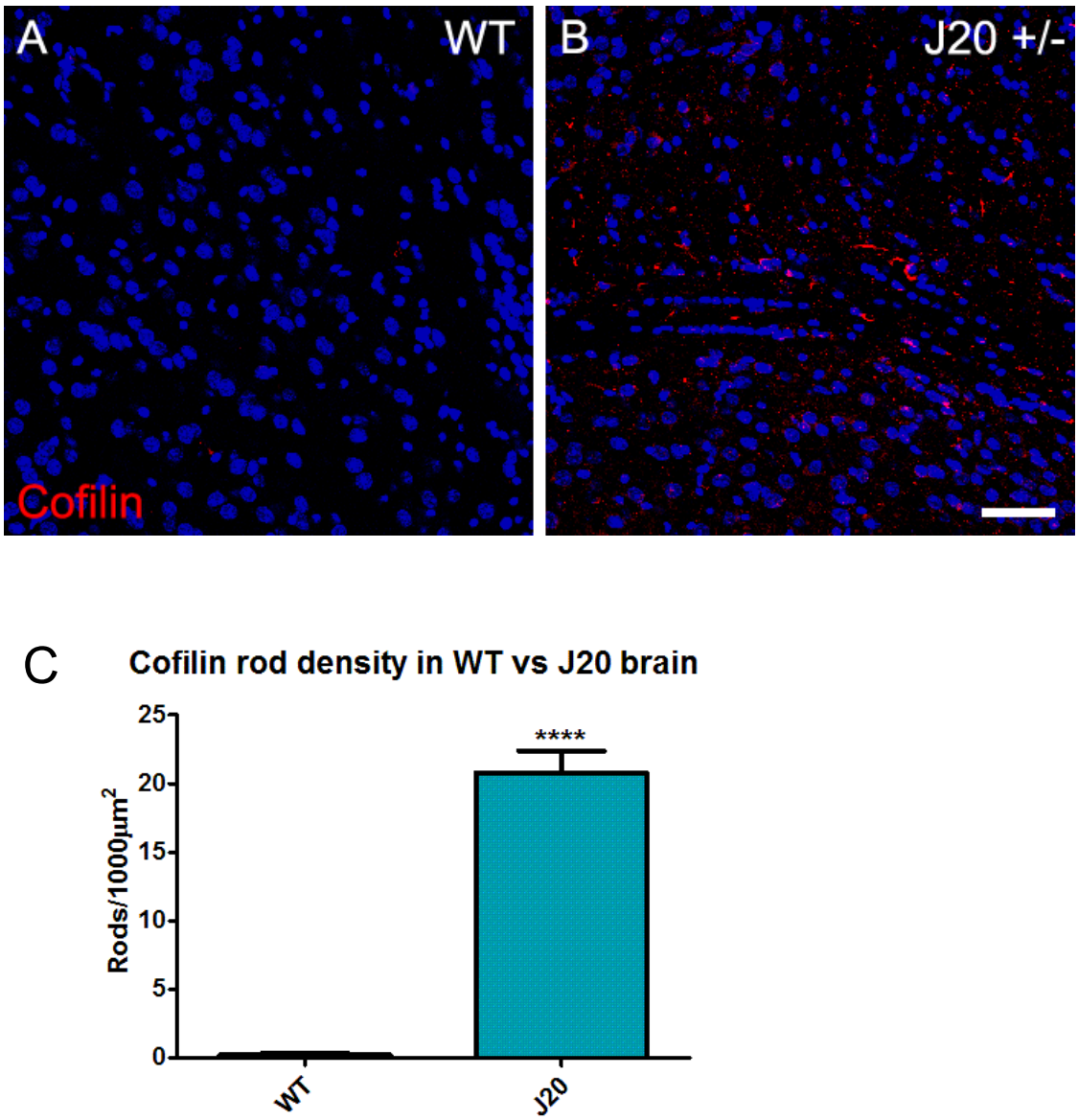

Figure 5-12. Cofilin rods form in the brains of J20 mice. *Cerebral cortex sections of wildtype (A) or J20 +/-* ***(B)*** *mice labelled with DAPI (blue) and anti-cofilin antibody (red). Cofilin-positive inclusions are small and rare in wildtype (arrows, A) but occur at much higher density in J20 mice (B), this is quantified in* ***(C)****. Images taken with identical confocal settings, scale bar = 50 µm, Mann Whitney U test. ****=p<0.0001.*

5.2.5 AIP blocks cofilin rod formation in cofilin overexpression

Having established a method for detecting and analysing rods in both fixed and live cells, and confirming rod formation is cofilin-dependent, AIP-1 was then expressed to assess whether the protein could modify rod formation under pathological conditions.

To further examine the potency of this effect, cofilin-GFP and AIP-1-Cardinal were co-expressed in neurons which were then fixed. In cells in which AIP-1 expression was high, cofilin-GFP formed elongated patches and blobs along the length of filopodia. In contrast, growth cones, in the same dish, expressing relatively low AIP-1 displayed the characteristic rod-like structures seen when wild-type cofilin is overexpressed (Fi*g. 5-13*). The effect was analysed by blinded classification of images into “high” or “low” AIP-1 expression and presence or absence of cofilin rods. Where AIP-1 expression was classed as low, 70% of growth cones displayed rod-like cofilin-GFP distribution (*Fig. 5-14*). In contrast, where AIP-1 expression was classed as high, 82% of growth cones displayed diffuse cofilin-GFP distribution. It is important to note this experiment was intended to demonstrate the cofilin redistribution capacity of AIP-1 and therefore fluorescently conjugated phalloidin was not used as a counterstain at this point.

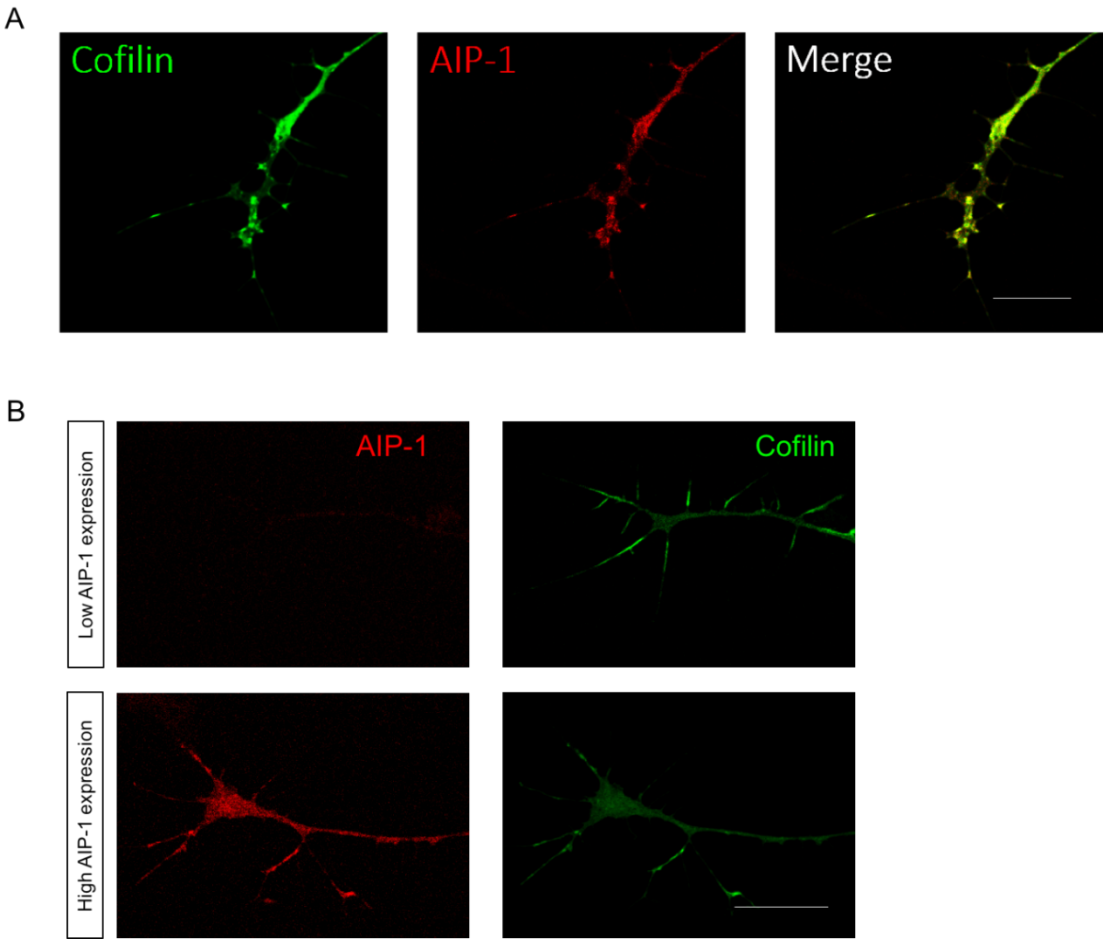

Figure 5-13. AIP redistributes cofilin and blocks rod formation.
(A) *Endogenous cofilin appears in round, punctate structures that co-localise with AIP-1 suggesting there is a spatial relationship between the proteins. Dissociated E7 dorsal root ganglia neurons were nucleofected with AIP-1-Cardinal (red), cultured for 24 hours then fixed and stained for cofilin (green).* ***(B)*** *Where AIP-1 expression is low, growth cones display typical rod-like structures seen when wild-type cofilin is overexpressed. Conversely, where AIP-1 expression is high, cofilin-GFP appears as elongated patches along filopodia and diffuse in the central domain of the growth cone. Dissociated E7 dorsal root ganglia neurons were co-nucleofected with wild-type cofilin and AIP-1-Cardinal and cultured for 24 hours before fixing.*

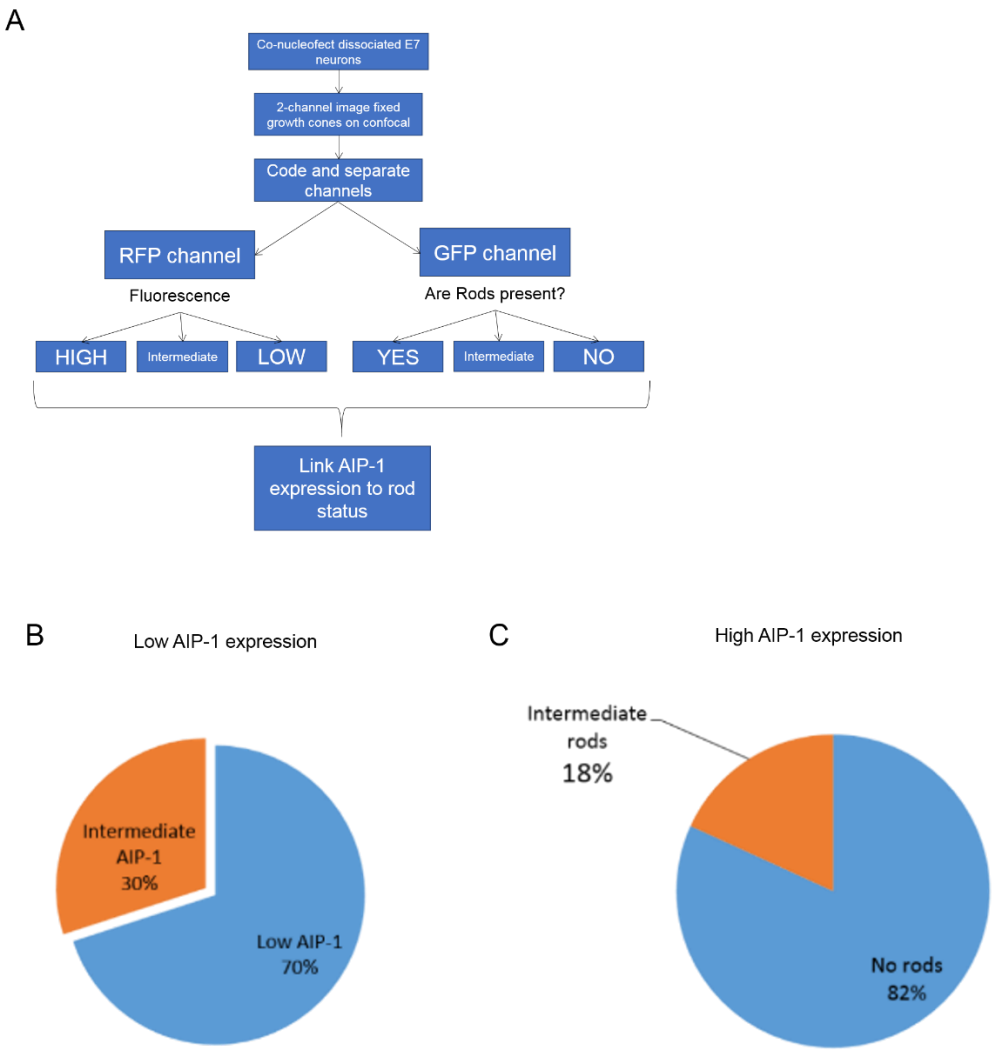

Figure 5-14. Quantification of rod frequency. (A) *Confocal images of dissociated E7 dorsal root ganglia neurons co-expressing wild-type cofilin-GFP and AIP-1-Cardinal were taken with fixed gain and offset levels for each channel to ensure comparative fluorescence intensities between growth cones. The channels for each image were separated and blindly coded. Average fluorescence intensity values for the Cardinal channel (AIP-1) for each image were extracted using FIJI and categorised as High, Intermediate, or Low. The GFP channel images were grouped according to whether rods were present or not. An intermediate category was included to classify neurons that had both rod-like structures and punctate spots. The file name from each file was revealed and matched with its counterpart channel. Percentages of growth cones were plotted according to AIP-1 expression levels* ***(B)*** *which shows that where AIP-1 expression is low, 70% of growth cones display rods whilst only 30% of growth cones expressing intermediate levels of AIP-1 display rods. When AIP-1 expression is high, 82% of growth cones have no rods, and only 18% have low levels of rods* ***(C)****.*

5.2.6 AIP-1 blocks rods formed by amyloid-β treatment

Having shown that AIP-1 can potently prevent rods forming in response to cofilin expression, I tested whether AIP-1 could counter rod formation induced by the presence of amyloid-β the principle constituent of plaques found in Alzheimer's brains. Amyloid-β comprises peptides of 36-43 amino acids, with the longer species being the most hydrophobic and fibrillogenic forms predominantly found in deposits within amyloid plaques (Barrow and Zagorski, 1991; Murphy and LeVine, 2010). Cofilin-actin rods are found in Alzheimer brains however a direct link to amyloid plaques has yet to be shown (Minamide et al., 2000).

E7 dorsal root ganglion neurons expressing AIP-1-mCardinal were acutely exposed to amyloid-$\beta_{1\text{-}42}$ oligomers for 1 hour at 37°C, fixed and labelled with anti-cofilin antibodies to assess rod formation. Fewer rods formed in AIP-1 expressing neurons than in their non-expressing counterparts (*Fig. 5-15A*). To quantify the effect, images were processed by a custom Matlab image analysis script *ROSA*, which measures eccentricity of objects to delineate between rod structures and those more circular in shape. Here, rod formation is reported as the rod index which indicates the presence of rods based on form, where zero is a perfect circle and values closer to 1 indicate shapes wider than they are long. Exposure of neurons to amyloid-$\beta_{1\text{-}42,}$ led to robust cofilin rod formation in control neurons (*Fig. 5-15B*) but only small cofilin-decorated fragments or no rods at all were observed in neurons transfected with AIP-1 ($p=0.0001$ Mann Whitney U test). This strongly supports the hypothesis that AIP-1 can play a key, protective role to prevent cofilin rod deposition in Alzheimer's disease.

A

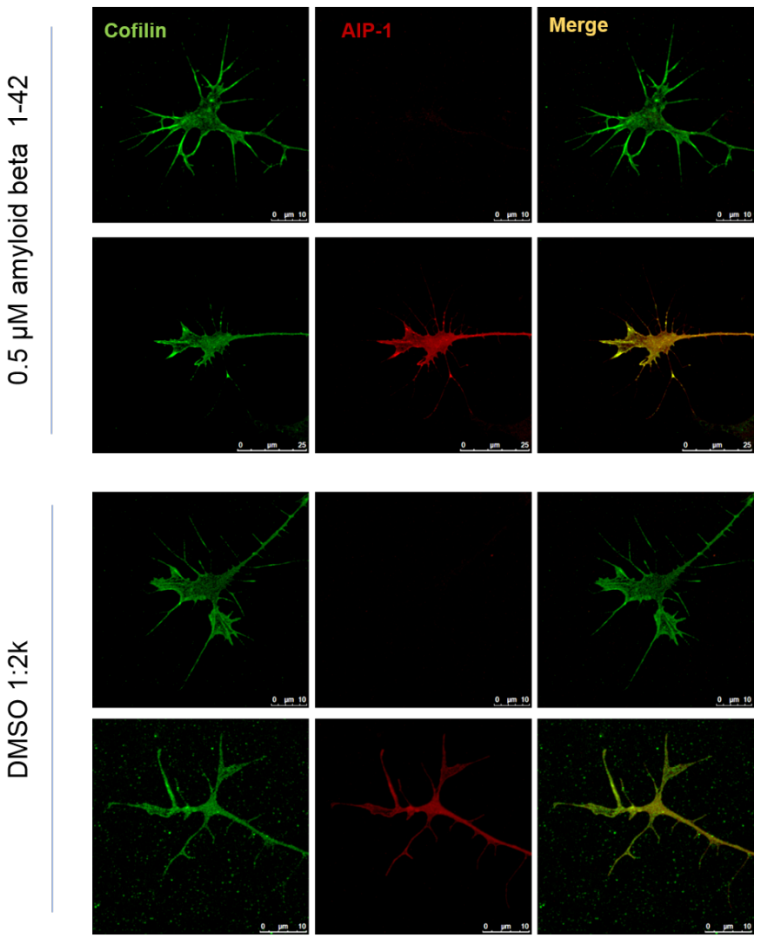

B

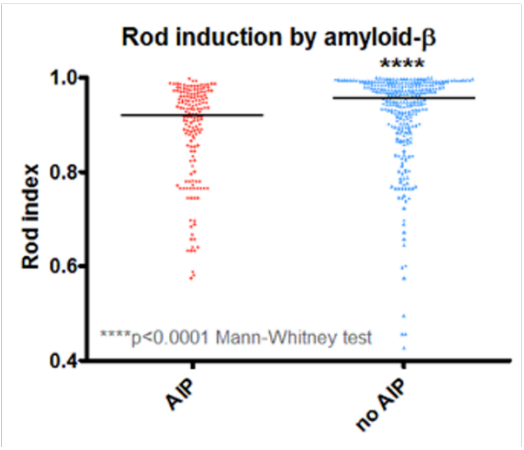

Figure 5-15. AIP-1 expression prevents cofilin rod induction by amyloid-β exposure. (A) *E7 chick dorsal root ganglia treated with amyloid-β_{1-42} oligomers for 1 hr, immunolabelled with anti-cofilin antibody (green).* ***(B)*** *Quantification of rod index using custom Matlab image analysis script ROSA. Higher values indicate increased rod formation (max. value 1). Median rod index in presence of AIP-1 = 0.92 (red circles) is significantly reduced compared to the absence of AIP-1 = 0.96 (blue triangles; p<0.0001 Mann-Whitney test). Scale bar = 10 µm.*

5.2.7 AIP-1 blocks rods formed by 2-DG treatment

The experimental use of amyloid-β is problematic in that the oligomers can aggregate before application and therefore must be handled with care. 2-DG was chosen as a more pragmatic rod inducer during the development of analytical tools for characterising the effect of AIP-1 on rod formation.

First, AIP-1 was confirmed to block 2-DG induced rod formation. Neurons overexpressing AIP-1-RFP were treated with 50mM 2-DG for 10 min at 37°C before fixation and staining with anti-cofilin antibodies and fluorescently conjugated phalloidin. The Matlab script, *Crod*, was then used to robustly quantify the effect of AIP-1 over expression on 2-DG induced rod formation. 2-DG induced rod formation was strongly repressed in growth cones overexpressing AIP-1 when compared to control (*Fig. 5-16*).

To reveal whether endogenous AIP-1 played a role in preventing the onset of rod formation, AIP-1 would need to be knocked down. To do this, pRNAiCAIP-1 was generated, as described in 4.2.5, for the production of specific siRNA. This hairpin was produced in house (kind gift of Dr J. Chilton), and its efficacy validated by immunofluorescence in DF-1 cells as the commercial antibodies (ab173574, Abcam; PA5-27645, Thermo Fisher) did not work well in chick DRG neurons. Further validation was attempted by Western blot but three attempts at enriching the hairpin expressing population of DF-1 cells failed and it was not technically possible to gather enough lysate from the primary neuronal cultures.

A chick derived fibroblast cell line, DF-1, was used too as the two anti-AIP-1 antibodies tested in DRG growth cones did not work. Furthermore, AIP-1 in

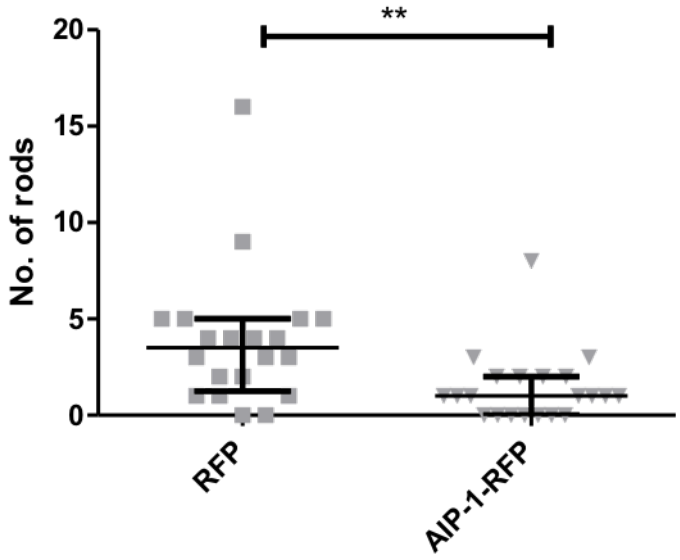

Figure 5-16. AIP-1 overexpression blocks 2-DG induced rod formation. *Median number of rods in growth cones overexpressing AIP-1 and treated with 50 mM 2-DG was significantly lower than in control growth cones (p=0.0016, Mann Whitney U-test, n ≥ 21).*

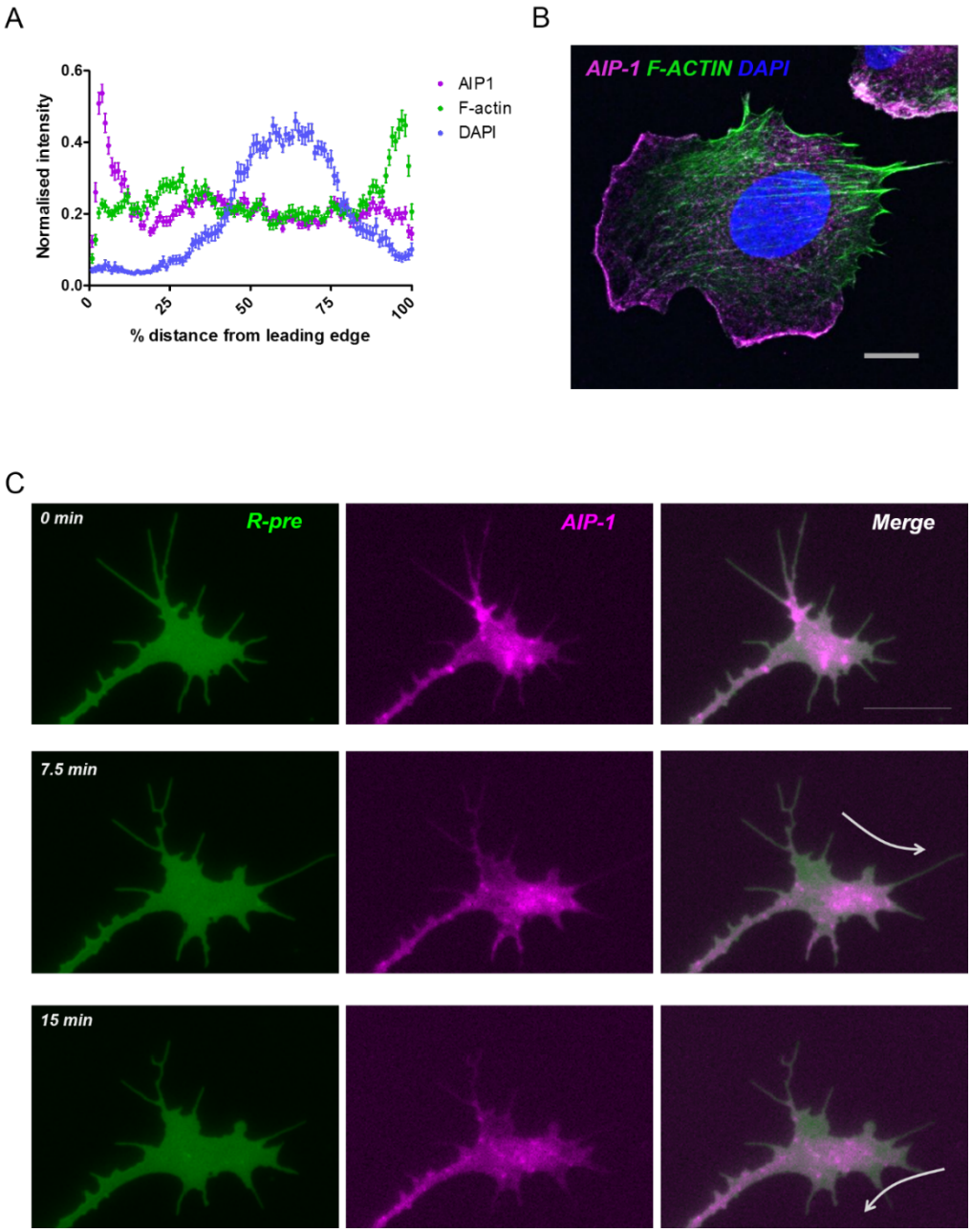

Figure 5-17. AIP-1 localises to areas of rapid actin turnover.
(A) *Assessment of AIP-1, phalloidin- AF488 and DAPI fluorescent intensities shows AIP-1 is collected at the leading edge of fixed DF-1 fibroblasts. Graph shows mean normalized intensity (+/- SEM) by the distance from the leading edge as a percentage of total cell length. N=41 linescans from 18 cells.*
(B) *AIP-1 (magenta) localises to the leading edge of polarized DF-1 fibroblast with lamellapodia. F-actin (green) forms stress fibres towards the rear of the cell at the trailing edge.Scale bar = 10μm, representative confocal image).*
(C) *AIP-1 patches shift to side of greatest protrusive activity. Stills taken from representative film of DRG growth cone co-expressing AIP-1-Cardinal (magenta) and R-Pre-YFP (green) a membrane marker at T= 0, 7.5min, 15min. No exogenous guidance cues added to induce turning. Arrows demonstrate direction of movement. Scale bar = 10μm. See Appendix E for Supplementary Media File 9.*

DF-1 cells localises to areas of active protrusion. AIP-1-Cardinal was expressed in primary neurons to assess AIP-1 localisation in neuronal growth cones. During live filming, AIP-1 patches shifted to areas of greatest protrusive activity of the growth cone which mirrors the findings in DF-1 cells and supports its role in the rapid actin turnover (*Fig 5.17*). This was seen in several live growth cones to varying degrees, but analysis was not performed as it was difficult to capture enough growth cones during turning and extension that were expressing the appropriate levels of the fusion proteins. Turning assays could be a viable technique to assist in reproducibility of inducing growth cone turning. 2-DG induced rod formation was increased when AIP-1 was knocked down using shRNAI specific for chick AIP-1 in comparison to the mock treated control.

If AIP-1 was able to reduce rod formation, it would be natural to hypothesise that knockdown would increase the number of rods induced by 2-DG treatment. However, this difference was not seen between the 2-DG treated AIP-1 knock down and control (*Fig. 5-18*). This could possibly be caused by increased frequency of coalescence of rods which creates structures bigger which means the constituent rods cannot be individually counted. When visually inspected positive rod-shaped structures appear bunched together rather than discrete rods. Another limitation is that false positives can be generated by patchy cofilin localisation as seen some mock treated growth cones. This primarily occurs in axons rather than growth cones and therefore could be readily discarded from the analysis (*Fig. 5-19*).

A

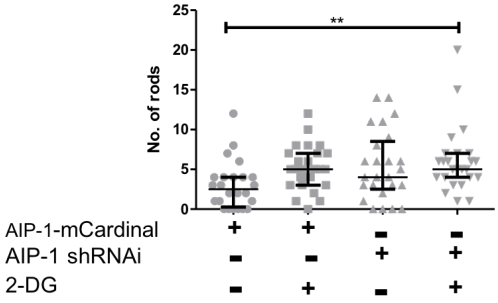

B

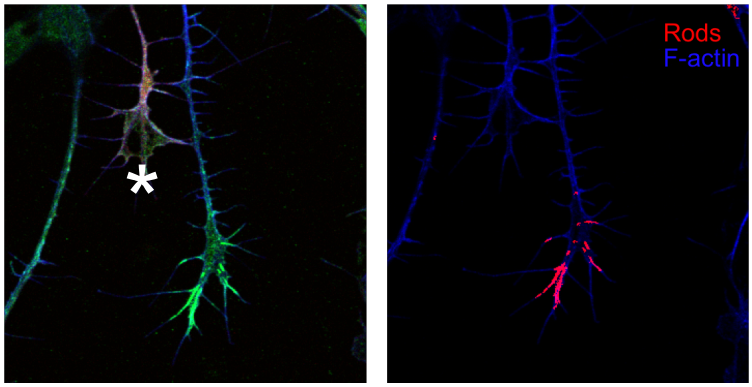

Figure 5-18. The effects of altering levels of AIP-1 expression
(A) *AIP-1 knockdown did not significantly increase rod formation when compared to control, but there was a significant difference between the mock treated controls and the AIP-1 knock down growth cones that had been treated with 50mM 2-DG (Kruskall-Wallis test, Dunn's post-hoc comparisons test, p=0.0065, n* ≥ 25 for each *condition).* ***(B)*** *Confocal image of a growth cone overexpressing AIP-1-RFP (asterisk) beside one that is not overexpressing AIP-1-RFP. There is a stark contrast in rod formation between the two examples. The hairpin efficacy validated by immunofluorescence in DF-1 cells as the commercial antibodies (ab173574, Abcam; PA5-27645, Thermo Fisher) did not work well in chick DRG neurons. Further validation was attempted by Western blot but three attempts at enriching the hairpin expressing population of DF-1 cells failed and it was not technically possible to gather enough lysate from the primary neuronal cultures.*

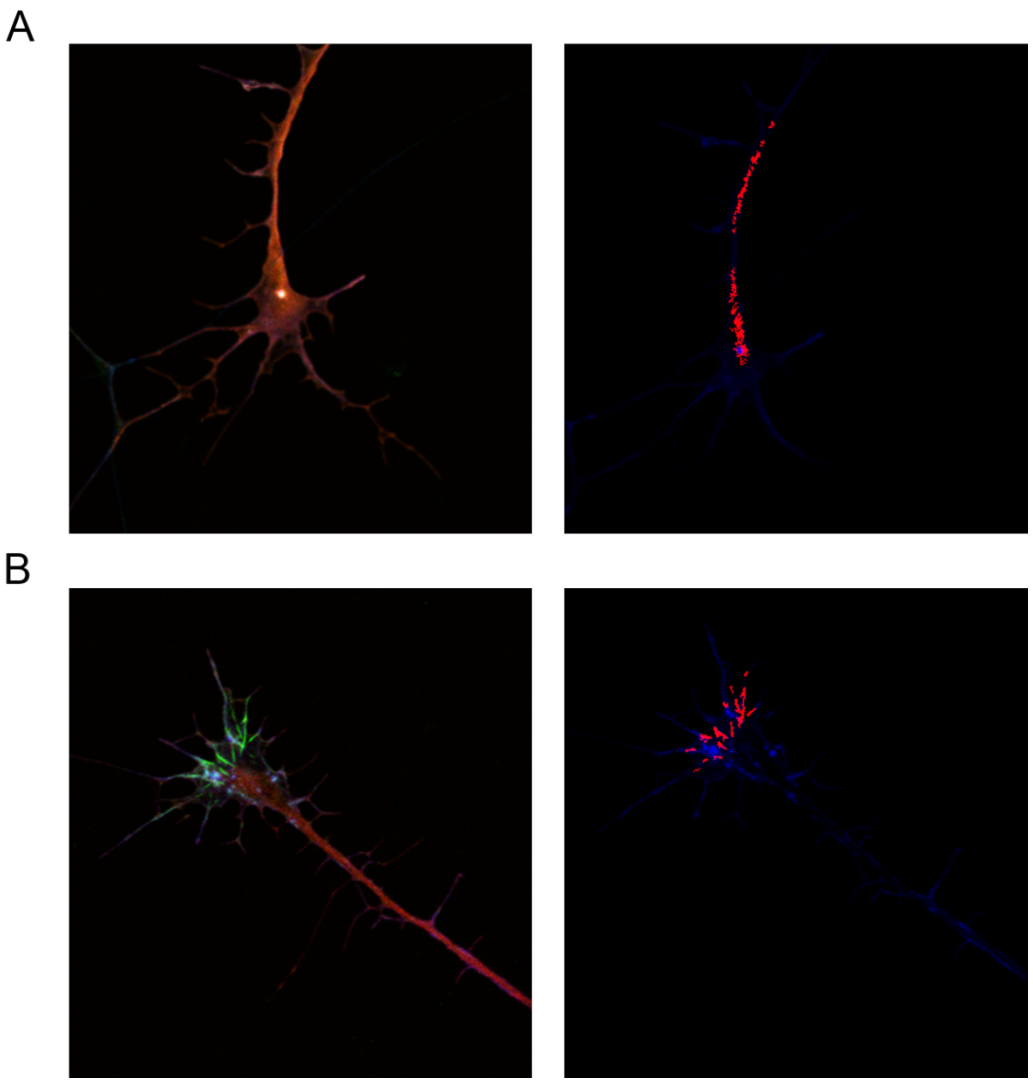

Figure 5-19. Rods display a variation in form. (A) *Left image shows a confocal image of growth cone with diffuse cofilin distribution, right shows how the image analysis algorithm can pick up a false positive.* ***(B)*** *Left image shows how rods can amalgamate potentially causing an underreporting of rod number.*

5.3 Discussion

The dysregulation of cofilin activity as a consequence of cellular stress can have huge impacts on cell function. In particular, the presence of cofilin rods in the growth cones of neurons is relevant to human disease as they are linked to a number of myopathies and several neurodegenerative diseases (Goebel and Warlo, 1997; Minamide et al., 2010; Minamide et al., 2000). Here, rods affect the formation and maintenance of synaptic morphology resulting in accelerated dysfunction associated with neurodegeneration. Cofilin rods are hypothesized to be transiently neuroprotective to acute insults in cellular models, but have been shown to contribute to neuronal toxicity in models of Huntington's disease and Alzheimer's disease. More importantly, rod formation is reversible and thus modulating aberrant rod formation could be of therapeutic benefit (Bamburg and Bernstein, 2016; Mi et al., 2013; Minamide et al., 2000; Shaw and Bamburg, 2017). This chapter assessed whether AIP-1 could block cofilin rod formation in the growth cones of DRG neurons, a model used to assess the underlying cellular principles of neurological disorders.

I have discovered that AIP-1 has a potent ability to prevent the formation of cofilin rods in neurons, even when they are treated with amyloid-$\beta_{1\text{-}42}$ oligomers or subjected to metabolic stress. This is the first study to demonstrate a molecular mechanism for preventing rod formation in the presence of a neuronal stressor and has the potential to protect against rod formation by other stressors such as those associated with disease *e.g.* inflammation and excitotoxicity.

AIP-1 is a highly conserved protein, found across eukaryotes, that functions with other regulators of actin dynamics such as cofilin and coronin (Kueh et al., 2008).

AIP-1 enhances the ability of cofilin to disassemble purified actin filaments as has been elegantly and extensively characterised *in vitro* (Gressin et al., 2015). Complete loss of AIP-1 causes embryonic lethality in mice (Kile et al., 2007), however, little is known about its role in neurons other than it is upregulated in the cochlea after noise damage (Oh et al., 2002). I hypothesised that AIP-1 could be used to block or reverse cofilin rod deposition (*Fig. 5-20*). When cofilin is overexpressed in neurons it severs actin filaments, decorates and stabilises the resulting fragments which then coalesce into rods. I then found that co-transfection with AIP-1 blocks rod induction and sequesters the cofilin. This effect is highly reproducible; in neurons classified as highly expressing AIP-1, fully formed rods were never seen even when cofilin is overexpressed. Furthermore, this suggests that AIP-1 enhances cofilin-mediated filament disassembly when filaments are highly decorated with cofilin decoration. This is supported by a previous study that revealed AIP-1 destabilises filaments in the presence of saturating amounts cofilin (Nadkarni and Brieher, 2014). One potential outcome of this finding is that cofilin saturated filaments could be specifically targeted for dismantling by AIP-1, allowing for normal cofilin function at sub-saturating concentrations.

Whilst AIP-1 is known to enhance cofilin-mediated disassembly, much of its study has been conducted at the molecular level using *in vitro* assays. One single study on intranuclear rod formation in *Dictyostelium* demonstrated that AIP-1 is involved in the formation of rods through maintenance of the actin monomer pool (Ishikawa-Ankerhold et al., 2017).

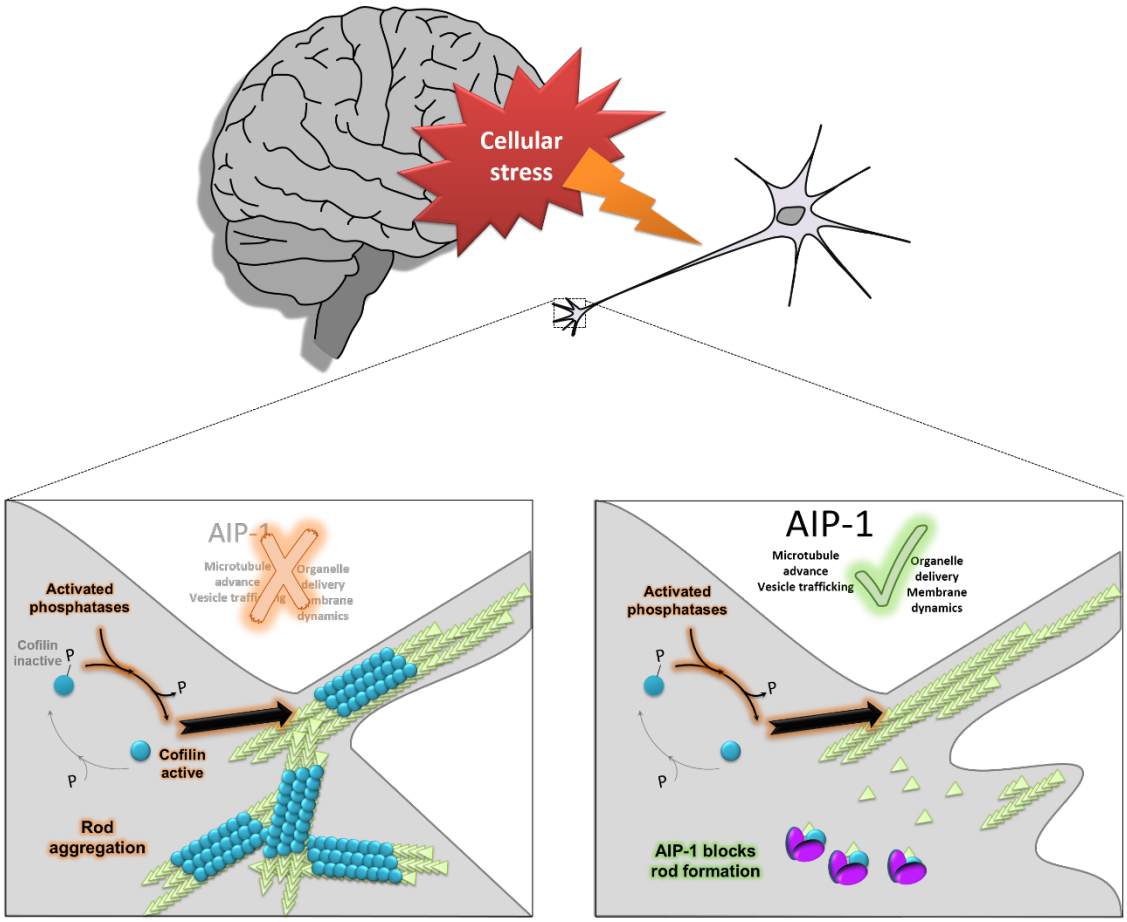

Figure 5-20. Proposed mechanism of action of AIP-1 in rescuing cytoskeletal dysfunction in neurodegeneration. *(Left) AIP-1 absent: The onset of cellular stress, such as amyloid-β exposure, causes activated phosphatases to dephosphorylate cofilin. Activated cofilin saturates actin filaments causing them to bundle into aberrant rod structures. These rods block major activities required for synapse formation resulting in the breakdown of synaptic function. (Right) AIP-1 present: AIP-1 enhances the depolymerisation of filaments that are decorated with cofilin. This allows normal functions required for maintenance of the synapse.*

The exact function of cofilin within the nucleus is unknown, however it is still thought to form part of a stress response (Munsie et al., 2012). Conversely, the results in neurons presented here show that overexpression of AIP-1 effectively prevents rod formation, potentially through enhancement of cofilin-mediated disassembly. Furthermore, no rods were observed in the nuclei of neurons (data not shown) which suggests that either, amyloid-β and 2-DG do not elicit intranuclear rod formation or that DRG neurons themselves do not display an intranuclear rod response. Evidence for rod formation in neuronal nuclei was never seen across all the experimental protocols, however it is possible this was overlooked due to focusing on growth cones.

Cofilin activity state plays important role in rod formation. Rod formation was observed in growth cones expressing constitutively active cofilin, but not in phosphomimetic cofilin, on 2-DG treatment when endogenous cofilin was knocked down. This suggests that cofilin must be dephosphorylated at Ser3 to form cofilin actin rods. Whether this escalation of cofilin activity is a result of reduced phosphorylation by LIMK or phosphatase activity is upregulated remains unknown. However, previous published findings showed cofilin phosphorylation induced by amyloid-β treatment could be repressed by addition of S3 peptide – a specific competitor for cofilin phosphorylation by LIMK (Heredia et al., 2006). It is possible that specific activation of cofilin in locations containing bundled F-actin, such as in filopodia, may be more susceptible to transformation into rods that occlude the filopodial lumen. Understanding whether actin architecture plays a part in rod formation is of importance as AIP-1 enhancement effect may be dependent upon the underlying actin architecture present (Gressin et al., 2015).

Filamentous actin within the growth cone is largely found in networks that form the lamellipodia and bundled into filopodia that extend out past the leading edge. Both structures are highly dynamic, requiring rapid reorganisation to respond to extracellular signals during motility. The localization of AIP-1 was found to coincide with the leading edge of fibroblasts – a zone with high actin turnover. This area is similar in behavior to the growth cone, and when assessed in neurons by fluorescent live cell imaging, AIP-1 was localized to regions of swift remodeling as growth cones formed asymmetric protrusions for turning. In particular, patches of AIP-1 appear at the base of highly active filopodia prior to extension. Similar behaviour has only been previously shown in yeast where AIP-1 localised to cortical actin patches the position of which correlates with polarized growth (Rodal et al., 1999; Waddle et al., 1996). This suggests that AIP-1 is supplying the demand of actin monomers for extension or generation of new filaments for rapid protrusive activity in neuronal growth cones, a hypothesis that has been previously proposed from observations in yeast (Okreglak and Drubin, 2010). Whilst this may seem counterintuitive based on enhancing cofilin severing activity, high actin turnover is associated with remodelling and extension rather than collapse as may be predicted.

The work in this chapter shows that AIP-1 can potently block the formation of cofilin rods which are thought to contribute to cellular dysfunction in several neurodegenerative disorders. AIP-1 offers the exciting possibility of a means to reverse cofilin rod formation and the subsequent cytoskeletal pathology associated with dementia and has potential for therapeutic exploitation in human disease. Furthermore, it is the first study to demonstrate that AIP-1 localises to areas of rapid actin remodeling in neuronal growth cones. However, many

questions remain such as to what extent is the cofilin rod response protective? Can modulating AIP-1 to prevent rods increase neuronal survival *in vivo*? If so, how can at risk neuronal populations be targeted? The J20 mouse line provides an ideal model of Alzheimer's to answer these key questions, and I have already confirmed that an increased density of cofilin aggregations can be visualised in the cortices of these animals compared to wildtype littermates. This model can be utilised in characterising the effect of rod formation electrophysiological responses of neurons to chronic amyloid-β exposure and most importantly how this can be modulated by AIP-1. Exploiting the action of AIP-1 therefore represents a potentially novel therapeutic avenue to tackle neurodegeneration. The generation of AIP-1 point mutants will further characterize AIP-1 function and perhaps point towards small peptide mimetic development.

CHAPTER 6

CONCLUDING DISCUSSION

CHAPTER 6
CONCLUDING DISCUSSION

There are many disorders of the central and peripheral nervous system; these severely impact the lives of hundreds of millions of people worldwide. The financial burden in Europe alone, in 2010, was estimated at a staggering €798 billion (Gustavsson et al., 2011). For many conditions, the underlying aetiology remains elusive. An increasing body of evidence suggests that mutations in the genes associated with neurological disease results in dysfunction of actin-based cytoskeletal activities, such as vesicle and organelle trafficking, and synaptic signalling, that are required for normal neuronal function. Defects of the cytoskeleton therefore potentially present a common mechanism that underlies a cascade of events that ultimately ends in neuronal loss in many neurological disorders. Therefore, understanding how the cytoskeleton and its associated regulatory proteins function in nervous system development is crucial for unpicking the complex pathogenesis that results in degeneration of neuronal function.

The aim of this study was to examine the role of the actin binding proteins drebrin and cofilin in the motility of neuronal growth cone and filopodial dynamics. These molecules were investigated due to their central role in the modulation of actin remodelling; Cofilin can sever and trigger the disassembly of filaments that form filopodia, whereas drebrin can stabilise and bundle. The combination of these actions leads to a highly responsive structure that underlies the plasticity of the nervous system, a feature that is disrupted in neurodegenerative and developmental disorders. Loss of drebrin in Alzheimer's disease is thought to contribute to cytoskeletal changes that precede the disappearance of synapses,

and dysregulated cofilin can cause formation of aggregates that disturbs synaptic health and thus impacts neuronal function. Despite their opposing molecular actions on actin filaments, cofilin and drebrin were unexpectedly found to have a synergistic relationship. Here, cofilin generates new barbed ends, seeding sites for actin filament extension which are then likely to be bundled and stiffened by drebrin, resulting in increased filopodial formation. This balance must be tightly regulated and dysregulation of upstream activators of cofilin and drebrin may disrupt the balance which results in the cytoskeletal abnormalities observed in disease. Furthermore, following acute treatment with low concentrations of the repulsive guidance cue sema 3A, neuronal growth cones expressing cofilin display increased morphological complexity and filopodial stability suggesting that traditional collapse signals may serve as pause signals allowing neurons to increase the surface area to sense the environment adequately and enable precise wiring decisions.

The synergistic relationship observed between cofilin and drebrin can also give insight to other fields of biology in which perturbations of the cytoskeleton are associated with disease. Epithelial-to-mesenchymal transition and subsequent migration that occurs in metastasis requires major reorganisation of the actin cytoskeleton (Shankar and Nabi, 2015; Yamaguchi and Condeelis, 2007). Cofilin activity is upregulated in cancer cell motility and invasion, though not through dephosphorylation events but rather through release of active cofilin by EGF-mediated PIP_2 hydrolysis. This is thought to drive the directed motility underlying invasive behaviour (Mouneimne et al., 2004). Additionally, drebrin has also been shown to facilitate shape changes in response to guidance cues in prostate cancer cells (Dart et al., 2017). The variations in expression of both cofilin and

drebrin could present a novel biomarker used to measure invasiveness and inform prognostic scoring for cancer outcome predictions.

Cofilin dysregulation can cause cytoskeletal dynamic arrest in cells exposed to a variety of stressors. Rapidly activated cofilin can saturate actin filaments causing them to aggregate into rod-shaped structures. This frees up ATP which can then be reassigned to processes required for cellular survival (Munsie and Truant, 2012). Neurons are particularly sensitive to stress conditions and these accumulations are linked to the demise of neuronal populations in proteinopathies such as Huntington's disease and Alzheimer's disease. Cofilin rods also form in retinal ganglion cells that are metabolically stressed *in vivo* which suggests that cofilin rods may contribute to the pathogenesis of diabetic retinopathy in which capillary degeneration leads to retinal ischemia (Kern and Barber, 2008). Most importantly, rod formation is reversible which renders them a novel therapeutic target in the alleviation of cell loss.

I have found that AIP-1 offers the exciting possibility of a means to reverse cofilin rod formation and the subsequent cytoskeletal pathology associated with dementia. This work shows that AIP-1 strongly inhibits rod formation in neurons during energy depletion and amyloid-β exposure, two major risk factors for dementia. Further understanding of how AIP-1 clears rods or blocks their deposition will open novel therapeutic avenues such as small molecule or peptide inhibitors to prevent or reverse disease progression. The role of AIP-1 in neurons is largely unknown; this is the first study to demonstrate by live cell imaging that AIP-1 is involved in the actin remodelling required for normal growth cone turning. However, further understanding of its function is necessary to develop therapies,

particularly those much needed for treating dementia. The next step would be to examine AIP-1 in a mouse model of Alzheimer's disease.

There is a growing appreciation that Alzheimer's disease, at least in its early stage, is predominantly a synaptopathy. Several groups have reported deficits in basal synaptic transmission in mice overexpressing amyloid; a smaller number have reported deficits in LTP (Randall et al., 2010). Nevertheless, there are few reports of deficits in basal synaptic transmission being normalized by molecular or pharmacological interventions. Therefore, understanding the time course of rod formation *in vivo* and whether AIP-1 can restore synaptic function would provide an important proof-of-principal that disrupting cofilin rod formation can ameliorate one of the key events in the Alzheimer's disease pathological pathway. Determining the mechanism of the protective action of AIP-1 to block and reverse cofilin rods in cultured neurons would further allow for the development of a targeted mimetic.

It is known that disruption to neuronal function occurs many decades before clinical symptoms of dementia are evident. However, very little is understood about the preclinical period, thus an advanced understanding of disease onset would be required to recognize when intervention would be best to promote neuronal survival and protect cognitive function.

APPENDICES

Appendix A

Supplementary Media File 1

Description:

The accompanying media file is a timelapse movie of a live DRG growth cone expressing drebrin-YFP (green). mRFP-R-Pre (magenta) was coexpressed to mark the plasma membrane. Images were captured every 15 seconds for 100 frames, using a 40x oil immersion objective, 2x2 binning.

Filename:
drebrin_rpre_growth_cone.avi

Appendix B

Supplementary Media File 2

Description:

The accompanying media file is a timelapse movie of a live DRG growth cone expressing mRFP-R-Pre (red) to mark the plasma membrane. Images were captured every 15 seconds for 240 frames, using a 40x oil immersion objective, 2x2 binning.

Filename:
rpre_growth_cone.avi

Appendix C

Supplementary Media File 3 & 4

Description:

Data file (3) is a timelapse movie of a live DRG growth cone co-expressing drebrin-Cherry (red) and cofilin-eGFP. Images were captured every 15 seconds for 100 frames, using a 40x oil immersion objective, 2x2 binning.

Media file (4) is the output from the customized Matlab image analysis script, *showOverlap4*, which was used to normalize fluorescence intensities for both channels in media file (3). A heatmap was applied to the channel ratio to reveal areas of co-occurrence

Filename:

Data file 3: dreb_cof_growth_cone.avi
Data file 4: dreb_cof_growth_cone_coloc_jet.avi

Appendix D

Supplementary Media File 5, 6, 7 & 8

Description:

This series of data files are timelapse movies of live DRG growth cones expressing either hair pins to knock down endogenous cofilin or scrambled control, along with cofilin R21Q-GFP to report rod formation on 50 mM 2-DG treatment. 2-DG or PBS (mock) was added at around 20-23 frames. Rods first emerge at roughly 6.5 minutes post-2-DG treatment and remained for the entirety of the imaging period. Images were captured every 15 seconds for 100 frames, using a 40x oil immersion objective, 2x2 binning.

Filename:

Data file 5: cofilin_knockdown_cofilinR21QGFP_2DG.avi
Data file 6: cofilin_knockdown_cofilinR21QGFP_mock .avi
Data file 7: scrambled_control_cofilnR21QGFP_2DG .avi
Data file 8: scrambled_control_cofilnR21QGFP_mock.avi

Appendix E

Supplementary Media File 9

Description:

The accompanying media file is a timelapse movie of a live DRG growth cone coexpressing AIP-1-cardinal (magenta) and eYFP-R-Pre (green).) AIP-1 patches shift to side of greatest protrusive activity. No exogenous guidance cues added to induce turning. Images were captured every 15 seconds for 100 frames, using a 40x oil immersion objective, 2x2 binning.

Filename:
AIP1cardinal_rpre_growth_cone.avi

Appendix F

Supplementary details of expression vector maps and cloning schemes for key genes

Cofilin fusion constructs with pClink expression vector

Cofilin-eGFP was first cloned from pEGFP-N1 human cofilin WT (Addgene, plasmid #50859) using custom designed primers with restriction overhangs BglII and XhoI (detailed in Table 2-2). Amplicons of the correct size were then ligated into pClink (*Fig. SM1)* digested with BamHI and XhoI which destroyed both these recognition sites. This was performed for cofilin mutants R21Q using the same primers, however the S3A and S3E mutant had specific forward primers.

For the cofilin-RFP constructs, cofilin alone was cloned using PCR and the same forward primers as for the eGFP version creating a BglII overhang on the N-terminal side. The reverse primer was designed to recognise the C-terminal end of cofilin and add a HindIII restriction overhang. The amplicon of the correct size was ligated into the shuttle vector pILES (*Fig. SM2)* containing mRFP digested with BglI and HindIII. Cofilin-mRFP was then excised using BglII and XhoI and ligated into pClink digested with BamHI and XhoI. Again, the BamHI/BglII site was destroyed (*Fig. SM3)*. This was performed for cofilin mutants R21Q using the same primers, however the S3A and S3E mutant had specific forward primers.

R-pre fusion constructs with pClink expression vector

mRFP-R-pre was first cloned from R-pre-mRFP (Addgene, plasmid #17275) using custom designed primers with restriction overhangs BamHI and SalI (detailed in Table XX). Amplicons of the correct size were then ligated into pClink digested with BamHI and XhoI, which destroyed the SalI/XhoI sites

For eYFP and mCardinal tagged R-pre, R-pre was cloned using primers with restriction overhangs for BamHI and SalI. This was then ligated with pILES containing either eYFP or mCardinal digested with BamHI and SalI. The fluorescent protein fused to the N-terminus of R-pre was then excised using BglII and SalI, then ligated with pClink digested with BamH1 and XhoI. Again, the BamHI/BglII and XhoI/SalI sites were destroyed (*Fig. SM4)*.

AIP-1 fusion constructs

Chicken AIP-1 was first cloned from chicken cDNA library using custom designed primers with restriction overhangs BamHI and HindIII (detailed in Table XX). Amplicons of the correct size were then ligated into pILES containing mRFP, eYFP and mCardinal, difested with BamHI and HindIII. The fluorescent protein fused to the C-terminus of AIP-1 was then excised using BamHI and SalI, then ligated with pClink digested with BamH1 and XhoI. The XhoI/SalI sites were destroyed.

The check if tagging affected AIP-1 translation or localisation, a construct was trialed with the N-terminus tag (*Fig. SM5*).

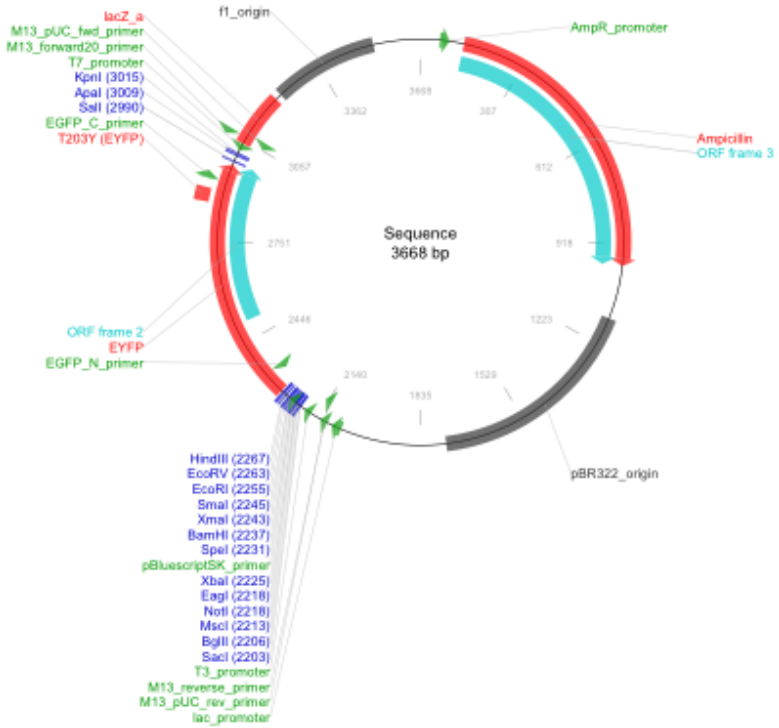

Figure SM1. Sequence map of pILES-YFP shuttle vector. *Based on the 2958-bp phagemid derived from pUC19 with an additional polylinker which adds the convenient restriction sites XhoI, BglII, MscI into the multiple cloning site.*

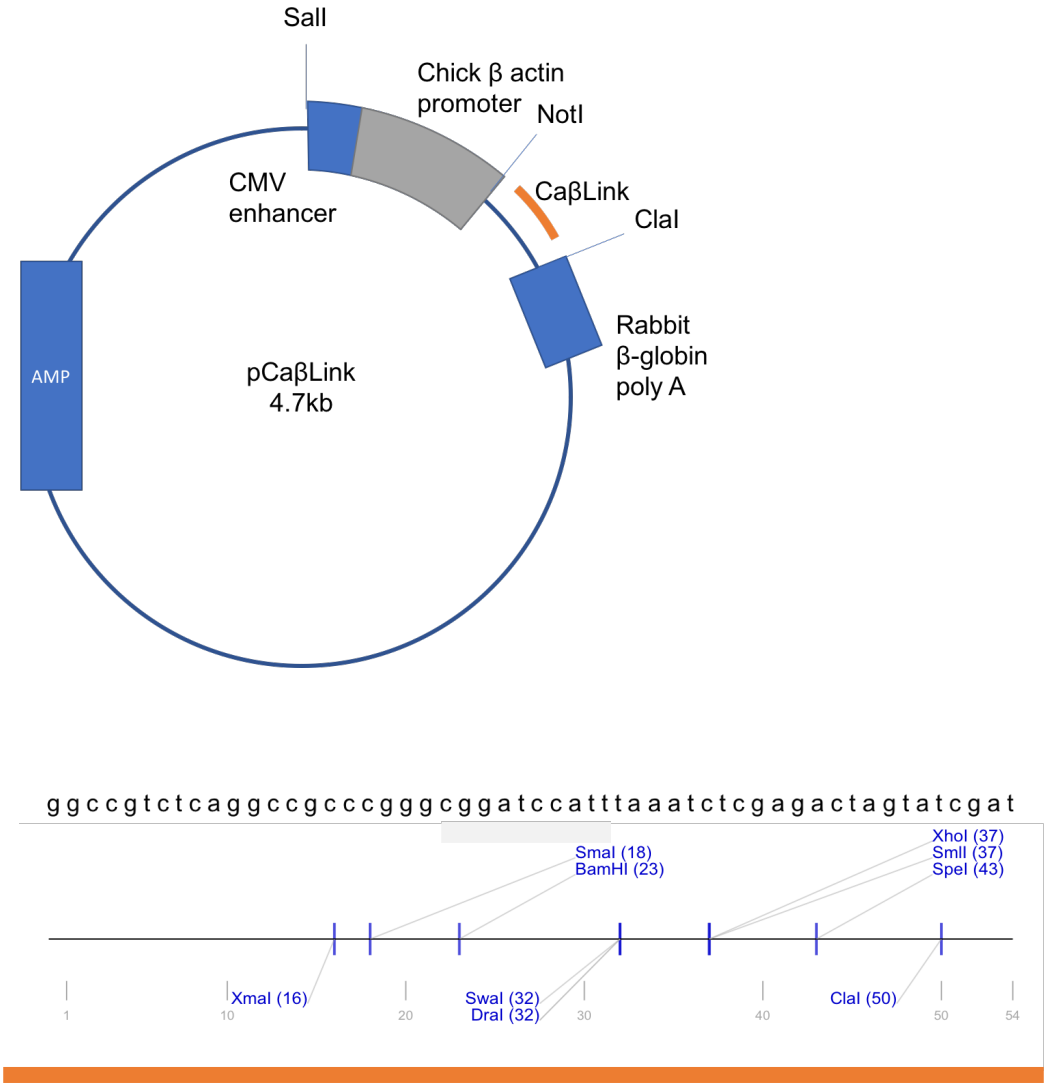

Figure SM2.Schematic of pCaLink expression vector. *pCaβLink is based upon the pCAAGS expresion vector which had the SV40 ori removed between two BamHI sites, these were filled and re-ligated. The resultant plasmid was then cut at NotI and Cla1 to remove all sequence (including lacZ) between the chick β-actin promoter and the rabbit β-globin poly and the expanded linker, CaβLink (orange), inserted. This expression vector contains the CMV enhancer and a chick β-actin promoter previously described (Fukuchi) for expression. Key, unique restriction sites are detailed in blue with DNA sequence above for the linker region.*

pClink Human Cofilin 1 – eGFP
Wild type, S3A, S3E, R21Q

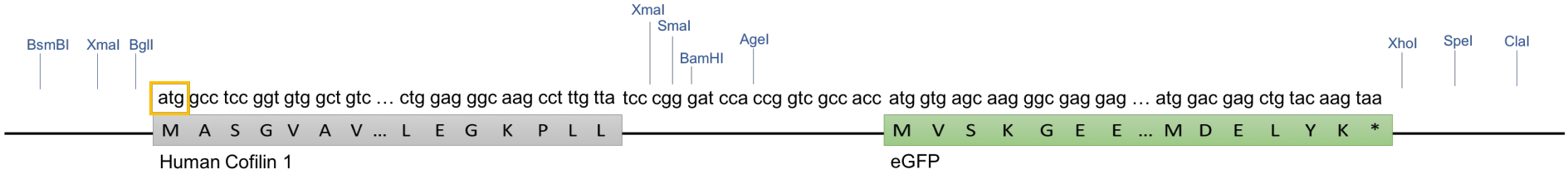

pClink Human Cofilin 1 – mRFP
Wild type, S3A, S3E, R21Q

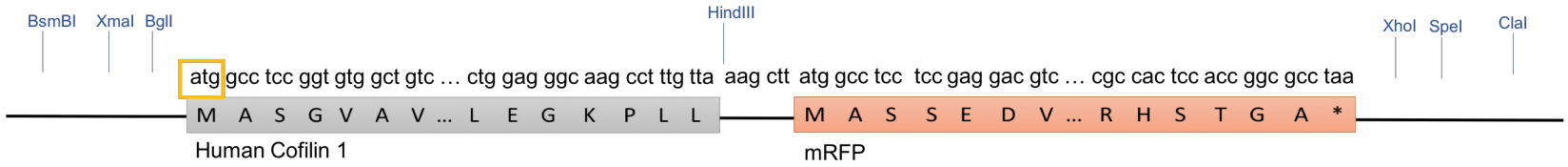

Figure SM3. *Schematic of cofilin fusion proteins, denoting restriction sites (in blue), start codon (yellow box) with DNA sequences above the amino acid sequences.*

pClink mRFP-R-Pre

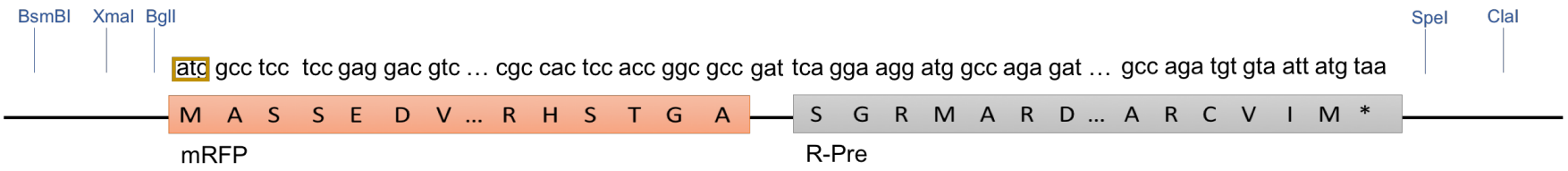

pClink mCardinal – R-PRe

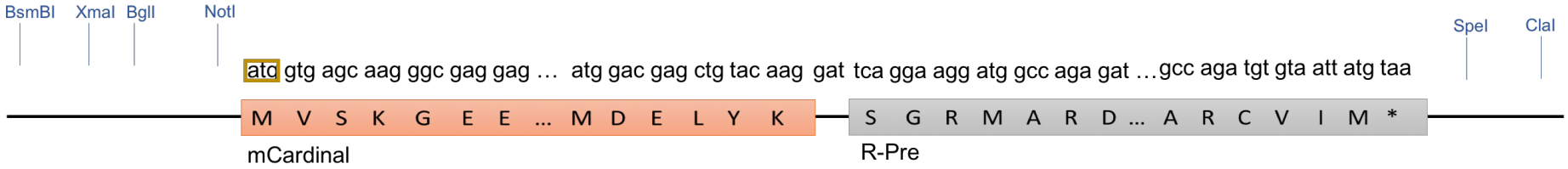

Figure SM4. *Schematic of R-pre fusion proteins, denoting restriction sites (in blue), start codon (yellow box) with DNA sequences above the amino acid sequences.*

pClink Mouse AIP-1 - mRFP

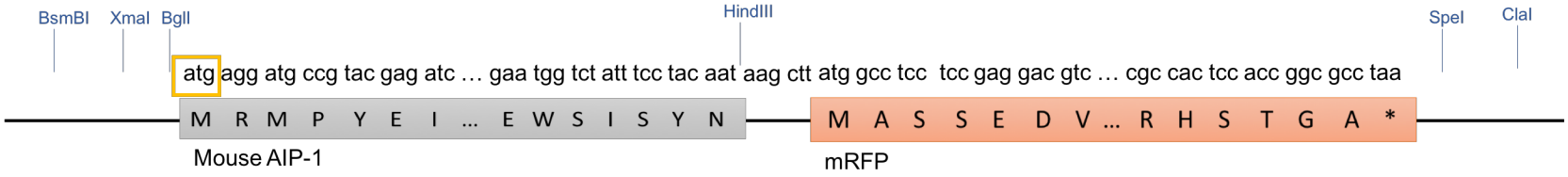

pClink Cardinal – Mouse AIP-1

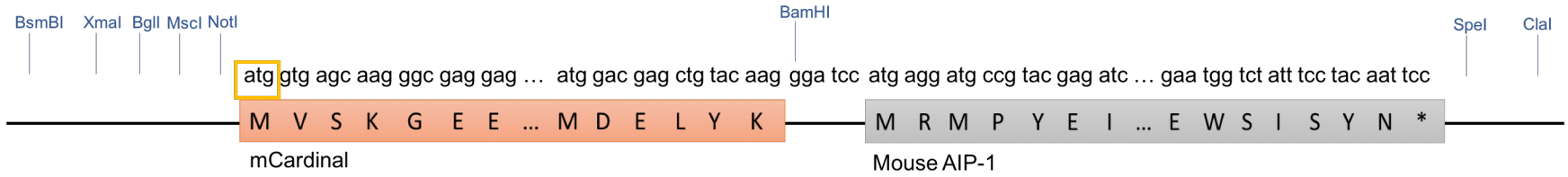

Figure SM5. *Schematic of Mouse AIP-1 fusion proteins, denoting restriction sites (in blue), start codon (yellow box) with DNA sequences above the amino acid sequences.*

Appendix G

Custom MATLAB scripts

AUTO
Used to analyse the live cell films presented in figure 4-10. It consists of 3 separate modules: *Data* extracts the data from the FIJI tracking output and calculates the filopodial length; *Export* exports the calculated lengths per frame into Excel spreadsheet format; *Normalise* plots the normalized data for the average number of filopodia per frame

Crod
Originally written to compare cofilin intensity with F-actin to identify rods. Subtracts background from image, normalises channels and then divides phalloidin channel by the cofilin channel. Ratio image is then thresholded to pixels where green:red ratio is greater than the ratio of the green to mean green + 1SD and spot noise removed. Remaining objects are 'rods'.

filMv5
Used to semi-automatically identify and track filopodia-like structures in films of live growth cones expressing fluorescently tagged proteins.

ROSA
A single script used to identify rod structures based on the ratio between width and length.

showOverlap4
Produces a heatmap of ratio of normalised fluorescent intensities.

tipTracks2
For reconstructing filopodial parameters from manually annotated co-ordinates of tips and bases using ImageJ.

AUTO-Data

```
%Change range of fileIndex according to min and max values of actual files
%to be analysed or to avoid repeating analysis of previous ones after e.g.
%a crash
for fileIndex=12:13
      close all
%Filename in '' in sprintf() below should exactly match name of files to be
%analysed with the number replaced by %d, e.g. Results_1a...Results_2a
%would be Results_%da
fileID = sprintf('Results_%da.xls',fileIndex);
if exist(fileID,'file')
inputxls=xlsread(fileID);
numTracks=max(inputxls(:,2));
allx=inputxls(:,4);
ally=inputxls(:,5);
allt=inputxls(:,3);
tipx=cell(numTracks/2,1);
basex=tipx;
tipy=tipx;
basey=tipx;
filoL=tipx;
tipt=tipx;
baset=basex;
emptyTrack=0;

%Find all the odd tracks, i.e. tips
for i=1:2:numTracks
thisFilo=find(inputxls(:,2)==i); %Get all slices for that track number
    if ~isempty(thisFilo)
    tipx{(i+1)/2}=allx(thisFilo);
    tipy{(i+1)/2}=ally(thisFilo);
    tipt{(i+1)/2}=allt(thisFilo);
    else
        emptyTrack=i;
    end
end
%Find all the odd tracks, i.e. bases
for i=2:2:numTracks
thisFilo=find(inputxls(:,2)==i);
basex{i/2}=allx(thisFilo);
basey{i/2}=ally(thisFilo);
baset{i/2}=allt(thisFilo);
    %Check equal number of tips and bases
    if length(basex{i/2})>length(tipx{i/2})
        basex{i/2}(length(tipx{i/2})+1:end)=[];
        basey{i/2}(length(tipx{i/2})+1:end)=[];
        baset{i/2}(length(tipx{i/2})+1:end)=[];
    end
    if length(tipx{i/2})>length(basex{i/2})
        tipx{i/2}(length(basex{i/2})+1:end)=[];
        tipy{i/2}(length(basex{i/2})+1:end)=[];
        tipt{i/2}(length(basex{i/2})+1:end)=[];
    end

end

%Calculate length of filopodia (filoL) over time
for i=1:length(tipx)
   filoL{i}=sqrt((tipx{i}-basex{i}).^2+(tipy{i}-basey{i}).^2);
```

```
end

%Find all the tracks present at each value of the slice (time) column
timepts=max(inputxls(:,3));
frameL=cell(1,timepts);
    %numFilo is vector of no. of filo at each timepoint
    numFilo=zeros(1,timepts);
    for t=1:timepts
        numFilo(t)=length(find(inputxls(:,3)==t))/2;
    %     %Find length of individual filopdia at each timepoint
    %     %Cycle through total number of filopodia, i.e. length of tipx
        for n=1:length(tipx)
            a=find(tipt{n}==t);
            if a
                if length(a)>1
                    a=a(1);
                end
               frameL{t}= [frameL{t} filoL{n}(a)];
            end
        end
    end

[y, life]=graphfiloAuto(fileID,numFilo,timepts,numTracks,...
    frameL,tipt,filoL,fileIndex);
[filoMassNorm,yNorm,numFiloNorm]=normFiloDataAuto(fileID,numFilo,...
    timepts,y,fileIndex);
exportExcelAuto(life,numFilo,y,fileIndex,filoMassNorm,yNorm,numFiloNorm);
plotFiloAuto(fileIndex, basey, basex, tipx, tipy, timepts, inputxls,tipt);

end
end
```

Published with MATLAB® R2014b

AUTO-Export

```
function exportExcelAuto(life,numFilo,y,filename,filoMassNorm,...
    yNorm,numFiloNorm)

if length(life)<length(numFilo)
    output=NaN(length(numFilo),3);
else
    output=NaN(length(life),3);
end
output(1:length(numFilo),1)=numFilo';
output(1:length(y),2)=y';
output(1:length(life),3)=life';
output(1:length(numFiloNorm),4)=numFiloNorm';
output(1:length(yNorm),5)=yNorm';
output(1:length(filoMassNorm),6)=filoMassNorm';
datasize=sprintf('A2:F%d',size(output,1));
headers={'No.filo','Mean length','Lifetimes','Norm. no. filo',...
    'Norm. length','Norm. filo mass'};
        savename=sprintf('%d.xls',filename);
        xlswrite(savename,headers)
        xlswrite(savename,output,datasize)
end
```

Published with MATLAB® R2014b

AUTO-Normalise

```
function [filoMassNorm,yNorm,numFiloNorm]=normFiloDataAuto(fileID,...
    numFilo,timepts,y,fileIndex)
%Normalise data
fig2name=sprintf('Normalised Filopodial Length And Tip Tracking Analysis - %s  %s',...
    fileID,date);
f2=figure('Visible','on','Units', 'Normalized',...
    'position',[0.02 0.1 0.95 0.8],...
    'Color',[0.925 0.904 0.982],'NumberTitle','off',...
    'Units','Normalized','ToolBar','none',...
    'Name',fig2name);

%normFrames is the number of frames averaged to obtain the normalisation
%factor
normFrames=5;

numFiloFactor=mean(numFilo(1:normFrames));
numFiloNorm=numFilo./numFiloFactor;
subplot(3,1,1)
plot(numFiloNorm)
xlim([1 timepts])
ylim([0 max(numFiloNorm)+1])
xlabel('Frame')
ylabel('No. filopodia')
title('Number of filopodia in each frame')

subplot(3,1,2)
% y=zeros(1,timepts);
% for i=1:timepts
%     y(i)=mean(frameL{i});
% end
yNormFactor=mean(y(1:normFrames));
yNorm=y./yNormFactor;
plot(yNorm)
xlim([1 timepts])
ylim([0 max(yNorm)+1])
xlabel('Frame')
ylabel('Mean length')
title('Mean length of filopodia per frame')

subplot(3,1,3)
filoMass=numFilo.*y;
filoMassFactor=mean(filoMass(1:normFrames));
filoMassNorm=filoMass./filoMassFactor;
plot(filoMassNorm)
xlim([1 timepts])
ylim([0 max(filoMassNorm)+1])
xlabel('Frame')
ylabel('Total filopodial mass')
title('Product of mean length and number of filopodia')

filename=sprintf('%d_norm.png',fileIndex);
saveas(gcf,filename);
end
```

Published with MATLAB® R2014b

Crod

```
%%Cofilin rod analysis
%Subtracts bgd from img, normalises channels and then divides green by red.
%Originally written to compare cofilin intensity with F-actin to identify
%rods.
%Ratio image is then thresholded to pixels where green:red ratio is greater
%than the ratio of the green to mean green + 1SD and spot noise
%removed. Remaining objects are 'rods'.

minobjsize=5; %minimum object size after thresholding
%Read in img file, assumes, format 'number.tif' from blind coding.
% filenum=input('Enter filename: ');
Nrods=0;
bgdxy=zeros(20,4);
filelet='115_Mock'; %CHANGE THIS!! and root name in line 22
%ALSO CHANGE CHANNELS IF NECESSARY (line 65)

%Loop below assumes 20 sequential files, also see lines 20 and 24 if files
%are non-sequential or have leading zeros
for filenum=1:20;
%   if filenum~=5 %include if need to skip files also line 114
    close all
filename=sprintf('115 DRGx 2DG Cof488 Phall568.lif_115 Mock
%d_z0.tif',filenum);

%%for filenames number with leading zeros
%to add zeros comment out line 22 and include lines 28-35
%number subtracted (line 30) should equal no. of digits in max value of i

%     str=num2str(filenum);
%
%     if length((num2str(filenum))-2) %#ok<*ISMT>
%         for n=1:(2-length(num2str(filenum)))
%             str=strcat('0',str);
%         end
%     end
%     filename=sprintf('Blinded DRG DEC 2016 S_Series0%s.tif',str);

% end of add zeros ---------------------

img=imread(filename);
figure;
imshow(img);
axis on;
%Obtain co-ords for bgd ROI, img axes x,y not matrix row, column
disp(filename);
x1=input('Enter bgd x1: ');
if x1<1 || x1>512
    x1=input('Enter bgd x1: ');
end
x2=input('Enter bgd x2: ');
if x2<1 || x2>512
    x2=input('Enter bgd x2: ');
end
y1=input('Enter bgd y1: ');
```

```
if y1<1 || y1>512
    y1=input('Enter bgd y1: ');
end
y2=input('Enter bgd y2: ');
if y2<1 || y2>512
    y2=input('Enter bgd y2: ');
end
bgdxy(filenum,1)=x1;
bgdxy(filenum,2)=x2;
bgdxy(filenum,3)=y1;
bgdxy(filenum,4)=y2;
%G=green channel (cofilin) R=F-actin channel
G=img(:,:,2);
R=img(:,:,1);
%Bgd subtraction, mean + 3SD
Gbgd=mean2(G(y1:y2,x1:x2))+3*std2(G(y1:y2,x1:x2));
Rbgd=mean2(R(y1:y2,x1:x2))+3*std2(R(y1:y2,x1:x2));
Gcorr=imsubtract(G,Gbgd);
Rcorr=imsubtract(R,Rbgd);
Gcorr=double(Gcorr);
Rcorr=double(Rcorr);
%Find mean green value + 1SD to set cut off for rod intensity
count=1;
pix=0;
for i=1:512;
    for j=1:512;
        if Gcorr(i,j)>0;
            pix(count)=Gcorr(i,j);
            count=count+1;
        end;
    end;
end
coeff=(mean(pix)+std(pix))/max(pix);
%Normalise
Gcorr=Gcorr./max(max(Gcorr));
Rcorr=Rcorr./max(max(Rcorr));
%Find ratio and threshold this
G2=Gcorr.*(1-Rcorr./Gcorr);
G2(G2<0)=0;
G2bw=zeros(size(G2));
G2bw(G2>coeff)=1;
G2bw=bwareaopen(G2bw,minobjsize);
figure;
[a,b]=size(G2);
imgout=zeros(a,b,3);
imgout=uint8(imgout);
imgout(:,:,1)=G2bw*255;
imgout(:,:,3)=R;

%Output img with rods marked in red on blue F-actin
imshow(imgout);
%Manual input of rod number
Nrods(filenum)=input('No. of rods: ');
%Save output img
%%Optional - add title
% text=sprintf('%s Rods (red) F-actin (blue)',filename);
% title(text);
```

```
savename=sprintf('%s%d_yarg.png',filelet,filenum);

imwrite(imgout,savename)
%   end %goes with if filenum~=...
end
%Save rod counts and bgd co-ords for current batch of files
rodout=sprintf('Rodcount_%s.xls',filelet);
if ~exist(rodout)
xlswrite(rodout,Nrods')
end
bgdout=sprintf('%s_bgd.mat',filelet);
if ~exist(bgdout)
save(bgdout,'bgdxy');
end
```

fiLIMv5

```
%%filopodia Localisation In Movies
%Semi-automated extractino of filopodial dynamics from fluorescent live
%cell imaging of growth cones
function filLIMv5(hObject,eventdata)
close all
%Figure window
f=figure('Visible','off','Units', 'Normalized',...
    'position',[0.02 0.1 0.95 0.8],...
    'Color',[0.925 0.904 0.982],'NumberTitle','off',...
    'Units','Normalized','MenuBar','none');
film=0;
cropped=0;
frames=0;
frameno=1;
lastframe=1;
tempdup=0;%stores extraction img until store is pressed to copy it to dupfr
tempdel=0;
score=0;
grow=0; shrink=0;
outlines=0;
outlineimg=0;
stored='empty';
origfr={};
storefr={};
labmat={};
cc=0;
fileID='No file.';
bw=0;
labelimg=0;
level=0;
delfr{1}='';%array of artefacts for each frame
filopodia=0; %No. of filopodia
serad=10; %Strel disk size
colwidth=0.225; %GUI Column width
colspace=0.005; %Column spacing
nocols=4; %No. of columns
col=zeros(nocols,1);
col(1)=0.01 ;
for co=2:nocols
col(co)=col(co-1)+colwidth+colspace; %Assign column x-coords
end
rowhigh=0.05; %GUI Row height
rowspace=0.005; %Row spacing
norows=19; %No.of rows
row=zeros(norows,1);
row(1)=0.025;
for ro=2:norows
row(ro)=row(ro-1)+rowhigh+rowspace; %Assign row y-coords
end
colormap(hsv)
cmap=colormap;
cmap(1,:)=[1 1 1]; cmap(64,:)=[0 0 0];
colormap(cmap)
set(0,'DefaultUicontrolFontunits','normalized');
set(0, 'DefaultAxesBox', 'off');
set(0,'DefaultUicontrolFontsize',0.4);
```

```
hfilmgrp=uibuttongroup('Units','normalized','Position',...
    [col(1) row(6) colwidth (rowhigh+rowspace)*3],'title','Film');
%Filename
currFile=uicontrol('Style','text','Units', 'Normalized','Parent',hfilmgrp,...
    'Position',[0 0.667 1 0.333],'String',fileID);
%hloadfilm
hloadfilm=uicontrol('Style','pushbutton','Units', 'Normalized',...
    'Parent',hfilmgrp,...
    'Position',[0 0.333 0.5 0.333],...
    'String','Load film','Callback',@loadfilm);
%hloadimg
hloadimg=uicontrol('Style','pushbutton','Units', 'Normalized',...
    'Parent',hfilmgrp,...
    'Position',[0.5 0.333 0.5 0.333],...
    'String','Load image','Callback',@loadimg);
hcrop=uicontrol('Style','pushbutton','Units', 'Normalized',...
    'Parent',hfilmgrp,'Position',[0 0 0.5 0.333],'String','Crop',...
    'Callback',@cropImg,'Visible','off');
hreset=uicontrol('Style','pushbutton','Units', 'Normalized',...
    'Parent',hfilmgrp,'Position',[0.5 0 0.5 0.333],'String','Reset',...
    'Callback',@reset,'Visible','off');

hframegrp=uibuttongroup('Units','normalized','Position',...
    [col(1) row(3) colwidth (rowhigh+rowspace)*3],...
    'title','Frame','Visible','off');
%hbwd
uicontrol('Style','pushbutton','Units', 'Normalized','Parent',hframegrp,...
    'Position',[0 0.667 0.15 0.333],'String','<<','Callback',@reverse);
%hfwd
uicontrol('Style','pushbutton','Units', 'Normalized','Parent',hframegrp,...
    'Position',[0.15 0.667 0.15 0.333],'String','>>','Callback',@advance);
hframeslider=uicontrol('Style','slider','Units', 'Normalized',...
    'Parent',hframegrp,'Position',[0.3 0.667 0.5 0.25],...
    'Min', 1, 'Max', 100,'Value',1,...
    'SliderStep',[0.01 0.1],'Callback',@jumpframe);
hframebox=uicontrol('Style','edit','Units', 'Normalized',...
    'Parent',hframegrp,'Position',[0.8 0.667 0.2 0.333],...
    'BackgroundColor','white','String','1','Callback',@frameslider);
hframecount=uicontrol('Style','text','Units', 'Normalized',...
    'Parent',hframegrp,'Position',[0 0.1 0.65 0.4], 'Visible','on');
hrunall=uicontrol('Style','pushbutton','Units', 'Normalized','Parent',...
    hframegrp,'Position',[0.65 0 0.35 0.5],...
    'String','Run all','Callback',@runall);

hthreshgrp=uibuttongroup('Units','normalized','Position',...
    [col(2) row(6) colwidth (rowhigh+rowspace)*3],'title','Threshold','Visible','off');
%Slider control and textbox
slhan=uicontrol('Style','slider','Units', 'Normalized','Parent',hthreshgrp,...
    'Position',[0 0.5 0.75 0.4],'Min', 0, 'Max', 1,'Value',0,...
    'SliderStep',[0.001 0.01],'BackgroundColor','white',...
    'Callback',@thresholdFrame);
slbox=uicontrol('Style','edit','Units', 'Normalized','Parent',hthreshgrp,...
    'Position',[0.75 0.5 0.25 0.4],'BackgroundColor','white',...
    'String',num2str(0),'Callback',@changeslider);
hfillHoles=uicontrol('Style','checkbox','Units', 'Normalized',...
    'Parent',hthreshgrp,'Position',[0 0.1 0.3 0.3],'Value',1,...
    'String',' Fill holes','Callback',@thresholdFrame);
hserad=uicontrol('Style','edit','Units', 'Normalized','Parent',hthreshgrp,...
    'Position',[0.75 0 0.25 0.4],'BackgroundColor','white',...
    'String',num2str(serad),'Callback',@thresholdFrame);
```

```
%hseradLabel
uicontrol('Style','text','Units', 'Normalized',...
    'Parent',hthreshgrp,'Position',[0.3 0 0.45 0.35],...
    'HorizontalAlignment','right','String','Filter width (px)  ');

hdatagrp=uibuttongroup('Units','normalized','Position',...
    [col(3) row(6) colwidth (rowhigh+rowspace)*3],'title','Data','Visible','off');
hnumfil=uicontrol('Style','text','Units', 'Normalized','Parent',hdatagrp,...
    'Position',[0 0.5 1 0.5],'fontsize',0.4,...
    'String','No. of filopodia:  0');
hstore=uicontrol('Style','pushbutton','Units', 'Normalized',...
    'Parent',hdatagrp,'Position',[0 0 0.5 0.5],'Fontsize',0.3,...
    'String','Store frame','Callback',@store);
hsave=uicontrol('Style','pushbutton','Units', 'Normalized',...
    'Parent',hdatagrp,'Position',[0.5 0 0.5 0.5],'Fontsize',0.3,...
    'String','Save frames','Callback',@saveframes);

hselectgrp=uibuttongroup('Units','normalized','Position',...
    [col(4) row(1) colwidth (rowhigh+rowspace)*8],'title','Select',...
    'Visible','off');
hremove=uicontrol('Style','listbox','Units', 'Normalized',...
    'Parent',hselectgrp,'Position',[0 0 0.4 1],...
    'String','None','min',0,'max',2,'Fontsize',0.04);
%hremovebutton
uicontrol('Style','pushbutton','Units', 'Normalized','Parent',hselectgrp,...
    'Position',[0.4 0.5 0.6 0.125],'String','Remove','Callback',@remove);
%hchoose
uicontrol('Style','pushbutton','Units', 'Normalized','Parent',hselectgrp,...
    'Position',[0.4 0.625 0.6 0.125],'String','Select',...
    'Callback',@choose);
%hzoom
uicontrol('Style','pushbutton','Units', 'Normalized','Parent',hselectgrp,...
    'Position',[0.4 0.875 0.6 0.125],'String','Zoom','Callback',@zoomIn);
%hpan
uicontrol('Style','pushbutton','Units', 'Normalized','Parent',hselectgrp,...
    'Position',[0.4 0.75 0.6 0.125],'String','Pan','Callback',@panImg);
hblackBgd=uicontrol('Style','checkbox','Units','Normalized',...
    'Parent',hselectgrp,'Position',[0.4 0.25 0.6 0.125],'Value',0,...
    'String','Black bgd','Callback',@showBlack);
houtline=uicontrol('Style','checkbox','Units','Normalized',...
    'Parent',hselectgrp,'Position',[0.4 0.375 0.6 0.125],'Value',1,...
    'String','Outline','Enable','off','Callback',@showOutline);

%axes
ax1=axes('Units', 'Normalized', 'Position',...
    [col(1) row(10) colwidth (rowhigh+rowspace)*8],'Visible','Off');
ax2=axes('Units', 'Normalized', 'Position',...
    [col(2) row(10) colwidth (rowhigh+rowspace)*8],'Visible','Off');
ax3=axes('Units', 'Normalized', 'Position',...
    [col(3) row(10) colwidth (rowhigh+rowspace)*8],'Visible','Off');
ax4=axes('Units', 'Normalized', 'Position',...
    [col(4) row(10) colwidth (rowhigh+rowspace)*8],'Visible','Off');
ax1title=uicontrol('Style','text','Units', 'Normalized','Position',...
    [col(1) row(9) colwidth rowhigh],'String','Original');
ax2title=uicontrol('Style','text','Units', 'Normalized','Position',...
    [col(2) row(9) colwidth rowhigh],'String','Threshold');
ax3title=uicontrol('Style','text','Units', 'Normalized','Position',...
    [col(3) row(9) colwidth rowhigh],'String','Filopodia');
ax4title=uicontrol('Style','text','Units', 'Normalized','Position',...
    [col(4) row(9) colwidth rowhigh],'String','Perimeter activity');
```

```
set (f,'Name','FilLIM - Filopodia Localisation In Movies');
set([ax1title,ax2title,ax3title,ax4title],...
    'fontsize',0.55,'BackgroundColor',[1 1 1]);
set([ax1title,ax2title,ax3title],...
    'ForegroundColor',[0.216 0.082 0.208],'Units','Normalized');
set(ax4title,...
    'ForegroundColor',[0.916 0.782 0.908],'Units','Normalized');

set(f,'Visible','on')
%Load film
function loadfilm(hObject,eventdata)
    fileID = uigetfile({'*.avi;',...
        'Movie files (*.avi)'},...
        'Select movie file to open');
% fileID='lactC2crop.avi';
    film=VideoReader(fileID);
    frames=read(film);
    lastframe=film.NumberOfFrames;
    frameno=1;
    origfr=cell(lastframe,1);
    delfr=origfr;
    storefr=origfr;
    filopodia=origfr;
    outlines=origfr;
    %labmat stores label matrix for each stored frame
    labmat=origfr;
    for i=1:lastframe
        origfr{i}=rgb2gray(frames(:,:,:,i));
        delfr{i}=zeros(size(origfr{i}));
    end
    tempdel=zeros(size(origfr{1}));
    score=tempdel;
    grow=tempdel; shrink=tempdel;
    set(currFile,'String',fileID);
    set(slhan,'Value',graythresh(origfr{frameno}));
    set(slbox,'String',num2str(graythresh(origfr{frameno})));
    set(hframeslider,'max',lastframe);
    set(hsave,'String','Save frames');
    set([hframegrp, hthreshgrp, hdatagrp, hselectgrp,hcrop,hreset,hstore,...
        houtline],...
        'Visible','on');
    set(hcrop,'Visible','off');
    set(hframecount,'String',...
        sprintf('Frame %d - %s\n (%d/%d) stored',...
        frameno, stored, sum(~cellfun('isempty',storefr)),...
        lastframe),'Visible','on');
    thresholdFrame;
    refreshView;
end


%Load image
function loadimg(hObject,eventdata)
 fileID = uigetfile({'*.mat;'...
     'Matlab data files (*.mat)'},...
        'Select dataset to open');
load(fileID,'cropped');
lastframe=size(cropped,4)
frames=cropped;
    frameno=1;
```

```
    origfr=cell(lastframe,1);
    delfr=origfr;
    storefr=origfr;
    filopodia=origfr;
    outlines=origfr;
    %labmat stores label matrix for each stored frame
    labmat=origfr;
    for i=1:lastframe
        origfr{i}=frames(:,:,:,i);
        delfr{i}=zeros(size(origfr{i}));
    end
    tempdel=zeros(size(origfr{1}));
    score=tempdel;
    grow=tempdel; shrink=tempdel;
    set(currFile,'String',fileID);
    set(slhan,'Value',graythresh(origfr{frameno}));
    set(slbox,'String',num2str(graythresh(origfr{frameno})));
    set(hframeslider,'max',lastframe);
    set(hsave,'String','Save frames');
    set([hframegrp, hthreshgrp, hdatagrp, hselectgrp,hcrop,hreset,hstore,...
        houtline],...
        'Visible','on');
    set(hcrop,'Visible','off');
    set(hframecount,'String',...
        sprintf('Frame %d - %s\n (%d/%d) stored',...
        frameno, stored, sum(~cellfun('isempty',storefr)),...
        lastframe),'Visible','on');
    thresholdFrame;
    refreshView;
end

%Threshold grey/rgb frame
function thresholdFrame(hObject,eventdata)
    level=get(slhan,'Value');
    checklevel;
    set(slbox,'String',num2str(level));
    bw=im2bw(origfr{frameno},level);
    hole=get(hfillHoles,'Value');
    if hole ==1
    bw=imfill(bw,'holes');
    end
    set(slbox,'String',num2str(level));
    axes(ax2);
    imagesc(bw)
    axis off;
    basefinder;
    refreshView;
end
%Adjust threshold
    function changeslider(hObject,eventdata)
        level=str2double(get(slbox,'string'));
        checklevel;
        set(slhan,'Value',level);
        thresholdFrame;
    end
%Enter frame number
function frameslider(hObject,eventdata)
        frameno=round(str2double(get(hframebox,'string')));
        if frameno<1 || frameno >lastframe
        errmsg=sprintf('Value must be between 1 and %d',lastframe);
```

```
        errordlg(errmsg,'Error','modal');
        return
        end
        set(hframeslider,'Value',frameno);
        jumpframe;
end
%Change frame with slider
function jumpframe(hObject,eventdata)
    frameno=round(get(hframeslider,'Value'));
    set(hframebox,'string',num2str(frameno));
    shiftframe;
end

%Update interface
function refreshView
    axes(ax1);
    imshow(origfr{frameno});
    axis off;
    axes(ax2);
    imagesc(im2bw(origfr{frameno},level));
    axis off;
    axes(ax3);
    if ~isempty(storefr{frameno})
        imagesc(label2rgb(storefr{frameno}))
        axis off
        set(hremove,'String',num2str(size(filopodia{frameno},1)));
            if get(hblackBgd,'Value')==1
            mask=makeBlack;
            imagesc(mask)
            axis off
            end
    else
    imshow(labelimg)
    axis off
            if get(hblackBgd,'Value')==1
            mask=makeBlack;
            imagesc(mask)
            axis off
            end

    end
    n=cc.NumObjects;
    C=(0:n)';
    set(hremove,'String',num2str(C));%Update listbox with no. filopodia
    set(f,'Visible','on');
    axis off
    if get(houtline,'Value')==1 && frameno>1
    axes(ax4)
    outlineimg=outline;
            imagesc(outlineimg);
            axis off
    else
        cla(ax4)
    end
end
%Valid slider value for threshold
function checklevel
    if level<0 || level >1
    errordlg('Value must be between 0 and 1',...
        'Error','modal');
```

```
    level=graythresh(origfr{frameno});
    set(slhan,'Value',level);
    set(slbox,'String',num2str(level));
    return
    end
end
%Convert to black background
function blackImg=makeBlack
    maskR=labelimg(:,:,1);
    maskG=labelimg(:,:,2);
    maskB=labelimg(:,:,3);
        maskR(tempdup==0)=0;
        maskG(tempdup==0)=0;
        maskB(tempdup==0)=0;
    blackImg = cat(3, maskR, maskG, maskB);
end
%Switch between black/white bgd
function showBlack(hObject,eventdata)
    axes(ax3)
    if get(hblackBgd,'Value')==1
        blackimg=makeBlack;
        imagesc(blackimg);
        axis off
    else
        imagesc(labelimg);
        axis off
    end
end
%Choose object with mouse
function choose(hObject,eventdata)
    lab=labelmatrix(bwconncomp(tempdup));
    [x,y]=ginput(1);%x,y origin = topleft of img and returns co-ords of
    %original img not scaled to size of axes
    x=floor(x); y=floor(y); pick=lab(y,x);
    set(hremove,'Value',pick+1);
end
%Zoom
function zoomIn(hObject,eventdata)
    axes(ax3);
    z=zoom;
    set(z,'Enable','on');
end
%Pan
function panImg(hObject,eventdata)
    axes(ax3);
    p=pan;
    set(p,'Enable','on');
end
%Crop image
    function cropImg(hObject,eventdata)
        crop=imcrop(ax1);
        origfr{1}=crop;
        tempdel=zeros(size(origfr{1}));
        thresholdFrame;
        refreshView;
    end
%Reset loaded image
    function reset(hObject,eventdata)
        storefr=cell(lastframe,1);
        delfr=storefr;
```

```
        for i=1:lastframe
            delfr{i}=zeros(size(origfr{1}));
        end
        stored='empty';
        filopodia=0;
        serad=3;
        frameno=1;
        set(currFile,'String',fileID);
    set(slhan,'Value',graythresh(origfr{frameno}));
    set(slbox,'String',num2str(graythresh(origfr{frameno})));
    set(currFile,'String',fileID);
    set(slhan,'Value',level);
    set(slbox,'String',num2str(level));
    set(hframebox,'String','1');
    set(hframeslider,'Value',1);
    set(hframecount,'String',...
        sprintf('Frame %d - %s\n (%d/%d) stored',...
        frameno, stored, sum(~cellfun('isempty',storefr)),...
        lastframe),'Visible','on');
        thresholdFrame;
        refreshView;
    end
%Move to next frame
function advance(hObject,eventdata)
    frameno=frameno+1;
    shiftframe;
end
%Move back one frame
function reverse(hObject,eventdata)
    frameno=frameno-1;
    shiftframe;
end
%Shift frame
function shiftframe
    if frameno>lastframe
        frameno=lastframe;
    end
    if frameno<1
        frameno=1;
    end
    if frameno==1
        set(houtline,'Enable','off');
        set(ax4title,...
    'ForegroundColor',[0.916 0.782 0.908],'Units','Normalized');
    else
        set(houtline,'Enable','on');
        set(ax4title,...
    'ForegroundColor',[0.216 0.082 0.208],'Units','Normalized');
    end
    tempdel(:,:)=0;
    if isempty(storefr{frameno})
        stored='empty';
    else
        stored='stored';
    end
    set(currFile,'String',fileID);
    set(slhan,'Value',level);
    set(slbox,'String',num2str(level));
    set(hframeslider,'Value',frameno);
    set(hframebox,'String',num2str(frameno));
```

```
    set(hframecount,'String',...
        sprintf('Frame %d - %s\n (%d/%d) stored',...
        frameno, stored, sum(~cellfun('isempty',storefr)),...
        lastframe),'Visible','on');
    thresholdFrame;
    refreshView;
end
%Store frame
function store(hObject,eventdata)
    ok=0;
    if ~isempty(storefr{frameno})
        ok=testclash;
    end
    if isempty(storefr{frameno}) || ok==1
    storefr{frameno}=tempdup;
    delfr{frameno}=tempdel;
    tempcc=bwconncomp(tempdup);
    labmat{frameno}=labelmatrix(tempcc);
    filoThin=bwmorph(storefr{frameno},'thin','Inf');
    CC2= bwconncomp(filoThin);
    filopodia{frameno}=cell2mat(struct2cell(regionprops(CC2,'Area')));
    set(hframecount,'String',...
    sprintf('Frame %d - stored\n (%d/%d stored)',...
    frameno, sum(~cellfun('isempty',storefr)),...
    lastframe));
if frameno>1
    outlines{frameno}=outlineimg*(frameno/lastframe);  %#ok<SETNU>
else
    outlines{frameno}=zeros(size(origfr{1}));
end
    if frameno<lastframe
    advance;
    end
    end
end
%Save frame data
function saveframes(hObject,eventdata)
    n=find(fileID=='.');
    savename=fileID(1:n-1);
    uisave({'filopodia','storefr','labmat'},savename);
end

%Remove filopodia
function remove(hObject,eventdata)
    CC = bwconncomp(tempdup);
    C=(0:CC.NumObjects)';
    set(hremove,'String',num2str(C));
    choices=get(hremove,'Value');
    L=labelmatrix(CC);
    if size(choices,2)>0 && choices(1)>1
        for k=1:size(choices,2)
        %fprintf('Filopodia number %d deleted\n',choices(k)-1);
            tempdel(L==choices(k)-1)=1;
            tempdup(L==choices(k)-1) = 0;
        end
    end
    CC = bwconncomp(tempdup);
    C=(0:CC.NumObjects)';
    set(hremove,'String',num2str(C));%Updates list of filopodia to select
    L=labelmatrix(CC);
```

```
    labelimg=label2rgb(L);
    set(hnumfil,'String',sprintf('No. of filopodia:  %d',CC.NumObjects));
    axes(ax3);
    if get(hblackBgd,'Value') == 1
        mask=makeBlack;
        imagesc(mask)
    else
        imagesc(labelimg)
    end
    axis off
    set(hremove,'Value',1);
end

%Check before overwriting frame
function ok=testclash
    clash=questdlg('You have already stored that frame. Do you want to overwrite?',...
    'Are you sure...?','Yes, overwrite','No, leave it','Yes, overwrite');
    switch clash
        case 'Yes, overwrite'
            ok=1;
        case 'No, leave it'
            ok=0;
    end
end

    function basefinder
%im2 is growth cone area
serad=round(str2double(get(hserad,'string')));
    if serad<1
    errordlg('Value must be positive',...
        'Error','modal');
    serad=1;
    set(hserad,'string','1');
    end
    set(hserad,'string',num2str(serad));
im2=imerode(bw, strel('disk',serad));
im2=bwareaopen(im2, 30);
im2=imdilate(im2, strel('disk',serad));
%im3 is filopodia, axon
im3=imsubtract(bw,im2);
im3=bwareaopen(im3,25);
%im4 should be the same as im2 but makes sure that erosion and dilation
%hasn't introduced px not in imbw
im4=bw & im2;
%im5 expands growth cone to find overlap (im6) with filopodia (im3) and
%therefore their base
im5=imdilate(im4,strel('disk',5));
im6=im3 & im5; %overlap
im6=bwareaopen(im6,8); %remove any spots caused by irregular outline rather
%than by filopodia

oldim3=labelmatrix(bwconncomp(im3));
overlap=im3 & im6;
if frameno>1
    tempvec=(delfr{frameno-1});
    if any(tempvec(:))
    merge=logical(delfr{frameno-1})&overlap;
    values=oldim3(merge);
    values=unique(values);
    values=values(values>0);
```

```
    for i=1:length(values)
    overlap(overlap==values(i))=0;
    end
    end
end
overlap=bwareaopen(overlap,12);
%find centres of regions where outline overlaps filopodia
s=regionprops(overlap,'Centroid','PixelList');
centres=cat(1,s.Centroid);
cc=bwconncomp(overlap);

%Take old index of protrusions (from threshold img) and replace with index
%of corresponding centre of overlap after cleaning up to renumber filopodia

tempdup=zeros(size(im3));
for i=1:cc.NumObjects
    oldim3val=oldim3(round(centres(i,2)),round(centres(i,1)));
    if oldim3val>0
    tempdup(oldim3==oldim3val)=i;
    else
        dist=zeros(size(s(i).PixelList,1),1);
        for j=1:size(s(i).PixelList,1)
            currpxX=s(i).PixelList(j,2);
            currpxY=s(i).PixelList(j,1);
            dist(j)=sqrt((currpxX-centres(i,2))^2+(currpxY-centres(i,1)));
        end
        closestpx=find(dist==(min(dist)));
    oldim3val=oldim3(s(i).PixelList(closestpx,2),s(i).PixelList(closestpx,1));
    tempdup(oldim3==max(oldim3val(:)))=i;
    end
end

labelimg=label2rgb(tempdup);
set(hnumfil,'String',sprintf('No. of filopodia:  %d',cc.NumObjects));
    end

function runall(hObject,eventdata)
    frameno=1;
    while frameno<lastframe
    basefinder;
    store;
    end
    frameno=lastframe;
    basefinder;
    store;
    saveframes;
end

%Create outline showing extension and retraction
    function imgout=outline
    f1bw=bwareaopen(bw,10);%Clean noise from threshold img
    f2bw=im2bw(origfr{frameno-1},level);%Threshold and clean frame-1
    hole=get(hfillHoles,'Value');
    if hole ==1
    f2bw=imfill(f2bw,'holes');
    end
    f2bw=bwareaopen(f2bw,10);
    f1bound=bwperim(f1bw);%Calculate boundaries
    f2bound=bwperim(f2bw);
    overlap=f1bound&f2bound;%Overlap i.e. no movement
```

```
    merge=zeros(size(f1bw));
    merge(overlap==1)=0;%No movement
    different=logical(imsubtract(f2bound,overlap));%Boundary px from...
    %current frame that have moved
    retract=different&f1bw;%Px that were also in frame-1 have retracted
    merge(retract==1)=1;
    score(retract==1)=score(retract==1)+1;
    shrink(retract==1)=shrink(retract==1)+1;
    extend=imsubtract(different,retract);%Remaining px that have moved...
    %have extended
    merge(extend==1)=3;
    score(extend==1)=score(extend==1)+1;
    grow(extend==1)=grow(extend==1)+1;
    cmap2=[1 0 0;1 1 1;0 1 0];%red-retraction white-static green-extension
    imgout=label2rgb(merge,cmap2,'k');
    end

    function showOutline(hObject,eventdata)
    axes(ax4)
        if get(houtline,'Value')==1
            outlineimg=outline;
            imagesc(outlineimg);
            axis off
            set(ax4title,...
    'ForegroundColor',[0.216 0.082 0.208],'Units','Normalized');
        else
            cla(ax4);
            set(ax4title,...
    'ForegroundColor',[0.916 0.782 0.908],'Units','Normalized');

        end
    end

end
```

Published with MATLAB® R2014b

ROSA

```
%Measurement of rod index
blobR=0; blobnoR=0; CCr=0;  Lr=0; SSr=0;
px=0;rosa=0;rods=0;

rods = imread('78 AIP.tif');
filename='ROSAtestnoR.xls';

rods=rods(:,:,2);

rodbw=im2bw(rods,0.21);
rodbw=bwareaopen(rodbw,5);
rodbw=imgbw2;
CCr=bwconncomp(rodbw);
Lr=labelmatrix(CCr);
blobR=zeros(size(rodbw,1),size(rodbw,2),max(max(Lr)));
for i=1:max(max(Lr))
    blobR(:,:,i)=(Lr==i);
    inv=imcomplement(blobR(:,:,i));
    dist=bwdist(inv);
    dist=max(max(dist));
    skel=bwmorph(blobR(:,:,i),'Skel','Inf');
    px=find(skel==1);
    rosa(i)=length(px)/dist;
end

xlswrite(filename,rosa')
```

Published with MATLAB® R2014b

showOverlap4

```
%%Heatmap of ratio of normalised fluorescent intensities
film=VideoReader('Series007_Crop001.avi');
frames=read(film);
clear figure;
firstF=34;
lastF=film.NumberOfFrames;
g=frames(:,1:214,2,firstF:lastF-1);
r=frames(:,1:214,1,firstF:lastF-1);
g=squeeze(g);
r=squeeze(r);
%crop to ROI
g=g(30:150,50:170,:);
r=r(30:150,50:170,:);
%subtract bgd on frame by frame basis
nF=size(g,3);%No. of frames

for i=1:nF
    gbgd=mean2(g(11:36,79:104,i));
    g(:,:,i)=imsubtract(g(:,:,i),gbgd);
    rbgd=mean2(r(11:36,79:104,i));
    r(:,:,i)=imsubtract(r(:,:,i),rbgd);
end
    g=double(g);
    r=double(r);

%Normalise over whole film
g=g./max(max(max(g)));
r=r./max(max(max(r)));
y=zeros(size(g));

for n=1:nF
    gtemp=g(:,:,n);
    rtemp=r(:,:,n);
    y(:,:,n)=(1-abs(r(:,:,n)-g(:,:,n))).*(r(:,:,n)+g(:,:,n))./2;
end

myVid=VideoWriter('coloc_jet.avi');
myVid.FrameRate=10;
myVid.Quality=90;
open(myVid);
for i=1:nF
    imagesc(y(:,:,i));
    colormap(jet);
    axis off;
    title('Correlation between drebrin and cofilin normalised intensities');
    colorbar;
    set(gca, 'clim', [0 1]);
    F=getframe(gcf);
    writeVideo(myVid,F);
end
close(myVid);
```

tipTracks2

```
%%For reconstructing filopodial parameters from manually annotated
%%co-ordinates of tips and bases using ImageJ
close all

fileID = uigetfile({'*.xls',...
     'Excel files (*.xls)'},...
        'Select Excel file to open');
inputxls=xlsread(fileID);
numTracks=max(inputxls(:,2));
allx=inputxls(:,4);
ally=inputxls(:,5);
allt=inputxls(:,3);
tipx=cell(numTracks/2,1);
basex=tipx;
tipy=tipx;
basey=tipx;
filoL=tipx;
tipt=tipx;
baset=basex;

%Find all the odd tracks, i.e. tips
for i=1:2:numTracks
thisFilo=find(inputxls(:,2)==i); %Get all slices for that track number
tipx{(i+1)/2}=allx(thisFilo);
tipy{(i+1)/2}=ally(thisFilo);
tipt{(i+1)/2}=allt(thisFilo);
end
%Find all the odd tracks, i.e. bases
for i=2:2:numTracks
thisFilo=find(inputxls(:,2)==i);
basex{i/2}=allx(thisFilo);
basey{i/2}=ally(thisFilo);
baset{i/2}=allt(thisFilo);
    %Check equal number of tips and bases
    if length(basex{i/2})>length(tipx{i/2})
        basex{i/2}(length(tipx{i/2})+1:end)=[];
        basey{i/2}(length(tipx{i/2})+1:end)=[];
        baset{i/2}(length(tipx{i/2})+1:end)=[];
    end
    if length(tipx{i/2})>length(basex{i/2})
        tipx{i/2}(length(basex{i/2})+1:end)=[];
        tipy{i/2}(length(basex{i/2})+1:end)=[];
        tipt{i/2}(length(basex{i/2})+1:end)=[];
    end

end

%Calculate length of filopodia (filoL) over time
for i=1:length(tipx)
   filoL{i}=sqrt((tipx{i}-basex{i}).^2+(tipy{i}-basey{i}).^2);
end

%Find all the tracks present at each value of the slice (time) column
timepts=max(inputxls(:,3));
frameL=cell(1,timepts);
    %numFilo is vector of no. of filo at each timepoint
    numFilo=zeros(1,timepts);
```

```
    for t=1:timepts
        numFilo(t)=length(find(inputxls(:,3)==t))/2;
    %     %Find length of individual filopdia at each timepoint
    %     %Cycle through total number of filopodia, i.e. length of tipx
        for n=1:length(tipx)
            a=find(tipt{n}==t);
            if a
                if length(a)>1
                    a=a(1);
                end
               frameL{t}= [frameL{t} filoL{n}(a)];
            end
        end
    end


plot(numFilo)
xlim([1 timepts])
ylim([0 max(numFilo)+1])
xlabel('Frame')
ylabel('No. filopodia')
title('Number of filopodia in each frame')
figure
for i=1:numTracks/2
    plot(tipt{i},filoL{i});
    hold on;
end
ymax=max(cellfun(@max,filoL));
xlim([1 timepts])
ylim([0 ceil(ymax/10)*10])
xlabel('Frame')
ylabel('Length')
title('Individual plots of each filopodium over time')
figure
y=zeros(1,timepts);
for i=1:timepts
    y(i)=mean(frameL{i});
end
plot(y)
xlim([1 timepts])
ylim([0 ceil(max(y)/10)*10])
xlabel('Frame')
ylabel('Mean length')
title('Mean length of filopodia per frame')
figure;
plot(numFilo.*y)
xlim([1 timepts])
xlabel('Frame')
ylabel('Total filopodial mass')
title('Product of mean length and number of filopodia')

%Export data to Excel
output(:,1)=numFilo';
output(:,2)=y';
savename=input('Enter filename for export (or n to cancel save): ','s');
    if savename~='n' && savename~='N'
        savename=sprintf('%s.xls',savename);
        xlswrite(savename,output)
    end
```

REFERENCES

Agnew, B.J., Minamide, L.S., Bamburg, J.R., 1995. Reactivation of Phosphorylated Actin Depolymerizing Factor and Identification of the Regulatory Site. Journal of Biological Chemistry 270, 17582-17587.

Agrawal, P.B., Joshi, M., Savic, T., Chen, Z., Beggs, A.H., 2012. Normal myofibrillar development followed by progressive sarcomeric disruption with actin accumulations in a mouse Cfl2 knockout demonstrates requirement of cofilin-2 for muscle maintenance. Hum Mol Genet 21, 2341-2356.

Aizawa, H., Wakatsuki, S., Ishii, A., Moriyama, K., Sasaki, Y., Ohashi, K., Sekine-Aizawa, Y., Sehara-Fujisawa, A., Mizuno, K., Goshima, Y., Yahara, I., 2001. Phosphorylation of cofilin by LIM-kinase is necessary for semaphorin 3A-induced growth cone collapse. Nature neuroscience 4, 367-373.

Amann, K.J., Pollard, T.D., 2001. Direct real-time observation of actin filament branching mediated by Arp2/3 complex using total internal reflection fluorescence microscopy. Proceedings of the National Academy of Sciences of the United States of America 98, 15009-15013.

Amberg, D.C., Basart, E., Botstein, D., 1995. Defining protein interactions with yeast actin in vivo. Nature Structural Biology 2, 28-35.

Aoki, C., Kojima, N., Sabaliauskas, N., Shah, L., Ahmed, T.H., Oakford, J., Ahmed, T., Yamazaki, H., Hanamura, K., Shirao, T., 2009. Drebrin a knockout eliminates the rapid form of homeostatic synaptic plasticity at excitatory synapses of intact adult cerebral cortex. J Comp Neurol 517, 105-121.

Aoki, C., Sekino, Y., Hanamura, K., Fujisawa, S., Mahadomrongkul, V., Ren, Y., Shirao, T., 2005. Drebrin A is a postsynaptic protein that localizes in vivo to the submembranous surface of dendritic sites forming excitatory synapses. J Comp Neurol 483, 383-402.

Araya, R., Vogels, T.P., Yuste, R., 2014. Activity-dependent dendritic spine neck changes are correlated with synaptic strength. Proceedings of the National Academy of Sciences of the United States of America 111, E2895-2904.

Arber, S., Barbayannis, F.A., Hanser, H., Schneider, C., Stanyon, C.A., Bernard, O., Caroni, P., 1998. Regulation of actin dynamics through phosphorylation of cofilin by LIM-kinase. Nature 393, 805-809.

Baier, H., Bonhoeffer, F., 1994. Attractive axon guidance molecules. Science 265, 1541-1542.

Bamburg, J.R., 1999. Proteins of the ADF/cofilin family: essential regulators of actin dynamics. Annual review of cell and developmental biology 15, 185-230.

Bamburg, J.R., Bernstein, B.W., 2016. Actin dynamics and cofilin-actin rods in Alzheimer disease. Cytoskeleton.

Bamburg, J.R., Bloom, G.S., 2009. Cytoskeletal pathologies of Alzheimer disease. Cell Motil Cytoskeleton 66, 635-649.

Bamburg, J.R., Harris, H.E., Weeds, A.G., 1980. Partial purification and characterization of an actin depolymerizing factor from brain. FEBS Lett 121, 178-182.

Barrow, C.J., Zagorski, M.G., 1991. Solution structures of Beta peptide and its consituent fragments. Science 253, 179-182.

Battye, R., Stevens, A., Jacobs, J.R., 1999. Axon repulsion from the midline of the Drosophila CNS requires slit function. Development 126, 6.

Behar, O., Golden, J.A., Mashimo, H., Schoen, F.J., Fishman, M.C., 1996. Semaphorin III is needed for normal patterning and growth of nerves, bones and heart. Nature 383, 525-528.

Bellenchi, G.C., Gurniak, C.B., Perlas, E., Middei, S., Ammassari-Teule, M., Witke, W., 2007. N-cofilin is associated with neuronal migration disorders and cell cycle control in the cerebral cortex. Genes & development 21, 2347-2357.

Bernstein, B.W., 2006. Formation of actin-ADF/cofilin rods transiently retards decline of
mitochondrial potential and ATP in stressed neurons. American journal of physiology. Cell physiology 291.

Bernstein, B.W., Shaw, A.E., Minamide, L.S., Pak, C.W., Bamburg, J.R., 2012. Incorporation of cofilin into rods depends on disulfide intermolecular bonds: implications for actin regulation and neurodegenerative disease. The Journal of neuroscience : the official journal of the Society for Neuroscience 32, 6670-6681.

Birgbauer, E., Oster, S.F., Severin, C.G., Sretavan, D.W., 2001. Retinal axon growth cones respond to EphB extracellular domains as
inhibitory axon guidance cues. Development, 8.

Blanchoin, L., Boujemaa-Paterski, R., Sykes, C., Plastino, J., 2014. Actin dynamics, architecture, and mechanics in cell motility. Physiol Rev 94, 235-263.

Bloom, O.E., Morgan, J.R., 2011. Membrane trafficking events underlying axon repair, growth, and regeneration. Molecular and cellular neurosciences 48, 339-348.

Bosch, M., Castro, J., Saneyoshi, T., Matsuno, H., Sur, M., Hayashi, Y., 2014. Structural and molecular remodeling of dendritic spine substructures during long-term potentiation. Neuron 82, 444-459.

Bradbury, S., 1979. Microscopical Image Analysis: Problems And Approaches*. Journal of Microscopy 115, 137-150.

Bravo-Cordero, J.J., Magalhaes, M.A., Eddy, R.J., Hodgson, L., Condeelis, J., 2013. Functions of cofilin in cell locomotion and invasion. Nat Rev Mol Cell Biol 14, 405-415.

Bray, D., Levin, M.D., Morton-Firth, C.J., 1998. Receptor clustering as a cellular mechanism to control sensitivity. Nature 393, 85-88.

Caja, S.R., 1899. Textura del Sistema Nervioso del Hombre y de los Vertebrados. , Madrid: Imprenta y Librería de Nicolás Moya.

Cajal, S.R., 1890. Notas anatómicas I. Sobre la aparición de las expansiones celulares en la médula embrionaria . Gac. Sant. Barc. 12, 412-419.

Calon, F., Lim, G.P., Yang, F., Morihara, T., Teter, B., Ubeda, O., Rostaing, P., Triller, A., Salem, N., Jr., Ashe, K.H., Frautschy, S.A., Cole, G.M., 2004. Docosahexaenoic acid protects from dendritic pathology in an Alzheimer's disease mouse model. Neuron 43, 633-645.

Campbell, D.S., Regan, A.G., Lopez, J.S., Tannahill, D., Harris, W.A., Holt, C.E., 2001. Semaphorin 3A Elicits Stage-Dependent Collapse, Turning, and Branching in Xenopus Retinal Growth Cones. Journal of neuroscience 21, 9.

Carlier, M.F., Laurent, V., Santolini, J., Melki, R., Didry, D., Xia, G.X., Hong, Y., Chua, N.H., Pantaloni, D., 1997. Actin depolymerizing factor (ADF/cofilin) enhances the rate of filament turnover: implication in actin-based motility. The Journal of cell biology 136, 1307-1322.

Carlier, M.F., Shekhar, S., 2017. Global treadmilling coordinates actin turnover and controls the size of actin networks. Nat Rev Mol Cell Biol 18, 389-401.

Carlsson, L., Nyström, L.E., Sundkvist, I., Markey, F., Lindberg, U., 1977. Actin polymerizability is influenced by profilin, a low molecular weight protein in non-muscle cells. Journal of molecular biology 115, 465-483.

Chae, T., Kwon, Y.T., Bronson, R., Dikkes, P., Li, E., Tsai, L.-H., 1997. Mice Lacking p35, a Neuronal Specific Activator of Cdk5, Display Cortical Lamination Defects, Seizures, and Adult Lethality. Neuron 18, 29-42.

Chao, M.V., 2003. Neurotrophins and their receptors: a convergence point for many signalling pathways. Nat Rev Neurosci 4, 299-309.

Chen, Q., Courtemanche, N., Pollard, T.D., 2015. Aip1 promotes actin filament severing by cofilin and regulates constriction of the cytokinetic contractile ring. The Journal of biological chemistry 290, 2289-2300.

Chilton, J.K., Dun, X.-P., 2010. Control of cell shape and plasticity during development and disease by the actinbinding protein Drebrin. Histol Histopathol 25.

Claessens, M.M., Bathe, M., Frey, E., Bausch, A.R., 2006. Actin-binding proteins sensitively mediate F-actin bundle stiffness. Nat Mater 5, 748-753.

Clark, C., Austen, O., Poparic, I., Guthrie, S., 2013. alpha2-Chimaerin regulates a key axon guidance transition during development of the oculomotor projection. The Journal of neuroscience : the official journal of the Society for Neuroscience 33, 16540-16551.

Clark, M.G., Teply, J., Haarer, B.K., Viggiano, S.C., Sept, D., Amberg, D.C., 2006. A genetic dissection of Aip1p's interactions leads to a model for Aip1p-cofilin cooperative activities. Molecular biology of the cell 17, 1971-1984.

Cooper, J.A., 1991. The role of actin polymerization in cell motility. Annu Rev Physiol 53, 585-605.

Dailey, M.E., Smith, S.J., 1996. The Dynamics of Dendritic Structure in Developing Hippocampal Slices. Journal of neuroscience 16.

Dart, A.E., Worth, D.C., Muir, G., Chandra, A., Morris, J.D., McKee, C., Verrill, C., Bryant, R.J., Gordon-Weeks, P.R., 2017. The drebrin/EB3 pathway drives invasive activity in prostate cancer. Oncogene 36, 4111-4123.

Das, R.M., Van Hateren, N.J., Howell, G.R., Farrell, E.R., Bangs, F.K., Porteous, V.C., Manning, E.M., McGrew, M.J., Ohyama, K., Sacco, M.A., Halley, P.A., Sang, H.M., Storey, K.G., Placzek, M., Tickle, C., Nair, V.K., Wilson, S.A., 2006. A robust system for RNA interference in the chicken using a modified microRNA operon. Dev Biol 294, 554-563.

Davenport, R.W., Dou, P., Rehder, V., Kater, S.B., 1993. A sensory role for neuronal growth cone filopodia. Nature 361, 721-724.

Davis, R.C., Maloney, M.T., Minamide, L.S., Flynn, K.C., Stonebraker, M.A., Bamburg, J.R., 2009. Mapping cofilin-actin rods in stressed hippocampal slices and the role of cdc42 in amyloid-beta-induced rods. J Alzheimers Dis 18, 35-50.

Dawe, H.R., Minamide, L.S., Bamburg, J.R., Cramer, L.P., 2003. ADF/Cofilin Controls Cell Polarity during Fibroblast Migration. Current Biology 13, 252-257.

Dent, E.W., Gertler, F.B., 2003. Cytoskeletal Dynamics and Transport in Growth Cone Motility and Axon Guidance. Neuron.

Dent, E.W., Gupton, S.L., Gertler, F.B., 2011. The growth cone cytoskeleton in axon outgrowth and guidance. Cold Spring Harb Perspect Biol 3.

Dessaud, E., McMahon, A.P., Briscoe, J., 2008. Pattern formation in the vertebrate neural tube: a sonic hedgehog morphogen-regulated transcriptional network. Development 135, 2489-2503.

Dickson, B.J., 2002. Molecular mechanisms of axon guidance. Science 298, 1959-1964.

Dickson, D.W., 1997. Neurodegenerative diseases with cytoskeletal pathology: a biochemical classification. Ann Neurol 42, 541-544.

Dominguez, R., Holmes, K.C., 2011. Actin structure and function. Annu Rev Biophys 40, 169-186.

Dottori, M., Hartley, L., Galea, M., Paxinos, G., Polizzotto, M., Kilpatrick, T., Bartlett, P.F., Murphy, M., Kontgen, F., Boyd, A.W., 1998. EphA4 (Sek1) receptor tyrosine kinase is required for the development of the corticospinal tract. Proceedings of the National Academy of Sciences 95, 13248-13253.

Drescher, U., Bonhoeffer, F., Müller, B.K., 1997. The Eph family in retinal axon guidance. Current opinion in neurobiology 7, 75-80.

Dun, X.P., Bandeira de Lima, T., Allen, J., Geraldo, S., Gordon-Weeks, P., Chilton, J.K., 2012. Drebrin controls neuronal migration through the formation and alignment of the leading process. Molecular and cellular neurosciences 49, 341-350.

Durand, C.M., Perroy, J., Loll, F., Perrais, D., Fagni, L., Bourgeron, T., Montcouquiol, M., Sans, N., 2012. SHANK3 mutations identified in autism lead to modification of dendritic spine morphology via an actin-dependent mechanism. Molecular psychiatry 17, 71-84.

Dwivedy, A., Gertler, F.B., Miller, J., Holt, C.E., Lebrand, C., 2007. Ena/VASP function in retinal axons is required for terminal arborization but not pathway navigation. Development 134, 2137-2146.

Edwards, D.C., Gill, G.N., 1999. Structural Features of LIM Kinase That Control Effects on the Actin Cytoskeleton. Journal of Biological Chemistry 274, 11352-11361.

Elder, G.A., Gama Sosa, M.A., De Gasperi, R., 2010. Transgenic mouse models of Alzheimer's disease. Mt Sinai J Med 77, 69-81.

Erskine, L., Williams, S.E., Brose, K., Kidd, T., Rachel, R.A., Goodman, C.S., Tessier-Lavigne, M., Mason, C.A., 2000. Retinal ganglion cell axon guidance in the mouse optic chiasm: expression and function of robos and slits. The Journal of neuroscience : the official journal of the Society for Neuroscience 20, 4975-4982.

Fan, J., Raper, J.A., 1995. Localized collapsing cues can steer growth cones without inducing their full collapse. Neuron 14, 263-274.

Fenstermaker, V., Chen, Y., Ghosh, A., Yuste, R., 2004. Regulation of dendritic length and branching by semaphorin 3A. Journal of neurobiology 58, 403-412.

Fiala, J.C., Feinberg, M., Popov, V., Harris, K.M., 1998. Synaptogenesis Via Dendritic Filopodia in Developing Hippocampal Area CA1. Journal of neuroscience 18, 11.

Fiala, J.C., Spacek, J., Harris, K.M., 2002. Dendritic Spine Pathology: Cause or Consequence of Neurological Disorders? Brain Research Reviews 39, 29-54.

Fifkova, E., Delay, R.J., 1982. Cytoplasmic Actin in Neuronal Processes as a Possible Mediator of Synaptic Plasticity. Journal of Cell Biology 95, 345-350.

Fletcher, D.A., Mullins, R.D., 2010. Cell mechanics and the cytoskeleton. Nature 463, 485-492.

Fox, J.W., Walsh, C.A., 1999. Periventricular heterotopia and the genetics of neuronal migration in the cerebral cortex. Am J Hum Genet 65, 19-24.

Francavilla, C., Loeffler, S., Piccini, D., Kren, A., Christofori, G., Cavallaro, U., 2007. Neural cell adhesion molecule regulates the cellular response to fibroblast growth factor. J Cell Sci 120, 4388-4394.

Freischmidt, A., Schopflin, M., Feiler, M.S., Fleck, A.K., Ludolph, A.C., Weishaupt, J.H., 2015. Profilin 1 with the amyotrophic lateral sclerosis associated mutation T109M displays unaltered actin binding and does not affect the actin cytoskeleton. BMC neuroscience 16, 77.

Fuhs, T., Goegler, M., Brunner, C.A., Wolgemuth, C.W., Kaes, J.A., 2014. Causes of retrograde flow in fish keratocytes. Cytoskeleton 71, 24-35.

Fujibuchi, T., Abe, Y., Takeuchi, T., Imai, Y., Kamei, Y., Murase, R., Ueda, N., Shigemoto, K., Yamamoto, H., Kito, K., 2005. AIP1/WDR1 supports mitotic cell rounding. Biochemical and biophysical research communications 327, 268-275.

Galloway, P.G., Perry, G., Gambetti, P., 1987. Hirano Body Filaments Contain Actin and Actin-Associated Proteins. Journal of Neuropathology and Experimental Neurology 46, 185-199.

Garvalov, B.K., Flynn, K.C., Neukirchen, D., Meyn, L., Teusch, N., Wu, X., Brakebusch, C., Bamburg, J.R., Bradke, F., 2007. Cdc42 regulates cofilin during the establishment of neuronal polarity. J Neurosci 27, 13117-13129.

Gasperini, R.J., Pavez, M., Thompson, A.C., Mitchell, C.B., Hardy, H., Young, K.M., Chilton, J.K., Foa, L., 2017. How does calcium interact with the cytoskeleton to regulate growth cone motility during axon pathfinding? Molecular and Cellular Neuroscience.

Geraldo, S., Khanzada, U.K., Parsons, M., Chilton, J.K., Gordon-Weeks, P.R., 2008. Targeting of the F-actin-binding protein drebrin by the microtubule plus-tip protein EB3 is required for neuritogenesis. Nature cell biology 10, 1181-1189.

Ghosh, M., Song, X., Mouneimne, G., Sidani, M., Lawrence, D.S., Condeelis, J.S., 2004. Cofilin promotes actin polymerization and defines the direction of cell motility. Science 304, 743-746.

Giger, R.J., Cloutier, J.-F., Sahay, A., Prinjha, R.K., Levengood, D.V., Moore, S.E., Pickering, S., Simmons, D., Rastan, S., Walsh, F.S., Kolodkin, A.L., Ginty, D.D., Geppert, M., 2000. Neuropilin-2 Is Required In Vivo for Selective Axon Guidance Responses to Secreted Semaphorins. Neuron 25, 29-41.

Goebel, H.H., Warlo, I., 1997. Nemaline myopathy with intranuclear rods—intranuclear rod myopathy. Neuromuscular Disorders 7, 13-19.

Gohla, A., Birkenfeld, J., Bokoch, G.M., 2005. Chronophin, a novel HAD-type serine protein phosphatase, regulates cofilin-dependent actin dynamics. Nature cell biology 7, 21-29.

Gohla, A., Bokoch, G.M., 2002. 14-3-3 Regulates Actin Dynamics by Stabilizing Phosphorylated Cofilin. Current Biology 12, 1704-1710.

Goldberg. D, J., Burmeister D, W., 1986. Stages in Axon Formation : Observations of Growth of
Aplysia Axons in Culture Using Video-enhanced
Contrast-Differential Interference Contrast Microscopy. The Journal of cell biology 103.

Goldman, J.E., Yen, S.H., 1986. Cytoskeletal protein abnormalities in neurodegenerative diseases. Ann Neurol 19, 209-223.

Gomez, T.M., Zheng, J.Q., 2006. The molecular basis for calcium-dependent axon pathfinding. Nature reviews. Neuroscience 7, 115-125.

Goodman, C.S., Kolodkin, A.L., Luo, Y., Püschel, A.W., Raper, J.A., 1999. Unified Nomenclature for the Semaphorins/Collapsins. Cell 97, 551-552.

Gorovoy, M., Niu, J., Bernard, O., Profirovic, J., Minshall, R., Neamu, R., Voyno-Yasenetskaya, T., 2005. LIM kinase 1 coordinates microtubule stability and actin polymerization in human endothelial cells. The Journal of biological chemistry 280, 26533-26542.

Grenningloh, G., Rehm, E.J., Goodman, C.S., 1991. Genetic analysis of growth cone guidance in Drosophila: fasciclin II functions as a neuronal recognition molecule. Cell 67, 45-57.

Gressin, L., Guillotin, A., Guerin, C., Blanchoin, L., Michelot, A., 2015. Architecture dependence of actin filament network disassembly. Curr Biol 25, 1437-1447.

Griffin, P., Furukawa, R., Piggott, C., Maselli, A., Fechheimer, M., 2014. Requirements for Hirano body formation. Eukaryot Cell 13, 625-634.

Grintsevich, E.E., Galkin, V.E., Orlova, A., Ytterberg, A.J., Mikati, M.M., Kudryashov, D.S., Loo, J.A., Egelman, E.H., Reisler, E., 2010. Mapping of drebrin binding site on F-actin. Journal of molecular biology 398, 542-554.

Grintsevich, E.E., Reisler, E., 2014. Drebrin inhibits cofilin-induced severing of F-actin. Cytoskeleton 71, 472-483.

Grintsevich, E.E., Yesilyurt, H.G., Rich, S.K., Hung, R.J., Terman, J.R., Reisler, E., 2016. F-actin dismantling through a redox-driven synergy between Mical and cofilin. Nature cell biology 18, 876-885.

Guglielmi, G., Falk, H.J., De Renzis, S., 2016. Optogenetic Control of Protein Function: From Intracellular Processes to Tissue Morphogenesis. Trends Cell Biol 26, 864-874.

Guild, G.M., Connelly, P.S., Vranich, K.A., Shaw, M.K., Tilney, L.G., 2002. Actin filament turnover removes bundles from Drosophila bristle cells. J Cell Sci 115, 641-653.

Gupton, S.L., Gertler, F.B., 2007. Filopodia: the fingers that do the walking. Science's STKE : signal transduction knowledge environment 2007, re5.

Gurniak, C.B., Perlas, E., Witke, W., 2005. The actin depolymerizing factor n-cofilin is essential for neural tube morphogenesis and neural crest cell migration. Dev Biol 278, 231-241.

Gustavsson, A., Svensson, M., Jacobi, F., Allgulander, C., Alonso, J., Beghi, E., Dodel, R., Ekman, M., Faravelli, C., Fratiglioni, L., Gannon, B., Jones, D.H., Jennum, P., Jordanova, A., Jonsson, L., Karampampa, K., Knapp, M., Kobelt,

G., Kurth, T., Lieb, R., Linde, M., Ljungcrantz, C., Maercker, A., Melin, B., Moscarelli, M., Musayev, A., Norwood, F., Preisig, M., Pugliatti, M., Rehm, J., Salvador-Carulla, L., Schlehofer, B., Simon, R., Steinhausen, H.C., Stovner, L.J., Vallat, J.M., Van den Bergh, P., van Os, J., Vos, P., Xu, W., Wittchen, H.U., Jonsson, B., Olesen, J., Group, C.D., 2011. Cost of disorders of the brain in Europe 2010. Eur Neuropsychopharmacol 21, 718-779.

Haas, J., Roth, S., Arnold, K., Kiefer, F., Schmidt, T., Bordoli, L., Schwede, T., 2013. The Protein Model Portal - a comprehensive resource for protein structure and model information.

Hamburger, V., Hamilton, H.L., 1992. A series of normal stages in the development of the chick embryo. 1951. Dev Dyn 195, 231-272.

Harigaya, Y., Shoji, M., Shirao, T., Hirai, S., 1996. Disappearance of actin-binding protein, drebrin, from hippocampal synapses in Alzheimer's disease. Journal of neuroscience research 43, 87-92.

Harrelson, A.L., Goodman, C.S., 1988. Growth cone guidance in insects: fasciclin II is a member of the immunoglobulin superfamily. Science 242, 700-708.

Harris, H.E., Bamburg, J.R., Weeds, A.G., 1980. Actin filament disassembly in blood plasma. FEBS letters 121, 175-177.

Harris, J.A., Devidze, N., Halabisky, B., Lo, I., Thwin, M.T., Yu, G.Q., Bredesen, D.E., Masliah, E., Mucke, L., 2010. Many neuronal and behavioral impairments in transgenic mouse models of Alzheimer's disease are independent of caspase cleavage of the amyloid precursor protein. The Journal of neuroscience : the official journal of the Society for Neuroscience 30, 372-381.

Hayashi, K., Ishikawa, R., Kawai-Hirai, R., Takagi, T., Taketomi, A., Shirao, T., 1999. Domain analysis of the actin-binding and actin-remodeling activities of drebrin. Exp Cell Res 253, 673-680.

Hayashi, K., Ishikawa, R., Ye, L.H., He, X.L., Takata, K., Kohama, K., Shirao, T., 1996. Modulatory role of drebrin on the cytoskeleton within dendritic spines in the rat cerebral cortex. Journal of Neuroscience 16, 7161-7170.

Hayashi, K., Shirao, T., 1999. Change in the shape of dendritic spines caused by overexpression of drebrin in cultured cortical neurons. The Journal of neuroscience : the official journal of the Society for Neuroscience 19, 3918-3925.

Henkemeyer, M., Orioli, D., Henderson, J.T., Saxton, T.M., Roder, J., Pawson, T., Klein, R., 1996. Nuk Controls Pathfinding of Commissural Axons in the Mammalian Central Nervous System. Cell 86, 35-46.

Henson, E.S., Gibson, S.B., 2006. Surviving cell death through epidermal growth factor (EGF) signal transduction pathways: implications for cancer therapy. Cellular signalling 18, 2089-2097.

Heredia, L., Helguera, P., de Olmos, S., Kedikian, G., Sola Vigo, F., LaFerla, F., Staufenbiel, M., de Olmos, J., Busciglio, J., Caceres, A., Lorenzo, A., 2006.

Phosphorylation of actin-depolymerizing factor/cofilin by LIM-kinase mediates amyloid beta-induced degeneration: a potential mechanism of neuronal dystrophy in Alzheimer's disease. The Journal of neuroscience : the official journal of the Society for Neuroscience 26, 6533-6542.

Hightower, R.C., Meagher, R.B., 1986. The molecular evolution of actin. Genetics 114, 315-332.

Hinsby, A.M., Lundfald, L., Ditlevsen, D.K., Korshunova, I., Juhl, L., Meakin, S.O., Berezin, V., Bock, E., 2004. ShcA regulates neurite outgrowth stimulated by neural cell adhesion molecule but not by fibroblast growth factor 2: evidence for a distinct fibroblast growth factor receptor response to neural cell adhesion molecule activation. Journal of neurochemistry 91, 694-703.

Hirano, A., 1994. Hirano bodies and related neuronal inclusions. Neuropathology and Applied Neurobiology 20, 3-11.

Honkura, N., Matsuzaki, M., Noguchi, J., Ellis-Davies, G.C., Kasai, H., 2008. The subspine organization of actin fibers regulates the structure and plasticity of dendritic spines. Neuron 57, 719-729.

Hotulainen, P., Llano, O., Smirnov, S., Tanhuanpaa, K., Faix, J., Rivera, C., Lappalainen, P., 2009. Defining mechanisms of actin polymerization and depolymerization during dendritic spine morphogenesis. The Journal of cell biology 185, 323-339.

Howard, J., 2008. Molecular Mechanics of Cells and Tissues. Cellular and Molecular Bioengineering 1, 24-32.

Hsia, A.Y., Masliah, E., McConlogue, L., Yu, G.Q., Tatsuno, G., Hu, K., Kholodenko, D., Malenka, R.C., Nicoll, R.A., Mucke, L., 1999. Plaque-independent disruption of neural circuits in Alzheimer's disease mouse models. Proceedings of the National Academy of Sciences 96, 3228-3233.

Huang, T.Y., Minamide, L.S., Bamburg, J.R., Bokoch, G.M., 2008. Chronophin mediates an ATP-sensing mechanism for cofilin dephosphorylation and neuronal cofilin-actin rod formation. Dev Cell 15, 691-703.

Hung, R.J., Pak, C.W., Terman, J.R., 2011. Direct redox regulation of F-actin assembly and disassembly by Mical. Science 334, 1710-1713.

Iida, K., Yahara, I., 1999. Cooperation of two actin-binding proteins, cofilin and Aip1, inSaccharomyces cerevisiae. Genes to Cells 4, 21-32.

Ishikawa, R., Hayashi, K., Shirao, T., Xue, Y., Takagi, T., Sasaki, Y., Kohama, K., 1994. Drebrin, a development-associated brain protein from rat embryo, causes the dissociation of tropomyosin from actin filaments. The Journal of biological chemistry 269, 29928-29933.

Ishikawa, R., Katoh, K., Takahashi, A., Xie, C., Oseki, K., Watanabe, M., Igarashi, M., Nakamura, A., Kohama, K., 2007. Drebrin attenuates the interaction between actin and myosin-V. Biochemical and biophysical research communications 359, 398-401.

Ishikawa-Ankerhold, H.C., Daszkiewicz, W., Schleicher, M., Muller-Taubenberger, A., 2017. Actin-Interacting Protein 1 Contributes to Intranuclear Rod Assembly in Dictyostelium discoideum. Scientific reports 7, 40310.

Ivanov, A., Esclapez, M., Pellegrino, C., Shirao, T., Ferhat, L., 2009. Drebrin A regulates dendritic spine plasticity and synaptic function in mature cultured hippocampal neurons. J Cell Sci 122, 524-534.

Jaiswal, R., Breitsprecher, D., Collins, A., Correa, I.R., Jr., Xu, M.Q., Goode, B.L., 2013. The formin Daam1 and fascin directly collaborate to promote filopodia formation. Curr Biol 23, 1373-1379.

Jansen, S., Collins, A., Chin, S.M., Ydenberg, C.A., Gelles, J., Goode, B.L., 2015. Single-molecule imaging of a three-component ordered actin disassembly mechanism. Nature communications 6, 7202.

Jensen, E.C., 2012. Use of fluorescent probes: their effect on cell biology and limitations. Anat Rec (Hoboken) 295, 2031-2036.

Jung, G., Kim, E.J., Cicvaric, A., Sase, S., Groger, M., Hoger, H., Sialana, F.J., Berger, J., Monje, F.J., Lubec, G., 2015. Drebrin depletion alters neurotransmitter receptor levels in protein complexes, dendritic spine morphogenesis and memory-related synaptic plasticity in the mouse hippocampus. Journal of neurochemistry 134, 327-339.

Kahn, O.I., Baas, P.W., 2016. Microtubules and Growth Cones: Motors Drive the Turn. Trends Neurosci 39, 433-440.

Kamiguchi, H., Lemmon, V., 1997. Neural cell adhesion molecule L1: signaling pathways and growth cone motility. J Neurosci Res 49, 1-8.

Kanellos, G., Frame, M.C., 2016. Cellular functions of the ADF/cofilin family at a glance. J Cell Sci 129, 3211-3218.

Kania, A., Klein, R., 2016. Mechanisms of ephrin-Eph signalling in development, physiology and disease. Nature reviews. Molecular cell biology 17, 240-256.

Kato, A., Kurita, S., Hayashi, A., Kaji, N., Ohashi, K., Mizuno, K., 2008. Critical roles of actin-interacting protein 1 in cytokinesis and chemotactic migration of mammalian cells. The Biochemical journal 414, 261-270.

Keleman, K., Dickson, B.J., 2001. Short- and Long-Range Repulsion by the Drosophila Unc5 Netrin Receptor. Neuron 32, 605-617.

Kennedy, T.E., Serafini, T., de la Torre, J., Tessier-Lavigne, M., 1994. Netrins are diffusible chemotropic factors for commissural axons in the embryonic spinal cord. Cell 78, 425-435.

Kern, T.S., Barber, A.J., 2008. Retinal ganglion cells in diabetes. The Journal of physiology 586, 4401-4408.

Ketschek, A., Gallo, G., 2010. Nerve growth factor induces axonal filopodia through localized microdomains of phosphoinositide 3-kinase activity that drive

the formation of cytoskeletal precursors to filopodia. The Journal of neuroscience : the official journal of the Society for Neuroscience 30, 12185-12197.

Ketschek, A., Spillane, M., Dun, X.P., Hardy, H., Chilton, J., Gallo, G., 2016. Drebrin Coordinates the Actin and Microtubule Cytoskeleton During the Initiation of Axon Collateral Branches. Developmental neurobiology.

Kidd, T., Bland, K.S., Goodman, C.S., 1999. Slit Is the Midline Repellent for the Robo Receptor in Drosophila. Cell 96, 785-794.

Kile, B.T., Panopoulos, A.D., Stirzaker, R.A., Hacking, D.F., Tahtamouni, L.H., Willson, T.A., Mielke, L.A., Henley, K.J., Zhang, J.G., Wicks, I.P., Stevenson, W.S., Nurden, P., Watowich, S.S., Justice, M.J., 2007. Mutations in the cofilin partner Aip1/Wdr1 cause autoinflammatory disease and macrothrombocytopenia. Blood 110, 2371-2380.

Kitsukawa, T., Shimizu, M., Sanbo, M., Hirata, T., Taniguchi, M., Bekku, Y., Yagi, T., Fujisawa, H., 1997. Neuropilin–Semaphorin III/D-Mediated Chemorepulsive Signals Play a Crucial Role in Peripheral Nerve Projection in Mice. Neuron 19, 995-1005.

Klejnot, M., Gabrielsen, M., Cameron, J., Mleczak, A., Talapatra, S.K., Kozielski, F., Pannifer, A., Olson, M.F., 2013. Analysis of the human cofilin 1 structure reveals conformational changes required for actin binding. Acta Crystallogr D Biol Crystallogr 69, 1780-1788.

Koganezawa, N., Hanamura, K., Sekino, Y., Shirao, T., 2017. The role of drebrin in dendritic spines. Molecular and cellular neurosciences.

Kojima, N., Hanamura, K., Yamazaki, H., Ikeda, T., Itohara, S., Shirao, T., 2010. Genetic disruption of the alternative splicing of drebrin gene impairs context-dependent fear learning in adulthood. Neuroscience 165, 138-150.

Kojima, N., Shirao, T., 2007. Synaptic dysfunction and disruption of postsynaptic drebrin-actin complex: a study of neurological disorders accompanied by cognitive deficits. Neuroscience research 58, 1-5.

Kolodkin, A.L., Hiesinger, P.R., 2017. Wiring visual systems: common and divergent mechanisms and principles. Curr Opin Neurobiol 42, 128-135.

Kolodkin, A.L., Levengood, D.V., Rowe, E.G., Tai, Y.-T., Giger, R.J., Ginty, D.D., 1997. Neuropilin Is a Semaphorin III Receptor. Cell 90, 753-762.

Konur, S., Yuste, R., 2004. Imaging the motility of dendritic protrusions and axon terminals: roles in axon sampling and synaptic competition. Molecular and cellular neurosciences 27, 427-440.

Konzok, A., Weber, I., Simmeth, E., Hacker, U., Maniak, M., Müller-Taubenberger, A., 1999. Daip1, aDictyosteliumHomologue of the Yeast Actin-Interacting Protein 1, Is Involved in Endocytosis, Cytokinesis, and Motility. The Journal of cell biology 146, 453-464.

Kreis, P., Hendricusdottir, R., Kay, L., Papageorgiou, I.E., van Diepen, M., Mack, T., Ryves, J., Harwood, A., Leslie, N.R., Kann, O., Parsons, M., Eickholt, B.J., 2013. Phosphorylation of the actin binding protein Drebrin at S647 is regulated by neuronal activity and PTEN. PloS one 8, e71957.

Kruger, R.P., Aurandt, J., Guan, K.L., 2005. Semaphorins command cells to move. Nat Rev Mol Cell Biol 6, 789-800.

Kubota, H., Ishikawa, R., Ohki, T., Ishizuka, J., Mikhailenko, S.V., Ishiwata, S., 2010. Modulation of the mechano-chemical properties of myosin V by drebrin-E. Biochemical and biophysical research communications 400, 643-648.

Kueh, H.Y., Charras, G.T., Mitchison, T.J., Brieher, W.M., 2008. Actin disassembly by cofilin, coronin, and Aip1 occurs in bursts and is inhibited by barbed-end cappers. The Journal of cell biology 182, 341-353.

Kullander, K., Croll, S.D., Zimmer, M., Pan, L., McClain, J., Hughes, V., Zabski, S., DeChiara, T.M., Klein, R., Yancopoulos, G.D., Gale, N.W., 2001. Ephrin-B3 is the midline barrier that prevents corticospinal tract axons from recrossing, allowing for unilateral motor control. Genes Dev 15, 877-888.

Lambrechts, A., Gevaert, K., Cossart, P., Vandekerckhove, J., Van Troys, M., 2008. Listeria comet tails: the actin-based motility machinery at work. Trends Cell Biol 18, 220-227.

Larsson, M., 2013. The optic chiasm: a turning point in the evolution of eye/hand coordination. Front Zool 10, 41.

Lee, D., Aoki, C., 2012. Presenilin conditional double knockout mice exhibit decreases in drebrin a at hippocampal CA1 synapses. Synapse 66, 870-879.

Lemmon, M.A., Schlessinger, J., 2010. Cell signaling by receptor tyrosine kinases. Cell 141, 1117-1134.

Lemmon, V., Farr, K.L., Lagenaur, C., 1989. L1-mediated axon outgrowth occurs via a homophilic binding mechanism. Neuron 2, 1597-1603.

Letourneau, P.C., 1975. Cell-to-substratum adhesion and guidance of axonal elongation. Developmental Biology 44, 92-101.

Letourneau, P.C., Condic, M.L., Snow, D.M., 1994. Interactions of developing neurons with the extracellular matrix. J Neurosci 14, 915-928.

Lewis, A.K., Bridgman, P.C., 1992. Nerve growth cone lamellipodia contain two populations of actin filaments that differ in organization and polarity. J Cell Biol 119, 1219-1243.

Li, D., Roberts, R., 2001. Human Genome and Diseases:¶WD-repeat proteins: structure characteristics, biological function, and their involvement in human diseases. Cellular and Molecular Life Sciences 58, 2085-2097.

Lilienbaum, A., Reszka, A.A., Horwitz, A.F., Holt, C.E., 1995. Chimeric integrins expressed in retinal ganglion cells impair process outgrowth in vivo. Molecular and cellular neurosciences 6, 139-152.

Lim, M.K., Kawamura, T., Ohsawa, Y., Ohtsubo, M., Asakawa, S., Takayanagi, A., Shimizu, N., 2007. Parkin interacts with LIM Kinase 1 and reduces its cofilin-phosphorylation activity via ubiquitination. Exp Cell Res 313, 2858-2874.

Lisabeth, E.M., Falivelli, G., Pasquale, E.B., 2013. Eph receptor signaling and ephrins. Cold Spring Harbor perspectives in biology 5.

Lumsden, A.G., Davies, A.M., 1986. Chemotropic effect of specific target epithelium in the developing mammalian nervous system. Nature 323, 538-539.

Luo, Y., Raible, D., Raper, J.A., 1993. Collapsin: A protein in brain that induces the collapse and paralysis of neuronal growth cones. Cell 75, 217-227.

Luo, Y., Shepherd, I., Li, J., Renzi, M.J., Chang, S., Raper, J.A., 1995. A family of molecules related to collapsin in the embryonic chick nervous system. Neuron 14, 1131-1140.

Ma, M., Zhou, L., Guo, X., Lv, Z., Yu, Y., Ding, C., Zhang, P., Bi, Y., Xie, J., Wang, L., Lin, M., Zhou, Z., Huo, R., Sha, J., Zhou, Q., 2009. Decreased cofilin1 expression is important for compaction during early mouse embryo development. Biochim Biophys Acta 1793, 1804-1810.

Maciver, S.K., Harrington, C.R., 1995. Two actin binding proteins, actin depolymerizing factor and cofilin, are associated with Hirano bodies. Neuroreport 6, 1985-1988.

Maciver, S.K., Hussey, P.J., 2002. The ADF/cofilin family: actin-remodeling proteins. Genome Biol 3, reviews3007.

Maness, P.F., Schachner, M., 2007. Neural recognition molecules of the immunoglobulin superfamily: signaling transducers of axon guidance and neuronal migration. Nat Neurosci 10, 19-26.

Manns, R.P., Cook, G.M., Holt, C.E., Keynes, R.J., 2012. Differing semaphorin 3A concentrations trigger distinct signaling mechanisms in growth cone collapse. The Journal of neuroscience : the official journal of the Society for Neuroscience 32, 8554-8559.

Marsh, L., Letourneau, P.C., 1984. Growth of Neurites without Filopodial or Lamellipodial Activity in the Presence of Cytochalasin-B. Journal of Cell Biology 99, 2041-2047.

Marsick, B.M., Flynn, K.C., Santiago-Medina, M., Bamburg, J.R., Letourneau, P.C., 2010. Activation of ADF/cofilin mediates attractive growth cone turning toward nerve growth factor and netrin-1. Developmental neurobiology 70, 565-588.

Marsick, B.M., Roche, F.K., Letourneau, P.C., 2012. Repulsive axon guidance cues ephrin-A2 and slit3 stop protrusion of the growth cone leading margin concurrently with inhibition of ADF/cofilin and ERM proteins. Cytoskeleton 69, 496-505.

McConnell, R.E., Edward van Veen, J., Vidaki, M., Kwiatkowski, A.V., Meyer, A.S., Gertler, F.B., 2016. A requirement for filopodia extension toward Slit during Robo-mediated axon repulsion. The Journal of cell biology 213, 261-274.

McCullough, B.R., Blanchoin, L., Martiel, J.L., De la Cruz, E.M., 2008. Cofilin increases the bending flexibility of actin filaments: implications for severing and cell mechanics. Journal of molecular biology 381, 550-558.

McGough, A., Pope, B., Chiu, W., Weeds, A., 1997. Cofilin changes the twist of F-actin: implications for actin filament dynamics and cellular function. The Journal of cell biology 138, 771-781.

McMurray, C.T., 2000. Neurodegeneration: diseases of the cytoskeleton? Cell Death Differ 7, 861-865.

Medalia, O., Beck, M., Ecke, M., Weber, I., Neujahr, R., Baumeister, W., Gerisch, G., 2007. Organization of actin networks in intact filopodia. Curr Biol 17, 79-84.

Mercer, J.C., Qi, Q., Mottram, L.F., Law, M., Bruce, D., Iyer, A., Morales, J.L., Yamazaki, H., Shirao, T., Peterson, B.R., August, A., 2010. Chemico-genetic identification of drebrin as a regulator of calcium responses. The international journal of biochemistry & cell biology 42, 337-345.

Merriam, E.B., Millette, M., Lumbard, D.C., Saengsawang, W., Fothergill, T., Hu, X., Ferhat, L., Dent, E.W., 2013. Synaptic regulation of microtubule dynamics in dendritic spines by calcium, F-actin, and drebrin. The Journal of neuroscience : the official journal of the Society for Neuroscience 33, 16471-16482.

Mi, J., Shaw, A.E., Pak, C.W., Walsh, K.P., Minamide, L.S., Bernstein, B.W., Kuhn, T.B., Bamburg, J.R., 2013. A genetically encoded reporter for real-time imaging of cofilin-actin rods in living neurons. PloS one 8, e83609.

Mikati, M.A., Grintsevich, E.E., Reisler, E., 2013. Drebrin-induced stabilization of actin filaments. The Journal of biological chemistry 288, 19926-19938.

Mills, E., Pham, E., Nagaraj, S., Truong, K., 2012. Engineered networks of synthetic and natural proteins to control cell migration. ACS Synth Biol 1, 211-220.

Minamide, L.S., Maiti, S., Boyle, J.A., Davis, R.C., Coppinger, J.A., Bao, Y., Huang, T.Y., Yates, J., Bokoch, G.M., Bamburg, J.R., 2010. Isolation and characterization of cytoplasmic cofilin-actin rods. The Journal of biological chemistry 285, 5450-5460.

Minamide, L.S., Striegl, A.M., Boyle, J.A., Meberg, P.J., Bamburg, J.R., 2000. Neurodegenerative stimuli induce persistent ADF/cofilin-actin rods that disrupt distal neurite function. Nature cell biology 2, 628-636.

Mogilner, A., Rubinstein, B., 2005. The physics of filopodial protrusion. Biophysical journal 89, 782-795.

Mohri, K., Ono, K., Yu, R., Yamashiro, S., Ono, S., 2006. Enhancement of actin-depolymerizing factor/cofilin-dependent actin disassembly by actin-interacting protein 1 is required for organized actin filament assembly in the Caenorhabditis elegans body wall muscle. Molecular biology of the cell 17, 2190-2199.

Moriyama, K., Iida, K., Yahara, I., 1996. Phosphorylation of Ser-3 of cofilin regulates its essential function on actin. Genes Cells 1, 73-86.

Mouneimne, G., Soon, L., DesMarais, V., Sidani, M., Song, X., Yip, S.C., Ghosh, M., Eddy, R., Backer, J.M., Condeelis, J., 2004. Phospholipase C and cofilin are required for carcinoma cell directionality in response to EGF stimulation. The Journal of cell biology 166, 697-708.

Mucke, L., E., M., Yu, G.Q., Mallory, M., Rockenstein, E.M., Tatsuno, G., Hu, K., Kholodenko, D., Johnson-Wood, K., McConlogue, L., 2000. High-Level Neuronal Expression of Aβ1–42 in Wild-Type Human Amyloid Protein Precursor Transgenic Mice: Synaptotoxicity without Plaque Formation. Journal of neuroscience 20.

Munsie, L., Caron, N., Atwal, R.S., Marsden, I., Wild, E.J., Bamburg, J.R., Tabrizi, S.J., Truant, R., 2011. Mutant huntingtin causes defective actin remodeling during stress: defining a new role for transglutaminase 2 in neurodegenerative disease. Hum Mol Genet 20, 1937-1951.

Munsie, L.N., Desmond, C.R., Truant, R., 2012. Cofilin nuclear-cytoplasmic shuttling affects cofilin-actin rod formation during stress. J Cell Sci 125, 3977-3988.

Munsie, L.N., Truant, R., 2012. The role of the cofilin-actin rod stress response in neurodegenerative diseases uncovers potential new drug targets. Bioarchitecture 2, 204-208.

Murphy, M.P., LeVine, H., 3rd, 2010. Alzheimer's disease and the amyloid-beta peptide. J Alzheimers Dis 19, 311-323.

Myers, J.P., Santiago-Medina, M., Gomez, T.M., 2011. Regulation of axonal outgrowth and pathfinding by integrin-ECM interactions. Dev Neurobiol 71, 901-923.

Nadkarni, A.V., Brieher, W.M., 2014. Aip1 destabilizes cofilin-saturated actin filaments by severing and accelerating monomer dissociation from ends. Curr Biol 24, 2749-2757.

Negishi, M., Oinuma, I., Katoh, H., 2005. Plexins: axon guidance and signal transduction. Cell Mol Life Sci 62, 1363-1371.

Niwa, R., Nagata-Ohashi, K., Takeichi, M., Mizuno, K., Uemura, T., 2002. Control of actin reorganization by Slingshot, a family of phosphatases that dephosphorylate ADF/cofilin. Cell 108, 233-246.

Nomura, K., Hayakawa, K., Tatsumi, H., Ono, S., 2016. Actin-interacting Protein 1 Promotes Disassembly of Actin-depolymerizing Factor/Cofilin-bound Actin Filaments in a pH-dependent Manner. The Journal of biological chemistry 291, 5146-5156.

Obinata, T., Nagaoka-Yasuda, R., Ono, S., Kusano, K., Mohri, K., Ohtaka, Y., Yamashiro, S., Okada, K., Abe, H., 1997. Low Molecular-weight G-actin Binding Proteins Involved in the Regulation of Actin Assembly during Myofibrillogenesis. Cell Struct Funct 22, 181-189.

Oh, S.H., Adler, H.J., Raphael, Y., Lomax, M.I., 2002. WDR1 colocalizes with ADF and actin in the normal and noise-damaged chick cochlea. J Comp Neurol 448, 399-409.

Ohshima, T., Ward, J.M., Huh, C.G., Longenecker, G., Veeranna, Pant, H.C., Brady, R.O., Martin, L.J., Kulkarni, A.B., 1996. Targeted disruption of the cyclin-dependent kinase 5 gene results in abnormal corticogenesis, neuronal pathology and perinatal death. Proceedings of the National Academy of Sciences of the United States of America 93, 11173-11178.

Okada, K., Ravi, H., Smith, E.M., Goode, B.L., 2006. Aip1 and cofilin promote rapid turnover of yeast actin patches and cables: a coordinated mechanism for severing and capping filaments. Molecular biology of the cell 17, 2855-2868.

Okamoto, K., Nagai, T., Miyawaki, A., Hayashi, Y., 2004. Rapid and persistent modulation of actin dynamics regulates postsynaptic reorganization underlying bidirectional plasticity. Nature neuroscience 7, 1104-1112.

Okenve-Ramos, P., Llimargas, M., 2014. A role for fascin in preventing filopodia breakage in Drosophila tracheal cells. Commun Integr Biol 7.

Okreglak, V., Drubin, D.G., 2010. Loss of Aip1 reveals a role in maintaining the actin monomer pool and an in vivo oligomer assembly pathway. The Journal of cell biology 188, 769-777.

Ono, S., 2001. The Caenorhabditis elegans unc-78 gene encodes a homologue of actin-interacting protein 1 required for organized assembly of muscle actin filaments. The Journal of cell biology 152, 1313-1319.

Ono, S., 2014. Regulation of structure and function of sarcomeric actin filaments in striated muscle of the nematode Caenorhabditis elegans. Anat Rec (Hoboken) 297, 1548-1559.

Parrini, E., Ramazzotti, A., Dobyns, W.B., Mei, D., Moro, F., Veggiotti, P., Marini, C., Brilstra, E.H., Dalla Bernardina, B., Goodwin, L., Bodell, A., Jones, M.C., Nangeroni, M., Palmeri, S., Said, E., Sander, J.W., Striano, P., Takahashi, Y., Van Maldergem, L., Leonardi, G., Wright, M., Walsh, C.A., Guerrini, R., 2006. Periventricular heterotopia: phenotypic heterogeneity and correlation with Filamin A mutations. Brain 129, 1892-1906.

Pasterkamp, R.J., 2012. Getting neural circuits into shape with semaphorins. Nature reviews. Neuroscience 13, 605-618.

Petros, T.J., Rebsam, A., Mason, C.A., 2008. Retinal axon growth at the optic chiasm: to cross or not to cross. Annu Rev Neurosci 31, 295-315.

Pollard, T.D., Blanchoin, L., Mullins, R.D., 2000. Molecular mechanisms controlling actin filament dynamics in nonmuscle cells. Annu Rev Biophys Biomol Struct 29, 545-576.

Pollard, T.D., Borisy, G.G., 2003. Cellular motility driven by assembly and disassembly of actin filaments. Cell 112, 453-465.

Polleux, F., 1998. Patterning of Cortical Efferent Projections by Semaphorin-Neuropilin Interactions. Science 282, 1904-1906.

Polleux, F., Morrow, T., Ghosh, A., 2000. Semaphorin 3A is a chemoattractant for cortical apical dendrites. Nature 404, 567-573.

Pope, B.J., Zierler-Gould, K.M., Kuhne, R., Weeds, A.G., Ball, L.J., 2004. Solution structure of human cofilin: actin binding, pH sensitivity, and relationship to actin-depolymerizing factor. The Journal of biological chemistry 279, 4840-4848.

Purpura, D.P., 1974. Dendritic Spine "Dysgenesis" and Mental Retardation. Science 186, 1126-1128.

Randall, A.D., Witton, J., Booth, C., Hynes-Allen, A., Brown, J.T., 2010. The functional neurophysiology of the amyloid precursor protein (APP) processing pathway. Neuropharmacology 59, 243-267.

Raper, J.A., Kapfhammer, J.R., 1990. The enrichment of a neuronal growth cone collapsing activity from embryonic chick brain. Neuron 4, 21-29.

Rehm, K., Panzer, L., van Vliet, V., Genot, E., Linder, S., 2013. Drebrin preserves endothelial integrity by stabilizing nectin at adherens junctions. J Cell Sci 126, 3756-3769.

Reinhard, J.R., Kriz, A., Galic, M., Angliker, N., Rajalu, M., Vogt, K.E., Ruegg, M.A., 2016. The calcium sensor Copine-6 regulates spine structural plasticity and learning and memory. Nat Commun 7, 11613.

Ren, N., Charlton, J., Adler, P.N., 2007. The flare gene, which encodes the AIP1 protein of Drosophila, functions to regulate F-actin disassembly in pupal epidermal cells. Genetics 176, 2223-2234.

Robertson, S.P., 2007. Otopalatodigital syndrome spectrum disorders: otopalatodigital syndrome types 1 and 2, frontometaphyseal dysplasia and Melnick-Needles syndrome. Eur J Hum Genet 15, 3-9.

Robertson, S.P., Twigg, S.R., Sutherland-Smith, A.J., Biancalana, V., Gorlin, R.J., Horn, D., Kenwrick, S.J., Kim, C.A., Morava, E., Newbury-Ecob, R., Orstavik, K.H., Quarrell, O.W., Schwartz, C.E., Shears, D.J., Suri, M., Kendrick-Jones, J., Wilkie, A.O., Group, O.P.-s.D.C.C., 2003. Localized mutations in the gene encoding the cytoskeletal protein filamin A cause diverse malformations in humans. Nat Genet 33, 487-491.

Rodal, A.A., Tetreault, J.W., Lappalainen, P., Drubin, D.G., Amberg, D.C., 1999. Aip1p interacts with cofilin to disassemble actin filaments. The Journal of cell biology 145, 1251-1264.

Rogers, E.M., Hsiung, F., Rodrigues, A.B., Moses, K., 2005. Slingshot cofilin phosphatase localization is regulated by receptor tyrosine kinases and

regulates cytoskeletal structure in the developing Drosophila eye. Mech Dev 122, 1194-1205.

Rosenblatt, J., Agnew, B.J., Abe, H., Bamburg, J.R., Mitchison, T.J., 1997. XenopusActin Depolymerizing Factor/Cofilin (XAC) Is Responsible for the Turnover of Actin Filaments inListeria monocytogenesTails. The Journal of cell biology 136, 1323-1332.

Saito, Y., Murakami, F., Song, W.-J., Okawa, K., Shimono, K., Katsumaru, H., 1992. Developing corticorubral axons of the cat form synapses on filopodial dendritic protrusions. Neuroscience Letters 147, 81-84.

Santiago, C., Bashaw, G.J., 2014. Transcription factors and effectors that regulate neuronal morphology. Development 141, 4667-4680.

Sarmiere, P.D., Bamburg, J.R., 2004. Regulation of the neuronal actin cytoskeleton by ADF/cofilin. Journal of neurobiology 58, 103-117.

Sasaki, Y., Hayashi, K., Shirao, T., Ishikawa, R., Kohama, K., 1996. Inhibition by drebrin of the actin-bundling activity of brain fascin, a protein localized in filopodia of growth cones. Journal of neurochemistry 66, 980-988.

Schlessinger, J., Ullrich, A., 1992. Growth factor signaling by receptor tyrosine kinases. Neuron 9, 383-391.

Schlüter, K., Jockusch, B.M., Rothkegel, M., 1997. Profilins as regulators of actin dynamics. Biochimica et Biophysica Acta (BBA) - Molecular Cell Research 1359, 97-109.

Serafini, T., Kennedy, T.E., Gaiko, M.J., Mirzayan, C., Jessell, T.M., Tessier-Lavigne, M., 1994. The netrins define a family of axon outgrowth-promoting proteins homologous to C. elegans UNC-6. Cell 78, 409-424.

Sernagor, E., Eglen, S.J., Wong, R.O., 2001. Development of retinal ganglion cell structure and function. Prog Retin Eye Res 20, 139-174.

Shankar, J., Nabi, I.R., 2015. Actin cytoskeleton regulation of epithelial mesenchymal transition in metastatic cancer cells. PloS one 10, e0119954.

Shao, X., Li, Q., Mogilner, A., Bershadsky, A.D., Shivashankar, G.V., 2015. Mechanical stimulation induces formin-dependent assembly of a perinuclear actin rim. Proc Natl Acad Sci U S A 112, E2595-2601.

Sharma, S., Grintsevich, E.E., Phillips, M.L., Reisler, E., Gimzewski, J.K., 2011. Atomic force microscopy reveals drebrin induced remodeling of f-actin with subnanometer resolution. Nano letters 11, 825-827.

Shaw, A.E., Bamburg, J.R., 2017. Peptide regulation of cofilin activity in the CNS: A novel therapeutic approach for treatment of multiple neurological disorders. Pharmacol Ther 175, 17-27.

Shim, K.S., Lubec, G., 2002. Drebrin, a dendritic spine protein, is manifold decreased in brains of patients with Alzheimer's disease and Down syndrome. Neuroscience Letters 324, 209-212.

Shinbrot, T., Young, W., 2008. Why decussate? Topological constraints on 3D wiring. Anat Rec (Hoboken) 291, 1278-1292.

Shirao, T., Inoue, H.K., Kano, Y., Obata, K., 1987. Localization of a developmentally regulated neuron-specific protein S54 in dendrites as revealed by immunoelectron microscopy. Brain Research 413, 374-378.

Shirao, T., Kojima, N., Nabeta, Y., Obata, K., 1989. Two forms of drebrins, developmentally regulated brain proteins, in rat. Proceedings of the Japan Academy. Ser. B: Physical and Biological Sciences 65, 169-172.

Shirao, T., Obata, K., 1985. Two Acidic Proteins Associated with Brain Development in Chick Embryo. Journal of neurochemistry 44, 1210-1216.

Sidani, M., Wessels, D., Mouneimne, G., Ghosh, M., Goswami, S., Sarmiento, C., Wang, W., Kuhl, S., El-Sibai, M., Backer, J.M., Eddy, R., Soll, D., Condeelis, J., 2007. Cofilin determines the migration behavior and turning frequency of metastatic cancer cells. The Journal of cell biology 179, 777-791.

Small, J.V., Auinger, S., Nemethova, M., Koestler, S., Goldie, K.N., Hoenger, A., Resch, G.P., 2008. Unravelling the structure of the lamellipodium. J Microsc 231, 479-485.

Smith, B.A., Gelles, J., Goode, B.L., 2014. Single-molecule studies of actin assembly and disassembly factors. Methods Enzymol 540, 95-117.

Sokac, A.M., Wieschaus, E., 2008. Zygotically controlled F-actin establishes cortical compartments to stabilize furrows during Drosophila cellularization. J Cell Sci 121, 1815-1824.

Song, X., Chen, X., Yamaguchi, H., Mouneimne, G., Condeelis, J.S., Eddy, R.J., 2006. Initiation of cofilin activity in response to EGF is uncoupled from cofilin phosphorylation and dephosphorylation in carcinoma cells. J Cell Sci 119, 2871-2881.

Sperry, R.W., 1963. CHEMOAFFINITY IN THE ORDERLY GROWTH OF NERVE FIBER PATTERNS AND CONNECTIONS. Proceedings of the National Academy of Sciences of the United States of America.

Spillane, M., Ketschek, A., Jones, S.L., Korobova, F., Marsick, B., Lanier, L., Svitkina, T., Gallo, G., 2011. The actin nucleating Arp2/3 complex contributes to the formation of axonal filopodia and branches through the regulation of actin patch precursors to filopodia. Developmental neurobiology 71, 747-758.

Star, E.N., Kwiatkowski, D.J., Murthy, V.N., 2002. Rapid turnover of actin in dendritic spines and its regulation by activity. Nature neuroscience 5, 239-246.

Stiles, J., Jernigan, T.L., 2010. The basics of brain development. Neuropsychol Rev 20, 327-348.

Stirnimann, C.U., Petsalaki, E., Russell, R.B., Muller, C.W., 2010. WD40 proteins propel cellular networks. Trends Biochem Sci 35, 565-574.

Stoeckli, E.T., Landmesser, L.T., 1998. Axon guidance at choice points. Curr Opin Neurobiol 8, 73-79.

Takahashi, H., Sekino, Y., Tanaka, S., Mizui, T., Kishi, S., Shirao, T., 2003. Drebrin-dependent actin clustering in dendritic filopodia governs synaptic targeting of postsynaptic density-95 and dendritic spine morphogenesis. The Journal of neuroscience : the official journal of the Society for Neuroscience 23, 6586-6595.

Takahashi, T., Fournier, A., Nakamura, F., Wang, L.-H., Murakami, Y., Kalb, R.G., Fujisawa, H., Strittmatter, S.M., 1999. Plexin-Neuropilin-1 Complexes Form Functional Semaphorin-3A Receptors. Cell 99, 59-69.

Tanabe, K., Yamazaki, H., Inaguma, Y., Asada, A., Kimura, T., Takahashi, J., Taoka, M., Ohshima, T., Furuichi, T., Isobe, T., Nagata, K., Shirao, T., Hisanaga, S., 2014. Phosphorylation of drebrin by cyclin-dependent kinase 5 and its role in neuronal migration. PloS one 9, e92291.

Taniguchi, M., Yuasa, S., Fujisawa, H., Naruse, I., Saga, S., Mishina, M., Yagi, T., 1997. Disruption of Semaphorin III/D Gene Causes Severe Abnormality in Peripheral Nerve Projection. Neuron 19, 519-530.

Tessier-Lavigne, M., Goodman, C.S., 1996. The molecular biology of axon guidance. Science 274, 1123-1133.

Tessier-Lavigne, M., Placzek, M., Lumsden, A.G., Dodd, J., Jessell, T.M., 1988. Chemotropic guidance of developing axons in the mammalian central nervous system. Nature 336, 775-778.

Theriot, J.A., 1997. Accelerating on a treadmill: ADF/cofilin promotes rapid actin filament turnover in the dynamic cytoskeleton. The Journal of cell biology 136, 1165-1168.

Thirion, C., Stucka, R., Mendel, B., Gruhler, A., Jaksch, M., Nowak, K.J., Binz, N., Laing, N.G., Lochmüller, H., 2001. Characterization of human muscle type cofilin (CFL2) in normal and regenerating muscle. European Journal of Biochemistry 268, 3473-3482.

Toda, M., Shirao, T., Minoshima, S., Shimizu, N., Toya, S., Uyemura, K., 1993. Molecular cloning of cDNA encoding human drebrin E and chromosomal mapping of its gene. Biochemical and biophysical research communications 196, 468-472.

Toshima, J., 2001. Cofilin Phosphorylation by Protein Kinase Testicular Protein Kinase 1 and Its Role in Integrin-mediated
Actin Reorganization and Focal Adhesion Formation.

Toshima, J., Ohashi, K., Okano, I., Nunoue, K., Kishioka, M., Kuma, K., Miyata, T., Hirai, M., Baba, T., Mizuno, K., 1995. Identification and characterization of a novel protein kinase, TESK1, specifically expressed in testicular germ cells. The Journal of biological chemistry 270, 31331-31337.

Toshima, J., Toshima, J.Y., Takeuchi, K., Mori, R., Mizuno, K., 2001. Cofilin phosphorylation and actin reorganization activities of testicular protein kinase 2

and its predominant expression in testicular Sertoli cells. The Journal of biological chemistry 276, 31449-31458.

Tseng, Y., Kole, T.P., Lee, J.S., Fedorov, E., Almo, S.C., Schafer, B.W., Wirtz, D., 2005. How actin crosslinking and bundling proteins cooperate to generate an enhanced cell mechanical response. Biochemical and biophysical research communications 334, 183-192.

Tseng, Y., Schafer, B.W., Almo, S.C., Wirtz, D., 2002. Functional synergy of actin filament cross-linking proteins. The Journal of biological chemistry 277, 25609-25616.

van Rheenen, J., Song, X., van Roosmalen, W., Cammer, M., Chen, X., Desmarais, V., Yip, S.C., Backer, J.M., Eddy, R.J., Condeelis, J.S., 2007. EGF-induced PIP2 hydrolysis releases and activates cofilin locally in carcinoma cells. The Journal of cell biology 179, 1247-1259.

Vartiainen, M.K., Mustonen, T., Mattila, P.K., Ojala, P.J., Thesleff, I., Partanen, J., Lappalainen, P., 2002. The three mouse actin-depolymerizing factor/cofilins evolved to fulfill cell-type-specific requirements for actin dynamics. Molecular biology of the cell 13, 183-194.

Vignjevic, D., Yarar, D., Welch, M.D., Peloquin, J., Svitkina, T., Borisy, G.G., 2003. Formation of filopodia-like bundles in vitro from a dendritic network. The Journal of cell biology 160, 951-962.

Voegtli, W.C., Madrona, A.Y., Wilson, D.K., 2003. The structure of Aip1p, a WD repeat protein that regulates Cofilin-mediated actin depolymerization. The Journal of biological chemistry 278, 34373-34379.

Wacker, A., Gerhardt, H., Phng, L.K., 2014. Tissue guidance without filopodia. Commun Integr Biol 7, e28820.

Waddle, J.A., Karpova, T.S., Waterston, R.H., Cooper, J.A., 1996. Movement of cortical actin patches in yeast. The Journal of cell biology 132, 861-870.

Wang, K.H., Brose, K., Arnott, D., Kidd, T., Goodman, C.S., Henzel, W., Tessier-Lavigne, M., 1999. Biochemical Purification of a Mammalian Slit Protein as a Positive Regulator of Sensory Axon Elongation and Branching. Cell 96, 771-784.

Wang, W., Eddy, R., Condeelis, J., 2007. The cofilin pathway in breast cancer invasion and metastasis. Nat Rev Cancer 7, 429-440.

Whiteman, I.T., Gervasio, O.L., Cullen, K.M., Guillemin, G.J., Jeong, E.V., Witting, P.K., Antao, S.T., Minamide, L.S., Bamburg, J.R., Goldsbury, C., 2009. Activated actin-depolymerizing factor/cofilin sequesters phosphorylated microtubule-associated protein during the assembly of alzheimer-like neuritic cytoskeletal striations. The Journal of neuroscience : the official journal of the Society for Neuroscience 29, 12994-13005.

Willmes, C.G., Mack, T.G., Ledderose, J., Schmitz, D., Wozny, C., Eickholt, B.J., 2017. Investigation of hippocampal synaptic transmission and plasticity in mice deficient in the actin-binding protein Drebrin. Scientific reports 7, 42652.

Wilson, L., Maden, M., 2005. The mechanisms of dorsoventral patterning in the vertebrate neural tube. Dev Biol 282, 1-13.

Wolf, M., Zimmermann, A.M., Görlich, A., Gurniak, C.B., Sassoè-Pognetto, M., Friauf, E., Witke, W., Rust, M.B., 2015. ADF/Cofilin Controls Synaptic Actin Dynamics and Regulates Synaptic Vesicle Mobilization and Exocytosis. Cereb Cortex 25, 2863-2875.

Worth, D.C., Daly, C.N., Geraldo, S., Oozeer, F., Gordon-Weeks, P.R., 2013. Drebrin contains a cryptic F-actin-bundling activity regulated by Cdk5 phosphorylation. The Journal of cell biology 202, 793-806.

Wu, C.H., Fallini, C., Ticozzi, N., Keagle, P.J., Sapp, P.C., Piotrowska, K., Lowe, P., Koppers, M., McKenna-Yasek, D., Baron, D.M., Kost, J.E., Gonzalez-Perez, P., Fox, A.D., Adams, J., Taroni, F., Tiloca, C., Leclerc, A.L., Chafe, S.C., Mangroo, D., Moore, M.J., Zitzewitz, J.A., Xu, Z.S., van den Berg, L.H., Glass, J.D., Siciliano, G., Cirulli, E.T., Goldstein, D.B., Salachas, F., Meininger, V., Rossoll, W., Ratti, A., Gellera, C., Bosco, D.A., Bassell, G.J., Silani, V., Drory, V.E., Brown, R.H., Jr., Landers, J.E., 2012. Mutations in the profilin 1 gene cause familial amyotrophic lateral sclerosis. Nature 488, 499-503.

Xiao, Y., Ma, H., Wan, P., Qin, D., Wang, X., Zhang, X., Xiang, Y., Liu, W., Chen, J., Yi, Z., Li, L., 2017. Trp-Asp (WD) Repeat Domain 1 Is Essential for Mouse Peri-implantation Development and Regulates Cofilin Phosphorylation. The Journal of biological chemistry 292, 1438-1448.

Yamaguchi, H., Condeelis, J., 2007. Regulation of the actin cytoskeleton in cancer cell migration and invasion. Biochimica et biophysica acta 1773, 642-652.

Yao, J., Hennessey, T., Flynt, A., Lai, E., Beal, M.F., Lin, M.T., 2010. MicroRNA-related cofilin abnormality in Alzheimer's disease. PloS one 5, e15546.

Yarmola, E.G., Bubb, M.R., 2006. Profilin: emerging concepts and lingering misconceptions. Trends Biochem Sci 31, 197-205.

Yehl, J., Kudryashova, E., Reisler, E., Kudryashov, D., Polenova, T., 2017. Structural Analysis of Human Cofilin 2/Filamentous Actin Assemblies: Atomic-Resolution Insights from Magic Angle Spinning NMR Spectroscopy. Scientific reports 7, 44506.

Yeung, T., Terebiznik, M., Yu, L., Silvius, J., Abidi, W.M., Philips, M., Levine, T., Kapus, A., Grinstein, S., 2006. Receptor activation alters inner surface potential during phagocytosis. Science 313, 347-351.

Yokoyama, N., Romero, M.I., Cowan, C.A., Galvan, P., Helmbacher, F., Charnay, P., Parada, L.F., Henkemeyer, M., 2001. Forward signaling mediated by ephrin-B3 prevents contralateral corticospinal axons from recrossing the spinal cord midline. Neuron 29, 85-97.

Yonezawa, N., Nishida, E., Iida, K., Yahara, I., Sakai, H., 1990. Inhibition of the interactions of cofilin, destrin, and deoxyribonuclease I with actin by phosphoinositides. The Journal of biological chemistry 265, 8382-8386.

Yonezawa, N., Nishida, E., Sakai, H., 1985. pH control of actin polymerization by cofilin. The Journal of biological chemistry 260, 14410-14412.

Yuan, A., Rao, M.V., Veeranna, Nixon, R.A., 2012. Neurofilaments at a glance. J Cell Sci 125, 3257-3263.

Yuan, B., Wan, P., Chu, D., Nie, J., Cao, Y., Luo, W., Lu, S., Chen, J., Yang, Z., 2014. A cardiomyocyte-specific Wdr1 knockout demonstrates essential functional roles for actin disassembly during myocardial growth and maintenance in mice. Am J Pathol 184, 1967-1980.

Zhao, H., Hakala, M., Lappalainen, P., 2010. ADF/cofilin binds phosphoinositides in a multivalent manner to act as a PIP(2)-density sensor. Biophysical journal 98, 2327-2336.

Zhou, Q., Homma, K.J., Poo, M.M., 2004. Shrinkage of dendritic spines associated with long-term depression of hippocampal synapses. Neuron 44, 749-757.

Zhu, H., Enaw, J.O., Ma, C., Shaw, G.M., Lammer, E.J., Finnell, R.H., 2007. Association between CFL1 gene polymorphisms and spina bifida risk in a California population. BMC Med Genet 8, 12.

Zhu, J., Li, W., Mao, Z., 2011. Cdk5: mediator of neuronal development, death and the response to DNA damage. Mech Ageing Dev 132, 389-394.

Zimmermann, A.M., Jene, T., Wolf, M., Görlich, A., Gurniak, C.B., Sassoè-Pognetto, M., Witke, W., Friauf, E., Rust, M.B., 2015. Attention-Deficit/Hyperactivity Disorder-like Phenotype in a Mouse Model with Impaired Actin Dynamics. Biol Psychiatry 78, 95-106.

Ziv, N.E., Smith, S.J., 1996. Evidence for a Role of Dendritic Filopodia in Synaptogenesis and Spine Formation. Neuron 17, 91-102.